

DISSERTATION

HYDRAULICS OF RIGID BOUNDARY BASINS

Submitted by
Frederick Jay Watts

In partial fulfillment of the requirements
for the Degree of Doctor of Philosophy
Colorado State University
Fort Collins, Colorado
August 1968

COLORADO STATE UNIVERSITY

August 1968

WE HEREBY RECOMMEND THAT THE DISSERTATION
PREPARED UNDER OUR SUPERVISION BY _____

Frederick Jay Watts

ENTITLED "HYDRAULICS OF RIGID BOUNDARY BASINS"

BE ACCEPTED AS FULFILLING THIS PART OF THE REQUIRE-
MENTS FOR THE DEGREE OF DOCTOR OF PHILOSOPHY

Committee on Graduate Work

D. B. Simons
Major Professor

M. L. ALBERTSON DBF

H. W. Shu

H. H. Hensinger

[Signature]
Head of Department

Examination Satisfactory

Committee on Final Examination

H. W. Shu

H. H. Hensinger

M. L. ALBERTSON DBF

D. B. Simons
Chairman

Permission to publish this dissertation or any part of it
must be obtained from the Dean of the Graduate School.

LIBRARIES

COLORADO STATE UNIVERSITY
Fort Collins, Colorado 80521
ii

ABSTRACT OF DISSERTATION

HYDRAULICS OF RIGID BOUNDARY BASINS

The object of the study was to develop design criteria for three classes (A, B & C) of rigid boundary energy dissipating structures. The Class A basin has a smooth floor and flaring vertical walls; the Class B basin is a rectangular basin with smooth floor and vertical walls; the Class C basin is a rectangular basin with smooth vertical walls and an artificially roughened floor.

Design aids developed during this study include: dimensionless coefficients for the energy and momentum equations which correct for nonhydrostatic pressure distribution and nonuniform velocity distribution at the outfall sections of circular and rectangular conduits; dimensionless water surface contours and velocity vectors for freely expanding jets supported on the bottom, downstream of circular and rectangular abrupt expansions; drag coefficients for roughness elements of known size and spacing; and other minor criteria.

Numerous existing criteria, including Blaisdell's criterion for wall flare, Ippen's relationships for predicting the angle of oblique standing waves and Albertson, et al.'s relationships for determining the properties of the flow field downstream of culvert outlets operating under high tailwater conditions were verified.

Design procedures based on continuity of flow and the balance of impulse and momentum from station to station are presented for the three classes of basins. Alternate refined procedures utilizing back-water computations are outlined for Class A and B basins.

Numerous example problems are solved in detail in Chapter VII. It is suggested that the energy basin be constructed within the roadway prism as an integral portion of the culvert barrel.

Discussions concerning the necessity of tailwater control and of other important factors which should be considered accompany the design computations.

Frederick Jay Watts
Department of Civil Engineering
Colorado State University
Fort Collins, Colorado
August 1968

ACKNOWLEDGMENTS

The writer wishes to thank his major professor, Dr. D. B. Simons, for his assistance, guidance and moral support throughout the study. The assistance and suggestions from other members of the graduate committee, Drs. H. W. Shen, M. L. Albertson and H. H. Frisinger, are gratefully acknowledged.

Helpful suggestions from M. Wacker of the Wyoming State Highway Commission and from H. Berger and H. Bossey of the Bureau of Public Roads contributed to the study.

The assistance of graduate students R. Stephan, T. Opie, J. Hamilton and others who participated in data collection and reduction was much appreciated.

The writer acknowledges the help and moral support of his wife, Betty, who typed the rough draft of the dissertation.

The services of numerous other personnel at the Engineering Research Center who helped construct facilities and produce the dissertation are noted.

Financial support from the Wyoming State Highway Commission and from Engineering Experiment Station at Colorado State University made this study possible.

TABLE OF CONTENTS

<u>Chapter</u>	<u>Page</u>
LIST OF TABLES	x
LIST OF FIGURES.	xi
I INTRODUCTION.	1
Flume Details.	4
Basin Classification	8
Experimental Program	8
II PRELIMINARY TESTS.	11
Preliminary Tests A - Class A Basin.	11
Basin Geometry	11
Method of Analysis	11
Apparatus for Measuring Velocities	14
Data Obtained	23
Analysis	23
Summary.	33
Preliminary Tests B.	34
Problem Statement.	34
Test Program	34
Data Obtained and Collection Method.	42
Data Reduction	48
Jet Divergence	48
Pipe Section, Outlet Configuration, and Eddy Pattern	58
Standing Waves	60

TABLE OF CONTENTS - Continued

<u>Chapter</u>	<u>Page</u>
Hydraulic Jump	71
Energy Losses.	73
Preliminary Tests C.	75
Run 39	75
Runs 40 through 42	77
Velocity Distribution.	78
Run 43 - High Tailwater.	78
Runs 44 through 50 - Low Tailwater	79
Summary.	88
III ENERGY AND MOMENTUM CORRECTION FACTORS	90
Problem Statement.	90
Theoretical Development.	92
Experimental Apparatus	97
CSU Calibration.	106
Measuring Procedure.	109
Test Facility.	112
Test Program and Range of Parameters	113
Presentation of Data	116
α and β Values.	116
Pressure Distribution.	119
Error Analysis	119
Energy Lines	130
IV WATER SURFACE CONTOURS AND VELOCITY DISTRIBUTION	132
Introduction	132

TABLE OF CONTENTS - Continued

<u>Chapter</u>		<u>Page</u>
	Test Program and Procedure	136
	Data Reduction and Presentation.	137
V	DRAG COEFFICIENTS.	150
	Problem Statement.	150
	Design Method.	151
	Experimental Procedure for Obtaining C_D	154
	Problem Analysis	157
	Test Program	158
	Operating Characteristics.	164
	Presentation of Data	165
VI	CHARACTERISTICS OF BASINS WITH HIGH TAILWATER.	177
	Problem Statement.	177
	Experimental Apparatus and Procedure	179
	Presentation of Data	186
	Results.	187
	$\frac{V_x \max}{V_o \max}$ versus $\frac{x}{D_o}$	192
	Q/Q_o versus x/D_o	194
	E/E_o versus x/D_o and M/M_o versus x/D_o	197
	Rate of Jet Expansion.	199
	Summary	199
VII	DESIGN OF ENERGY BASINS	204
	Class A Basin.	204
	Class B Basin.	211

TABLE OF CONTENTS - Continued

<u>Chapter</u>		<u>Page</u>
	Class C Basin	222
	Combined Basin.	229
	High Tailwater Basins	231
VIII	CONCLUSIONS	234
	BIBLIOGRAPHY.	237

LIST OF TABLES

<u>TABLE</u>		<u>Page</u>
I	FLOW PARAMETERS - PRELIMINARY TESTS A	29
II	FLOW PARAMETERS - PRELIMINARY TESTS B	41
III	FLOW PARAMETERS - TESTS C	80
IV	FLOW PARAMETERS FOR ENERGY AND MOMENTUM EXPERIMENTS	115
V	LENGTH OF SMOOTH FLOOR FOR MOMENTUM	156
VI	DATA FOR DRAG COEFFICIENT EVALUATION	160
VII	L DATA	207

LIST OF FIGURES

<u>Figure</u>		<u>Page</u>
1	Outdoor flume detail	5
2	Outdoor flume	6
3	Outdoor flume	6
4	Basin floor elevations.	7
5	Rating curve for 15-foot sharp-crested weir	9
6	Class A basin details	12
7,8	Centerline velocity profile Q = 14.1 cfs Run 1 smooth floor.	15,16
9,10,11,12	Isovels and velocity profiles Q = 14.1 cfs Run 1 smooth floor.	17-20
13,14	Centerline velocity profile Q = 21.5 cfs Run 2 smooth floor.	21,22
15,16,17,18	Isovels and velocity profiles Q = 21.5 cfs Run 2 smooth floor.	24-27
19	Energy, ζ depth, and mean depth Q = 14.1 cfs Run 1 smooth floor.	31
20	Energy, ζ depth, and mean depth Q = 21.5 cfs Run 2 smooth floor.	32
21	Smooth floor plain end Run 11 Q = 21.3 cfs	36
22	1" x 4" element plain end Run 12 Q = 14.6 cfs	36
23	2½" x 9" element standard transition Run 26 Q = 14.9 cfs	37
24	2½" x 9" element 45° flare Run 21 Q = 21.7 cfs	37

LIST OF FIGURES - Continued

<u>Figure</u>		<u>Page</u>
25	Roughness pattern and roughness elements.	38
26	Smooth floor plain end Run 29 Q = 23.1 cfs	39
27	2½" x 9" element 45° flare Run 37 Q = 23.2 cfs	39
28	Test program.	40
29-56	Energy line and water surfaces Run 10 through 37	43-46
57	Pitot tube.	47
58-85	Basin plan and cross section Run 10 through 37	49-55
86	Smooth floor 45° flare Run 17 Q = 21.6 cfs	61
87	Smooth floor plain end Run 10 Q = 14.9 cfs	61
88	Definition sketch for R-jump.	67
89	Variation of Y_t/Y_o with F_o for R-jump.	67
90	Study of the consolidated shear force coefficient C_s	68
91	Study of the length L_1 of R-jump	68
92-102	Energy lines and water surfaces Run 40 through 5081,82
103-111	Velocity distribution Run 42 through 50	83-85
112	2½" x 9" element submerged flow Run 43 Q = 23 cfs.	86
113	2½" x 9" element submerged flow Run 43 Q = 23 cfs.	86
114	16 rows of 2½" x 9" elements Run 44 Q = 23.3 cfs.	87

LIST OF FIGURES - Continued

<u>Figure</u>		<u>Page</u>
115	16 rows of 2½" x 9" elements Run 44 Q = 23.3 cfs.	87
116	Definition sketch	93
117	Yaw and pitch probes.	98
118	Yaw probe calibration factor.	100
119	Mean calibration factors.	101
120	Curve for K	103
121	Curve for K ₆	104
122	Pitch probe calibration angle of yaw versus deduced velocity	107
123	Pitch probe calibration angle of yaw versus deduced head	108
124	Measuring grid at the outfall section	110
125	Measuring grid at downstream sections	111
126	Energy and momentum coefficients, outfall section circular approach pipe.	117
127	Energy and momentum coefficients, outfall section rectangular approach pipe	118
128-131	Dimensionless pressure plots circular outfall	120-123
132-134	Dimensionless pressure plots rectangular outfall. . .	124-126
135	Velocity comparison Pitch probe versus yaw probe Pitch probe versus Ott meter.	127
136	Total head comparison Pitch probe versus yaw probe.	128
137	Energy lines Runs 1-φ-P through 12-□-P.	131
138-141	Dimensionless water surface contours and relative velocities Circular outfall.	138-141

LIST OF FIGURES - Continued

<u>Figure</u>		<u>Page</u>
142-147	Dimensionless water surface contours and relative velocities Rectangular outfall	142-147
148	Dimensionless water surface contours.	148
149	Definition sketch for drag coefficient evaluation .	152
150	Centerline profiles for drag coefficient evaluation	156
151	Run 37R Q = 17.3 cfs $\frac{W_2}{W_0} = 4$ 2½" x 9" elements Row 2, 3, 5 & 6	163
152	Run 35R Q = 17.3 cfs $\frac{W_2}{W_0} = 4$ 2½" x 9" elements Row 1, 2, 3, 4, 5, & 6	163
153	Run 34R Q = 12.1 cfs $\frac{W_2}{W_0} = 4$ 2½" x 9" elements Row 1, 2, 3, 4, 5, & 6	166
154	Run 34R Q = 12.1 cfs $\frac{W_2}{W_0} = 4$ 2½" x 9" elements Row 1, 2, 3, 4, 5, & 6	166
155	Run 32R Q = 12.0 cfs $\frac{W_2}{W_0} = 4$ 2½" x 9" elements Row 1, 2, 3, & 4	167
156	Run 32R Q = 12.0 cfs $\frac{W_2}{W_0} = 4$ 2½" x 9" elements Row 1, 2, 3, & 4	167
157	Run 41R Q = 12.3 cfs $\frac{W_2}{W_0} = 8$ 2½" x 9" elements Row 1, 2, 3, 4, 5, & 6	168
158	Run 42R Q = 17.8 cfs $\frac{W_2}{W_0} = 8$ 2½" x 9" elements Row 1, 2, 3, 4, 5, & 6	168
159	Run 21R Q = 11.5 cfs $\frac{W_2}{W_0} = 4$ 1¼" x 9" elements Row 1, 2, 3, 4, 5, & 6	169
160	Run 55R Q = 10.8 cfs $\frac{W_2}{W_0} = 8$ 1¼" x 9" elements Row 1, 2, 3, & 4	169

LIST OF FIGURES - Continued

<u>Figure</u>		<u>Page</u>
161-164	Coefficients of drag for roughness elements Rectangular approach pipe	170-171
165-171	Coefficients of drag for roughness elements Circular approach pipe.	172-174
172-177	Centerline velocity profiles Isovels Transverse velocity profiles.	181-185
178	Description sketch Jet diffusion	188
179	Distribution of centerline velocity for flow from orifice	190
180	Distribution of centerline velocity for flow from submerged outlets	191
181	Distribution of volume and energy flux downstream from orifice	196
182	Distribution of momentum flux downstream from orifice.	198
183	Distribution of longitudinal velocity in zone of establishment of flow	200
184	Distribution of longitudinal velocity in zone of established flow.	200
185	A comparison of jet widths, predicted versus measured, at height $\frac{D_o}{2}$	201
186	Class A basin	206
187	Dimensionless water surface contours and relative velocities Class A basin	209
188	Class B basin	212
189	Dimensionless water surface contours and relative velocities Class B basin.	216
190	General relations for F_1 , Q , β , y_2/y_1 , F_2	218

LIST OF FIGURES - Continued

<u>Figure</u>		<u>Page</u>
191	Definition sketch for backwater computations Class B basin	220
192	Class C basin	223
193	Definition sketch Trajectory equations.	228

Chapter I

INTRODUCTION

Scour at the outlet of conduits is a familiar problem to hydraulic and highway engineers. Among the possible results are untidy scour holes, excessive deposition of scoured material downstream, and occasional structural collapse resulting from foundation removal.

Traditionally, an energy dissipating basin such as the St. Anthony Falls basin (1), Bureau of Reclamation stilling basin (2), the New South Wales jump basin (3), or some other basin which has previously proven satisfactory has been placed at the outlet of large structures with high efflux velocity. For small diameter conduits which flow infrequently and at moderate velocities (4 to 8 fps), the various agencies have usually treated scour as a maintenance problem. If serious erosion occurred, the hole would be filled with broken concrete or large rock, reliance being placed on the judgment of the local foreman rather than on specific design criteria.

Numerous publications by government agencies, such as "Shore Protection Planning and Design," Corps of Engineers (4), "Riprap Requirements for Overflow Embankments," Corps of Engineers (5), and "Bank and Shore Protection," California Division of Highways (6), suggest design criteria. The usual form is a chart of rock diameter versus mean velocity or near bed velocity with empirical multiplying factors where flow is likely to impinge on the surface such as on the banks of bends.

The use of formulas or design charts based on uniform mean flow conditions for three dimensional, highly turbulent, non-uniform,

plunging flow found at culvert outlets is questionable. For this reason, the State Highway Commission of Wyoming, in conjunction with the Bureau of Public Roads, inaugurated a basic research program aimed at producing suitable design criteria for local scour with particular emphasis placed on culvert outlets.

The problems to be investigated were formulated by the staff of the State Highway Commission of Wyoming in consultation with personnel of Colorado State University and the Bureau of Public Roads. The project was initiated by the signing of the agreement "Engineering Investigations Pertaining to Flow Protection of Bridges and Culverts," dated February 16, 1966.

The project was subdivided into three phases:

Phase I Channel stabilization in the vicinity of and downstream of culvert outlets.

Phase II Channel stabilization in the vicinity of and downstream of bridges.

Phase III Investigation of the use of special materials and techniques to develop economical methods of stabilizing channels where there is no gravel or rock available and where special problems require the use of other materials and methods of stabilization.

The supporting agency showed little interest in rigid boundary basins. The bulk of the work was to be directed at obtaining a satisfactory design procedure for riprapped basins. However, it was presumed that flow characteristics of rigid boundary dissipating basins would have to be evaluated before attempting study of the more complex erodible basins.

This dissertation presents results of preliminary studies and experimental investigations of the hydraulic characteristics of non-erodible basins. The objectives are as follows:

1. Define and discuss common regimes of flow that occur under various operating conditions.
2. Present pertinent information from previous well-documented research studies that relate directly to the basin problems and show how the results of these studies are applicable.
3. Where deficiencies exist in available information, introduce experimentally or analytically obtained results to bridge the gap.
4. Report new information concerning losses of energy near conduit outlets where concentrated flow is allowed to plunge and expand.
5. Present new information concerning the pressure and velocity distribution at the conduit outlet section.
6. Present new information defining surface contours of an expanding free jet. This information is necessary for the design of basins where walls are not used for confining the expanding jet.
7. Utilize flow measurements for the purpose of deducing drag coefficients for roughness elements of known dimensions and ultimately apply this information for design purposes.
8. Present experimental findings concerning the properties of an expanding jet discharging into a high tailwater basin where the jet is bounded on the top by a free surface and on the bottom by a rough rigid boundary. A comparison is made between the properties displayed by the culvert basin and those of a three-dimensional jet dispersing in an infinite basin.

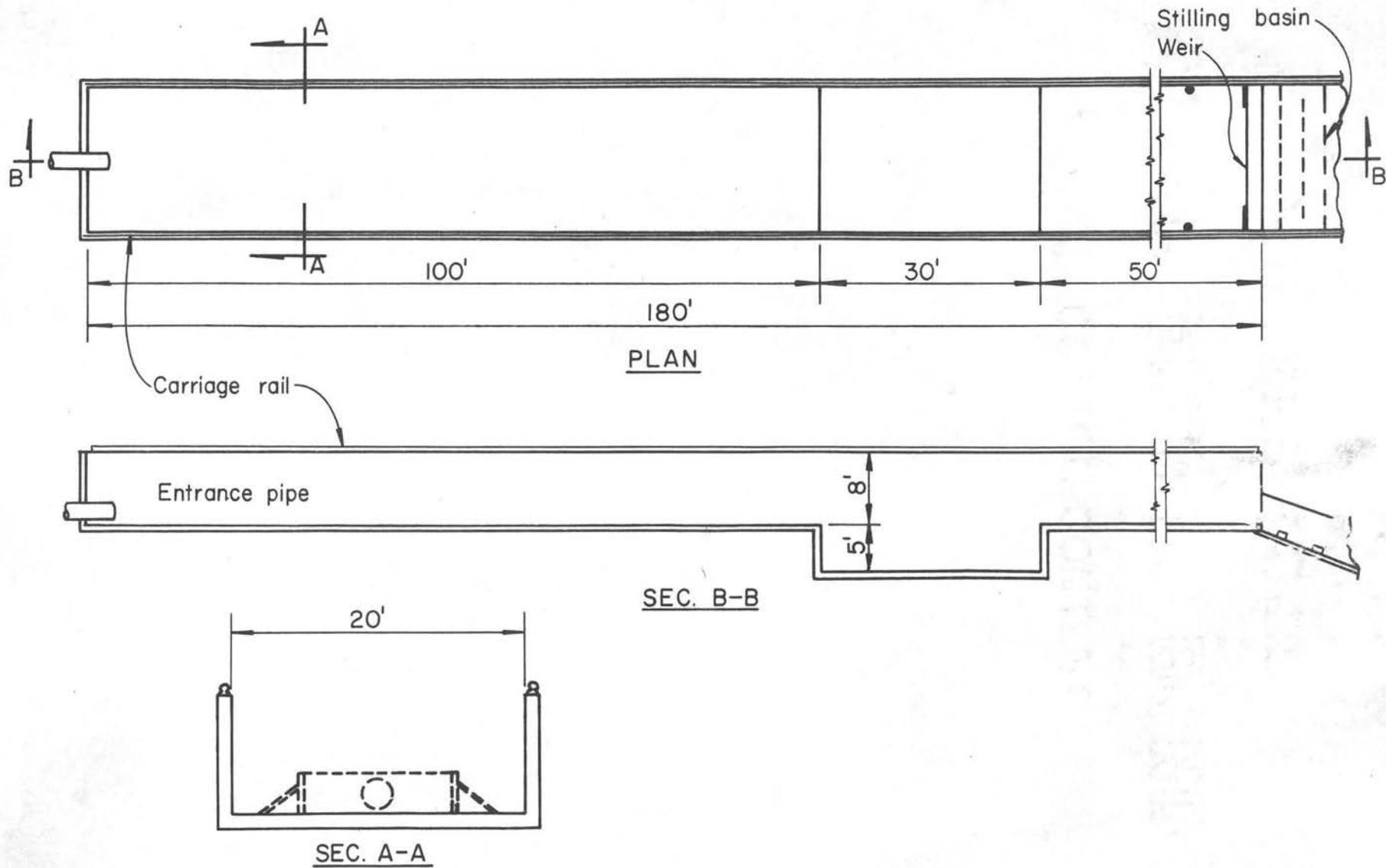
9. Integrate the various relationships (some already available, others developed during this study) into a logical design procedure.

Flume Details

All experimental work described in this paper was conducted in an outdoor, reinforced concrete flume 185 feet long, 20 feet wide, and 8 feet deep (with a 5 foot deep recessed center portion for future test programs), constructed on the site of the Colorado State University (CSU) Outdoor Hydraulics Laboratory. The flume was equipped with a movable, overhead personnel and instrument carriage which spanned from wall to wall. The carriage was mounted on crane rails carefully placed to grade, ($\pm 1/16''$), on top of the flume walls. A sketch of the flume is shown in Fig. 1, and photographs of the flume and carriage are shown in Fig. 2 and Fig. 3. Only the upstream 100 feet of the flume were used for this test program.

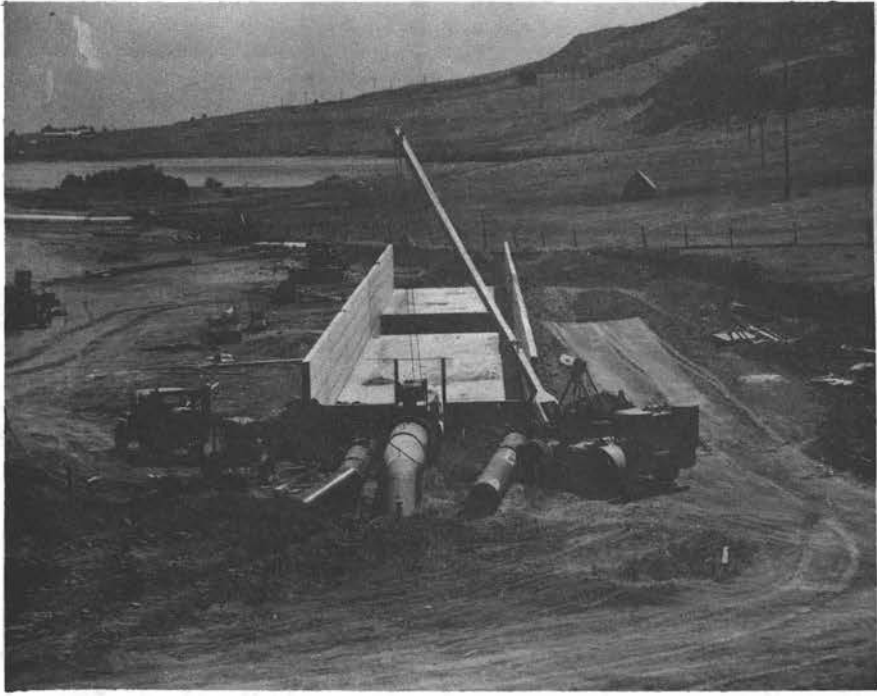
The floor of the flume was hand-finished concrete with a horizontal surface. At one section, finishing techniques led to a deviation from horizontal of three-eighths of an inch. Relative elevations of the floor surface as determined by conventional leveling techniques are shown in Fig. 4.

For all phases of testing, the water was recirculated. Water in College Lake was pumped through a 24 in. circular pipe to the upper end of the flume, then flowed from the flume down a natural channel back to the lake. The pump was capable of delivering from 20 to 27 cfs at the entrance of the flume, depending on the surface elevation of College Lake. A variable-speed, single-stage, deep-well turbine pump was used.



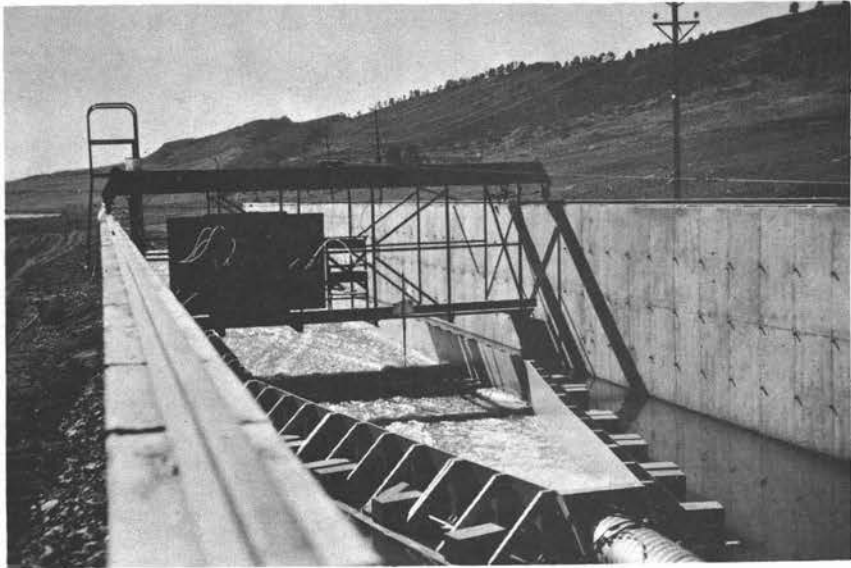
Outdoor Flume Detail

Fig. 1



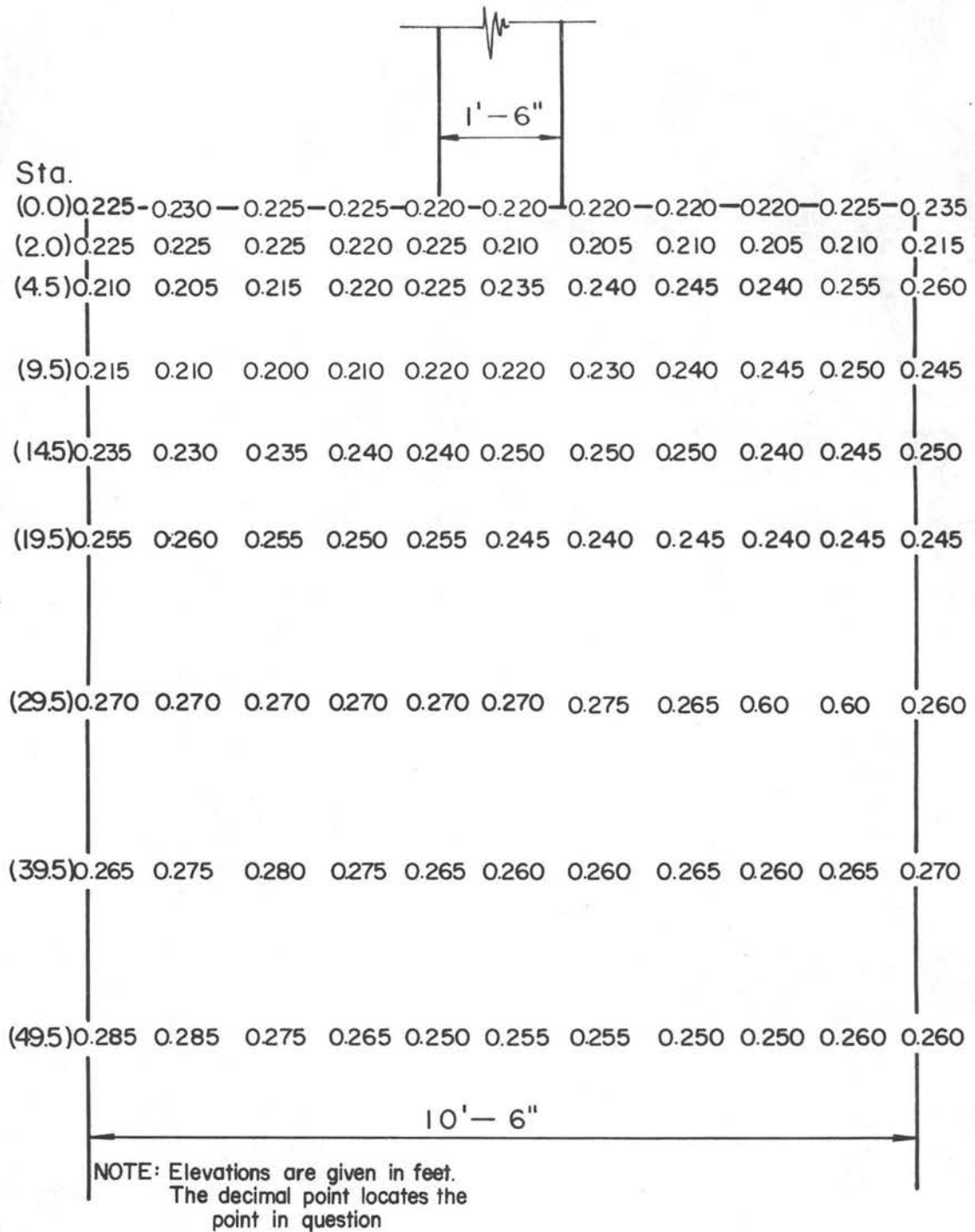
Outdoor Flume

Fig. 2



Outdoor Flume

Fig. 3



Basin Floor Elevations
Plan View

Fig. 4

Discharge (Q) was measured in two different ways. In some cases, Q was obtained by integrating the velocity data taken at each cross section. For other situations, a rectangular, sharp-crested weir installed at the lower end of the flume was used. Calibration of the weir was accomplished by volumetric, dye dilution, and current meter techniques. Weir dimensions, calibration points and rating curves are shown in Fig. 5.

Basin Classification

The energy dissipation basins discussed in this paper are classified as follows:

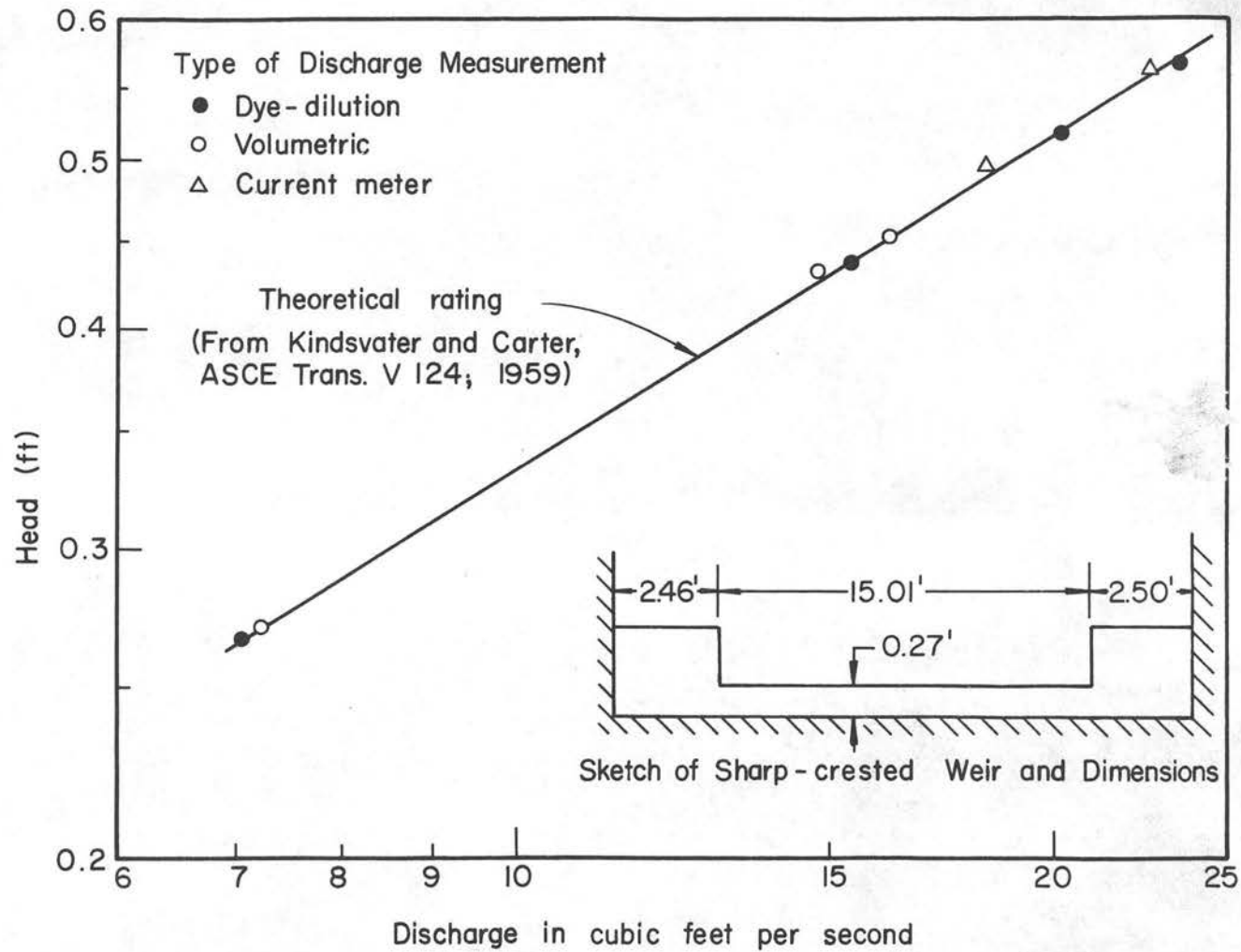
Class A - A basin with a smooth floor and vertical walls which flare from the culvert outlet to a long rectangular basin. The flare angle is maintained sufficiently small so that the flow occupies the entire section.

Class B - A rectangular basin with vertical walls and a smooth floor, directly downstream of the culvert outlet. Essentially, the culvert walls terminate abruptly and the channel floor continues at the same slope.

Class C - A Class B basin with roughness elements attached to the floor. The elements are particular size and are placed in an appropriate pattern. The purpose of the elements is to disrupt the high-speed expanding jet downstream of the culvert outlet.

Experimental Program

The various studies are presented in chronological order. Three series of preliminary tests of rigid boundary basins with smooth and artificially roughened floors are described in Chapter II. The purpose



Rating Curve for 15 Foot Sharp-Crested Weir

Fig. 5

of the tests was to compile a large quantity of information concerning the basin characteristics. The flow field and geometry displayed by the various basins was then examined, and, where aspects of the flow were hydraulically similar, comparison was made between observed basin characteristics and those estimated from existing hydraulic criteria. A major purpose of these tests was to delineate areas where additional information was needed prior to establishing a general, systematic design procedure.

The additional studies which were considered essential are described in Chapters III through VI. In the concluding chapter, the relationships derived from the CSU studies (from this point on, "CSU study" will refer to the research and analysis conducted for this current project as opposed to the work described in numerous references that will be cited), in addition to existing hydraulic design criteria, are integrated into a systematic design procedure. A number of example basins are analyzed in the concluding chapter.

Chapter II

PRELIMINARY TESTS

Preliminary Tests A - Class A Basin

The purposes of preliminary tests A were to check the suitability of the Blaisdell (7) criterion for basin wall divergence downstream of circular approach pipes, to examine the flow fields and energy losses in Class A basins, and to evaluate the necessity of detailed velocity measurements for energy computation.

Basin Geometry

A smooth floor basin with vertical walls flaring 1:4 from the pipe outlet to a rectangular basin 10' 9" wide was constructed downstream of an 18" hel-cor pipe.

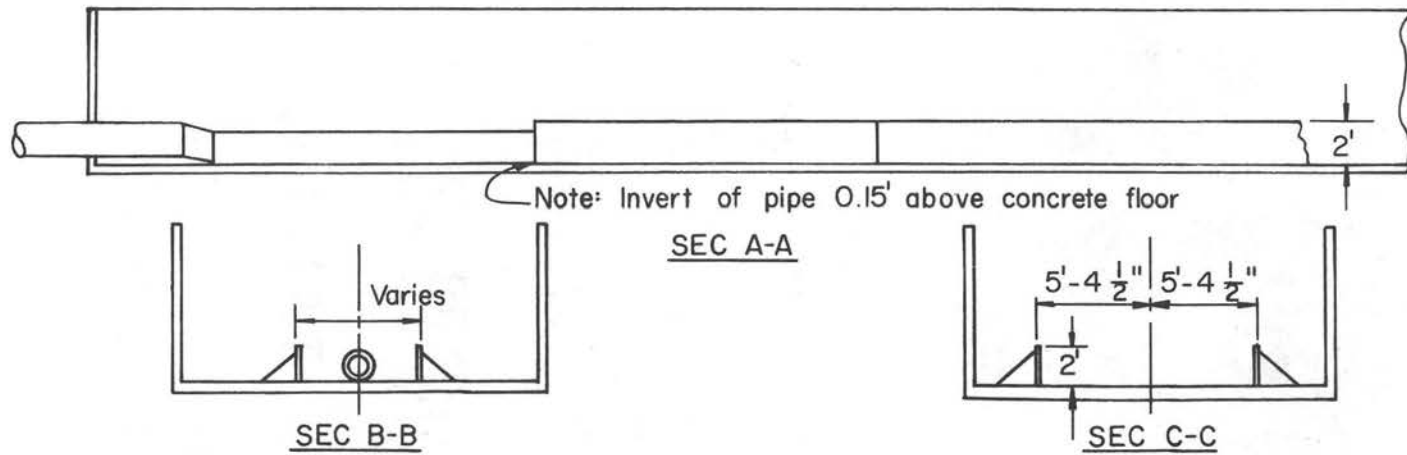
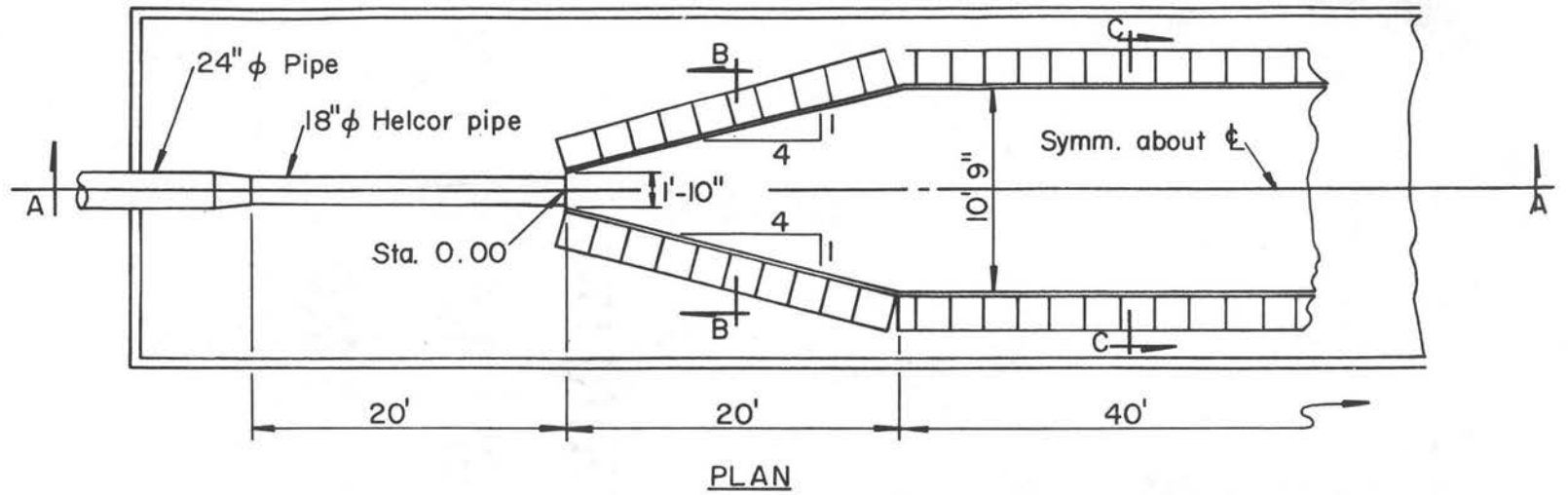
The criterion suggested by Blaisdell (7),

$$u = 3F_0 \quad (2-1)$$

was used to establish the flare of the walls. The length u is the longitudinal distance per transverse unit of divergence along a wall, and $F_0 = \frac{V_0}{\sqrt{gy_0}}$. For this test, V_0 was assumed to be the average exit velocity from the pipe for the maximum discharge to be tested, y_0 was assumed to be the depth of flow at the exit of the pipe, and g is the acceleration due to gravity. The general plan of the basin and significant dimensions are shown in Fig. 6. Figure 3 is a photograph showing the basin.

Method of Analysis

The major interest of this study was the dissipation of energy as the flow moved downstream from the culvert outlet. For the



Class A Basin Details

Fig. 6

preliminary runs, sufficient data were obtained to precisely define the specific energy E . E was computed by two methods.

$$(i) \quad E = (Q/A)^2/2g + y \quad , \quad (2-2)$$

where Q is the total discharge passing through a section, A is the area of the wetted section, and y is the average depth of flow

$$(ii) \quad E = \frac{\sum \left[\left(\frac{q_i}{a_i} \right)^2 / 2g + y_i \right]}{n} \quad (2-3)$$

where q_i is the discharge passing through a vertical strip, a_i is the area of the vertical strip, y_i the mean depth of the vertical strip, and n is the number of vertical strips in the complete section. The width of the vertical strips was arbitrarily set at 0.50 ft for Sta. 0.0 through Sta. 14.5, and at 1.00 ft for the remaining stations. A velocity traverse was necessary at the centerline of each of these strips. The computation method was devised so that the effect of the velocity distribution (both transverse and vertical) could be determined. No attempt was made to evaluate the direction of flow and include all velocity components in the analysis.

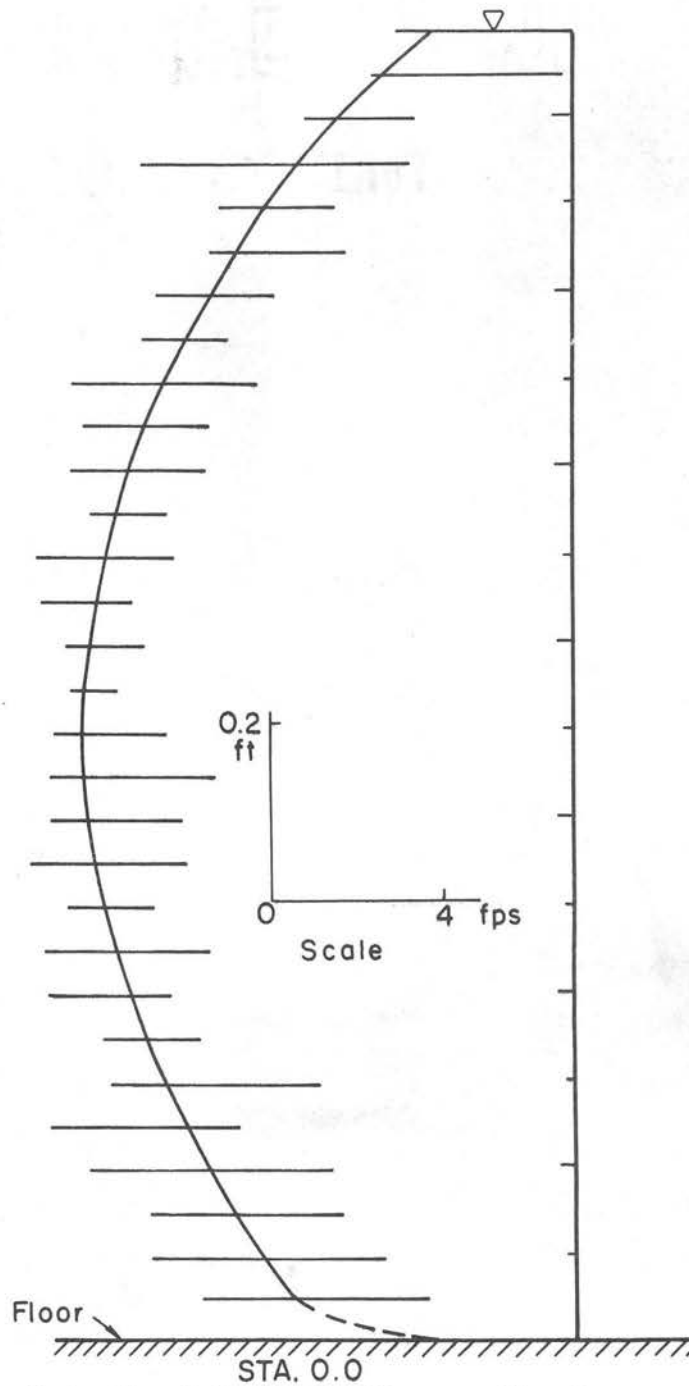
Two discharges, $Q = 14.1$ cfs and $Q = 21.5$ cfs, were examined. In order to check duplicability of the data, the water surface profiles for the 14.1 cfs discharge were measured twice. The pump was set for a given discharge and a complete run was made. Subsequently, the same discharge was established and water surface profiles were measured again. Agreement between data from the two runs was good, as illustrated by the fit of the triangular and circular points shown on the isovel plots, Fig. 9 through Fig. 12 (figures to be discussed in a later section).

Apparatus for Measuring Velocities

A system comprised of a pitot-static tube in series with a differential pressure transducer, square root circuit, and an x-y plotter was built. Output from the system was a direct plot of velocity versus height above the floor. The flume arrangement precluded the possibility of positioning the transducer below the level of the static-pitot inlets. This resulted in an induced negative head between the pitot and the transducer. A manifold bleedout device was constructed so that when in position for measurement, both sides of the pitot could be thoroughly flushed with water prior to each traverse, ridding the connecting tubes of any accumulation of air which might have come out of solution while under negative head. The arrangement was not totally satisfactory, for reasons which will be explained later.

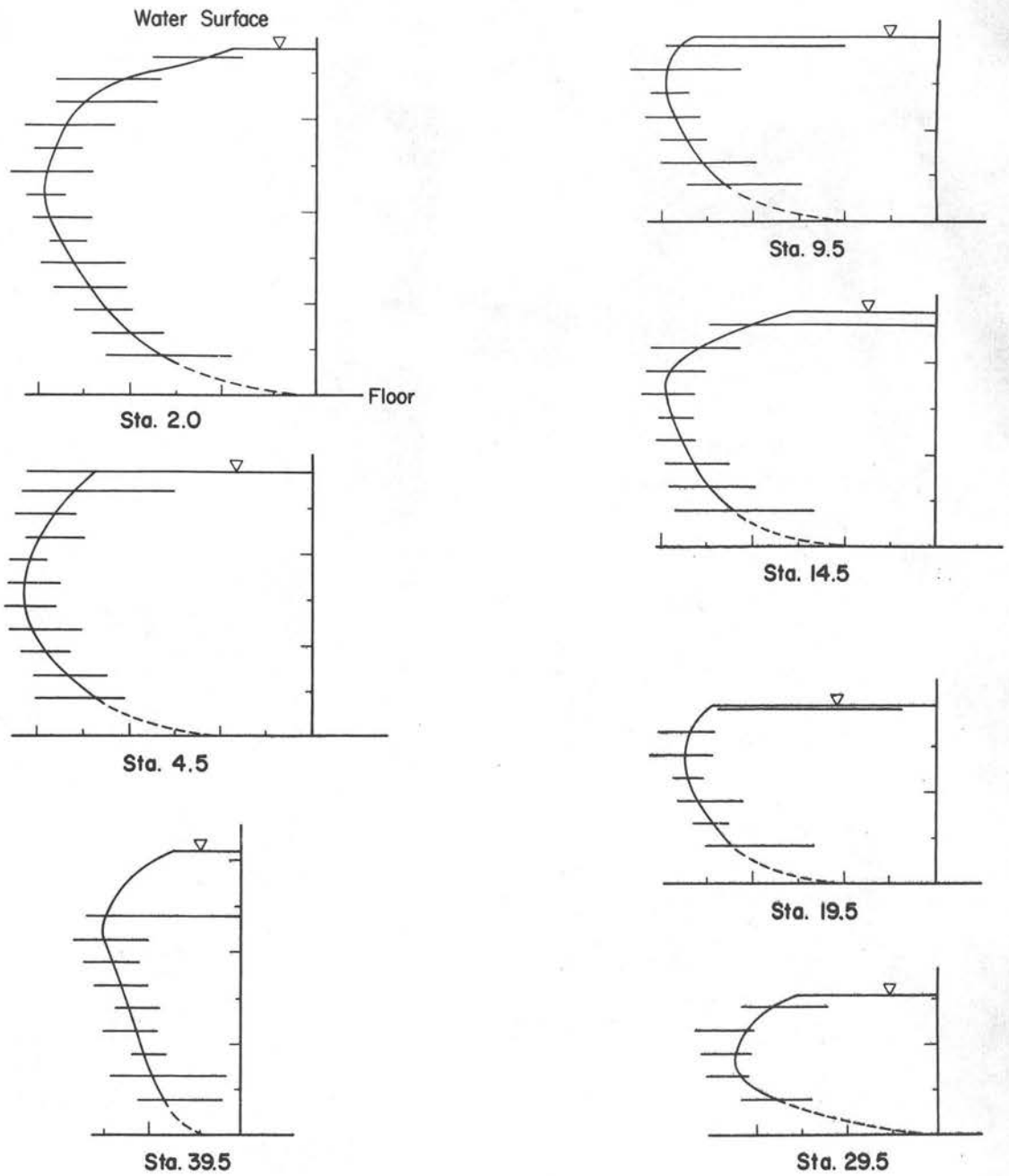
Typical output from the system is shown in Figs. 7, 8, 13, and 14. The horizontal slash lines indicate the maximum sweep of the pen during the traversing operation. Since a plus or minus deviation from the mean velocity was equally probable, the mean velocity profile was sketched in by eye.

No attempt was made to align the pitot-static tube along the stream filament. All velocities were measured with the axis of the tube parallel to the centerline of the channel and on a plane parallel to the floor surface. According to information presented in Ref. 8, the pitot-static tube is capable of measuring velocity within ± 2 percent if the yaw angle does not exceed 15 degrees. This condition was met at all times with the exception of Sta. 2.0 and, in some instances, Sta. 4.5, where the simultaneous plunging of the water and lateral spreading may have led to a yaw angle in excess of 15 degrees.



Centerline Velocity Profile
Q = 14.1 cfs
Run 1 Smooth Floor

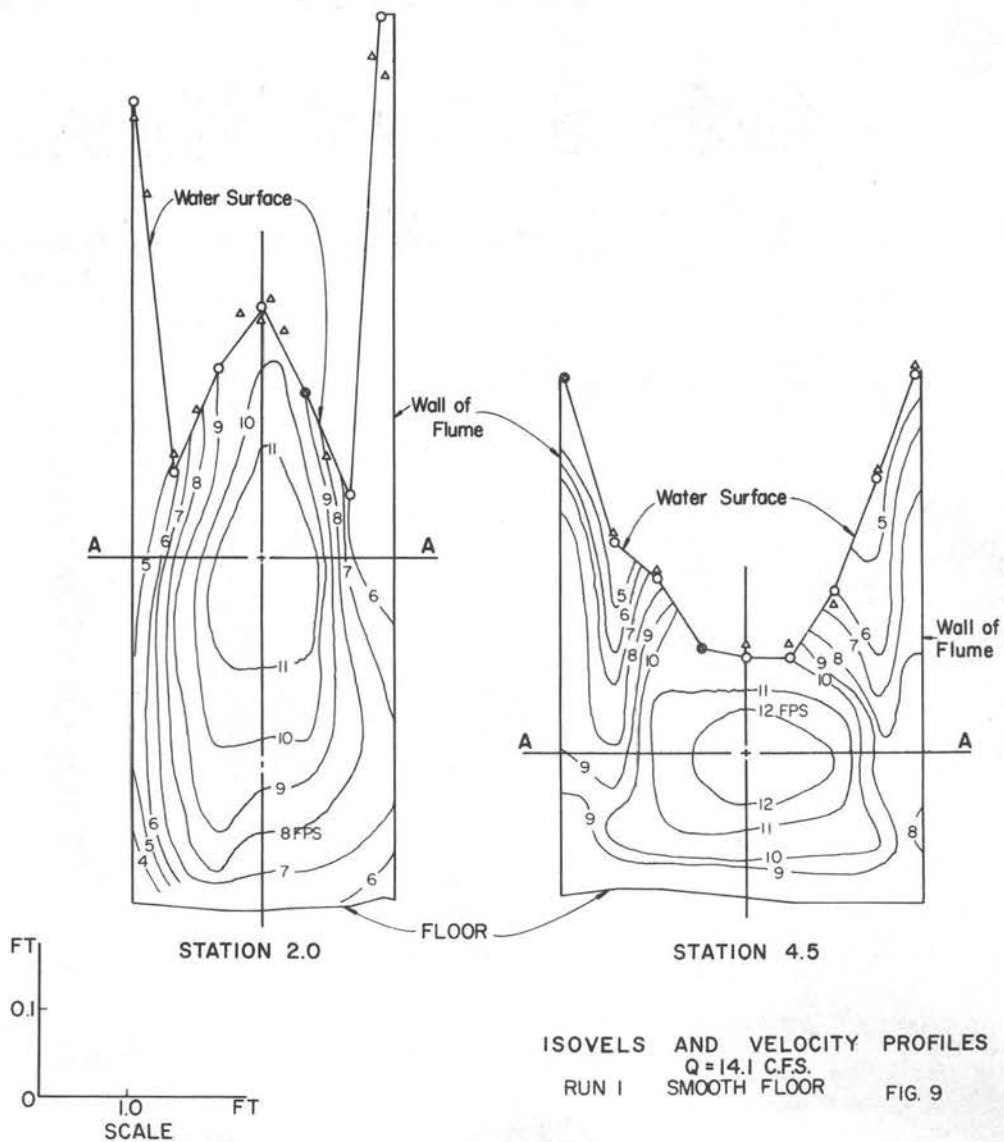
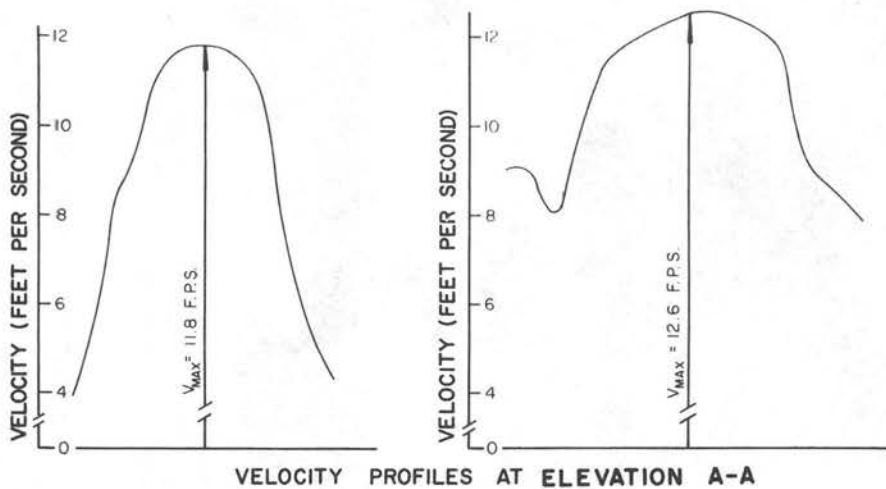
Fig. 7

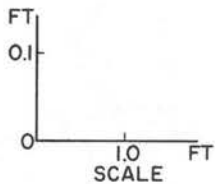
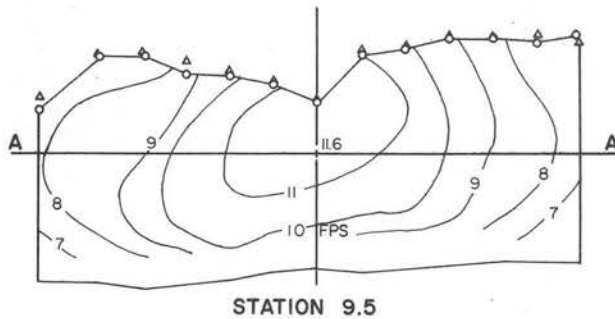
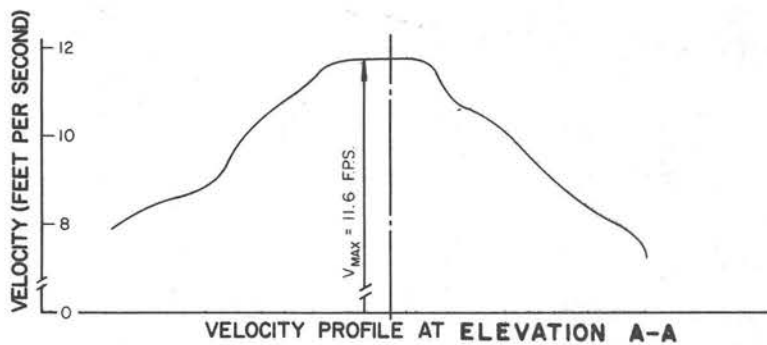
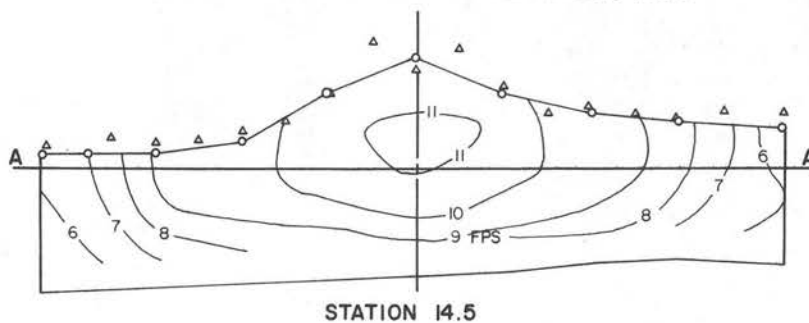
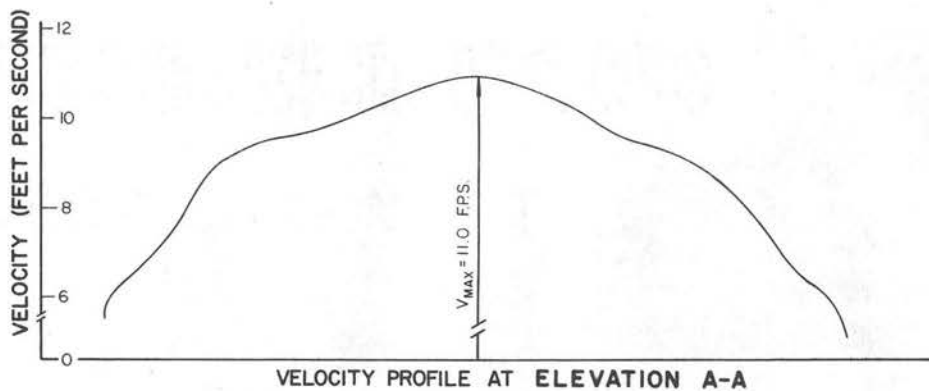


Centerline velocity profile
 $Q = 14.1 \text{ c.f.s.}$
 Run I Smooth floor

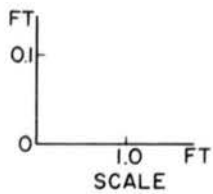
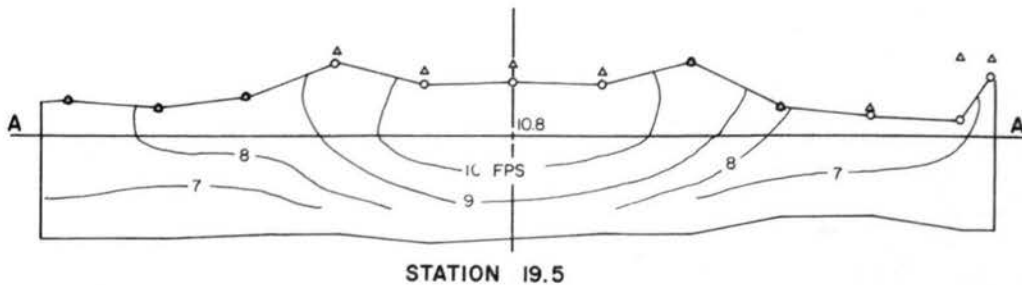
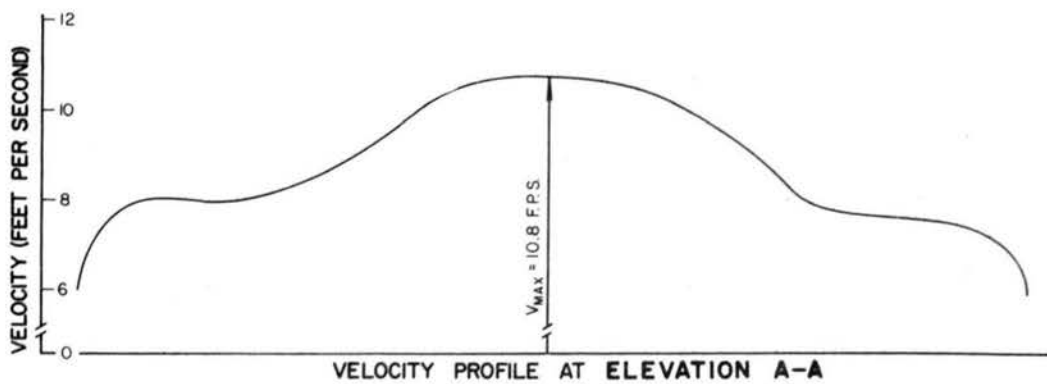
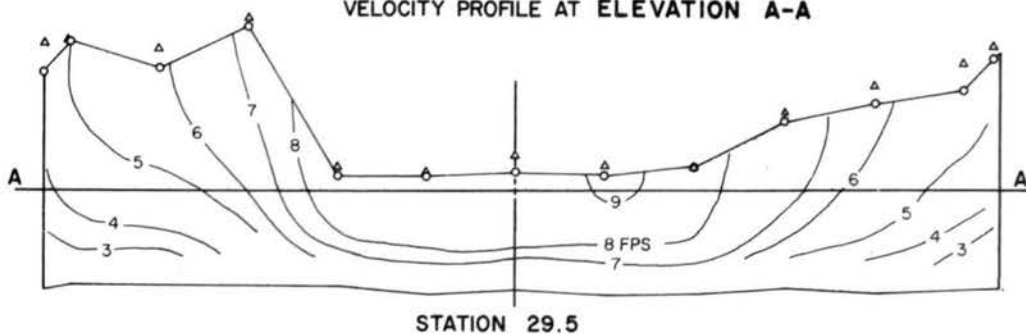
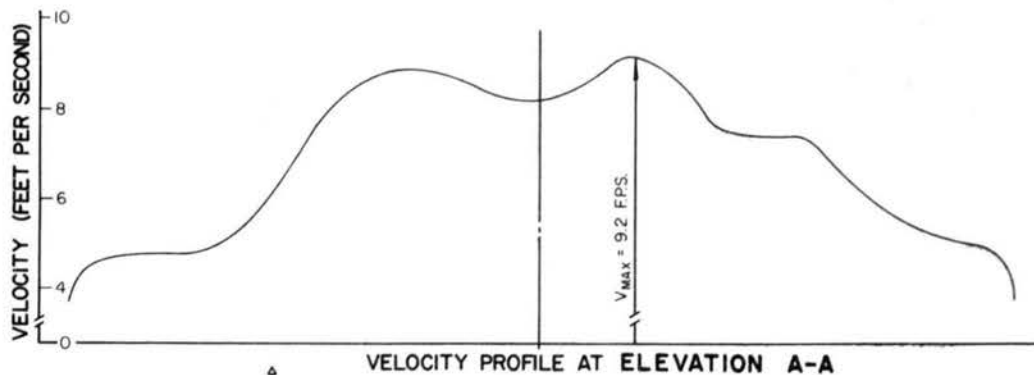
FT
 0.1
 4 FPS
 SCALE

FIG. 8

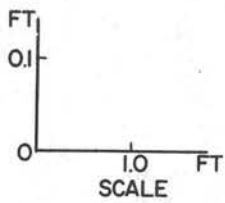
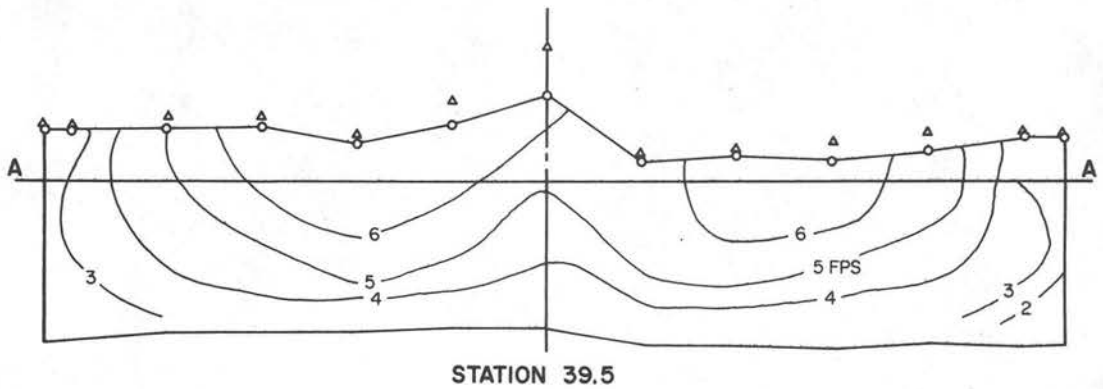
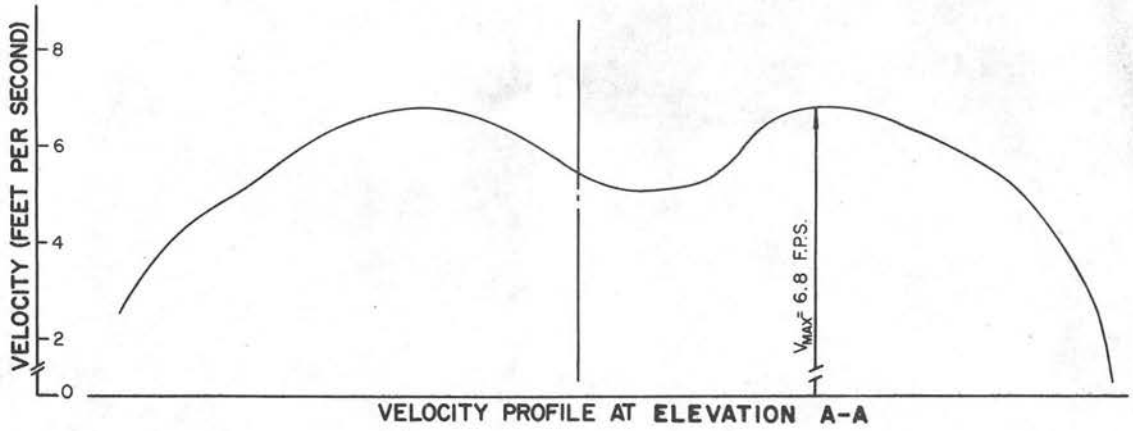




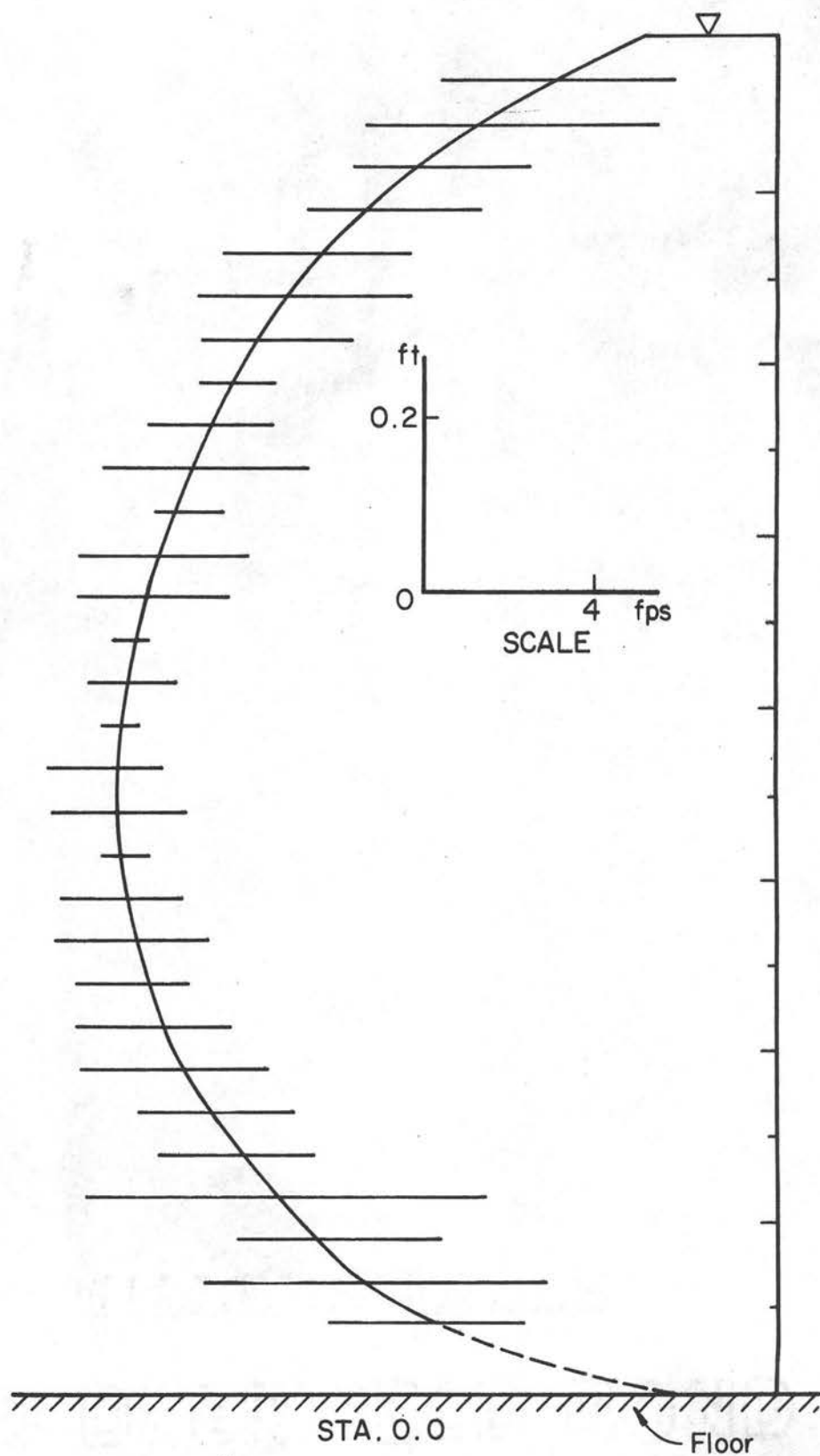
ISOVELS AND VELOCITY PROFILES
 Q = 14.1 C.F.S.
 RUN I SMOOTH FLOOR FIG. 10



ISOVELS AND VELOCITY PROFILES
 $Q = 14.1$ CFS.
 RUN I SMOOTH FLOOR FIG. II

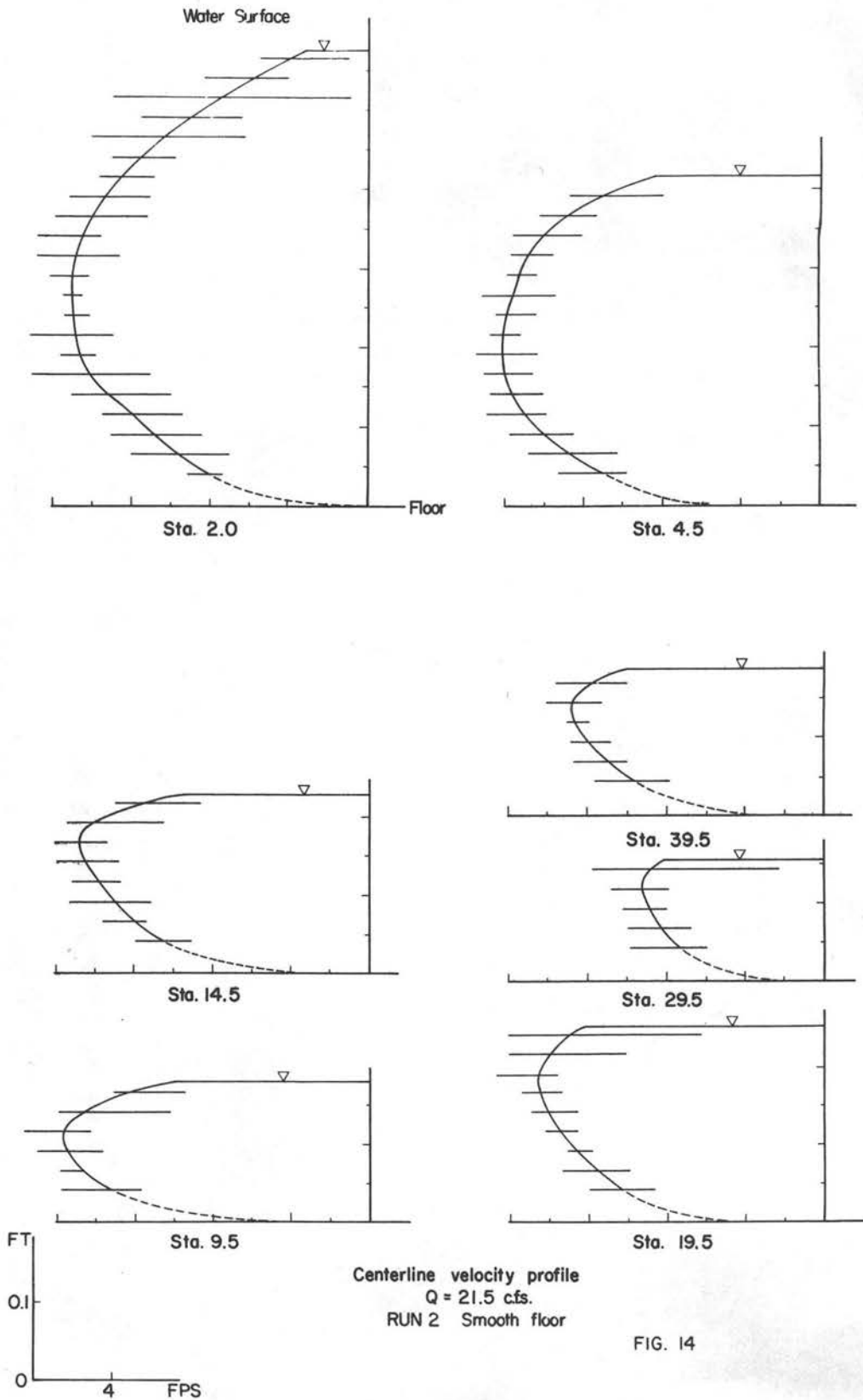


ISOVELS AND VELOCITY PROFILE
 $Q = 14.1 \text{ C.F.S.}$
 RUN I SMOOTH FLOOR FIG. 12



Centerline Velocity Profile
Q = 21.5 cfs
Run 2 Smooth Floor

Fig. 13



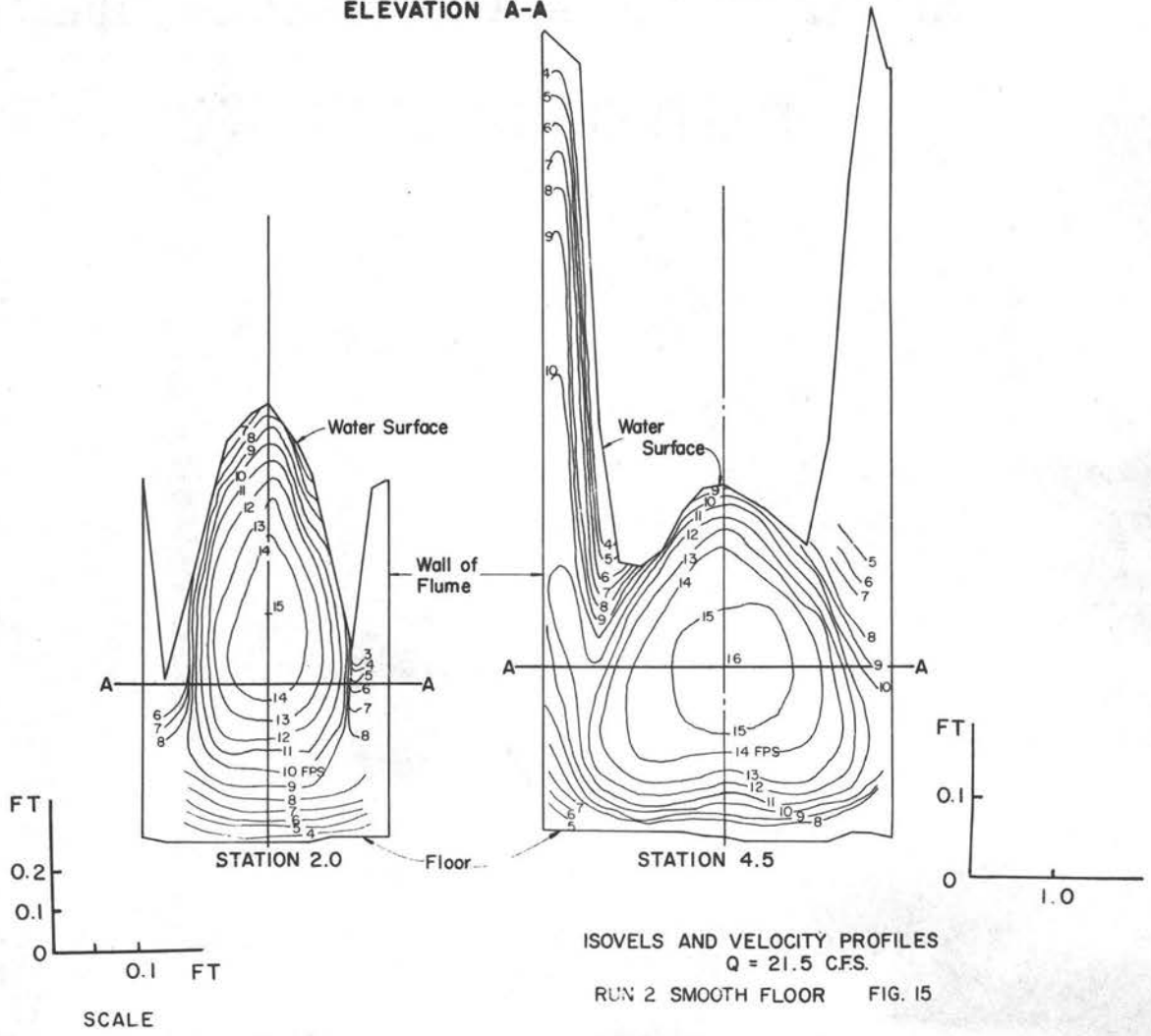
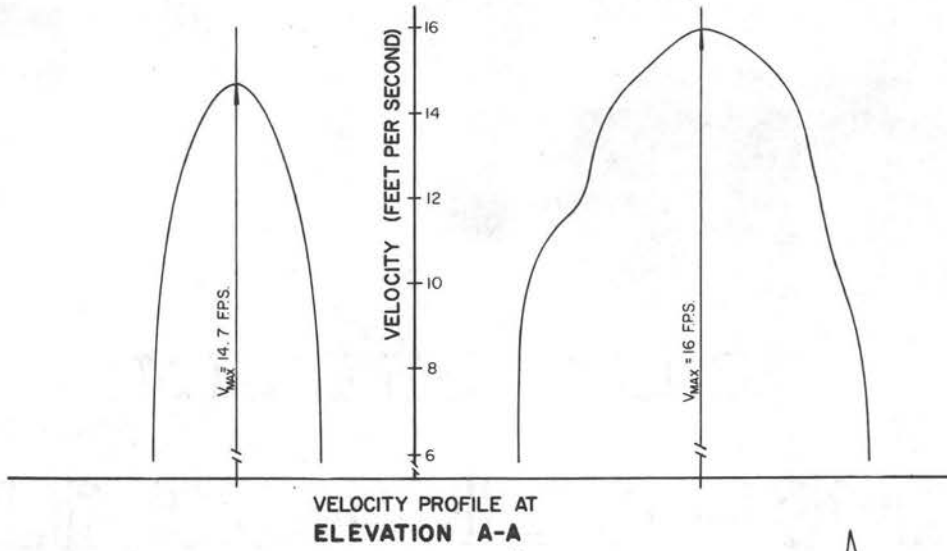
Data Obtained

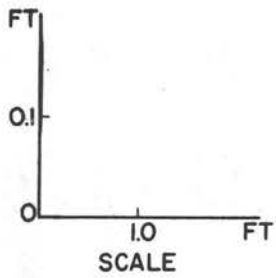
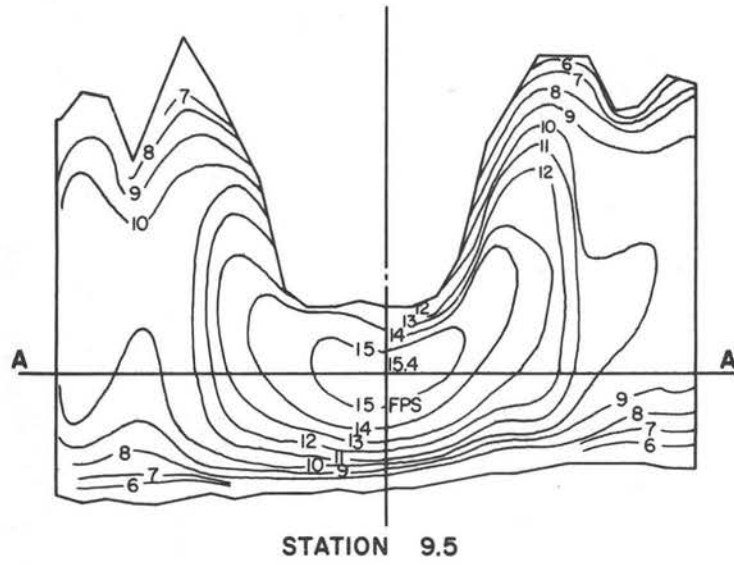
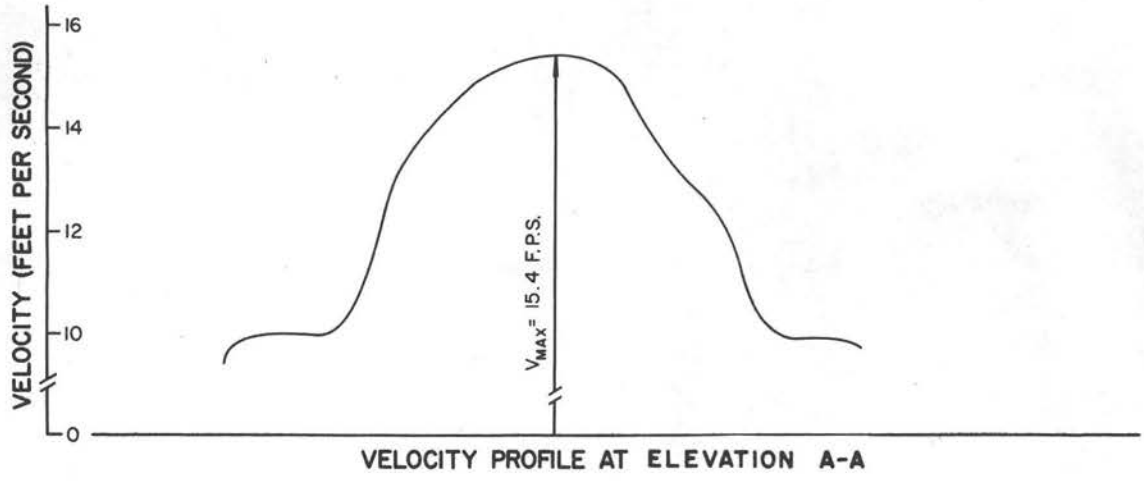
Data were collected at the following cross sections: the outlet of the pipe, Sta. 0.0 (centerline traverse only), Sta. 2.0, Sta. 4.5, Sta. 9.5, Sta. 15.5, Sta. 19.5, and Sta. 39.5. Throughout this paper, the station number corresponds to the distance in feet between the pipe outlet and the section in question. The voluminous amount of data collected precludes its publication; however, it is available to interested parties.

Figures 7 and 8 show the vertical velocity traverse obtained at the centerline of each section for a discharge of 14.1 cfs. The fluctuations of velocity (the magnitude is indicated by the span of the horizontal slash lines) are due to turbulence and transducer response to vibrations induced by drag forces on the probe submerged in the flow. Figures 9 through 12 are isovels constructed from the velocity traverses. Figures 13 and 14 show the vertical velocity traverse obtained for a discharge of 21.5 cfs; Figs. 15 through 18 are isovels constructed from these data.

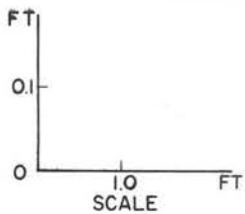
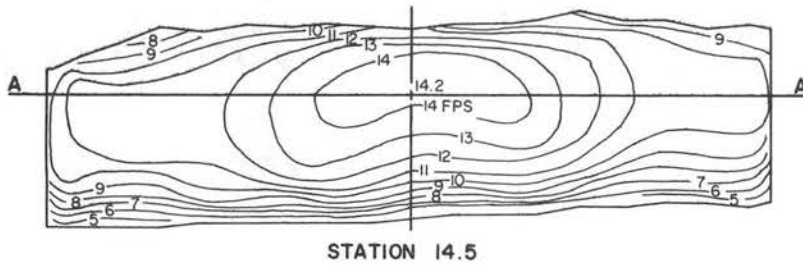
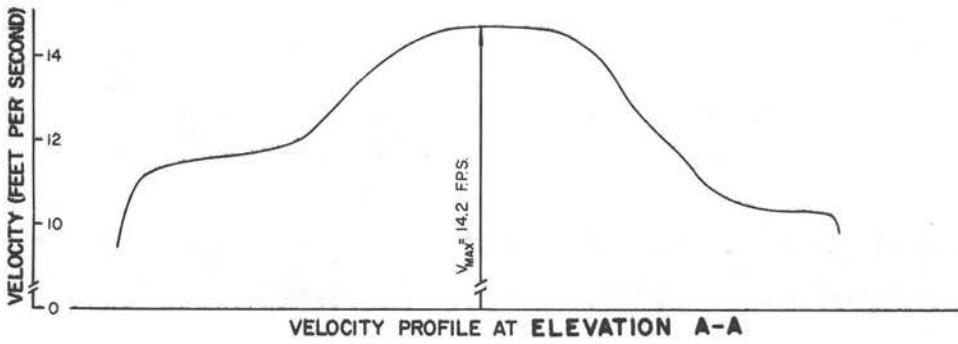
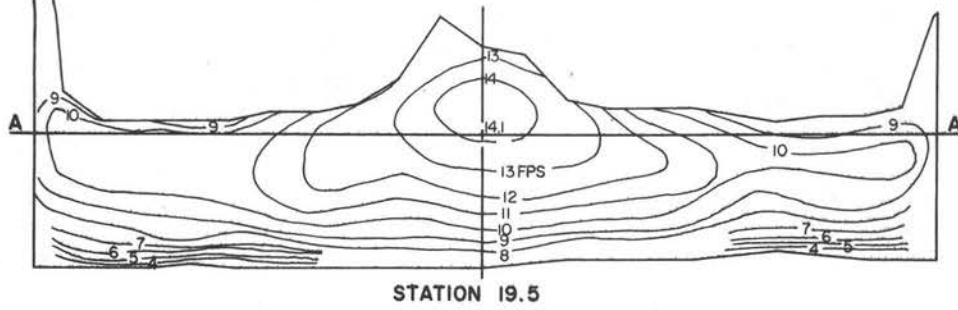
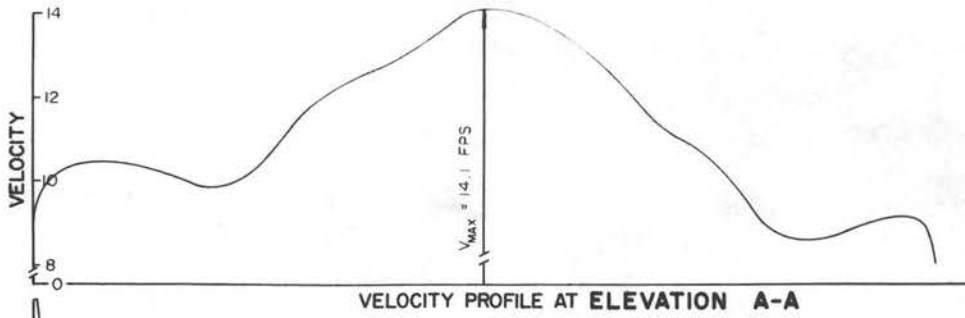
Analysis

The discharges passing through each section were obtained by a graphical integration procedure. Each strip of area, associated with a vertical velocity profile, was subdivided into incremental areas 0.5 ft high by 0.5 or 1.0 ft wide. The velocity passing through the centroid of the area was then scaled from the velocity traverse, and the product of the velocity and area was found. These products, for the entire section, were then summed to obtain the discharge.



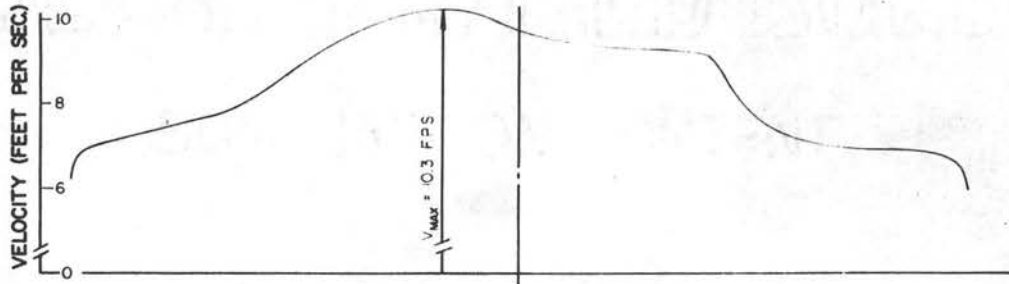


ISOVELS AND VELOCITY PROFILE
 $Q = 21.5 \text{ C.F.S.}$
 RUN 2 SMOOTH FLOOR FIG. 16

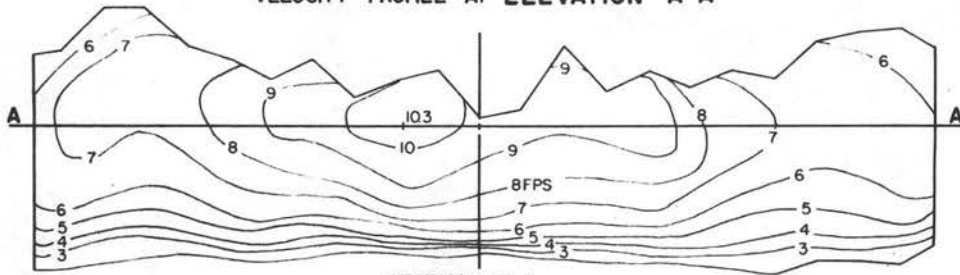


ISOVELS AND VELOCITY PROFILE
Q = 21.5 CFS.

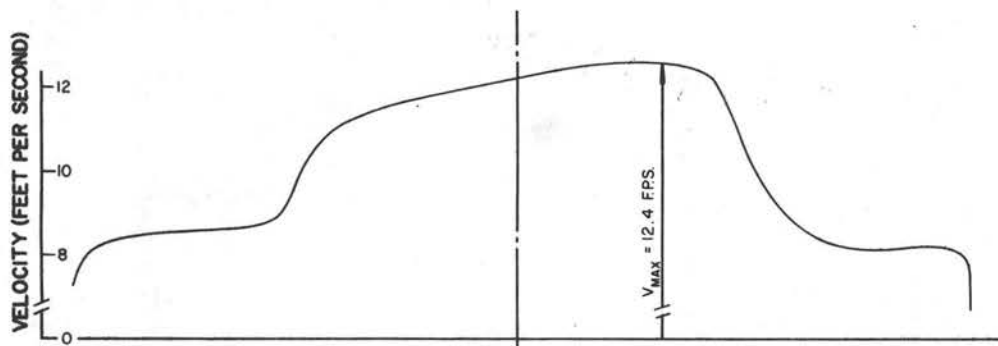
RUN 2 SMOOTH FLOOR FIG. 17



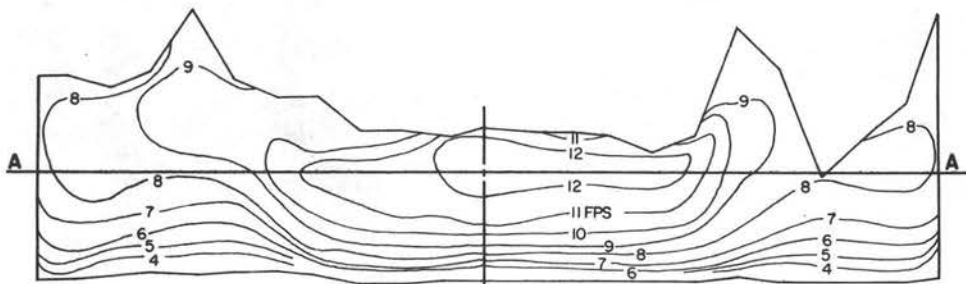
VELOCITY PROFILE AT ELEVATION A-A



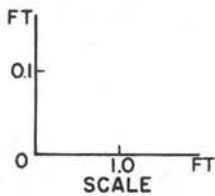
STATION 39.5



VELOCITY PROFILE AT ELEVATION A-A



STATION 29.5



ISOVELS AND VELOCITY PROFILES
 Q = 21.5 C.F.S.
 RUN2 SMOOTH FLOOR FIG. 18

As a check on the consistency of the data, a comparison was made between the discharges at each cross section. This information is shown in Table I.

For both runs (particularly for $Q = 14.1$ cfs), it is obvious that the discharges obtained at Sta. 29.5 and Sta. 39.5 are too low. Several weeks were spent rechecking measurements, replacing valves, and recalibrating equipment. During this time, several partial runs were completed with similar results. It was deduced that the negative head between the differential transducer and the pitot was the source of the trouble. It did not appear practical to place the differential transducer below the pitot as this would necessitate building a false floor in the bottom of the flume with a trench along one side. Subsequent investigation of the energy line characteristics indicated that the traversing procedure was not necessary, at least in the zone of gradually varied flow, Sta. 9.5 and beyond.

Despite the discrepancy in integrated discharge, the overall isovel pattern seemed consistent and usable. To obtain a reasonable comparison of energy level from section to section, an average of four integrated discharges, discarding the three lowest values, was used as the discharge, Q average, for a given run. For computational purposes, each point velocity was adjusted by multiplying it by a ratio of " Q average" over " Q integrated" for that section, so that the adjusted discharges passing each section would be equal. This adjustment was used for computation only; the velocity traverses and isovels presented are measured values.

Initially, 25 vertical velocity traverses were selected, and the corrective coefficient for non-uniform velocity (Ref. 9)

TABLE I - FLOW PARAMETERS - PRELIMINARY TESTS A

Run No.	Sta.	Q integrated cfs	Q average cfs	D _o pipe dia. ft	W ₂ basin width ft	V _Q fps	y _o ft	F _o = $\frac{V_o}{\sqrt{gy_o}}$	$\frac{Q}{D_o^{5/2}}$
1	0.0	-	14.1	1.50	10.75	8.0	1.50	1.15	5.1
	2.0	15.1							
	4.5	14.5							
	9.5	13.4							
	14.5	12.3							
	19.5	13.1							
	29.5	11.5							
	39.5	9.6							
2	0.0	-	21.5	1.50	10.75	12.2	1.50	1.76	7.8
	2.0	22.1							
	4.5	21.3							
	9.5	21.1							
	14.5	21.6							
	19.5	21.1							
	29.5	19.5							
	39.5	18.7							

$$\alpha_1 = \frac{\sum v_i^3 \Delta A_i}{V^3 A} \quad (2-4)$$

was computed. v_i is the mean velocity of a vertical increment of 0.05 ft of a velocity traverse, ΔA_i is the incremental area, $A = \sum \Delta A_i$ of a vertical strip and $V = \frac{\sum v_i \Delta A_i}{A}$. Values of α ranged from 1.03 to 1.12, consistent with values for concrete lined canals obtained at Colorado State University during an earlier study, Ref. 10. Since the variation was minor, the value of α was assumed to be one for all verticals.

The next step was to compute the specific energy at each section in two different ways:

$$E = \frac{(Q/A)^2}{2g} + y \quad (2-2)$$

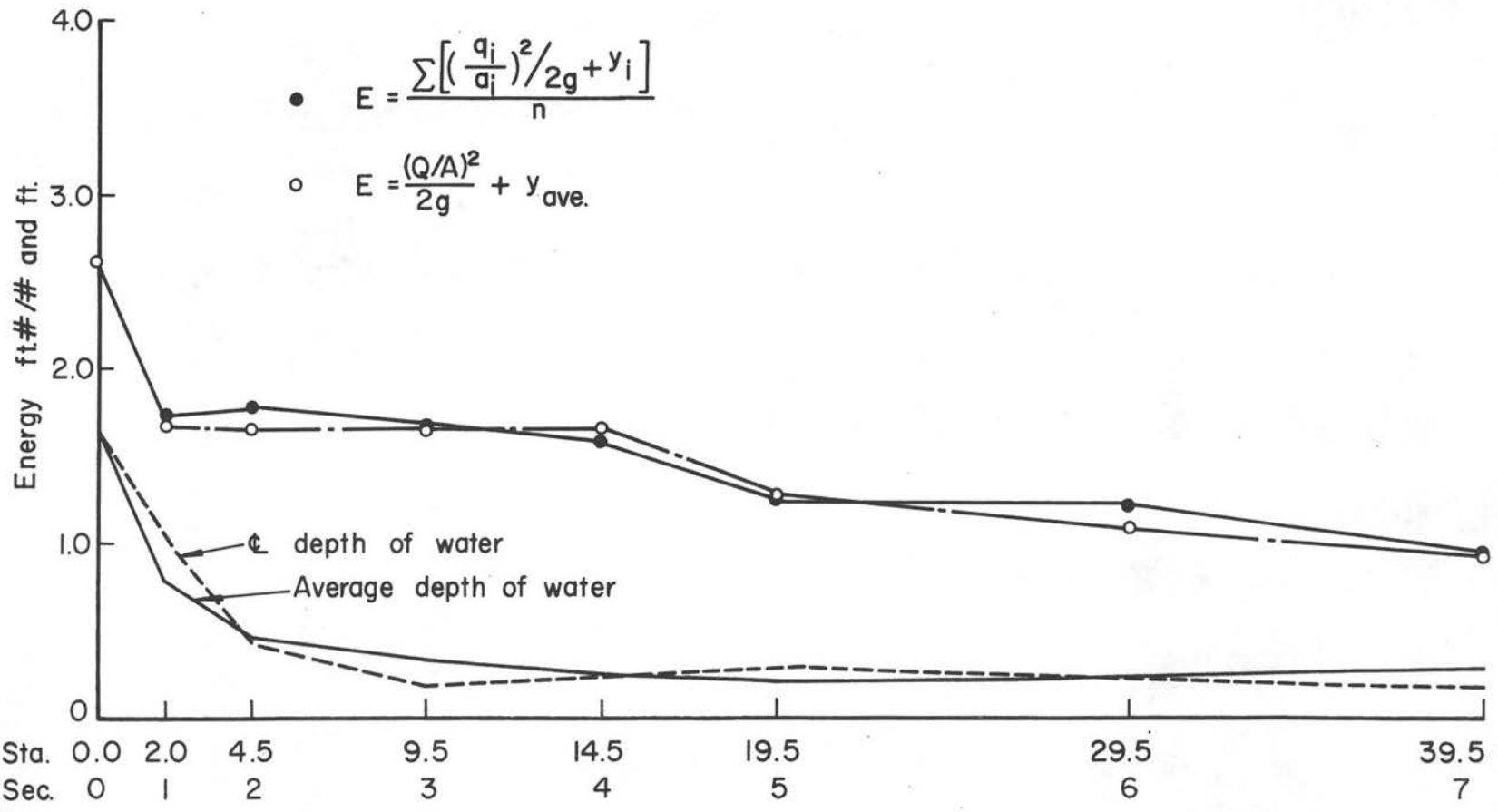
and

$$E = \frac{\sum \left[\left(\frac{q_i}{a_i} \right)^2 / 2g + y_i \right]}{n} \quad (2-3)$$

The results of these computations together with mean depth of flow and the depth of flow at the centerline of the sections are shown in Fig. 19 and Fig. 20.

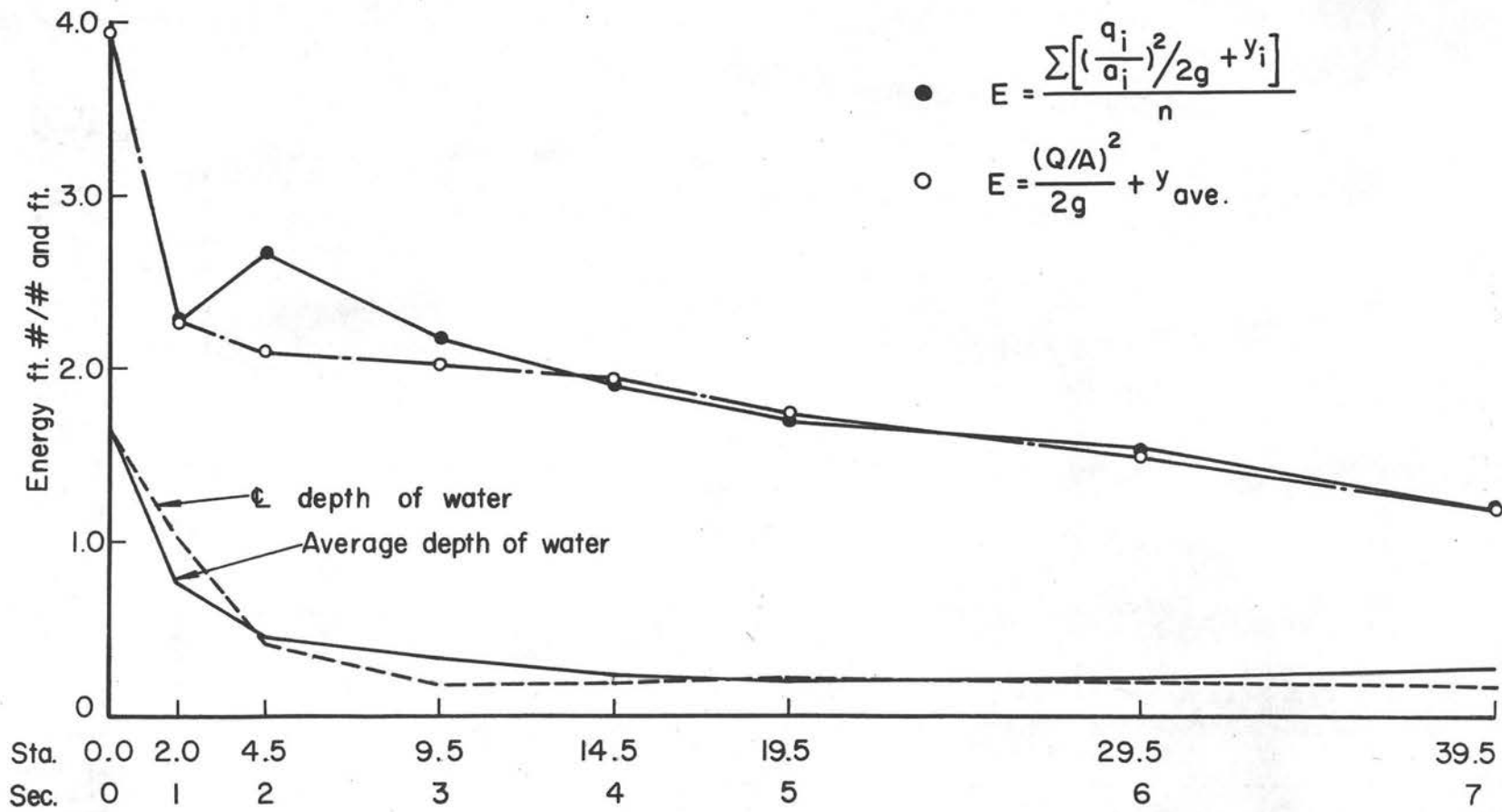
It is apparent that a considerable amount of energy is dissipated in the region adjacent to the pipe outlet. Examination of Fig. 20 shows that for $Q = 21.5$ cfs the specific energy is decreased by 46 percent at a point nine and one-half feet downstream of the outlet. Using the Darcy-Weisbach formula modified for open channel flow,

$$h_f = \frac{f L V^2}{8gd} \quad (2-5)$$



Energy, ζ Depth, and Mean Depth
 $Q = 14.1$ cfs
 Run 1 Smooth Floor

Fig. 19



Energy, ζ Depth, and Mean Depth Fig. 20
 Q = 21.5 cfs
 Run 2 Smooth Floor

where L is the length of the reach (9.5 ft), d is the mean depth of flow in the reach, V is the mean velocity in the reach, and $f = 0.04$ (high, but consistent with values shown in Ref. 9), about one-half foot of this loss can be accounted for. The energy loss across the waves originating from the walls can be estimated by a formula equally useful for an oblique wave (Ref. 11) or a normal jump,

$$\Delta E = \frac{(d_2 - d_1)^3}{4d_2 d_1} \quad (2-6)$$

where d_1 is the depth upstream of the wave and d_2 is the downstream depth. The oblique wave accounts for less than 0.1 ft of loss.

For $Q = 14.1$, a 37 percent decrease in energy occurred. Again, losses computed by conventional techniques can account for only a portion of this apparent loss.

Summary

The major portion of the energy loss near the pipe outlet must be due to a turbulent energy loss associated with the rapid changes in direction that the water undergoes as it emerges from the pipe, spreads rapidly, and undergoes a redistribution of velocity. Despite an attempt to flare the walls in an efficient manner (i.e., to minimize loss), a large loss occurred.

The losses associated with run up on the transition walls, where the jet lands and spreads radially, could not account for much loss since only a small percentage of the water was directly involved.

Though small interference waves were apparent both near the outfall and at the junction of the walls, as can be seen by examining the water surface elevations shown in the isovel plots, the Blaisdell

criterion for flare angle, presented originally for rectangular approach pipes, appears to be satisfactory for circular approach pipes.

A major interest of the preliminary study was how many data are necessary to define the energy line. A comparison of the energy lines shown in Figs. 19 and 20 indicates little difference in the position of points when the more elaborate and time-consuming integration procedure was used. For this reason, it did not appear necessary to carry on with detailed velocity measurements for the runs described in the next section.

Preliminary Tests B

Problem Statement

The major interest of this phase of study was the magnitude of energy dissipation throughout the basin for a given discharge, pipe outlet configuration, pipe section, and floor roughness. Other points of interest were the location of the boundary of the diverging jet, the angle of impingement of the jet striking the boundary, the relative depth and bearing of the standing waves, the location of the hydraulic jump, the effect of the pipe section and outlet configuration on the location of the hydraulic jump, and the eddy patterns.

Test Program

Twenty-eight runs were made. An 18 in. diameter hel-cor pipe twenty feet long was used as the approach pipe for runs 10 through 27. Three outlet configurations were tested; without end section, hereafter referred to as "plain end", commercial end section hereafter referred to as a "standard transition", and vertical wingwalls flaring

45 degrees. The basin was 10 ft 6 in. wide by 60 ft 0 in. long with vertical walls. For each outlet configuration, three floor surfaces, one of smooth concrete and two with roughness elements, were tested. Figures 21 through 24 show various outlet configurations.

The artificial roughness was created by bolting short pieces of angle iron to the floor. Figure 25 shows the geometric dimensions of the basin and the spacing pattern and dimensions of the roughness elements. The spacing of the roughness elements and the geometric ratios

$$\frac{\text{width of element}}{\text{height of element}} = 3.9 \quad \text{and} \quad \frac{\text{longitudinal spacing of element}}{\text{height of element}} = 6$$

were selected because a large amount of experimental data with these approximate ratios was available, Sayre and Albertson (12).

Each of the arrangements mentioned above was run with two discharges, approximately 15 cfs and 22 cfs

For runs 28 through 37, an 18 in. square, smooth, sheet metal approach pipe 20 ft long was used. Two outlet configurations, plain end and vertical wingwalls flaring 45 degrees, were tested. The same three floor conditions described above were examined. Photographs of the basins are shown in Figs. 26 and 27.

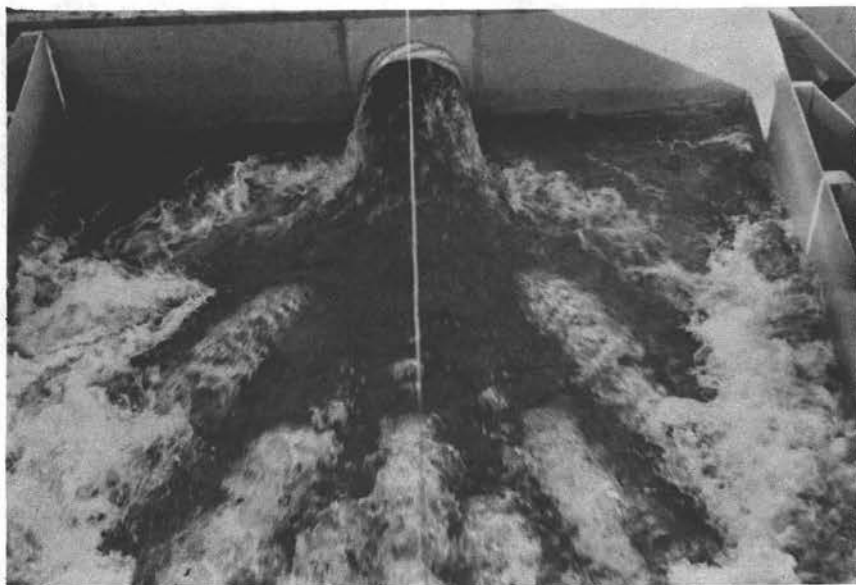
The basins with plain end pipes and smooth floors are Class B basins. The same arrangement with elements attached to the floors are Class C basins.

An outline of the test program showing the approach pipe, outlet configuration, condition of the floor, the test discharge, and the run number is shown in Fig. 28. Other significant variables are listed in Table II.



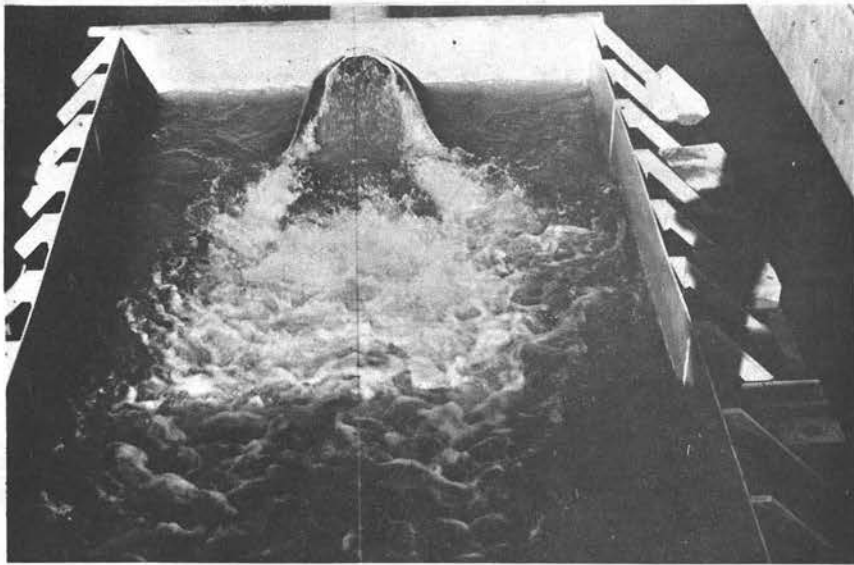
Smooth Floor Plain End
Run 11 $Q = 21.3$ cfs

Fig. 21



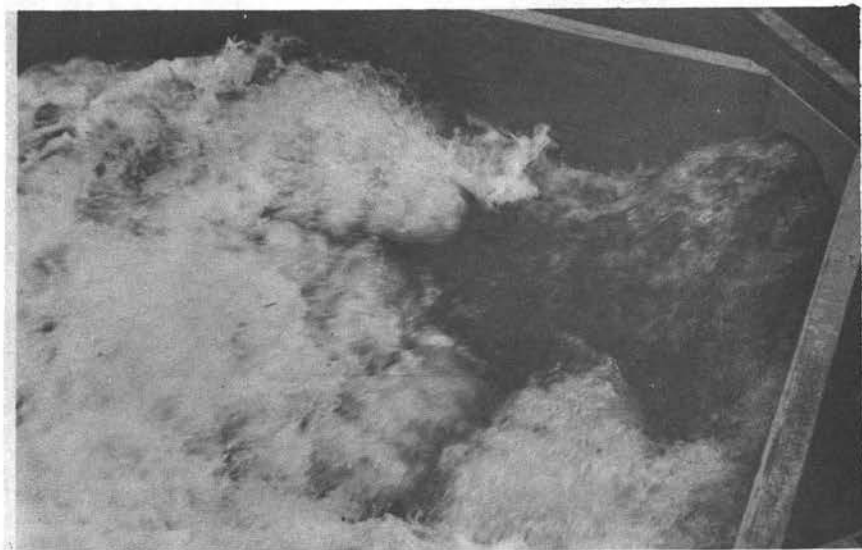
1" x 4" Elements Plain End
Run 12 $Q = 14.6$ cfs

Fig. 22



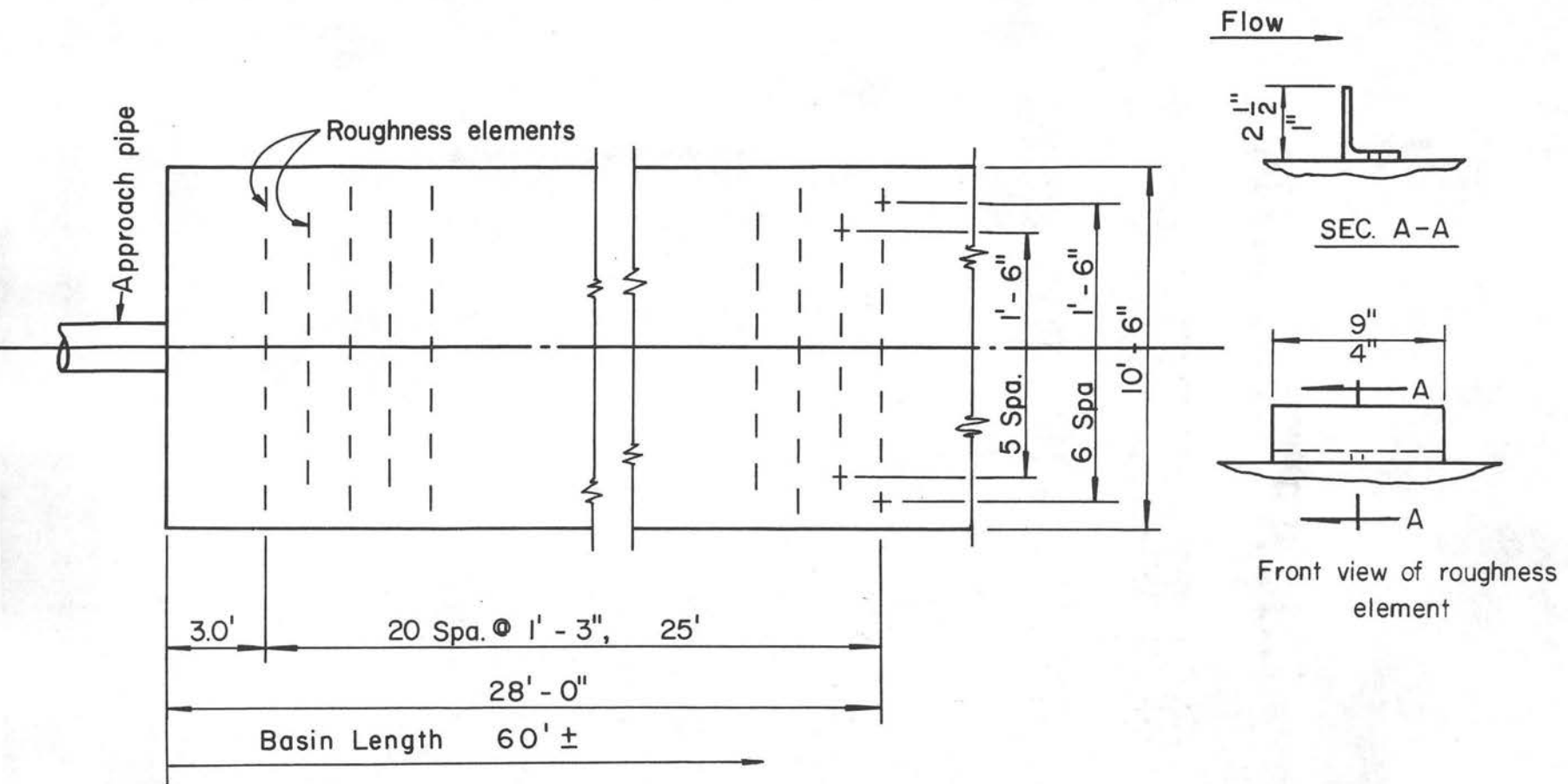
2½" x 9" Elements Standard Transition
Run 26 Q = 14.9 cfs

Fig. 23

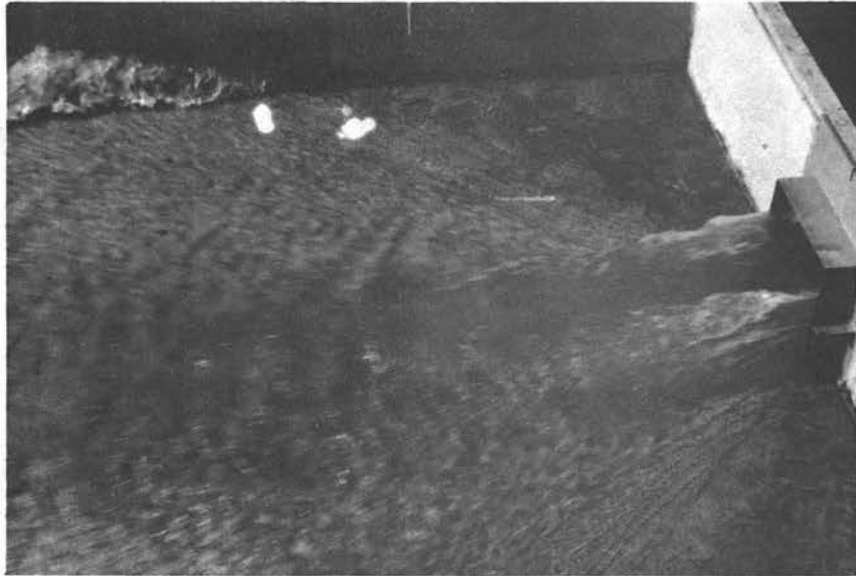


2½" x 9" Elements 45° Flare
Run 21 Q = 21.7 cfs

Fig. 24

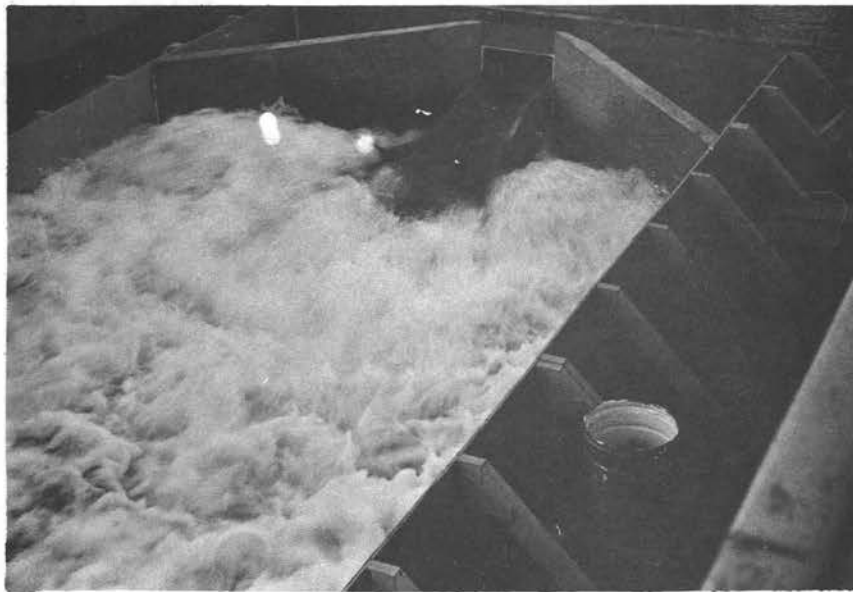


Roughness Pattern and Roughness Elements Fig. 25
 Typical all runs 10 through 37 excepting smooth floor runs



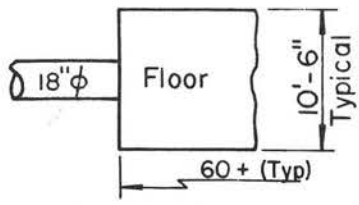
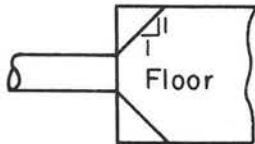
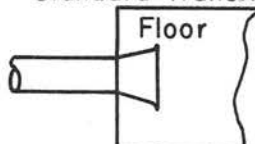

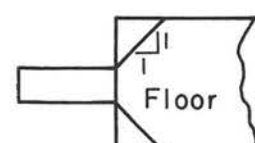
Smooth Floor Plain End
Run 29 $Q = 23.1$ cfs

Fig. 26



2½" x 9" Elements 45° Flare
Run 37 $Q = 23.2$ cfs

Fig. 27

	Floor Surface	Disch. cfs	Run No.
 <p>18" ϕ Floor 10'-6" Typical 60+ (Typ) Round Pipe</p>	Smooth	14.9	10
	"	21.3	11
	4"x1" Roughness elem.	14.6	12
	"	21.5	13
	9"x2 1/2" Rough. elem.	14.6	14
"	21.2	15	
 <p>Round Pipe</p>	Smooth	14.8	16
	"	21.6	17
	4"x1" Roughness elem.	14.4	18
	"	21.5	19
 <p>Standard Transition Round Pipe</p>	Smooth	15.2	22
	"	21.8	23
	4"x1" Roughness elem.	14.9	24
	"	21.3	25
 <p>18" \square Floor Square Pipe</p>	Smooth	16.4	28
	"	23.1	29
	4"x1" Roughness elem.	16.4	30
	"	23.2	31
 <p>Square Pipe</p>	Smooth, not run, Edge of jet, runs 28, 29, downstream of wall		
	4"x1" Roughness elem.	16.4	34
	"	23.3	35
	9"x2 1/2" Rough. elem.	16.2	36
"	23.2	37	

Note: All walls vertical

TABLE II (continued)

Run No.	Q (cfs)	V ave at pipe outlet (fps)	Depth at pipe outlet d_1 (ft)	Fr = $\frac{V}{\sqrt{gd_1}}$	E Total Energy at outlet ft. lb/lb	Hydraulic Jump Data					Standing Wave Data											
						Location (sta.)	Up-stream depth d_1 (ft)	Down-stream depth d_2 (ft)	ΔE computed ft lb/lb	ΔE scaled ft lb/lb	d_1 (ft)		d_2 (ft)		ΔE ft. lb/lb Computed		β ($^\circ$) Observed		θ ($^\circ$) Computed		θ ($^\circ$) Observed	
											Left	Right	Left	Right	Left	Right	Left	Right	Left	Right	Left	Right
10	14.9	8.43	1.5	1.2	2.75	20	.17	.55	.15	.35	.07	.10	.28	.26	.12	.04	76	74	46	47	63	64
11	21.3	12.06		1.7	3.91	28	.22	.71	.19	.48	.10	.10	.32	.30	.08	.07	56	65	47	52	41	54
12	14.6	8.26		1.2	2.71																	
13	21.6	12.22		1.8	3.97																	
14	14.5	8.20		1.2	2.69																	
15	21.2	12.00		1.7	3.89																	
16	14.8	8.37		1.2	2.74	25	.20	.67	.19	.26	.06	.08	.26	.26	.13	.07	48	48	36	36	32	31
17	21.6	12.22		1.8	3.97	31	.22	.71	.19	.45	.04	.06	.26	.28	.25	.16	51	49	46	44	39	39
18	14.4	8.15		1.2	2.68																	
19	21.6	12.22		1.8	3.97																	
20	14.6	8.26		1.2	2.71																	
21	21.7	12.28		1.8	3.99																	
22	15.2	8.60		1.2	2.80	25	.16	.62	.24	.32	.07	.08	.23	.22	.06	.04	73	58	49	44	62	48
23	21.7	12.28		1.8	3.99	31	.24	.71	.15	.50	.08	.09	.29	.27	.10	.06	72	61	55	49	60	52
24	14.9	8.43		1.2	2.75																	
25	21.3	12.05		1.7	3.91																	
26	14.9	8.43	Y	1.2	2.75																	
27	22.7	12.84	1.5	1.8	4.21																	
28	16.4	12.32	.888	2.3	3.25	29	.14	.59	.27	.43	.06	.06	.24	.23	.10	.10	59	58	50	50	49	49
29	23.1	15.46	.995	2.7	4.70	39	.19	.77	.33	.92	.08	.10	.28	.32	.09	.08	56	56	48	48	48	48
30	16.4	12.04	.908	2.2	3.16																	
31	23.2	15.52	.996	2.7	3.74																	
32	16.4	11.80	.926	2.2	3.09																	
33	23.6	15.60	1.011	2.7	4.79																	
34	16.4	12.32	.889	2.3	3.25																	
35	23.2	15.57	.992	2.8	4.75																	
36	16.5	12.03	.912	2.2	3.16																	
37	23.5	15.74	.996	2.8	4.85																	

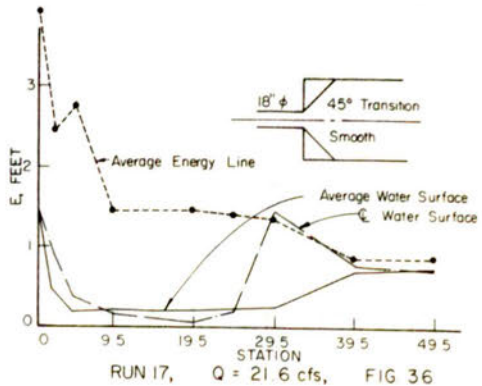
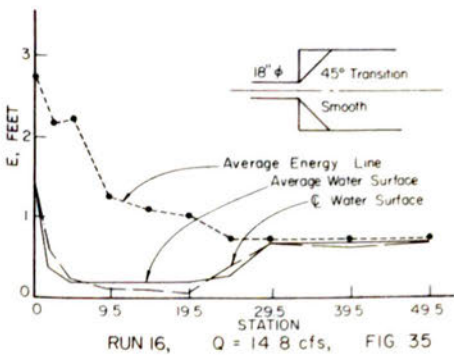
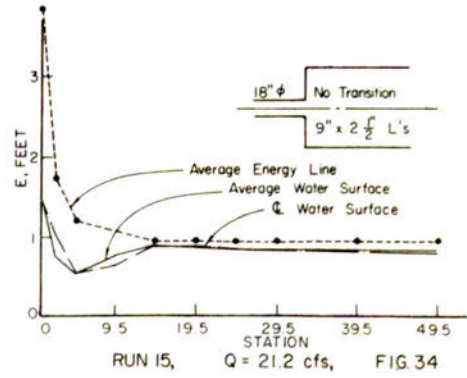
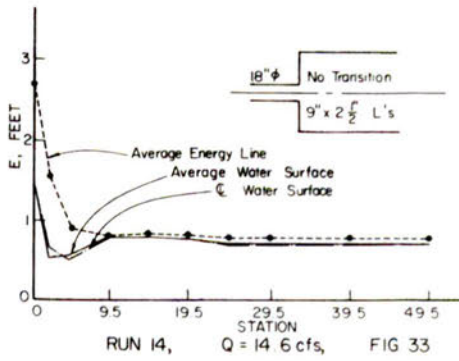
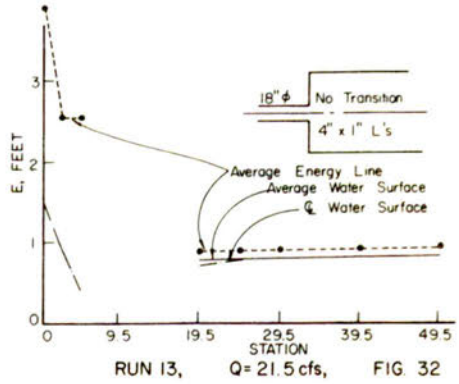
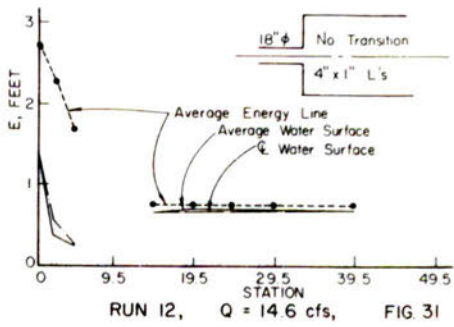
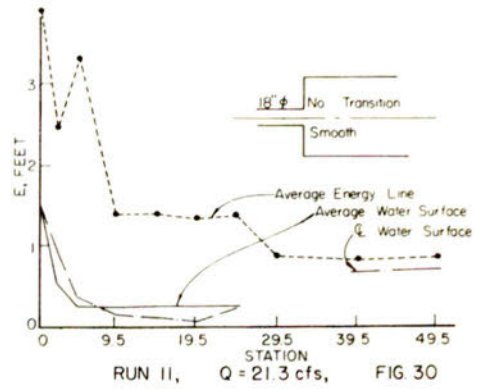
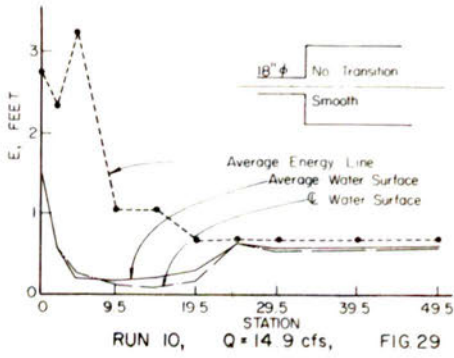
Data Obtained and Collection Method

Information gathered during preliminary tests A in the smooth basin indicated that the energy line could be adequately defined (at least in the lower regions of the basin) if the cross-sectional area at a station and the discharge passing through it were known. For the rough basins, the mixing and churning created by high speed flow impinging on the roughness elements should result in an even more uniform velocity distribution. For the above reasons, velocity traversing was abandoned. The water surface profile was measured at the pipe outlet, if it was not flowing full, and at successive downstream stations. The stations at which data were taken are shown by the filled circles that define the energy line (Figs. 29 through 56). The data collection stations varied slightly from run to run because of the poorly defined water surface over the upper portion of the roughness field and in the area adjacent to the hydraulic jump in the smooth floor basin.

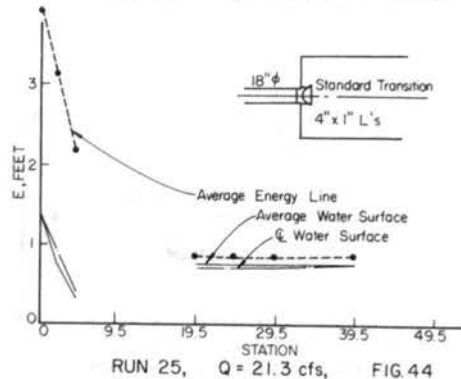
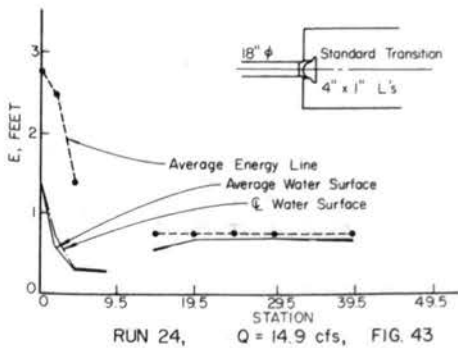
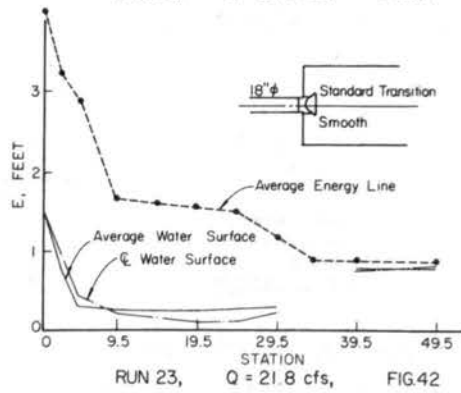
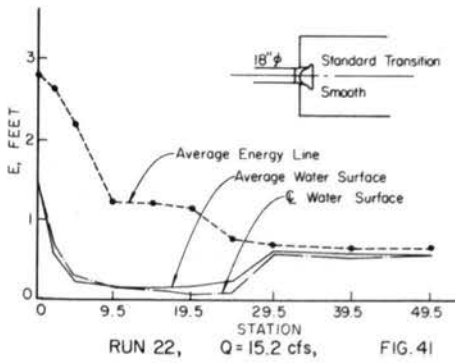
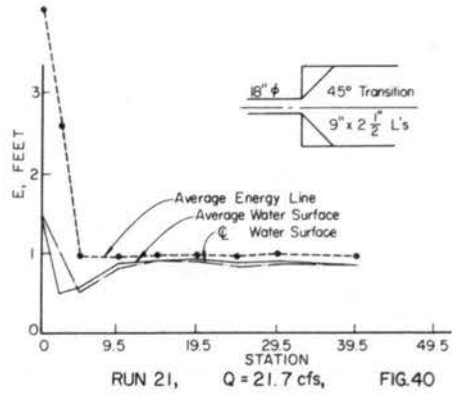
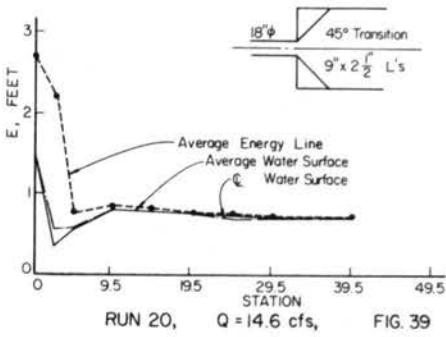
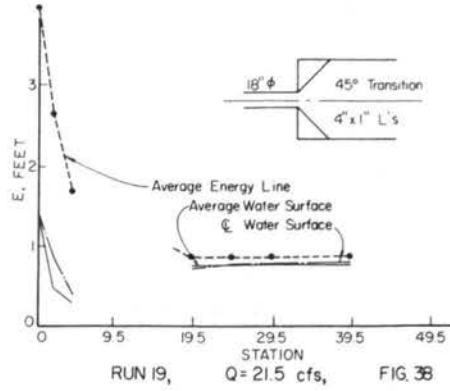
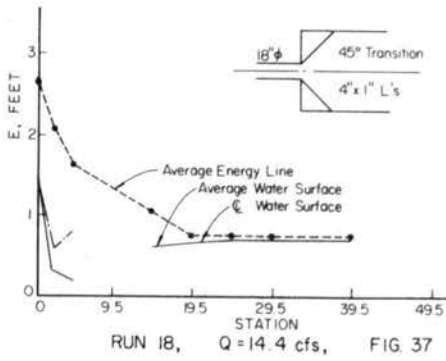
The pitot tube already described was used for locating the water surface. Water continuously ejected through the center tube was used as a pointer. This proved to be a very effective means for picking up the high speed rough surface. Elevations were recorded to 0.01 feet and, when waves were not present, were repeatable within ± 0.01 ft. Figure 57 shows the tube in position for a measurement.

The discharge measurements were obtained from the sharp-crested weir previously described. Four discharge readings (two at the beginning, two after completion) were taken for each run.

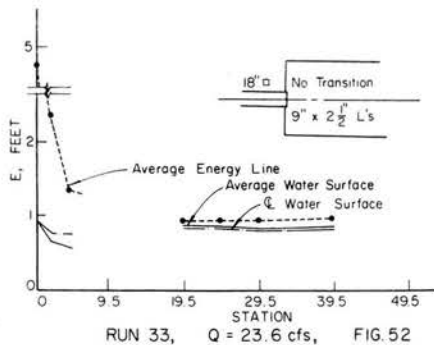
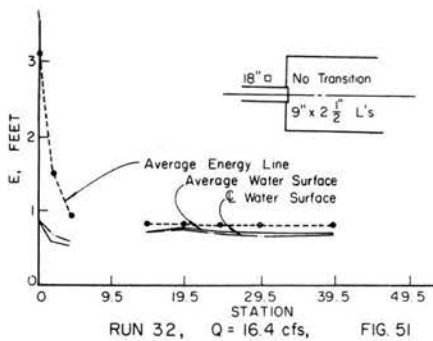
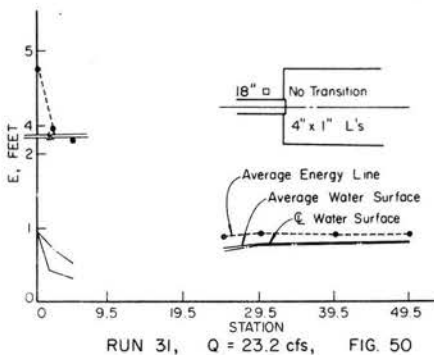
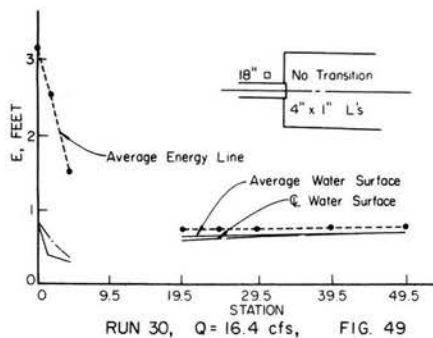
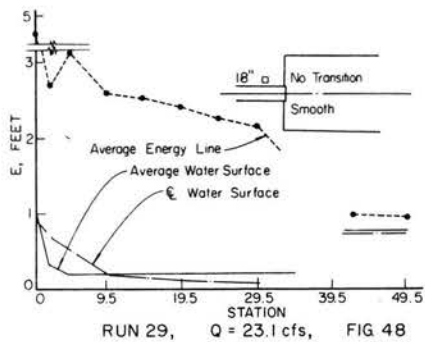
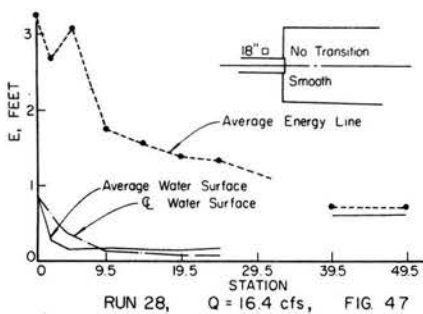
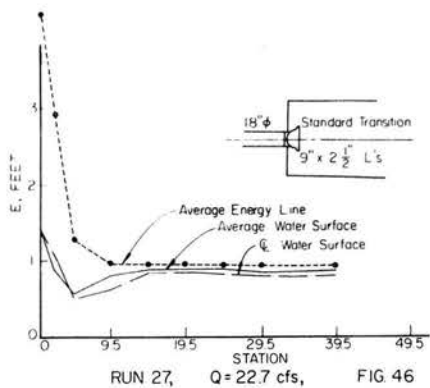
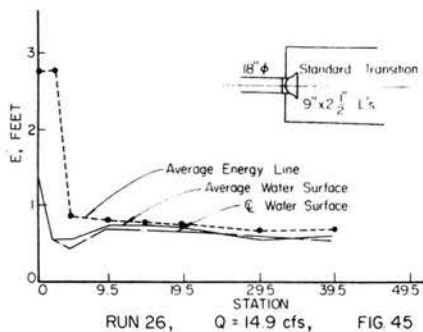
In addition to the above measurements, the location of the edge of the diverging jet downstream of the outlet, the location of the



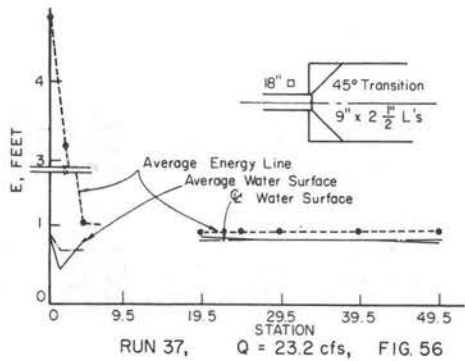
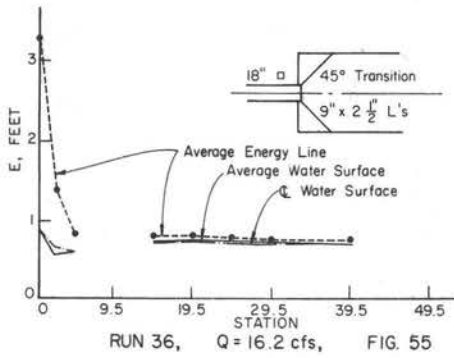
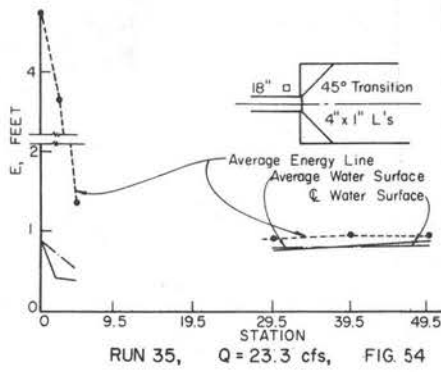
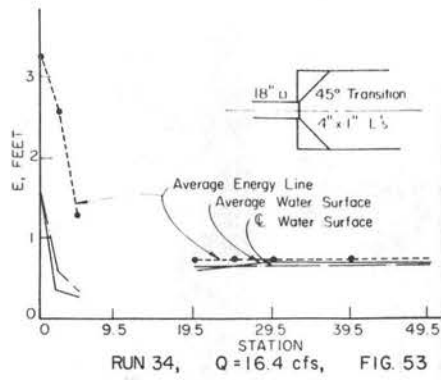
ENERGY LINE AND WATER SURFACES



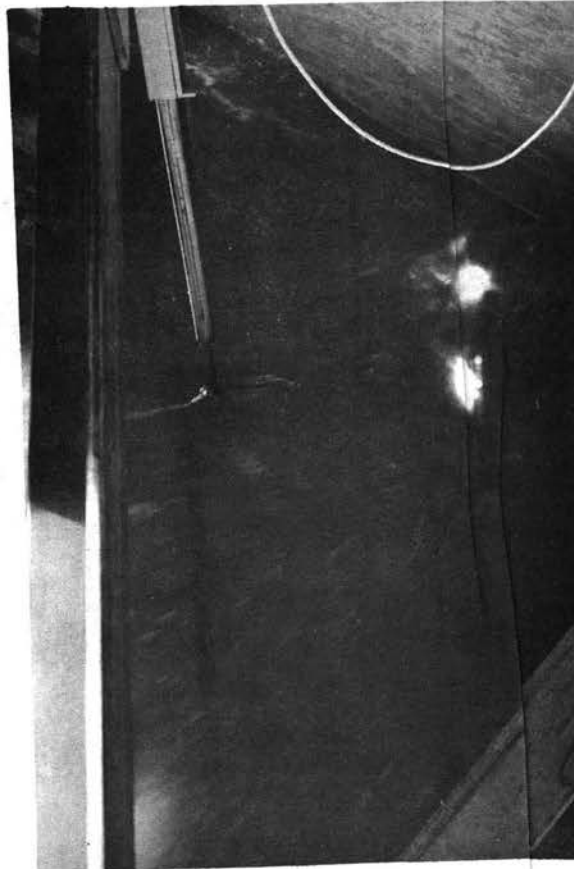
ENERGY LINE AND WATER SURFACES



ENERGY LINE AND WATER SURFACES



ENERGY LINE AND WATER SURFACES



Pitot Tube

Fig 57

oblique standing waves and the transverse hydraulic jump (for smooth basin flow) were recorded.

Data Reduction

Specific energy $E = \frac{(Q/A)^2}{2g} + y$ (Eq. 2-2) was computed.

To expedite computations, a computer program was written. The output was E and y .

The following data were plotted:

Energy lines

Centerline depth and mean depth

} Figs. 29 through 56

Plan view of the basin showing the edge of the expanding jet and the location of the standing wave

Cross sections at Sta 0.0, 2.0, 4.5 and 9.5

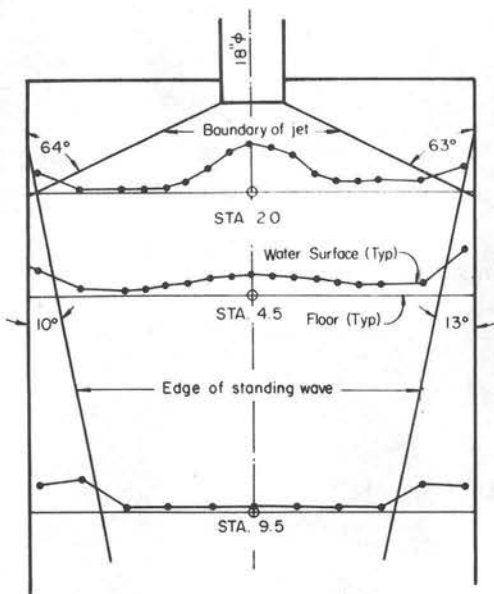
} Figs. 58 through 85.

No sections are shown for the round pipe at Sta 0.0 since the pipe flowed full at all times. The 15 cfs discharge occasionally broke away from the top surface, dropping two or three inches below the crown of the pipe.

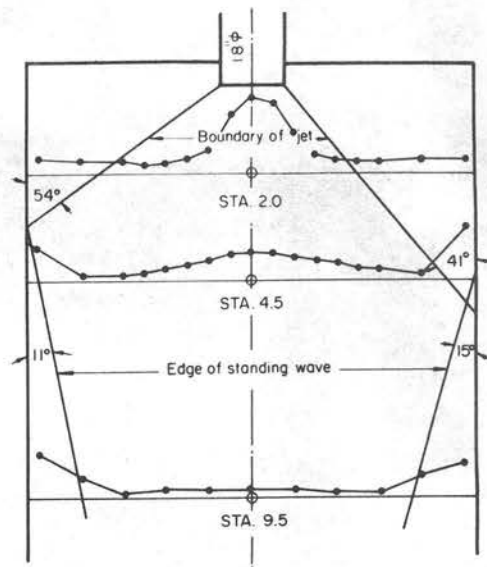
Jet Divergence

Figures 58 through 85 graphically display the approximate boundary of the expanding jet. The location of the edge of the jet was a matter of judgment. The zone of turbulence and air entrainment along the side of the high speed core was located by eye and the coordinates recorded.

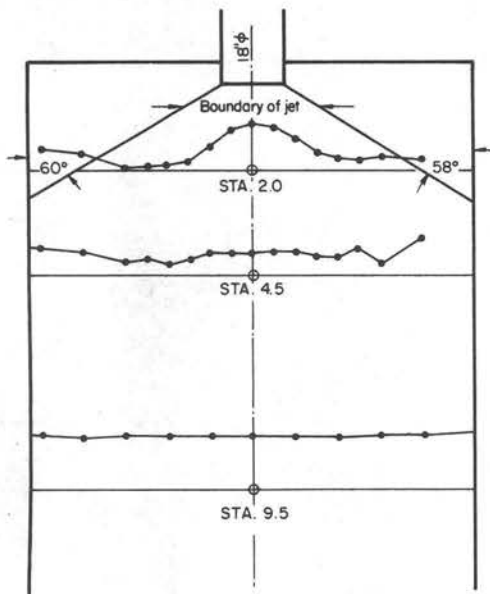
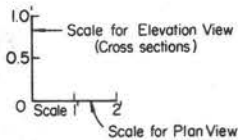
Lateral confinement of the jet by tailwater materially affected divergence. Surface disturbances and the additional depth made it very



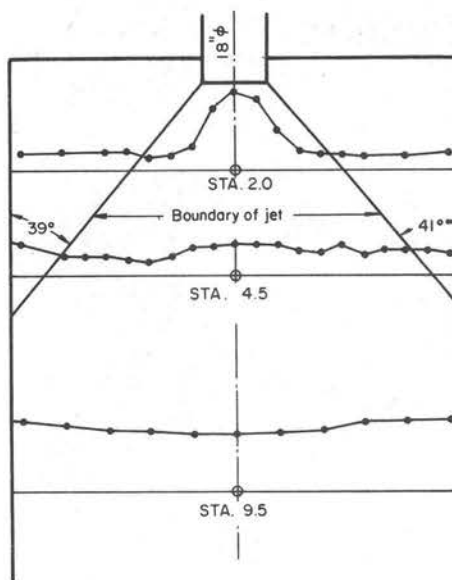
RUN 10, Q = 14.9 cfs, FIG. 58
SMOOTH FLOOR



RUN 11, Q = 21.3 cfs, FIG. 59
SMOOTH FLOOR

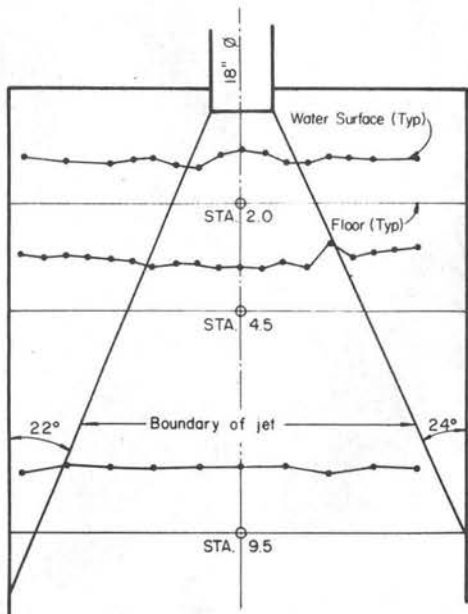


RUN 12, Q = 14.6 cfs, FIG. 60
4"x1" ELEMENTS

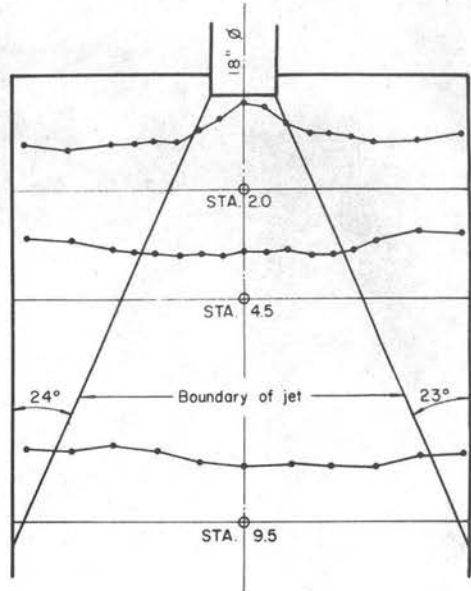


RUN 13, Q = 21.5 cfs, FIG. 61
4"x1" ELEMENTS

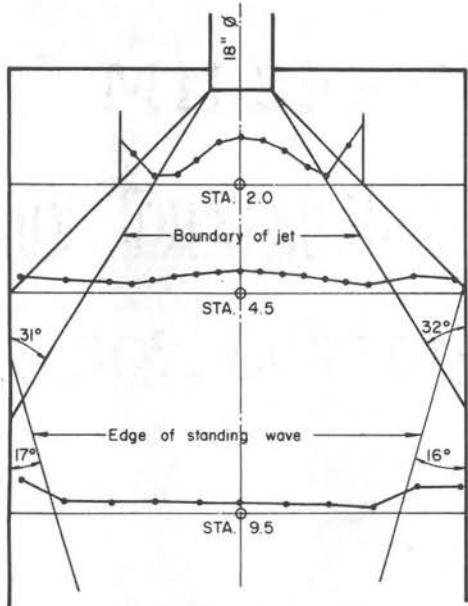
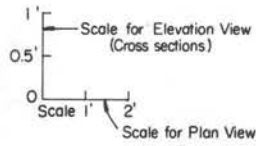
BASIN PLAN AND CROSS SECTIONS



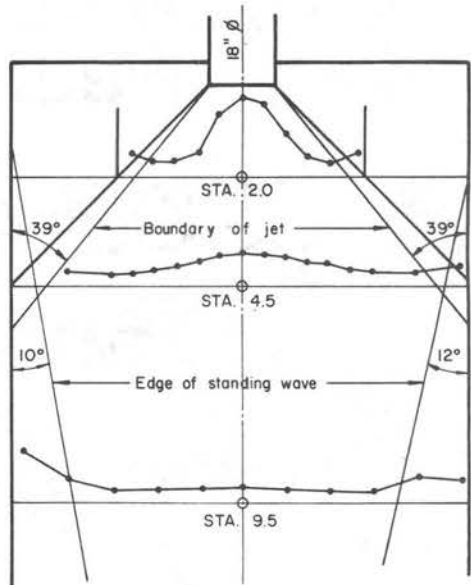
RUN 14, $Q = 14.6$ cfs, FIG. 62
 $9'' \times 2\frac{1}{2}''$ ELEMENTS



RUN 15, $Q = 21.2$ cfs, FIG. 63
 $9'' \times 2\frac{1}{2}''$ ELEMENTS

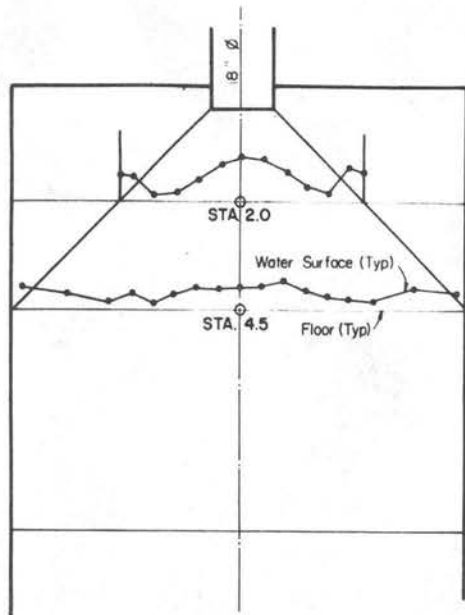


RUN 16, $Q = 14.8$ cfs, FIG. 64
 SMOOTH FLOOR

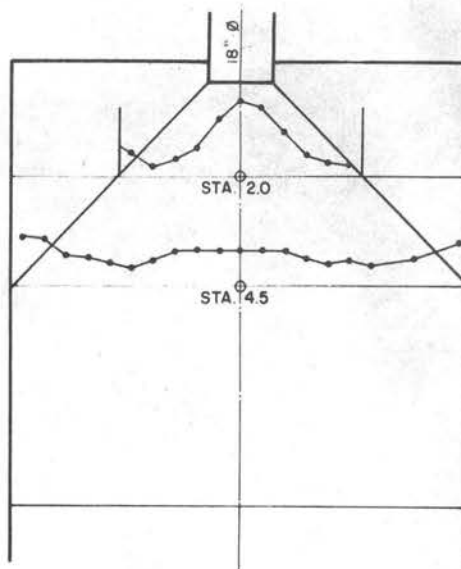


RUN 17, $Q = 21.6$ cfs, FIG. 65
 SMOOTH FLOOR

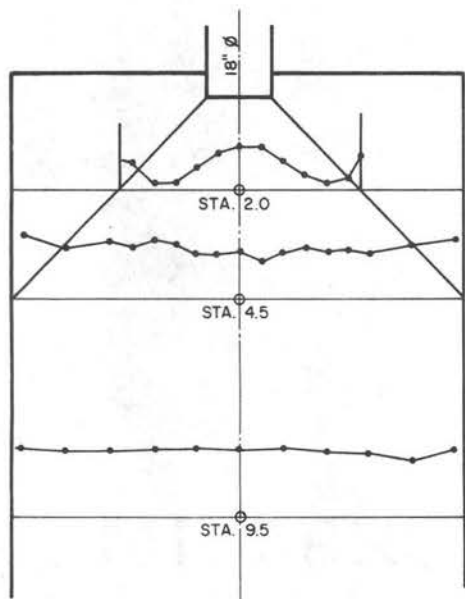
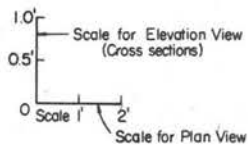
BASIN PLAN AND CROSS SECTIONS



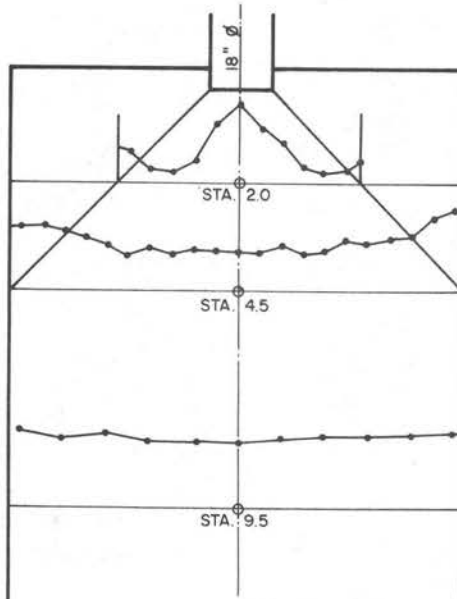
RUN 18, Q = 14.4 cfs, FIG. 66
4" x 1" ELEMENTS



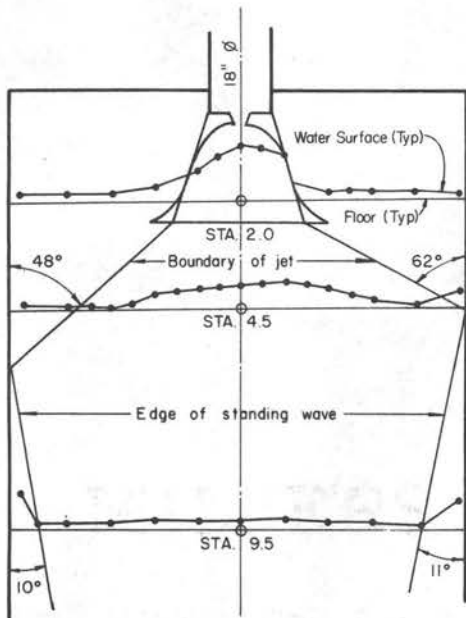
RUN 19, Q = 21.5 cfs, FIG. 67
4" x 1" ELEMENTS



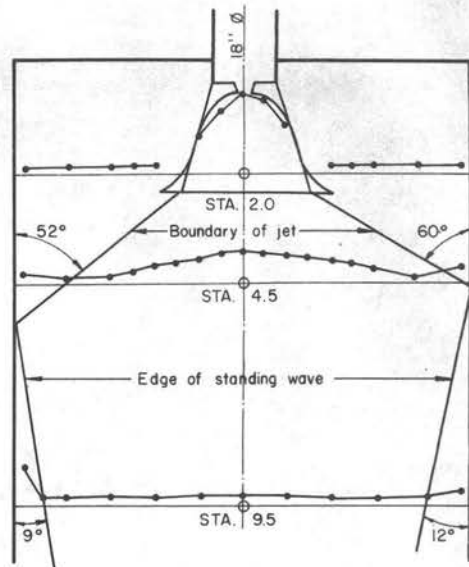
RUN 20, Q = 14.6 cfs, FIG. 68
9" x 2 1/2" ELEMENTS



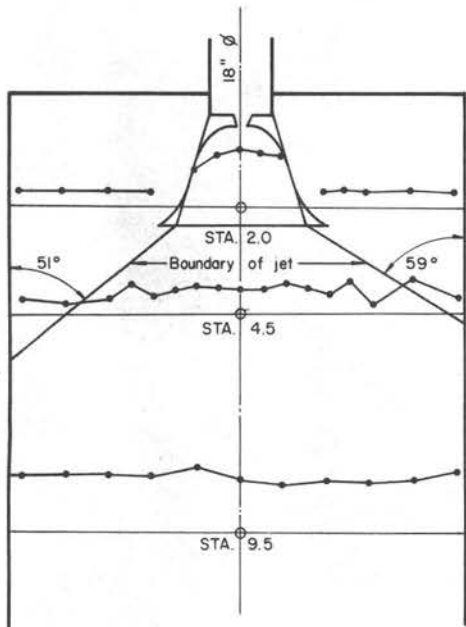
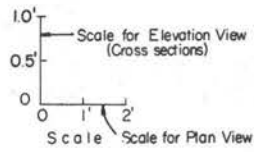
RUN 21, Q = 21.7 cfs, FIG. 69
9" x 2 1/2" ELEMENTS



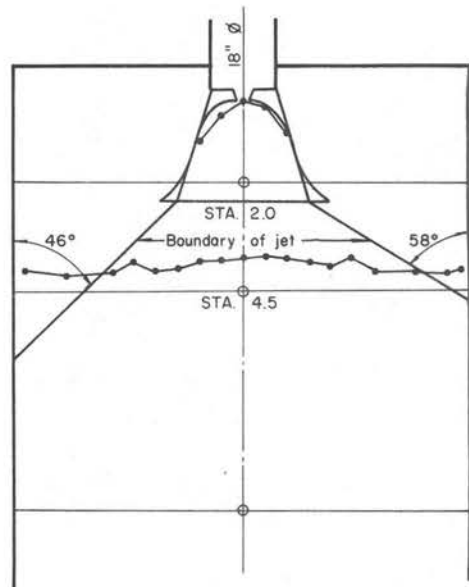
RUN 22, Q = 15.2 cfs, FIG. 70
SMOOTH FLOOR



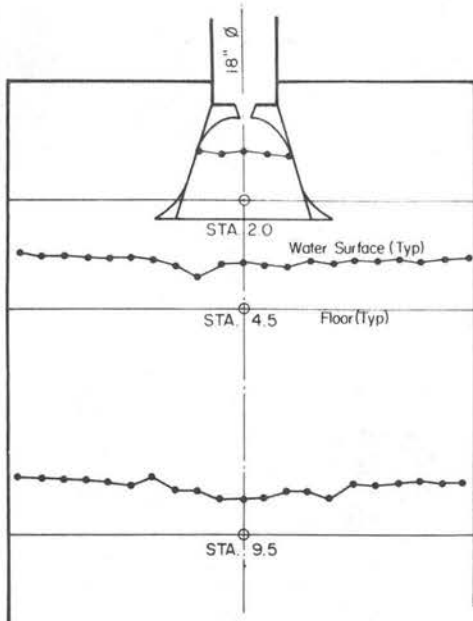
RUN 23, Q = 21.8 cfs, FIG. 71
SMOOTH FLOOR



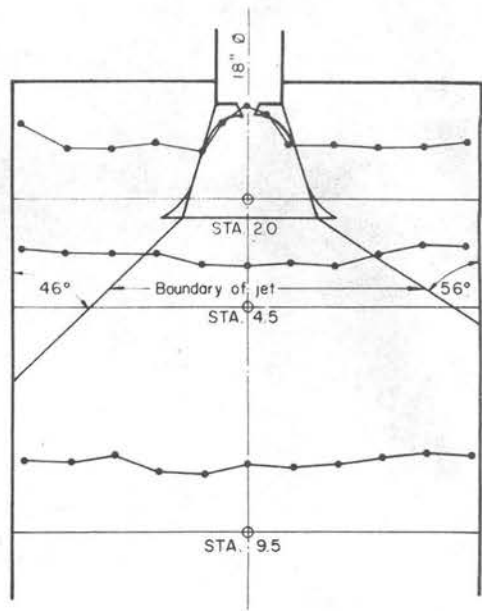
RUN 24, Q = 14.9 cfs, FIG. 72
4"x1" ELEMENTS



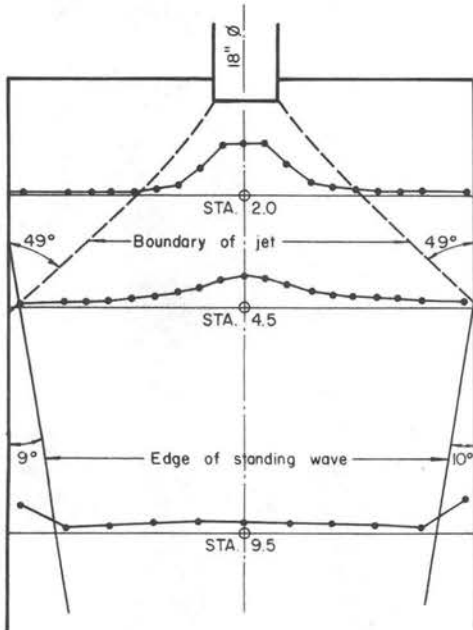
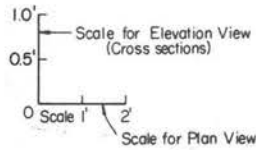
RUN 25, Q = 21.3 cfs, FIG. 73
4"x1" ELEMENTS



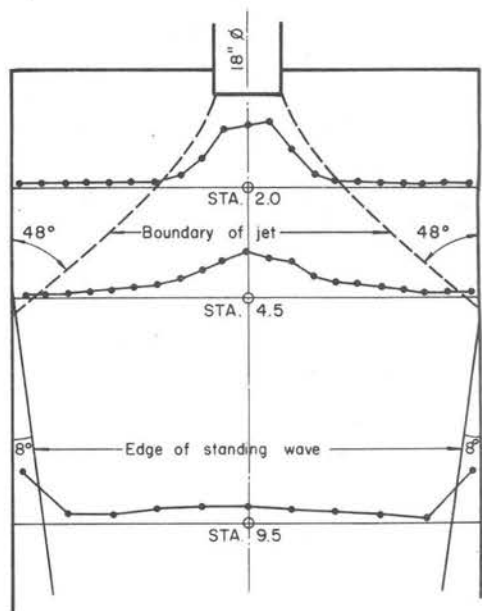
RUN 26, $Q=14.9$ cfs, FIG. 74
 $9'' \times 2\frac{1}{2}''$ ELEMENTS



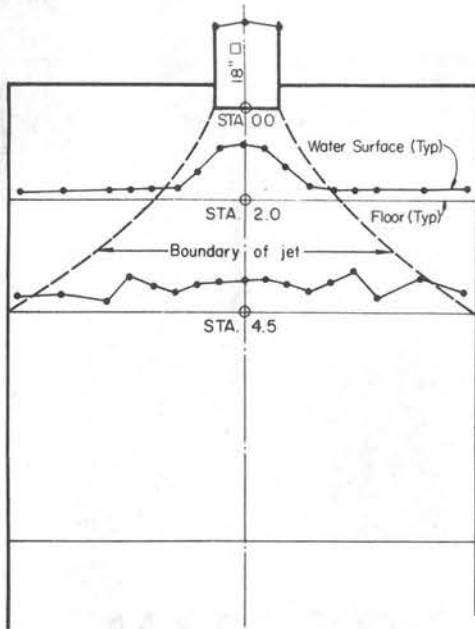
RUN 27, $Q=22.7$ cfs, FIG. 75
 $9'' \times 2\frac{1}{2}''$ ELEMENTS



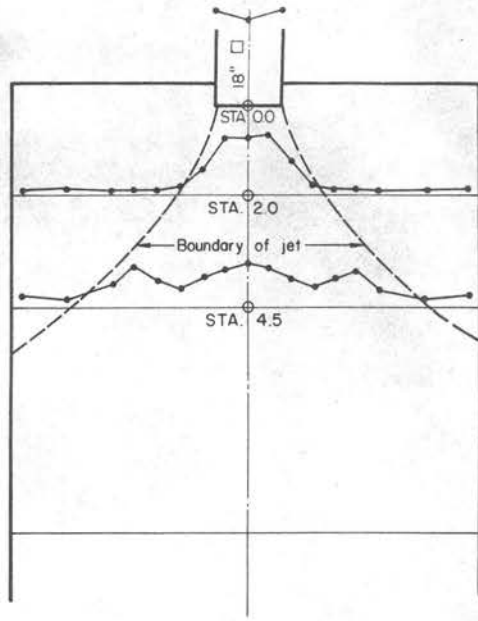
RUN 28, $Q=16.4$ cfs, FIG. 76
 SMOOTH FLOOR



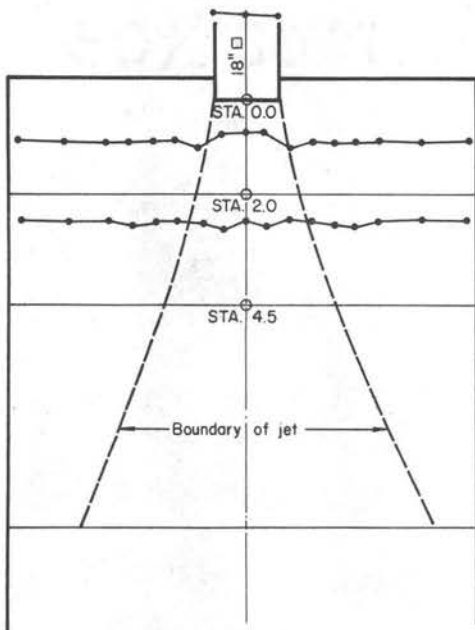
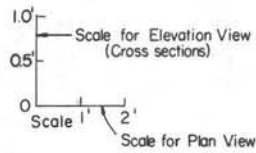
RUN 29, $Q=23.1$ cfs, FIG. 77
 SMOOTH FLOOR



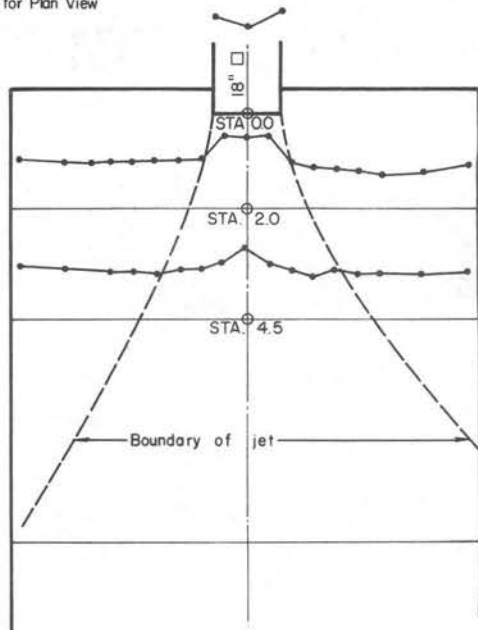
RUN 30, Q = 16.4 cfs, FIG. 78
4" x 1" ELEMENTS



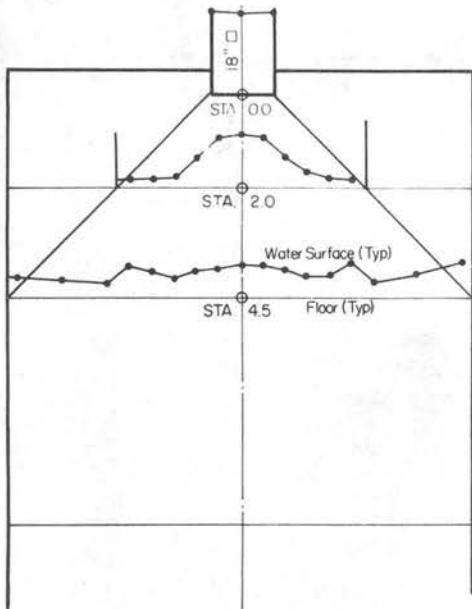
RUN 31, Q = 23.2 cfs, FIG. 79
4" x 1" ELEMENTS



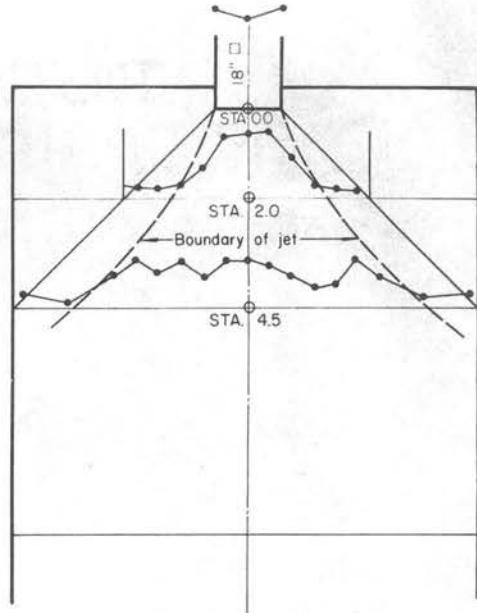
RUN 32, Q = 16.4 cfs, FIG. 80
9" x 2 1/2" ELEMENTS



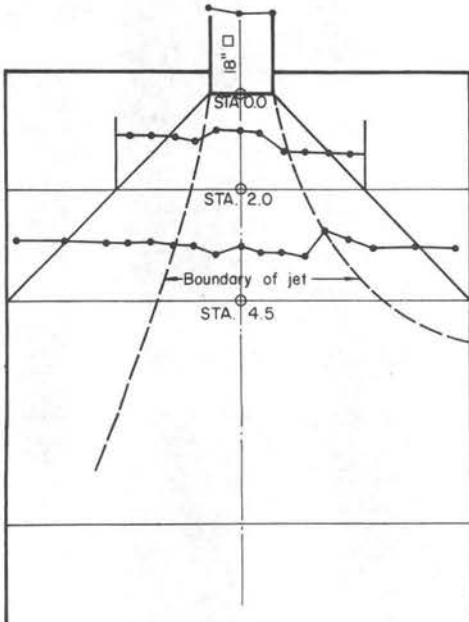
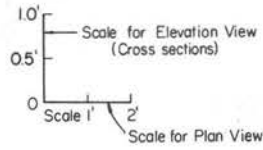
RUN 33, Q = 23.6 cfs, FIG. 81
9" x 2 1/2" ELEMENTS



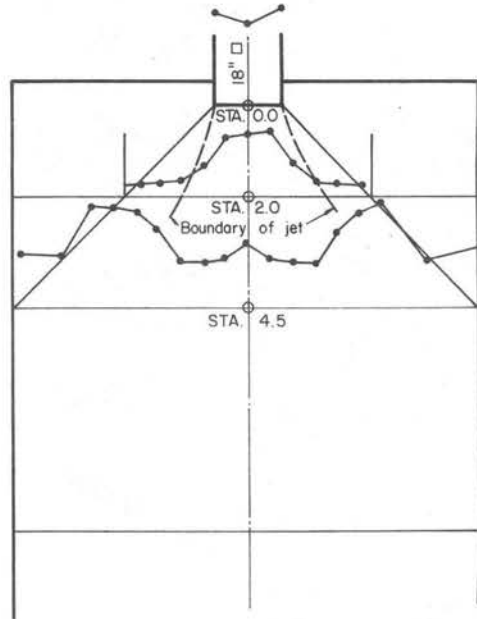
RUN 34, $Q = 16.4$ cfs, FIG. 82
4"x1" ELEMENTS



RUN 35, $Q = 23.3$ cfs, FIG. 83
4"x1" ELEMENTS

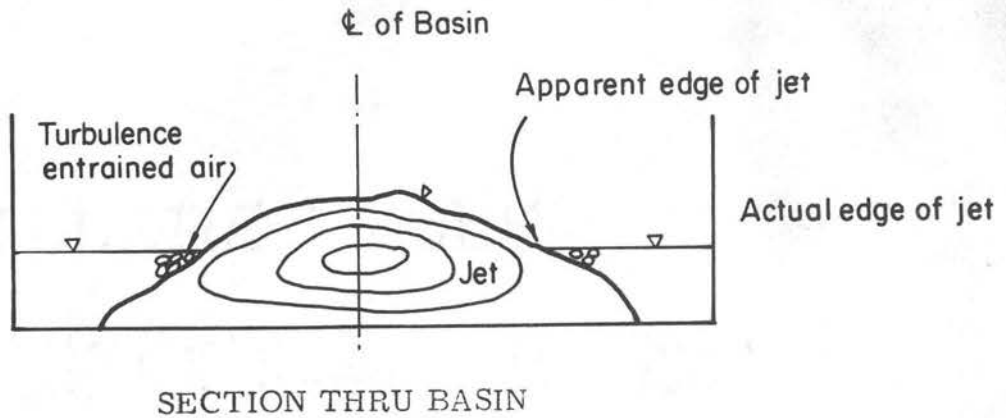


RUN 36, $Q = 16.2$ cfs, FIG. 84
9"x 2 1/2" ELEMENTS



RUN 37, $Q = 23.2$ cfs, FIG. 85
9"x 2 1/2" ELEMENTS

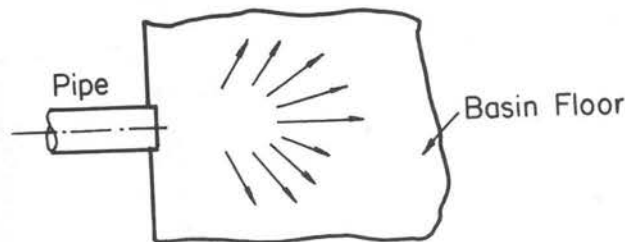
difficult to locate the edge of the jet, and therefore the coordinate may not have been accurate. The accompanying sketch illustrates the problem.



Because of the depth problem, the lower boundary of the jet may well diverge at a more rapid rate than indicated on the drawings.

All other conditions being equal, the jet issuing from the smooth square pipe tended to remain concentrated and did not diverge as rapidly as the flow from the circular pipe. Some of the conditions that seem pertinent are:

A. The cylindrical unsupported jet discharging from the pipe tended to plunge to the floor and spread radially.



PLAN VIEW

The slightly higher invert elevation, about 0.15 ft due to the corrugations, and the higher crest elevation tended to augment this phenomenon. From the viewpoint of stability, this landing area will be a critical zone for rock surfaced basins.

B. The water discharging from the hel-cor pipe, particularly at the higher discharge, exhibited a rough, turbulent, corrugated surface which must have been moving at a slower rate than the main core. This contrasted with the smooth side surfaces displayed by the water flowing from the square pipe.

C. The exit velocities of the rectangular pipe were about 20 to 40% higher than those associated with the round pipe for a similar discharge, and therefore the water particles were carried farther out into the basin prior to gravity dispersion. There were several reasons for the higher exit velocity from the rectangular approach pipe.

- (1) The water was delivered to the rectangular barrel through a 1.5 foot diameter circular pipe (cross-sectional area 78% of 1.5 foot by 1.5 foot rectangular pipe). This, in conjunction with slightly higher discharges, resulted in a much higher entrance velocity.
- (2) The rectangular pipe had smooth walls and floor (as contrasted to the corrugated pipe) and was set on a slight slope, about 1%. This resulted in the conduit running only partially full.

These conditions in combination resulted in a significantly higher exit velocity.

Lack of symmetry of the jet is apparent in some of the basins. For the circular pipe, there may have been a slight spiral effect

caused by the helical corrugations. For those basins with roughness elements, the edge of the jet was hardly discernible because of the disturbed condition. The position of the edge of the jet varied considerably, depending on how the water separated around the roughness elements.

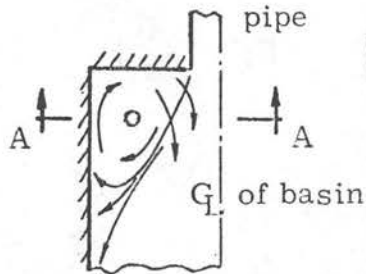
Pipe Section, Outlet Configuration, and Eddy Pattern

It did not appear that the shape of the pipe section materially affected the hydraulic characteristics of the basin. As already mentioned, discharge from the round, rough pipe tended to plunge a little more rapidly. The result of this radial flow was a little more concentration of flow along the wall for the circular approach pipe. From run to run, considering the energy level at the outfall section, little variation in the location of the hydraulic jump was noted.

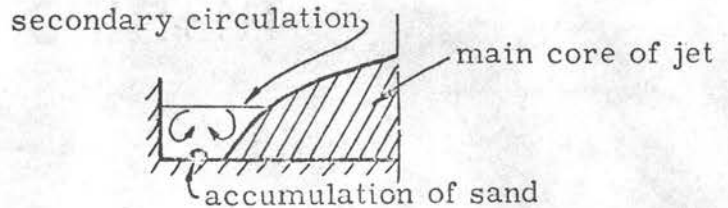
For the pipes with plain ends discharging into rectangular basins, well developed eddies occurred in the upper corners. The mechanism which drives these jets is usually attributed to friction between the water stored in corners and the high speed core of water. Though this mechanism is probably dominant in relatively deep flow, it was not the major factor in these basins. Typically, water impinged on the walls and then split, most of it flowing downstream and the remainder upstream. The water flowing upstream tended to raise the eddy area surface. When the water surface in the eddy area rose slightly above the lowest elevation of the high speed core, water flowed onto the jet and was swept downstream.

In the cases where roughness elements were used (particularly the large elements), water diverted by the elements drove the eddies at a high speed. No measurement of the eddy velocity was made.

Judging from the accumulation of sand particles in the center of the eddies, the circulation would appear to have been as shown:



PLAN VIEW



Sec A-A

This transverse velocity (secondary circulation) increases the scour capacity of the water. Because of the rather small quantity of water (0.1 to 0.3 feet deep) involved in these eddies, they do not contribute greatly to energy dissipation.

The standard transition confines the jet. As will be discussed in a later section, little loss of energy occurred between the pipe outlet and the transition outlet. Whereas this "efficiency" may be highly desirable from the viewpoint of minimizing pipe entrance loss, it is undesirable from the viewpoint of scour potential. A transition is needed that maximizes energy dissipation, providing installation conditions are such that this does not affect the capacity of the pipe.

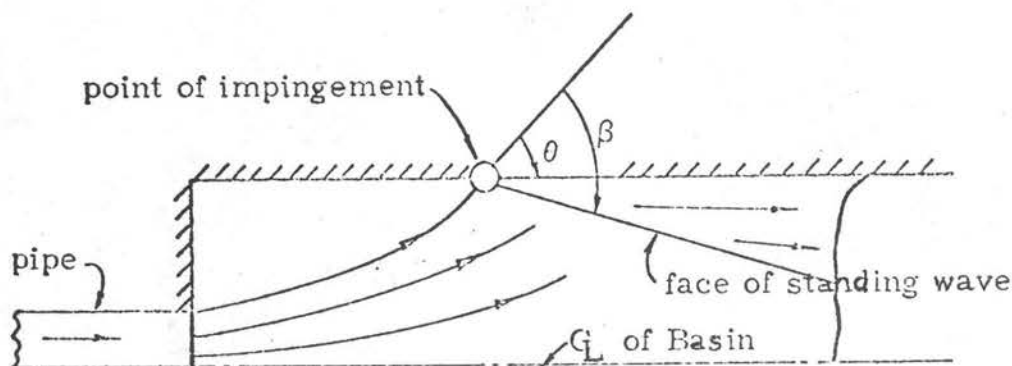
All in all, it appears that from a design viewpoint, wing walls flaring at about 45 degrees from the centerline are adequate. In all instances, the main jet fell within the walls. The small amount of water between the jet and the wall acted as a cushion, yet was not of sufficient width to allow the large eddies to grow.

Standing Waves

The location of the standing waves in smooth basins is shown graphically in Figs. 58 through 85. Water depths on each side of the waves are shown on the cross sections displayed in the same figures. A compilation of the wave angle, depths each side of the waves, and some of the computed and measured variables are shown in Table II. Figures 86 and 87 are photographs showing the oblique standing waves and hydraulic jump.

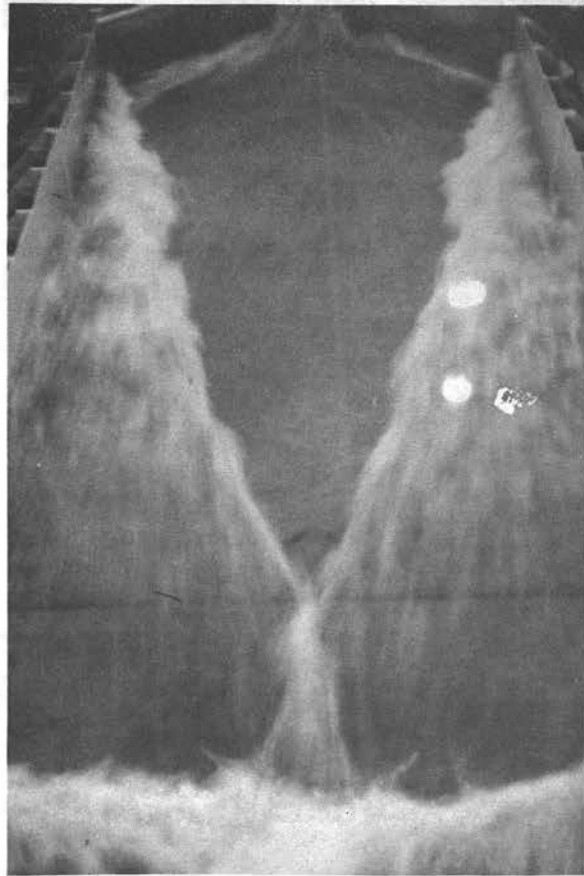
From the design viewpoint, two areas of major interest are:

(a) what is the runup height of the wave (see sketch below) where it strikes the wall at the point of impingement? (b) what is the energy loss associated with the standing waves?

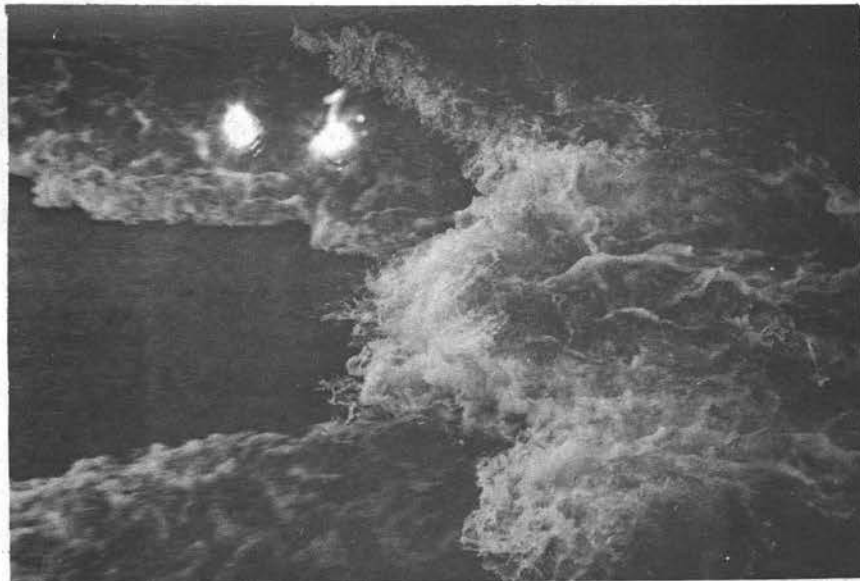


PLAN VIEW

A conservative answer to the first question can be obtained by solving the Bernoulli equation for a surface stream filament, assuming that the transverse component of velocity is totally converted to elevation head. The approximate equation would be



Smooth Floor 45° Flare Fig. 86
Run 17 $Q = 21.6$ cfs



Smooth Floor Plain End Fig. 87
Run 10 $Q = 14.9$ cfs

$$d_2 = \frac{(V \sin\theta)^2}{2g} + d_1 \quad (2-7)$$

where d_2 is the maximum height that the water could reach and d_1 is the height of the approach water surface. For the condition where the basin has flaring walls, θ is defined. V could be assumed to be the mean velocity at the pipe exit. As an example, using data from run 16,

$$\theta = 31^\circ \quad V = 8.4 \text{ fps} \quad Q = 14.8 \text{ cfs}$$

$$d_1 = \frac{Q}{(\text{width})(V)} = \frac{14.8}{(10.5)(8.4)} = 0.17$$

$$d_2 = \left[\frac{(8.4)(0.515)}{64.4} \right]^2 + 0.17 = \underline{\underline{0.46 \text{ ft}}}$$

Though no data are available for the point of impingement (see run 16, Fig. 35), about 2 ft downstream, a runup of 0.4 ft is indicated. For run 17, comparative depths would be d_2 computed 1.1 ft and d_2 measured 0.7 ft. This procedure is admittedly conservative, as it presumes total conversion of velocity head to elevation head. On the other hand, the approach velocity may well be higher than the mean exit velocity, particularly if the elevation head is large compared to the velocity head at the pipe exit. A better approximation of d_1 and V can be obtained from Figs. 138 through 148 found in Chapter IV. These figures are recommended for design use.

For the situation where the pipe discharges into a rectangular basin, θ and V are unknown. Generalized surface contours prepared by Rouse, Bhoota and Hsu (13) are of limited use. For a given exit condition, the surface contours could be superimposed on the basin plan. Unfortunately, for usual Froude numbers, this information will define

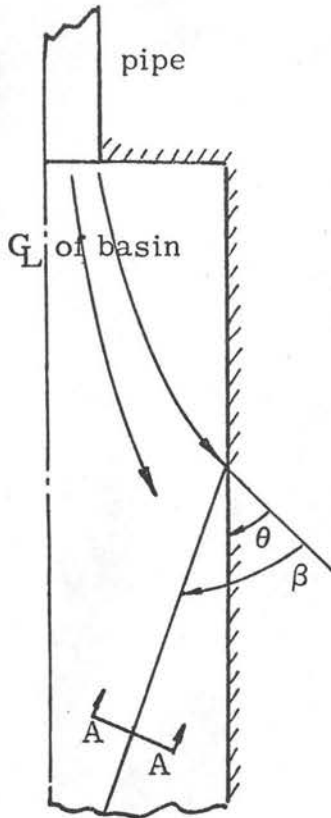
the water surface for only about two pipe diameters downstream and is therefore of limited use. Also, there is no way of estimating the direction or the magnitude of velocity in the flow field. Again the reader is referred to Chapter IV for further discussion and solution of this problem.

To estimate the energy loss associated with the standing wave, the relationship from Ref. 11 (also found in many other hydraulics tests),

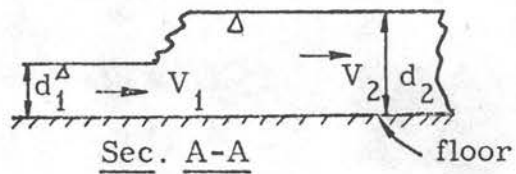
$$\Delta E = \frac{(d_2 - d_1)^3}{4 d_2 d_1} \quad (2-8)$$

was used. The flow depths on either side of the wave, d_2 and d_1 , were scaled from cross sections at Sta. 14.5 or 19.5 (about midway along the face of the jump at a sufficient distance away from the wall). The computed energy losses are shown in Table II. The maximum loss computed was 0.25 ft; the average loss was about 0.1 ft. This loss appears insignificant when contrasted with the overall loss exhibited by the energy lines for the upper portion of the basins.

Another correlation was attempted. Utilizing the relationships and curves established by Ippen (11), "Mechanics of Supercritical Flow", a comparison was made between the theoretical approach angle θ_t and the measured approach angle θ_m . Significant excerpts from this paper are shown below. Values of θ_m and β were scaled from Figs. 58 through 85; d_2 and d_1 were obtained as described in the previous paragraph. A comparison of θ_m and θ_t is shown in Table II. The agreement is excellent for the two runs with the rectangular approach pipe. Though not developed for circular approach pipe, the relationships appear to describe satisfactorily the flow with possibly the



PLAN VIEW



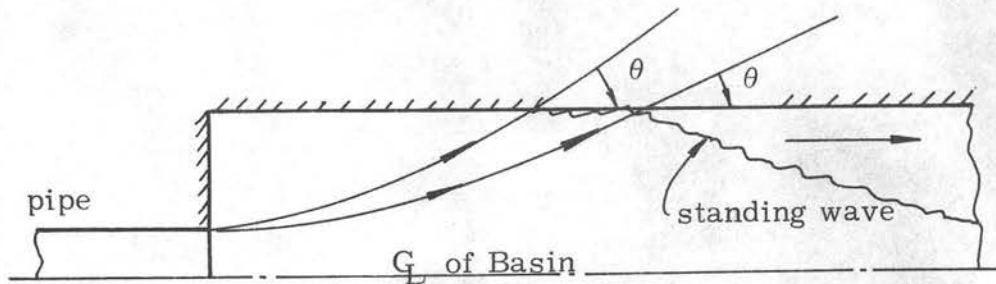
$$\frac{d_2}{d_1} = \frac{1}{2} \left[\sqrt{1 + 8 F_1^2 \sin^2 \beta} - 1 \right]$$

$$F_1 = \frac{V_1}{\sqrt{g d_1}} \quad ; \quad \frac{d_2}{d_1} = \frac{\tan \beta}{\tan(\beta - \theta)}$$

$$\tan \theta = \frac{\tan \beta \left(\sqrt{1 + 8 F_1^2 \sin^2 \beta} - 3 \right)}{2 \tan^2 \beta + \sqrt{1 + 8 F_1^2 \sin^2 \beta} - 1}$$

Equations and graphical solution to the above equations are shown on p. 287, Ref. 11 or p. 431, Ref. 3.

exception of the plain end pipe condition. According to Ippen's work, for given approach Froude numbers and depth ratios, there is a maximum value of θ beyond which the jump theoretically cannot form. This value was exceeded according to the CSU measurements. For some runs, it was observed that the standing wave tended to cling to the wall for a few feet prior to angling off into the flow (Fig. 21). This would effectively decrease θ (see sketch).



PLAN VIEW

The agreement between the predicted and measured angle of the standing wave is good enough to warrant the use of the Ippen criterion for prediction of the angle of the standing wave.

The relative depths of the standing waves, the ratio of the downstream depth divided by the upstream depth, d_2/d_1 , were computed from the measured data. These ratios were compared (Table II) with the predicted ratios based on the Ippen criterion. The predicted ratios are two to three times larger than the measured ratios; therefore, the Ippen criterion is not recommended for design use.

With the exception of run 17, the measured relative depths were restricted to a rather narrow range, 3.1 to 4.0. Despite a large variation of Froude number (1.2 to 2.8), the relative depth remained essentially constant.

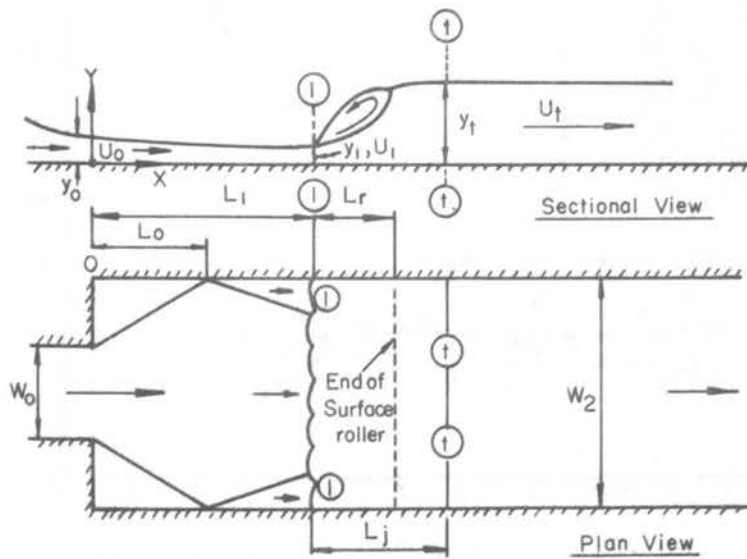
To determine the effect of relative width, W_2/W_0 , on the relative depth, a comparison was made between the relative depths of flow for basins with $W_2/W_0 = 7$, Preliminary Tests B just described, and relative depth of flow for basins with $W_2/W_0 = 4$, tests

described in Chapter III. For the six runs ($1.3 < \text{Froude number} < 2.3$, $W_2/W_0 = 4$) where sufficient data were collected to define the standing wave adequately, the relative depths varied from 3.6 to 4.1, essentially the same range as for the basins with $W_2/W_0 = 7$. It is apparent that the effect of relative width ratio is negligible, at least for the range of $4 < W_2/W_1 < 7$. There was no correlation between the relative depth and Froude number for either of the two series of tests. For design purposes, it is suggested that the relative depth d_2/d_1 be assumed constant and equal to 3.5.

As explained in Chapter VII, both the angle and the depth of the standing wave is necessary for the design of certain types of Class B basins.

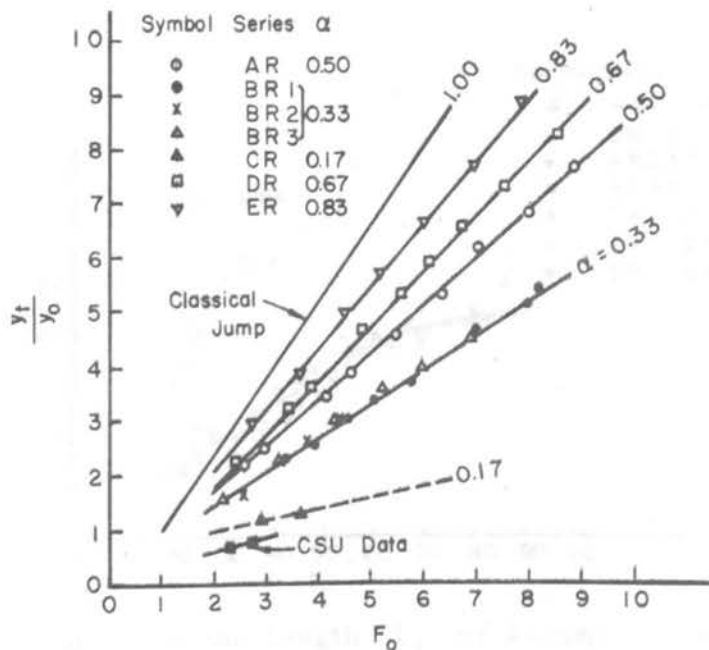
Recently, N. Rajaratnam and K. Subramanya (14) presented numerous empirical relationships for predicting the characteristics of hydraulic jumps downstream of abrupt symmetrical expansions. The jump that is similar to those observed in the CSU smooth basin studies was classified as an R-jump.

With a known discharge Q , outfall flow depth y_0 , outfall width W_0 , and basin width W_2 (see definition sketch, Fig. 88), relationships are given for predicting the sequent depth downstream of the jump (y_t), total bed shear (P_f) exerted by the flow on the floor between the outfall section and the hydraulic jump, and the distance from the outlet to the face of the jump, L_1 . Figures 1, 2, 5, and 7 from Ref. 14 are reproduced in this report as Figs. 88, 89, 90, and 91, respectively.



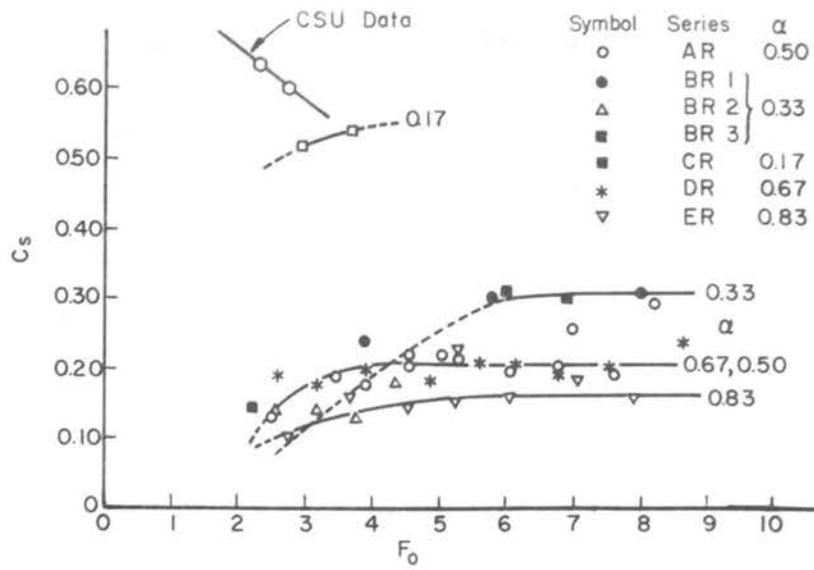
Definition Sketch for R-Jump
Reproduced from Ref. 14

Fig. 88



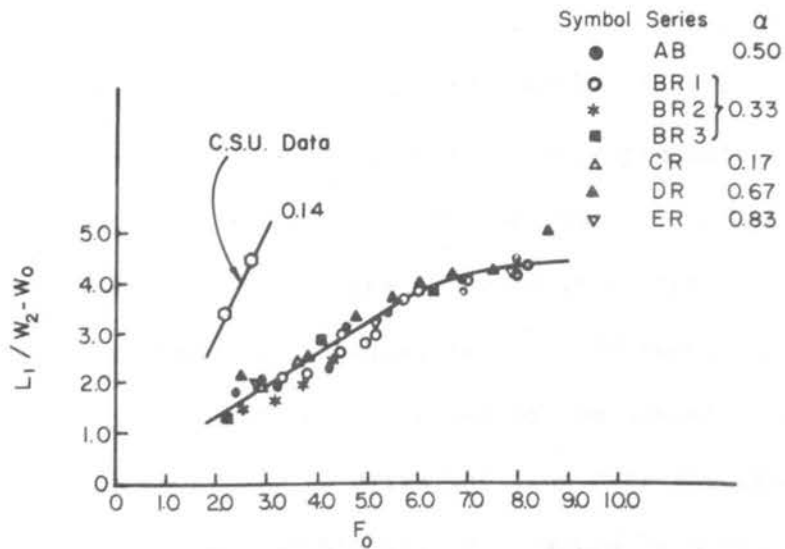
Variation of y_t/y_0 With F_0 for R-Jump
Reproduced from Ref. 14

Fig. 89



Study of the Consolidated
Shear Force Coefficient C_s
Reproduced from Ref. 14

Fig. 90



Study of the Length L_1 of R-Jump
Reproduced from Ref. 14

Fig. 91

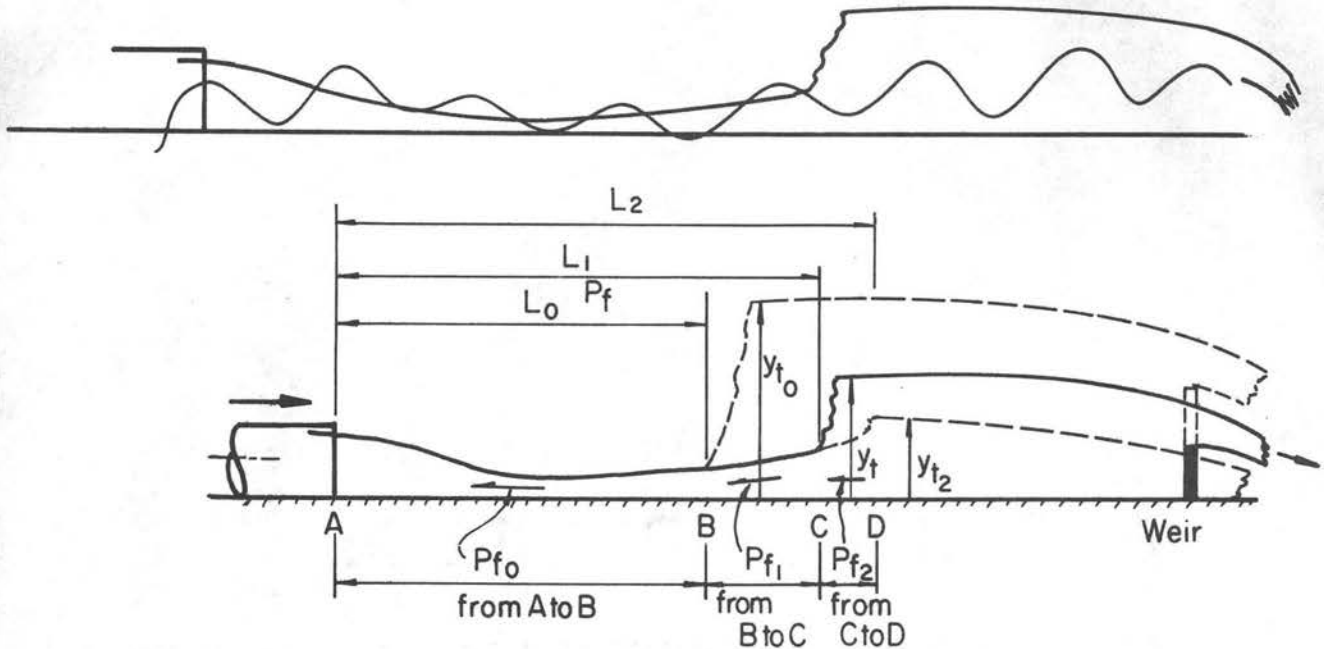
Two parameters are defined: the Froude number at the outfall, $F_o = \frac{Q}{W_o y_o \sqrt{g y_o}}$, and the ratio of the approach channel width to basin width, $\alpha = \frac{W_o}{W_2}$. The usual momentum equation, with modifying assumptions, is written between the outlet (Sta. 0.0) and Sta. t-t, a short distance downstream of the jump;

$$\frac{1}{2} \gamma W_o y_o^2 + \rho Q U_o = \frac{1}{2} \gamma W_2 y_t^2 + \rho Q V_t + \underbrace{P_f}_{C_s \rho Q U_o} .$$

In Fig. 89, the variation of y_t/y_o versus F_o , with α as a third parameter, is presented. This graph is supposed to be useful for predicting y_t , the sequent depth: i.e., for a given relative width α , approach flow depth y_o and approach Froude number F_o , y_t can be predicted. This is an illogical plot. The sequent depth y_t can only be a function of Q and downstream channel characteristics. Since the flow in this zone is subcritical, it is subject to downstream control.

Data from the only two CSU runs (28 and 29) that were approximately equivalent to experimental evidence presented in Ref. 14 are plotted in Fig. 89. F_o for the CSU runs was 2.3 and 2.7, and $\alpha = 0.14$. The apparent "fit" of the CSU data is deceptive. As one can clearly see from the sketch below, for the CSU runs, given a discharge Q , y_t is a function of the sum of the downstream weir height and the head necessary to drive the flow over the crest of the weir. If the weir had been 6" higher, y_{t_o} would be about 6" larger than y_t , and the jump face would have moved upstream to position B. That is, the jump would shift to such a position that a balance would be obtained between the upstream and downstream momentum flux and

pressure forces. If the weir had been removed, y_{t_2} would be smaller than y_t by about the depth of the weir, and the jump face would have moved downstream to D.



Centerline Section Through Basin

A similar argument can be used against the validity of Fig. 90.

With reference to the momentum equation,

$$\underbrace{\frac{1}{2} \gamma W_0 y_0^2 + \rho Q U_0}_{\text{constant}} = \underbrace{\frac{1}{2} \gamma W_2 y_t^2 + \rho}_{1} + \underbrace{P_f}_{2}$$

and the sketch above, the terms on the left side remain constant for a given set-up. The flow upstream of B is unaffected by downstream conditions; thus, the integrated floor shear P_{f_0} remains constant upstream of B. It is obvious by examining the equation above that there must be an interchange between terms 1 and 2 depending on the position of the jump face, i.e., P_f must vary in accordance with the tailwater depth. When the jump is at position C, the total bed shear is equal

to $P_{f_0} + P_{f_1}$; when at D, the total bed shear must equal $P_{f_0} + P_{f_1} + P_{f_2}$, and, therefore, cannot take on a constant value except for a given flow condition and geometry. The apparent approximate fit of the CSU data is again coincidental.

A more realistic appraisal of the relationships presented in Ref. 14 is shown by the poor fit of the CSU data in Fig. 91. This plot, of course, is the significant plot as far as basin design is concerned, i.e., what length of basin is required to ensure subcritical flow downstream of the basin?

Utilizing Fig. 91 for CSU run 28 ($F_0 = 2.3$), the predicted location of the hydraulic jump is 13 feet compared to the measured length of 29 feet. For run 29, the predicted location is 17 feet compared to the measured length of 39 feet.

This relationship obviously doesn't scale well. Though simplified empirical relationships are convenient, they must scale. For this reason, criteria presented in Ref. 14 are not recommended for design purposes.

The writer prefers a solution based on known hydraulic principles, as outlined and illustrated in Chapter VII.

Hydraulic Jump

Table II lists the location of the jumps for the various runs. For nearly identical discharges and tailwater conditions, the locations of the hydraulic jump for the standard transition and 45 degree wing wall end conditions are not perceptibly different. For the plain end condition, sufficient energy is dissipated in the outlet region to shift the jump 3 to 5 feet upstream. This again points out the efficiency of

the standard transition; i.e., the energy level at the end of the transition $2\frac{1}{2}$ feet downstream of the outlet is essentially the same as the energy level at the pipe outlet.

A comparison was made between the computed theoretical energy loss

$$\Delta E = \frac{(d_2 - d_1)^3}{4d_2d_1}$$

where d_2 and d_1 are the mean depths before and after the jump and the measured loss as determined by scaling the vertical discontinuity of the energy line at the point of the jump (see runs 10, 11, 16, 17, 22, 23, 28 and 29, Figs. 29 through 56). The results are listed in Table II. There was little agreement.

Several reasons for the discrepancy are apparent. These jumps are not ordinary jumps. They were quite unsymmetrical at times and always unsteady. The jump moved continuously up or down the channel. The tailwater would build up slightly, generally on one side of the channel and slowly push the jump upstream. In the tailwater region, surface flow in the upstream direction along the sides of the channel was noticeable. After the wave advanced a certain distance upstream, the whole jump would suddenly be swept downstream, sometimes as much as four feet.

At all times, the high speed flow was concentrated along the channel centerline. By assuming a mean depth of flow for d_1 , the computed energy loss would necessarily be too low. Lack of velocity profiles precluded any rigorous energy analysis.

The velocity distribution immediately downstream of the jump was not uniform. The velocity was concentrated along the center third

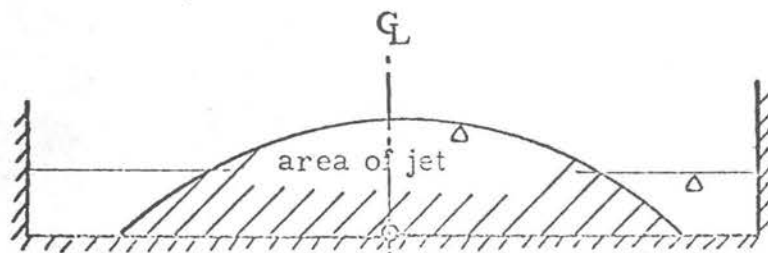
of the channel width. Prior to jet dispersion by normal frictional effects, the energy level would be higher than the plotted points indicated.

Energy Losses

A computer program was used for data reduction. Input included depth of flow at each vertical, the strip width, and the discharge passing through the gross section. Total energy and mean depth of flow were the output.

Pressure distribution correction (Ref. 15) or velocity distribution correction terms were not applied to this data. The energy was computed by formula 2-2, $E = \frac{(Q/A)^2}{2g} + y$. The depth y was obtained by dividing the flow area by the channel width. At the outlet of the circular pipe, it was necessary to add the 0.15 ft vertical discontinuity, the depth of corrugation, to the energy quantity.

For situations where the jet width did not fill the complete width of the basin (Sta. 2.0 and 4.5), the area through which the water passed had to be estimated. The operator examined the plotted section and estimated the location of the jet edge. If the total area of the section had been used for the velocity computation ($V = Q/A$), the result would have been gross underestimate of the velocity head



SECTION THRU BASIN

term. If the area assumed was too small, the result was an excessive velocity head and a consequent apparent (but impossible) gain of energy (run 10 is an example). Also, for this series of runs, there is no way of estimating the effect of the direction of flow on the magnitude of the energy. With the exception of Sta. 2.0 for the runs using the standard transition, the energy points shown at Sta. 2.0 and 4.5 are of no value. They are presented merely because data were taken at these stations. The centerline depths and mean depths are correct.

By the time the water had reached Sta. 9.5 or 14.5, the flow was fairly well oriented downstream, and, though some transverse flow was noticeable (necessary to maintain the oblique standing wave in the smooth basins), the energy computations should be reasonably valid.

Over the field of roughness elements, a slight underestimate of the energy is probable. After striking the first 6 to 10 rows of elements, the flow tended to stabilize above the angles and flow over them as though they were a rough floor. The result was a zone of low velocity in among the elements. No good way of estimating the true depth of the flow is available, so the gross area was used for computation.

Several results appear obvious: even without the roughness elements (runs 10, 11, 16, 17, 22, 23, 28, and 29), a large portion of the energy is dissipated in the upper portion of the basin. With reference to Chapter IV, the estimated outlet energy based on gross flow parameters and y is too high. The remaining portion of the apparent loss is associated with a much higher Darcy-Weisbach friction loss in the non-uniform, rapidly varied flow region than is usually assumed.

In situations where the concentrated flow can be spread laterally and consequently flows at a shallower depth, the small

roughness elements are quite effective in dissipating kinetic energy. A major portion of the energy is dissipated in the first few rows of elements. After passing through and over the first 4 to 10 rows of elements, the flow appears to ride up over the angles. Though not apparent to the eye, an undular jump occurs followed by subcritical flow. After this occurs, the angles are much less efficient and have the effect of a roughened floor rather than individual impact blocks. The significant fact is that the elements can cause the jump to occur and thus, significantly reduce the velocity of the flow.

Preliminary Tests C

After completion of Preliminary Tests B, several miscellaneous experiments were carried out.

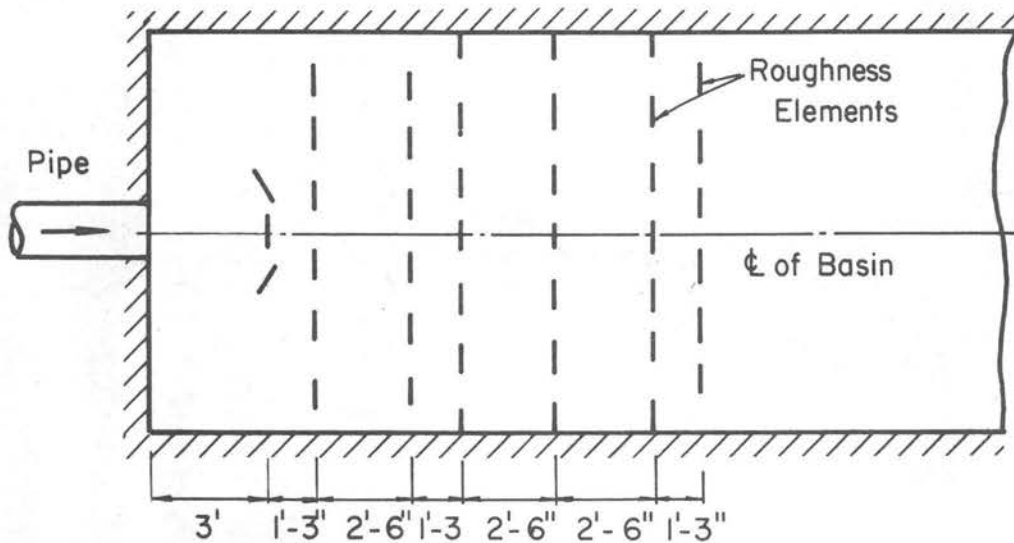
Run 39

An examination of the energy lines for the roughened basins indicated that only the first few rows of elements were effective. It appeared that the first few rows of elements triggered a hydraulic jump resulting in subcritical flow over the remainder of the elements. The depth of the subcritical flow was controlled by the downstream measuring weir as previously explained.

The following experiment was conducted to determine the number of rows of elements required to ensure subcritical flow within the field of elements.

The basin set-up used for run 33, Preliminary Tests B, (1.5 ft square approach pipe, basin width 10.5 ft, 9 in. x 2½ in. roughness elements) was reconstructed and subjected to a discharge of 23 cfs.

The angles were systematically removed a row at a time until a well defined jump became obvious downstream of the angles. Nine rows of angles were necessary to ensure that the jump fell in the field of roughness. An unsteady 1. level jump was visible upstream of the last one or two rows of angles. With eight rows, the jump shifted about two feet downstream and was quite distinct, though unsteady in position. By doubling the spacing of some of the rows of angles and



PLAN VIEW

rotating two of the angles in the first row so that they would be normal to the flow, it was possible to reduce the number of rows to seven and still maintain the jump in the roughness area. Several arrangements were tried. The one shown above seemed the most efficient.

The larger gap between the rows allowed the water previously thrown into the air to drop back to the floor and thus be in position to strike the following row at an angle more favorable for energy

dissipation. This spreading out of rows reduced the number of roughness elements from 55 to 42.

Runs 40 through 42

The purpose of these runs was to determine the effectiveness of the roughness elements in a narrow channel as compared to the effectiveness of the elements in a wide channel. For these runs, the channel width was reduced to six feet. The relative width, W_2/W_0 , was four, compared to seven for the similar runs 32 and 33, described previously.

The spacing and number of elements are shown in the inserts of Figs. 92, 93, and 94.

During runs 40 and 41, it was observed that high speed flow concentrated along the sides of the basin. This was due to the large pile-up and consequent runoff along the sides and the smooth floor condition (4 in. gap) that existed between the angle roughness and the wall (see insert, Fig. 93). To overcome the latter problem, 2 in. x 2 in. x 4 in. blocks were nailed to the wall flush with the floor in line with alternate rows of roughness elements plugging the gap (insert, Fig. 94). Following this modification, data were taken again at the higher discharge, run 42. At this time, several point velocities were measured at Sta. 10.3, 14.8, 30, and 40 with a Price current meter.

The data collected during these runs were processed and plotted in the same manner as the data described for Preliminary Tests B. The energy lines are shown in Figs. 40, 41, and 42.

It is apparent from the energy line configuration shown in Fig. 96 that the elements were very effective even in the narrower basin. A comparison between this energy line and the one displayed in Fig. 52 for an equivalent flow in the 10.5 ft wide basin shows that the energy level is about 25% higher in the narrow basin, the result of the channel being narrower, rather than any inefficiency of the elements. The minimum specific energy for 23 cfs in the six ft wide channel is 1.15 ft, approximately the height of the energy line shown in Fig. 94, compared to the minimum specific energy of 0.8 ft for 23 cfs in a 10.5 ft wide channel.

Velocity Distribution

At Sta. 14.5, the velocity at the elevation of the top of the angles was measured. At this elevation the meter was positioned midway between the rows of angles. Very low velocity is apparent at this elevation (see Fig. 103). In general, the velocity distribution at Sta. 29.5 and 39.5 was very uniform, evidence substantiating a prior assumption of uniform velocity downstream of the angle field.

Run 43 - High Tailwater

The effect of high tailwater was observed during this run. Downstream of the basin, previously described for run 42, a timber dam was constructed with sufficient height to cause tailwater of 18 inches at Sta. 29.5.

Figures 112 and 113 are photographs of the basin operating at a discharge of 23 cfs. The thalweg attached to the left side of the basin, and reverse flow up the right side of the basin was evident.

Velocities measured with a Price meter are shown in Fig. 104. Although the mean exit velocity must have been at least 14 fps, the maximum velocity measured at Sta. 10.2 was about 6 fps and at Sta. 14.5 was about 7.8 fps. The thalweg may have been centered between the measured verticals at Sta. 10.2. Extreme difficulty in stabilizing the Price meter may also have contributed to the low measured velocity. In any event, the velocity decay is rapid. Despite the large depth of flow over the roughness elements, they were quite effective.

Runs 44 through 50 - Low Tailwater

After completion of run 43, the dam and measuring weir were removed from the flume, thus reducing tailwater to a minimum. The variable during these runs was the number of rows of roughness elements. Each pattern of elements was subjected to one discharge, about 23 cfs.

Data for energy computation and velocity plots were collected at Sta. 10.3, 14.8, 30, and 40. An Ott minor meter mounted on the instrument carriage probe was used for velocity measurements.

The discharges were obtained by averaging the integrated discharges at Sta. 29.5 and 39.5. Because of the high degree of turbulence, entrained air (conditions under which the Ott meter tends to overestimate velocity) and the unknown flow area over the angle field, the integrated discharges at Sta. 10.5 and 14.9 always indicated a discharge that was too high and therefore were not included in the average.

Figures 92 through 102 show the energy lines for the various runs. Figures 103 through 111 are plots of the measured velocity at the various stations. Other run data are listed in Table III.

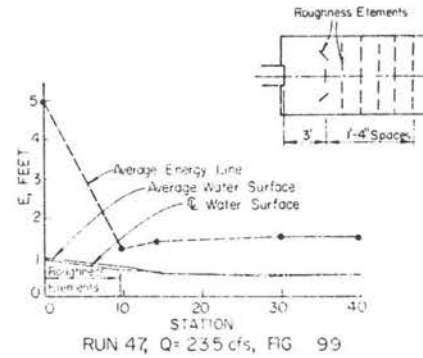
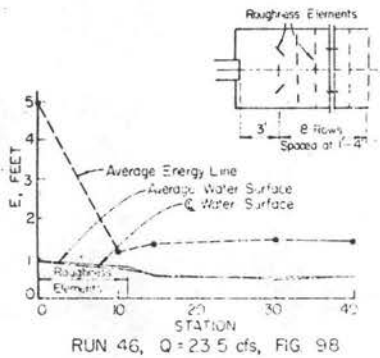
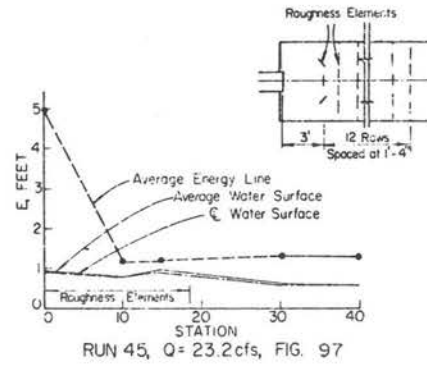
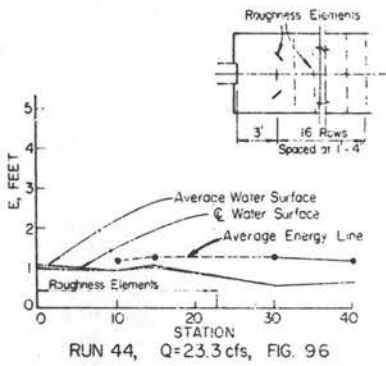
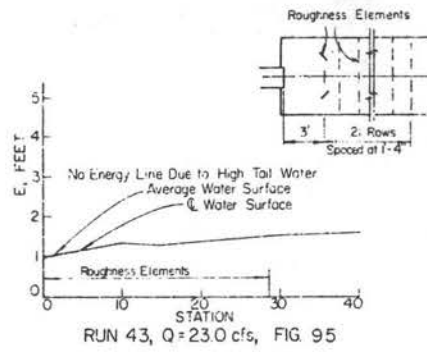
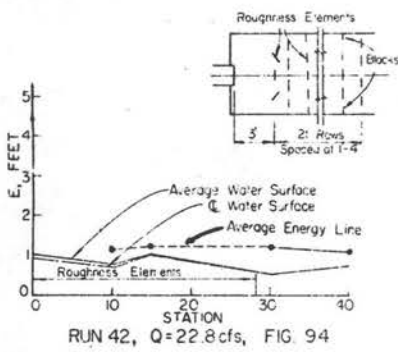
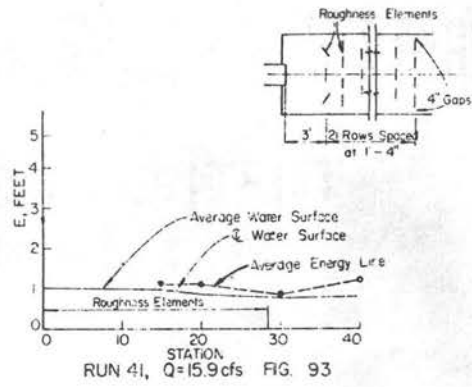
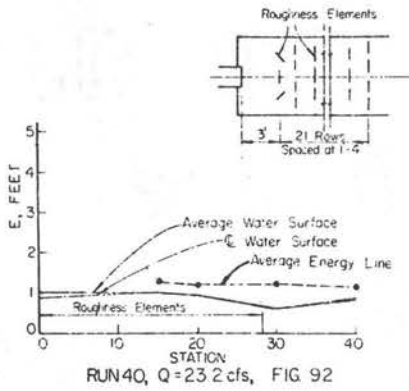
TABLE III - FLOW PARAMETERS - TESTS C

Run No.	No. of Rows of Angles	Q integ @ Sta. 29.5 (cfs)	Q integ @ Sta. 39.5 (cfs)	Q ave (cfs)	Mean Depth @ Outlet (ft)	Remarks
40	21			23.2*	1.01	measuring weir in place
41	21			15.9*	----	weir in place
42	21			22.8*	1.02	weir in place
43	21	----	----	----	----	1'-6" tailwater
44	16	23.4	23.2	23.3	1.01	weir removed
45	12	23.3	23.1	23.2	0.98	weir removed
46	8	23.5	23.5	23.5	0.99	weir removed
47	6	23.8	23.2	23.5	0.99	weir removed
48	4	22.7	22.4	22.5	0.99	weir removed
49	2	23.1	23.4	23.3	0.99	weir removed
50	0	25.3	23.4	24.3	1.00	weir removed

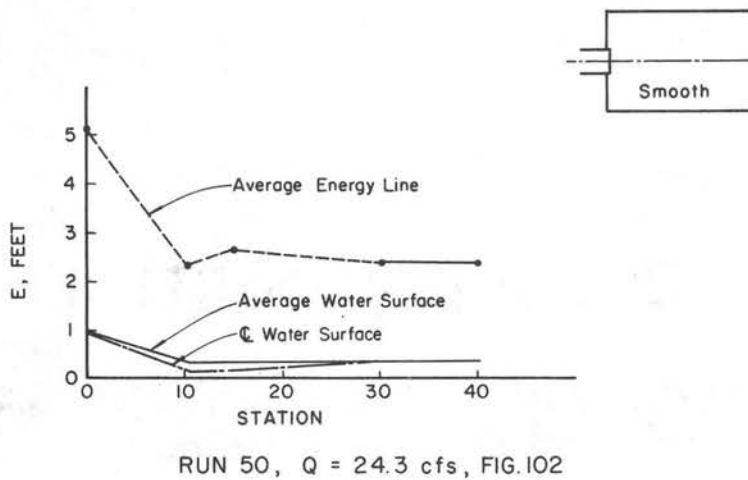
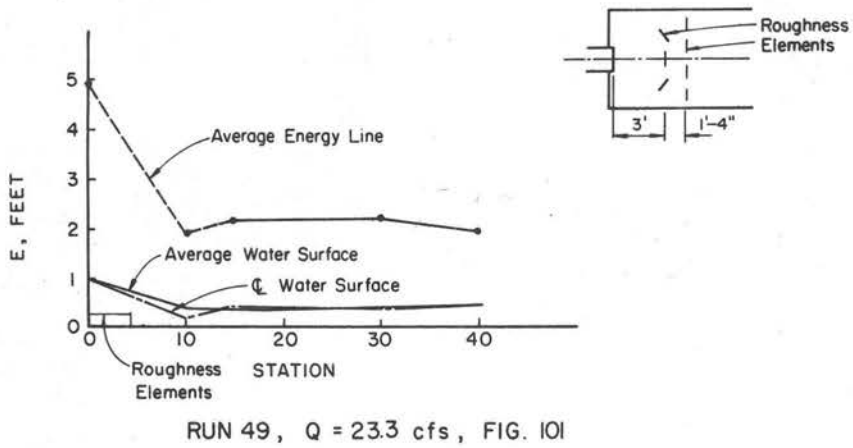
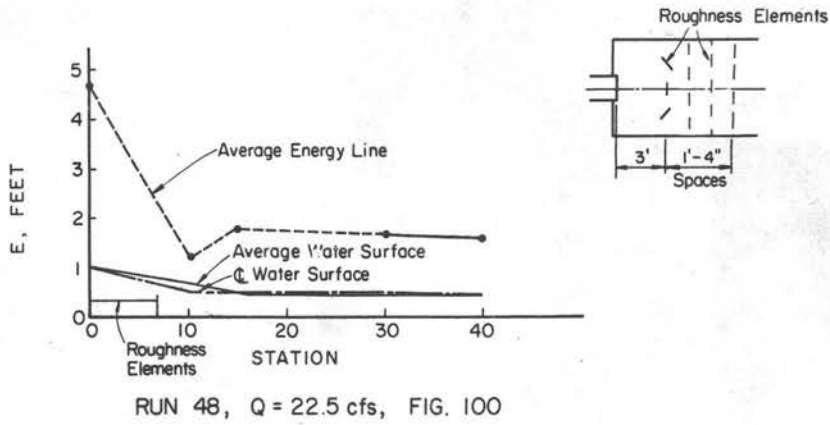
* Discharge measured by notched weir.

Note: 6'-0 wide x 48'-0 basin with vertical walls, typical run No. 40 through 50

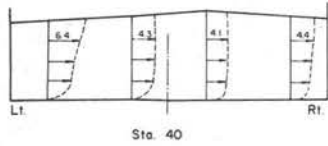
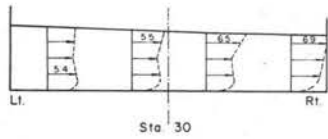
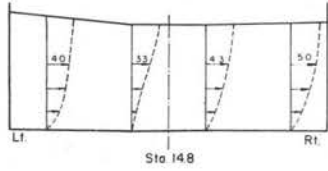
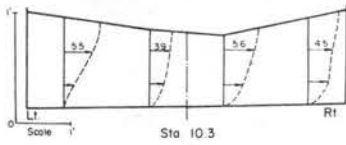
$$F_o = \frac{V_o}{\sqrt{gy_o}} \approx 2.8 \text{ all runs}$$



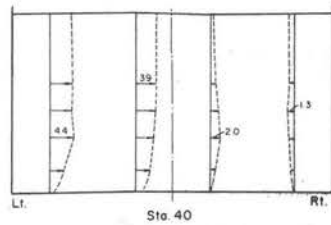
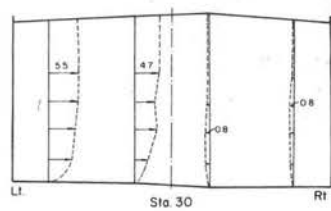
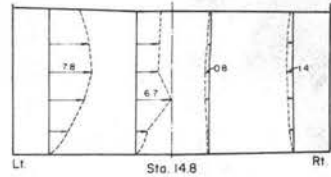
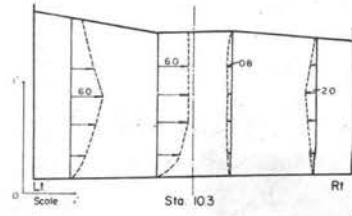
Energy Line and Water Surfaces



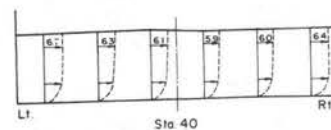
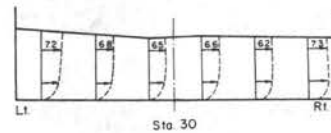
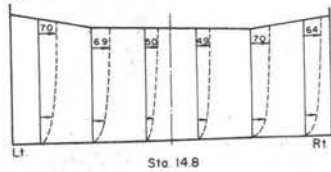
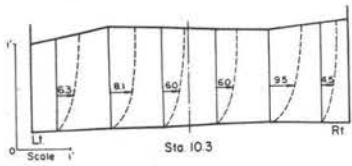
ENERGY LINE AND WATER SURFACES



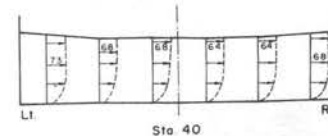
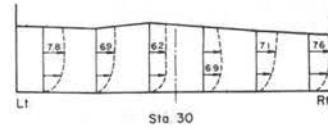
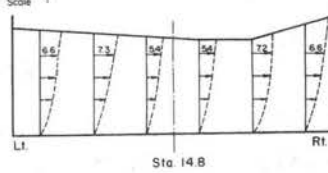
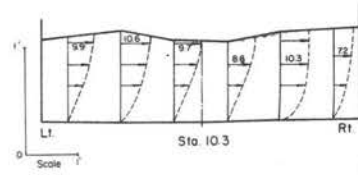
VELOCITY DISTRIBUTION
 RUN 42, Q = 22.8 cfs, FIG. 103
 21 ROWS OF 9" x 2 1/2" ELEMENTS



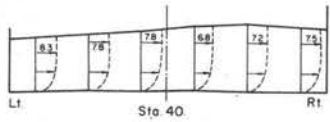
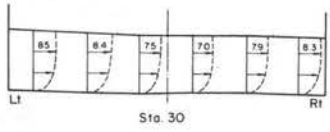
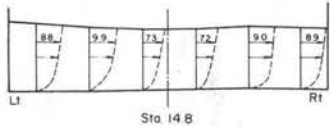
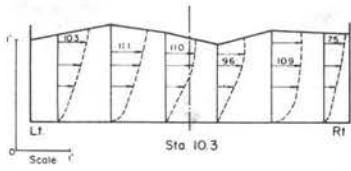
VELOCITY DISTRIBUTION
 RUN 43, Q = 23 cfs, FIG. 104
 21 ROWS OF 9" x 2 1/2" ELEMENTS



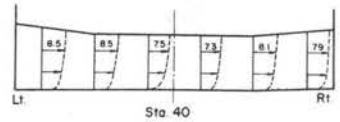
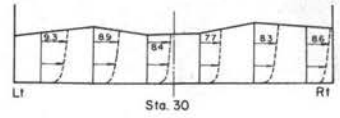
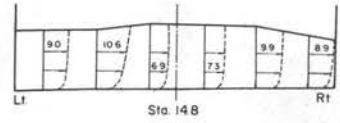
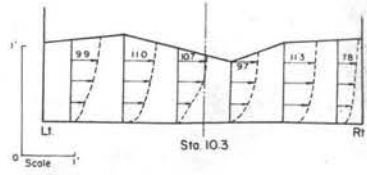
VELOCITY DISTRIBUTION
 RUN 44, Q = 23.3 cfs, FIG. 105
 16 ROWS OF 9" x 2 1/2" ELEMENTS



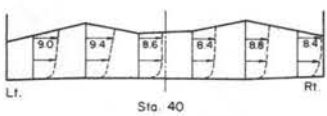
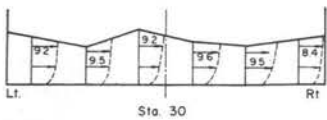
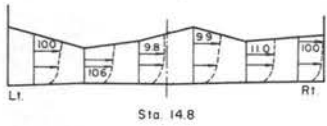
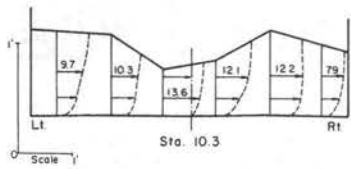
VELOCITY DISTRIBUTION
 RUN 45, Q = 23.2 cfs, FIG. 106
 12 ROWS OF 9" x 2 1/2" ELEMENTS



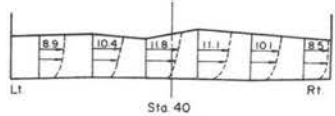
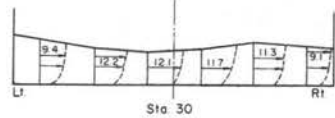
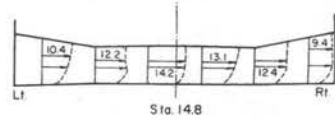
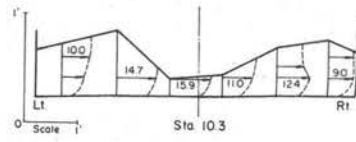
VELOCITY DISTRIBUTION
 RUN 46, Q = 23.5 cfs, FIG. 107
 8 ROWS OF 9" x 2 1/2" ELEMENTS



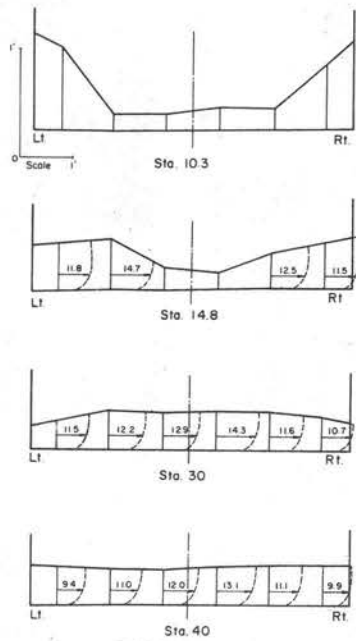
VELOCITY DISTRIBUTION
 RUN 47, Q = 23.5 cfs, FIG. 108
 6 ROWS OF 9" x 2 1/2" ELEMENTS



VELOCITY DISTRIBUTION
 RUN 48, Q = 22.5 cfs, FIG. 109
 4 ROWS OF 9" x 2 1/2" ELEMENTS

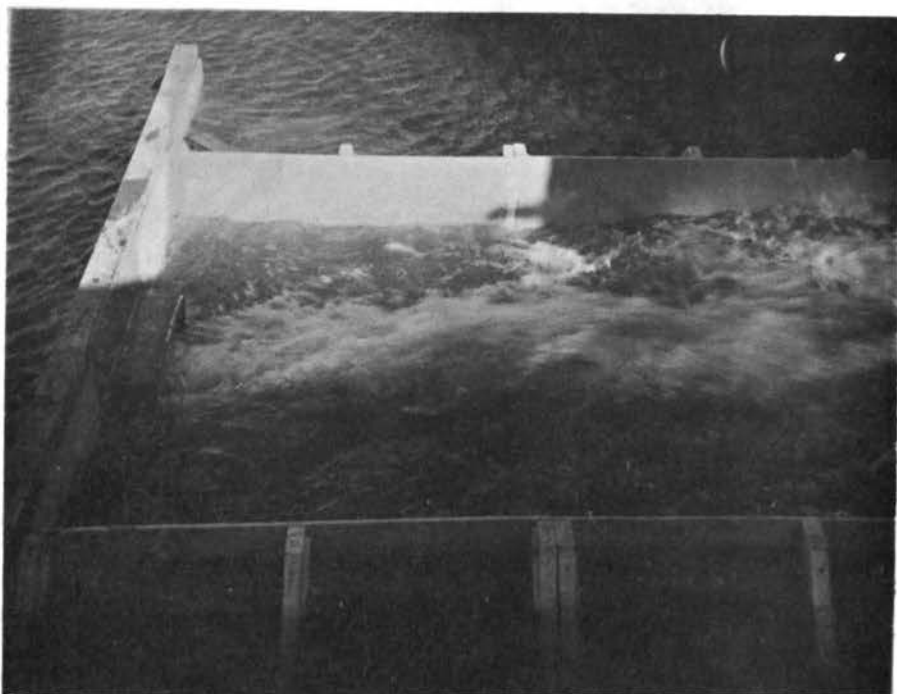


VELOCITY DISTRIBUTION
 RUN 49, Q = 23.3 cfs, FIG. 110
 2 ROWS OF 9" x 2 1/2" ELEMENTS



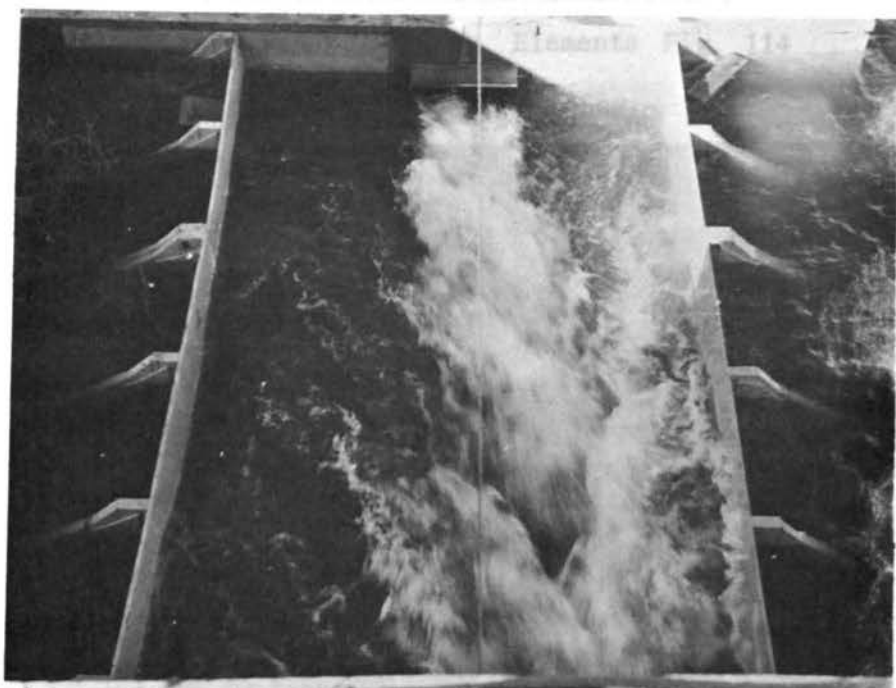
VELOCITY DISTRIBUTION

RUN 50, Q = 24.3 cfs FIG. III
SMOOTH FLOOR



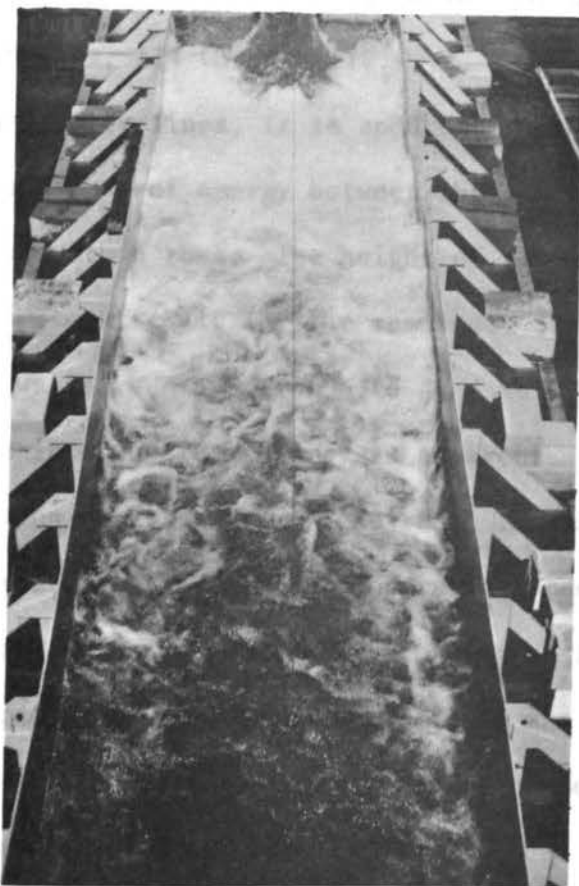
2½" x 9" Elements Submerged Flow
Run 43 Q = 23 cfs

Fig. 112

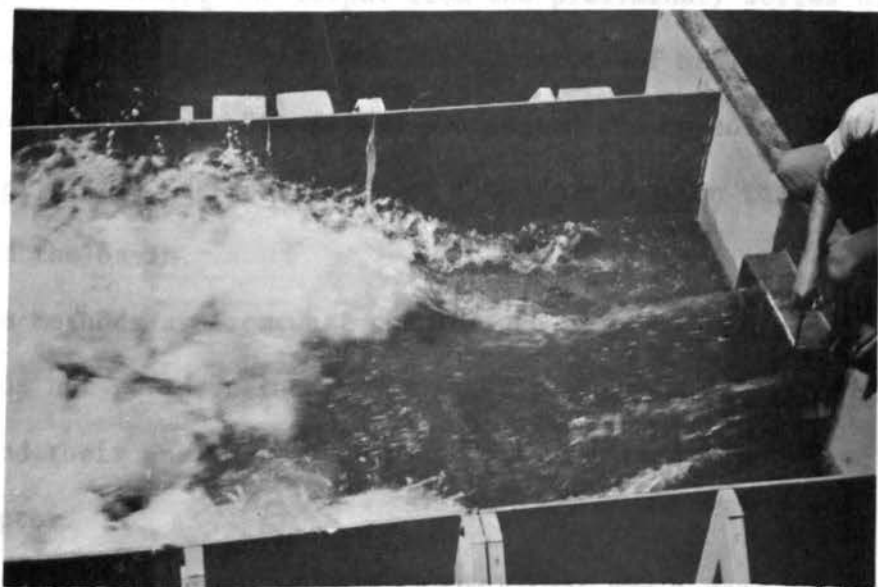


2½" x 9" Elements Submerged Flow
Run 43 Q = 23 cfs

Fig. 113



16 Rows of $2\frac{1}{2}$ " x 9" Elements Fig. 114
Run 44 $Q = 23.3$ cfs



16 Rows of $2\frac{1}{2}$ " x 9" Elements
Run 44 $Q = 23.3$ cfs

Fig. 115

Several photographs of flow during these runs and descriptive titles are shown in Figs. 114 through 117.

By comparing energy lines, it is apparent that there is little variation in the magnitude of energy between the run with 21 rows of elements and the run with 6 rows. The height of the energy line varies significantly and systematically for the remainder of the basins, i.e., as the number of rows is reduced (from 6 to 4, 4 to 2, and 2 to 0), a systematic increase in downstream energy is apparent.

After examining the data from these runs, it was apparent that basins with four or six rows of elements operating under minimum tail-water conditions were effective energy dissipating basins. The encouraging output from this abbreviated set of runs was the motivating factor for the development of a systematic design procedure for Class C basins presented in Chapter V and Chapter VII.

Summary

After examining the output from the preliminary series of tests, methods of design for each of the three classes of basins, Class A, B, and C, were developed. The design procedures are based on the impulse-momentum principle and continuity of flow from section to section throughout the basin.

The methods are somewhat complex and require several additional design aids not yet described. For these reasons, a description of the methods and their application to practical problems is deferred to the final chapter.

Criteria discussed in this chapter that are a part of the design procedure are:

Design aids are described in the next four chapters.

(a) The Blaisdell criterion for the design of the wall flare, Eq. 1-2.

(b) Ippen's relationship for predicting the angle of the face of standing waves.

(c) The relative depth ratio $d_2/d_1 = 3.5$ predicting the downstream depth of standing waves.

(d) Equation 2-7 for predicting the height of wave runup on the basin walls.

Additional generalized criteria that are required include:

1) Coefficients β_1 and β_2 , factors applied to terms in the usual momentum equations, which correct for non-hydrostatic pressure distribution and non-uniform velocity distribution at the outfall section of a culvert. The culvert outlet is the starting point for all computations, and therefore it is essential that these quantities be correct.

Additionally, sufficient data were gathered at this time to determine where the large loss of energy occurred in the region adjacent to the outlet section.

2) Dimensionless water surface profiles and velocity vectors for the expanding jet downstream of an abrupt expansion.

3) Approximate drag coefficients for roughness elements of known dimension and pattern.

4) A design criterion for predicting the rate of decay of velocity and approximate width of the expanding jet downstream of culvert outlets where high tailwater prevails.

The studies conducted for the purpose of establishing these design aids are described in the next four chapters.

Chapter III

ENERGY AND MOMENTUM CORRECTION FACTORS

Problem Statement

The design procedure requires an accurate estimate of the momentum flux and pressure force term, computed for a specific discharge, at the outfall section of circular and rectangular culverts. The primary purpose of the experiments described in this chapter was the evaluation of these factors.

The precise description of the energy line in the region adjacent to the outlet, though not required for design, was also a matter of interest. The data shown in Chapter II indicated that a large loss of energy occurred. The question that arose was, did the loss occur in the rapidly varied flow zone from the outlet to about two or three pipe diameters downstream, or from the latter location on downstream in the shallow, high-speed flow? The data described in Chapter II were not sufficiently detailed to determine this.

The specific energy equation for non-uniform flow can be written as $E = \alpha_1 \frac{(Q/A)^2}{2g} + \alpha_2 y$ where α_1 and α_2 are corrective coefficients that compensate for the variable distribution of velocity and the non-hydrostatic pressure distribution. α_1 is always larger than 1.0 and, for usual pipe flow, generally varies from 1.01 to 1.10. Since α_1 was assumed to be 1.0 for the analysis in the previous chapter, the kinetic energy term should be slightly smaller. Any α_1 greater than 1.0 is a correction in the wrong direction. The only

possibility for an overestimate of specific energy is in the piezometric head term, y .

The most comprehensive treatment of this subject was found in Ref. 15, "Pressure and Resistance Characteristics of a Model Pipe Culvert," by J. L. French. The piezometric grade line was established for the interior uniform flow zone within the pipe and linearly extended through the plane of the outlet. A ratio of the elevation of the piezometric line at this plane over the depth of flow was found. The resulting ratio was designated as the correction factor. A relationship was established between the Froude number at the outlet section and the correction factor. Information is given for both rectangular and trapezoidal discharge channels downstream of a circular approach pipe for the condition where the jet is supported on the bottom by a floor and for the condition where the jet was allowed to fall freely without bottom support. Values of the correction factor ranged from 0.57 to 0.85.

This paper provides appropriate correction factors for the pressure head term of the specific energy equation for circular pipes.

The design methods developed during the CSU study require similar correction factors for the pressure quantity in the momentum equation for both circular and rectangular approach pipes.

A comprehensive experimental program was devised whereby the energy level and momentum at the outlet and at successive stations throughout the basin were evaluated by integrating quantities obtained by direct measurement within the flow field. These quantities were then used to deduce appropriate correction factors.

Theoretical Development

At any cross section, be it open channel or closed conduit, the amount of energy per pound of water at any point in the section is the sum of the potential and kinetic energy. In usual hydraulic nomenclature, the energy equation is

$$H = \alpha_1 \left(\frac{P}{\gamma} + y \right) + \alpha_2 \frac{V^2}{2g} \quad (3-1)$$

where

P = pressure intensity at the point in lbs/sq ft,

γ = unit weight of the fluid in lbs/cu ft,

y = elevation in ft of the point with respect to the datum,

V = magnitude of the velocity vector at the point in ft/sec,

g = gravitational acceleration in ft/sec², and

α_1 and α_2 = corrective coefficients already described.

Where non-uniform steady flow conditions prevail, it is convenient to evaluate the power of the flow at a section. This is accomplished by multiplying the quantity of energy per pound of water by the number of pounds of water per second which pass through the incremental area surrounding the point, i.e.,

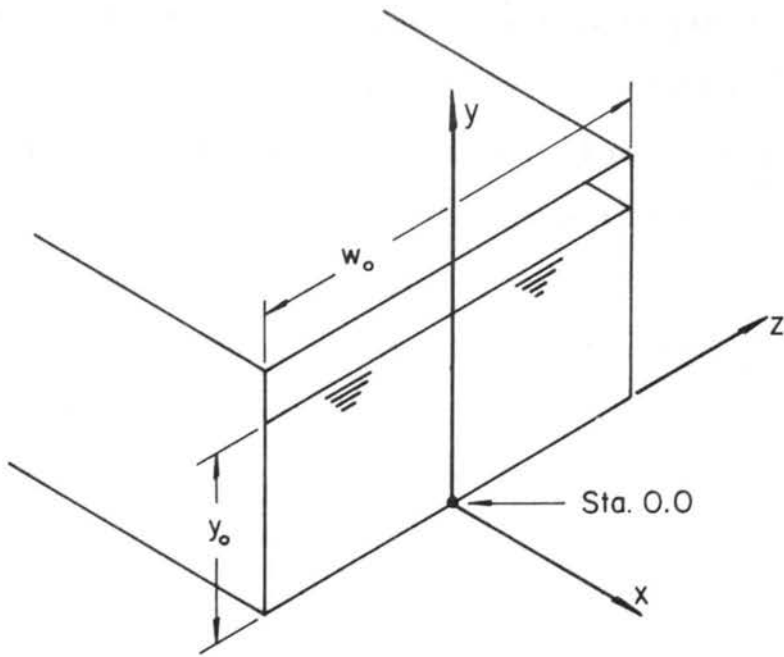
$$\Delta P = \left[\left(\frac{P}{\gamma} + y \right) + \frac{V^2}{2g} \right] \gamma dQ \quad (3-2)$$

Referring to Fig. 116,

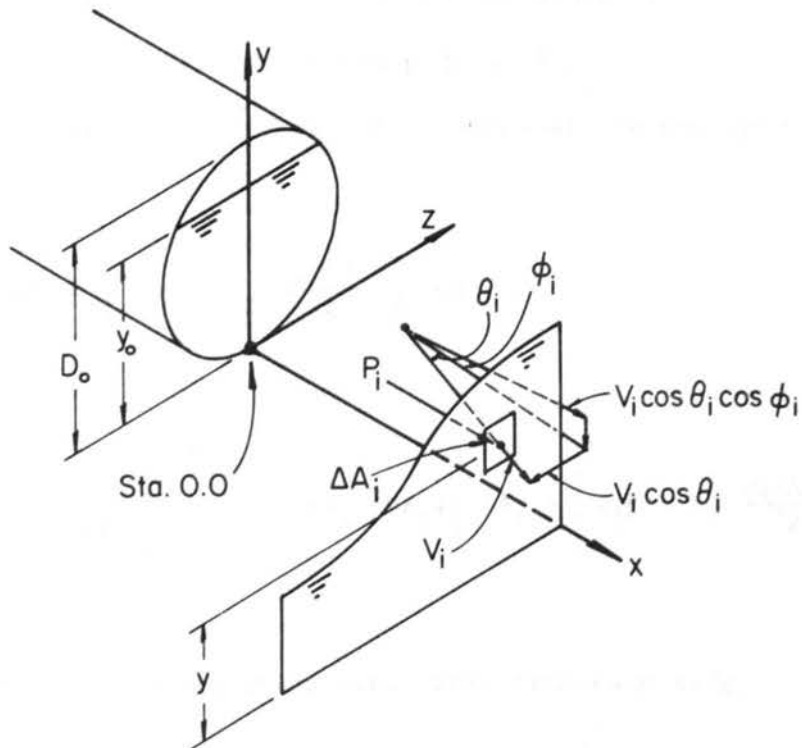
$$dQ_i = V_i \cos \theta_i \cos \phi_i \Delta A_i \quad (3-3)$$

At any cross section, the total power available is

$$P = \sum_i \left[\left(\frac{P}{\gamma} + y \right)_i + \frac{V_i^2}{2g} \right] \left[\gamma V_i \cos \theta_i \cos \phi_i \right] \Delta A_i \quad (3-4)$$



Definition Sketch: Rectangular Pipe



Definition Sketch: Circular Pipe

Fig. 116

where the sum is taken over the entire section in question. The subscript i implies that all quantities are associated with an incremental area, i . The sum sign is usually shown as an integral, but of necessity, the equation must be in differential form if measured quantities are used to evaluate P .

The specific energy equation that is the most convenient is made up of gross flow quantities,

$$H = \alpha_1 y + \alpha_2 \frac{(Q/A)^2}{2g} \quad (3-5)$$

where

Q = total discharge passing through the cross section ft^3/sec ,

A = wetted cross-sectional area ft^2 , and

y = mean depth of flow = Q channel width ft .

Other variables have been identified previously.

To convert this to power, it is necessary to multiply H by γQ ,

$$P = HQ\gamma = \left(\alpha_1 y + \alpha_2 \frac{(Q/A)^2}{2g} \right) \gamma Q \quad (3-6)$$

Equating Eqs. 3-5 and 3-6,

$$\sum_i \left[\left(\frac{P}{\gamma} + y \right)_i + \frac{V_i^2}{2g} \right] \left[\gamma V_i \cos\theta_i \cos\phi_i \Delta A_i \right] = \left[\alpha_1 y + \alpha_2 \frac{(Q/A)^2}{2g} \right] \gamma Q \quad (3-7)$$

Canceling out γ , and equating like terms from each side,

$$\alpha_1 y Q = \sum_i \left[\left(\frac{P}{\gamma} + y \right)_i \left(V_i \cos\theta_i \cos\phi_i \Delta A_i \right) \right]$$

or

$$\alpha_1 = \frac{\sum_i \left[\left(\frac{P}{\gamma} + y \right)_i (V_i \cos \theta_i \cos \phi_i \Delta A_i) \right]}{(y) (Q)} \quad (3-8)$$

and

$$Q \alpha_2 \frac{(Q/A)^2}{2g} = \sum_i \left(\frac{V_i^2}{2g} \right) V_i \cos \theta_i \cos \phi_i \Delta A_i$$

or

$$\alpha_2 = \frac{\sum_i (V_i^3 \cos \theta_i \cos \phi_i \Delta A_i)}{Q^3/A^2} \quad (3-9)$$

Switching to the impulse and momentum principle and using a similar line of reasoning, it can be shown in differential form that the external force and momentum flux at any cross section is

$$F = \sum_i P_i \Delta A_i + \sum_i \rho V_i^2 \cos^2 \theta_i \cos \phi_i^2 \Delta A_i \quad (3-10)$$

where ρ = mass density, $\frac{\gamma}{g}$, (lbs sec²/ft³).

The convenient expression of momentum and pressure force in terms of gross flow quantities is

$$F = \beta_1 \frac{\gamma Y^2}{2} W + \beta_2 Q \rho V \quad (3-11)$$

where

W = width of wetted section,

β_1 = correction factor which compensates for the non-hydrostatic pressure distribution, and

β_2 = correction factor which compensates for the non-uniform distribution of velocity.

Equating Eqs. 3-10 and 3-11 and sorting out similar terms, it is easily shown that

$$\beta_1 = \frac{\sum_i P_i \Delta A_i}{y \left(\frac{\gamma}{2}\right) A} \quad (3-12)$$

and

$$\beta_2 = \frac{\sum_i \left[V_i^2 \cos^2 \theta_i \cos_i^2 \phi \Delta A_i \right]}{Q^2/A} \quad (3-13)$$

where

A = the wetted area at the outfall section for either circular or rectangular conduits.

Equations 3-4 and 3-10 are general. There are no limiting assumptions; i.e., if the quantities can be measured precisely and if the incremental areas are taken small enough so that the summation is a good approximation of the integral, the quantities found are correct for that particular cross section.

The procedure used to evaluate these quantities was to divide each cross section into a grid, measure the velocity, total head and elevation at the centroidal point of each incremental area, deduce the pressure at the point by subtracting the sum of the velocity head and elevation head from the measured total head and perform the various summations. Yaw and pitch probes were used in combination to obtain the yaw (horizontal) angle and pitch (vertical) angle of the velocity vector simultaneously with the measurements of total head and velocity magnitude at each grid point.

Using the measured data, Eqs. 3-8, 3-9, 3-12 and 3-15 were solved. A large portion of the computation was performed on the CSU CDC 6400 computer. An example showing the computational sequence commencing with experimentally obtained data and carried through to the final quantities is shown in Appendix A.

Experimental Apparatus

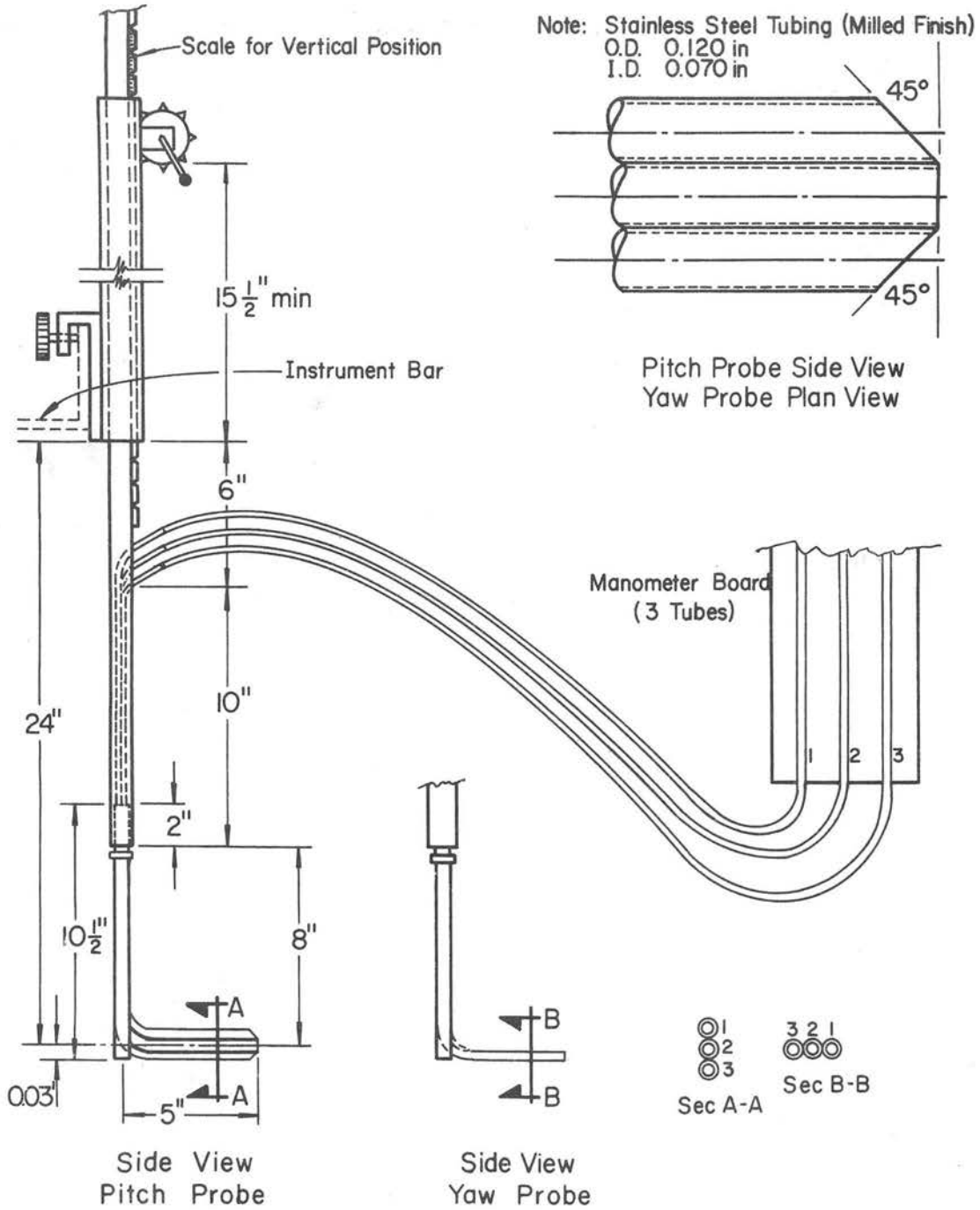
After much consideration, a three tube yaw probe used in conjunction with a three tube pitch probe was selected for velocity measurements. Some of the factors considered in the selection of these probes were ease of use, duplication of calibration data for velocities ranging from 3.0 fps to 10 fps, ease of construction of the instruments, ease of obtaining yaw and pitch angle of the flow, and the fact that the center tube of the probe could be used as a total head tube independent of the bounding tubes.

A thorough description of the development of the probes, including calibration technique and recommended operating procedure is given in Ref. 16, prepared by N. Rajaratnam and D. Muralidhar. The following is taken from this reference and is repeated here for clarity.

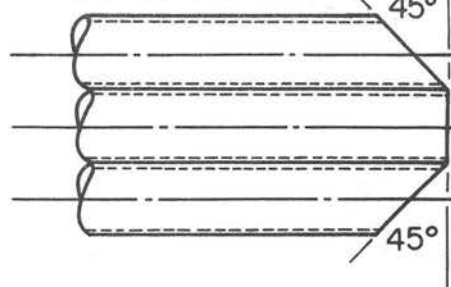
Three probes were constructed and calibrated. The yaw probe and first pitch probe were constructed of three lengths of stainless steel tubing of 3 mm external diameter and an internal diameter of 1.8 mm. The three tubes were soldered together side by side in a horizontal plane for the yaw probe, in a vertical plane for the pitch probe. The nose of the probes was milled so that the face of the central tube was perfectly flat and the side tubes were chamfered at an angle of 45° . (A detail drawing of the probes and supporting equipment constructed for the CSU study is shown in Fig. 117.)

An additional pitch probe was constructed to about half scale with 1.3 mm external diameter and 0.8 mm internal diameter steel tubing.

All three probes were calibrated in the potential core of a plane turbulent wall jet produced by a deeply submerged sluice gate.

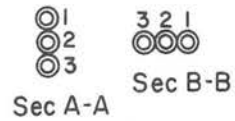


Note: Stainless Steel Tubing (Milled Finish)
 O.D. 0.120 in
 I.D. 0.070 in



Pitch Probe Side View
 Yaw Probe Plan View

Manometer Board
 (3 Tubes)



Yaw and Pitch Probes

Fig. 117

The theory of the probes is as follows. For two dimensional flows at a given point where the flow velocity is V , the static piezometric head is H_0 and the angle of attack is θ ; the piezometric heads indicated by the three tubes of a probe can be written as

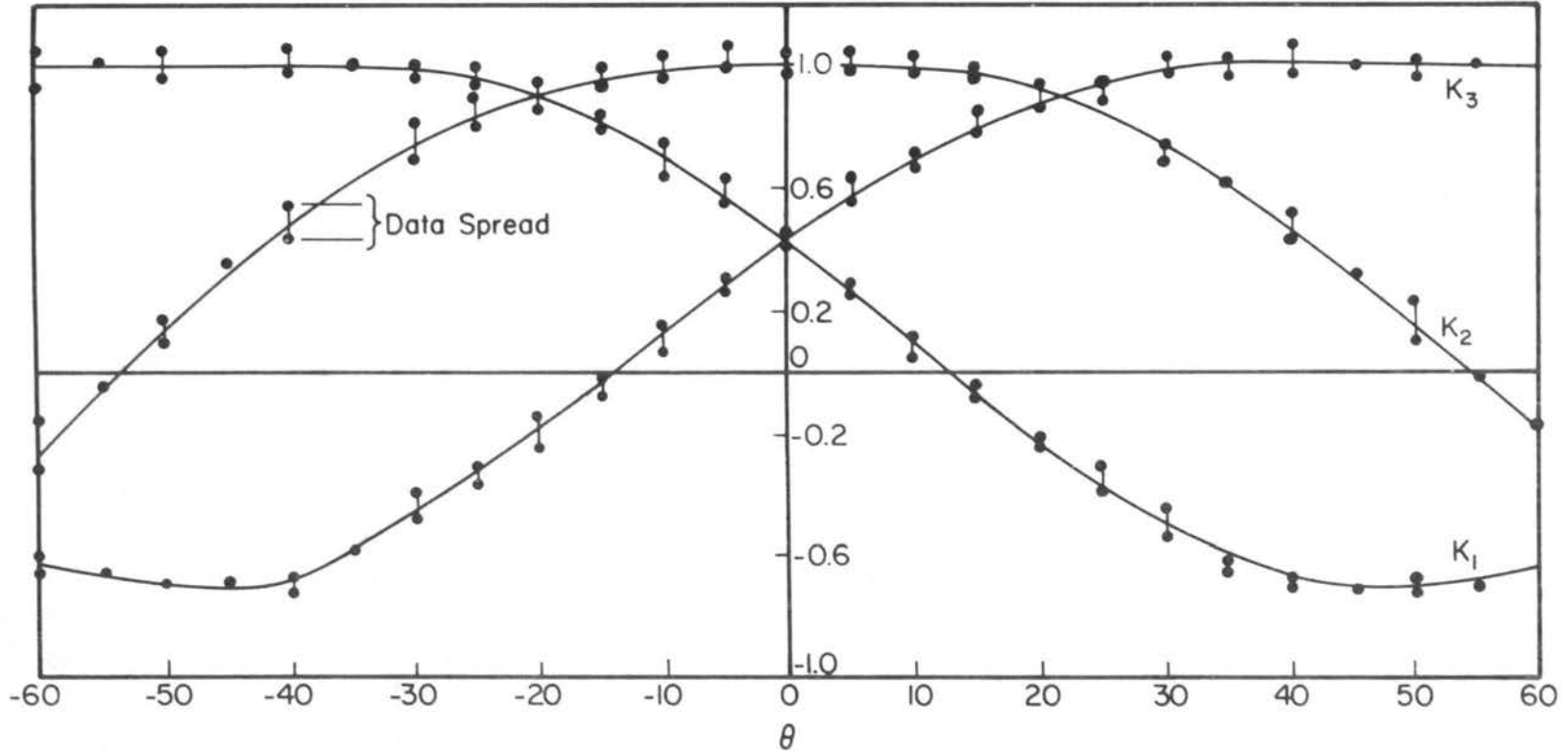
$$h_1 = h_0 + K_1 V^2/2g \quad (3-14)$$

$$h_2 = h_0 + K_2 V^2/2g \quad (3-15)$$

$$h_3 = h_0 + K_3 V^2/2g \quad (3-16)$$

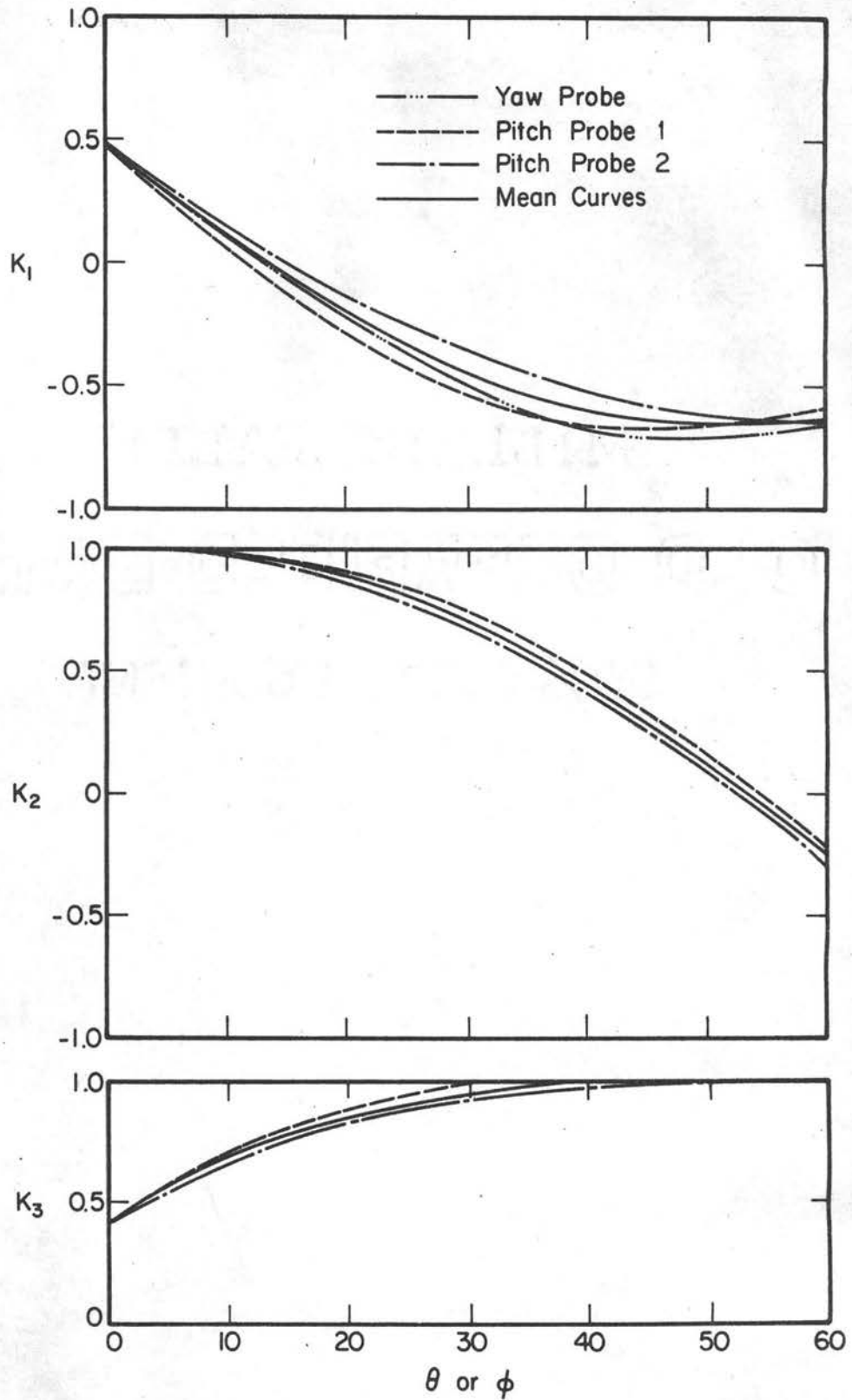
where K_1 , K_2 , and K_3 are calibration coefficients and are functions only of θ , neglecting viscous and other minor effects.

The yaw probe was calibrated for seven velocities ranging from 1.47 to 10.39 fps, with a range of θ from 0° to 60° . The large pitch probe was calibrated for velocities from 1.41 to 10.0 fps with a range of ϕ from 0° to 60° , and the smaller pitch probe was calibrated with velocities of 3.06 and 7.56 fps with the pitch angle varying from 0° to 60° . A plot of θ versus K_1 , K_2 , and K_3 and the data scatter is reproduced as Fig. 118. The mean values for K_1 , K_2 , and K_3 for all three probes were collected and are reproduced as Fig. 119. Agreement between the data for all three probes was sufficiently good that mean curves could be drawn which were suitable for any of the three probes; i.e., the calibration for the half-scale probe was the same as for the full scale probe. Digressing for a moment, this was a major point in the selection of the yaw and pitch probe for the CSU study. If a probe constructed to half scale yielded the same calibration data as the full scale probe, then certainly probes constructed



Yaw Probe Calibration Factors
 Reproduced from Ref. 16

Fig. 118



Mean Calibration Factors
 Reproduced from Ref. 16

Fig. 119

at CSU to the same specifications and dimensions as the larger probes could be used without much additional calibration.

Using the three calibration factors, K_1 , K_2 , and K_3 , a fourth factor K was defined as

$$K = \frac{K_3 - K_2}{K_1 - K_2} \quad (3-17)$$

Combining Eq. 3-17 with Eqs. 3-14, 3-15 and 3-16, the relationship

$$K = \frac{h_3 - h_2}{h_1 - h_2} \quad (3-18)$$

is obtained.

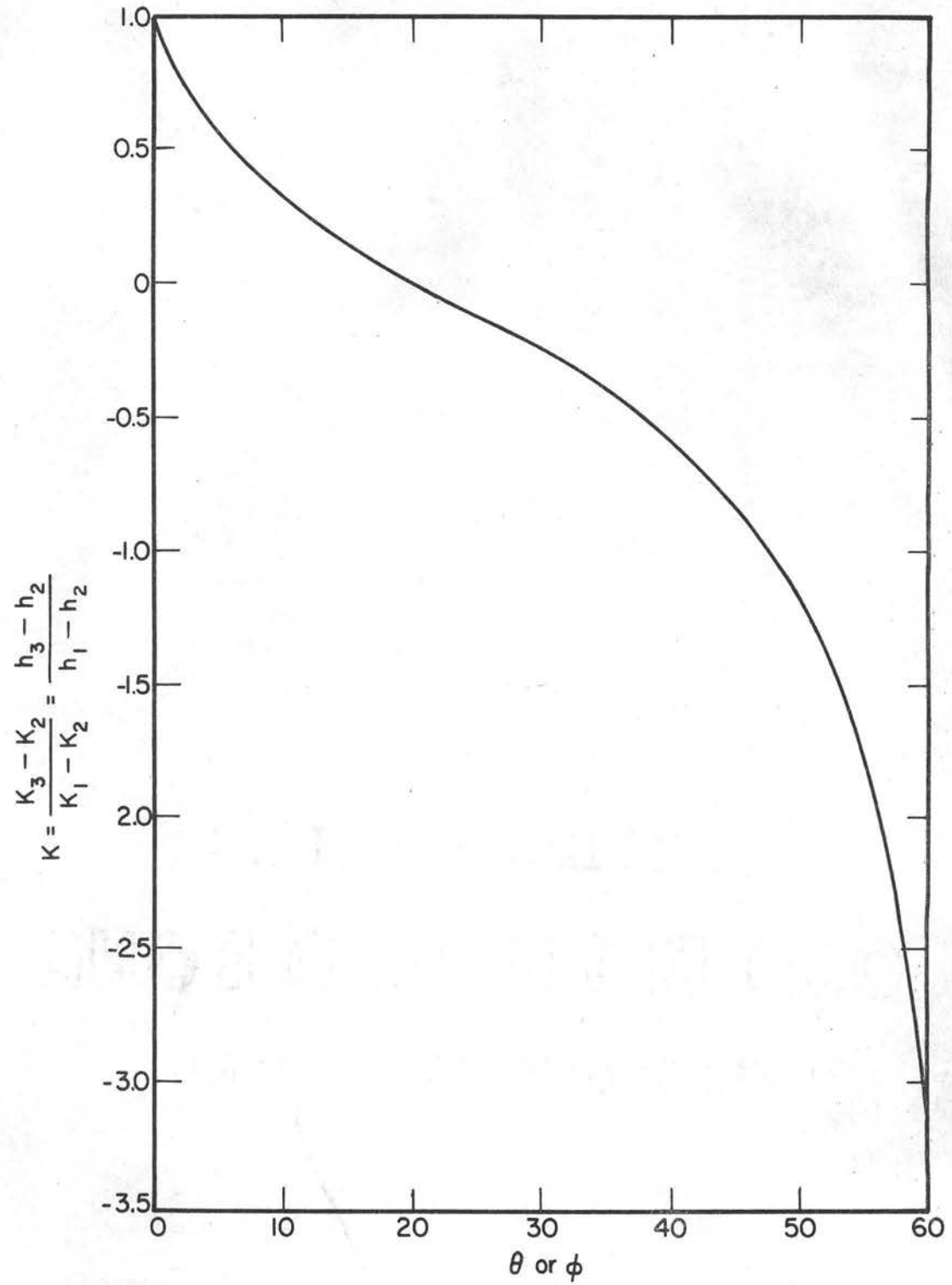
By equating h_0 of Eqs. 3-14 and 3-15, it is easily shown that

$$V = \frac{\sqrt{2g (h_1 - h_2)}}{\sqrt{K_1 - K_2}}$$

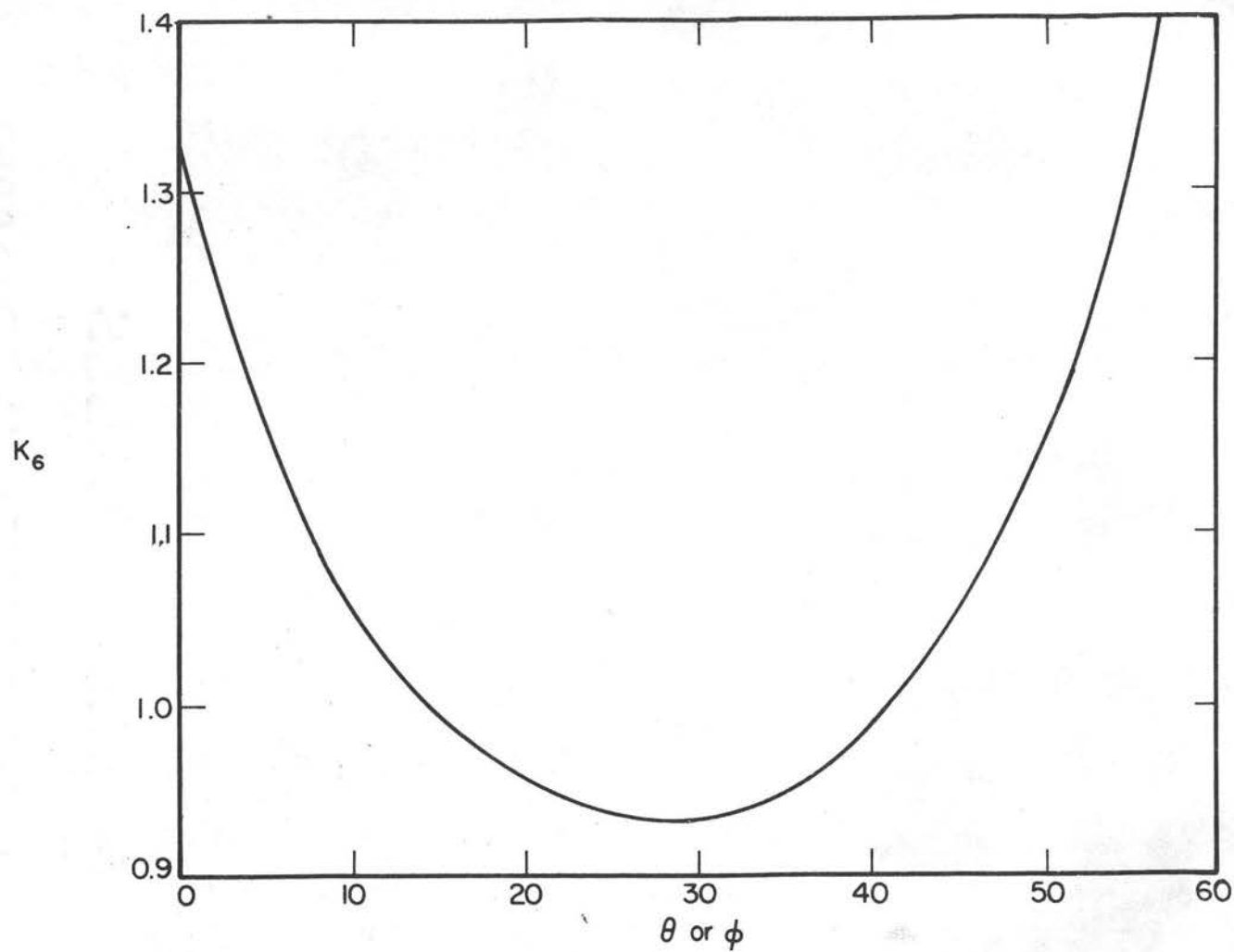
Letting $K_6 = \frac{1}{\sqrt{K_1 - K_2}}$,

$$V = K_6 \sqrt{2g (h_1 - h_2)} \quad (3-19)$$

where K_6 is only a function of θ . To apply these equations, compute the quantity K , Eq. 3-18, with the measured data, obtain θ from Fig. 120; with this value of θ , obtain K_6 from Fig. 121, compute $h_1 - h_2$ from the measured data, and evaluate Eq. 3-19. Thus, both the angle and the magnitude of the velocity can be determined. All calibration was conducted in two dimensional flow.



Curve for K Fig. 120
Reproduced from Ref. 16



Curve for K_6 Fig. 121
Reproduced from Ref. 16

For the CSU study, the pressure at the point in question was obtained by an indirect computation. All probe readings were obtained with the manometer referenced to the floor ($y = 0$); therefore, the center tube of the probe (yaw or pitch) gave the total head directly. By careful bookkeeping, the elevation of the probe above the floor, plus the velocity head term, was subtracted from the total head reading. The remaining quantity is the pressure head.

Returning to the CSU study, it was assumed that at the outlet section, the flow would be essentially two dimensional, at least in the vertical plane. The walls of the pipe would train the flow and, therefore, little deviation from the horizontal was expected. The major angle would be in the vertical plane, particularly for the situations where the pipe was emitting partial flow. Measured yaw and pitch angles verified these assumptions with the exception of a very trivial region around the periphery of the pipe. Because of the very small yaw angle and the relatively large pitch angle, the data from the pitch probe was considered the primary data; the yaw probe data provided the yaw angle and was used as an independent check on the pitch probe data.

In the sections downstream of the outlet, the reverse situation occurred. The water surface was more or less horizontal, and the major angle was in the horizontal plane; therefore, the yaw probe data was used as the primary data.

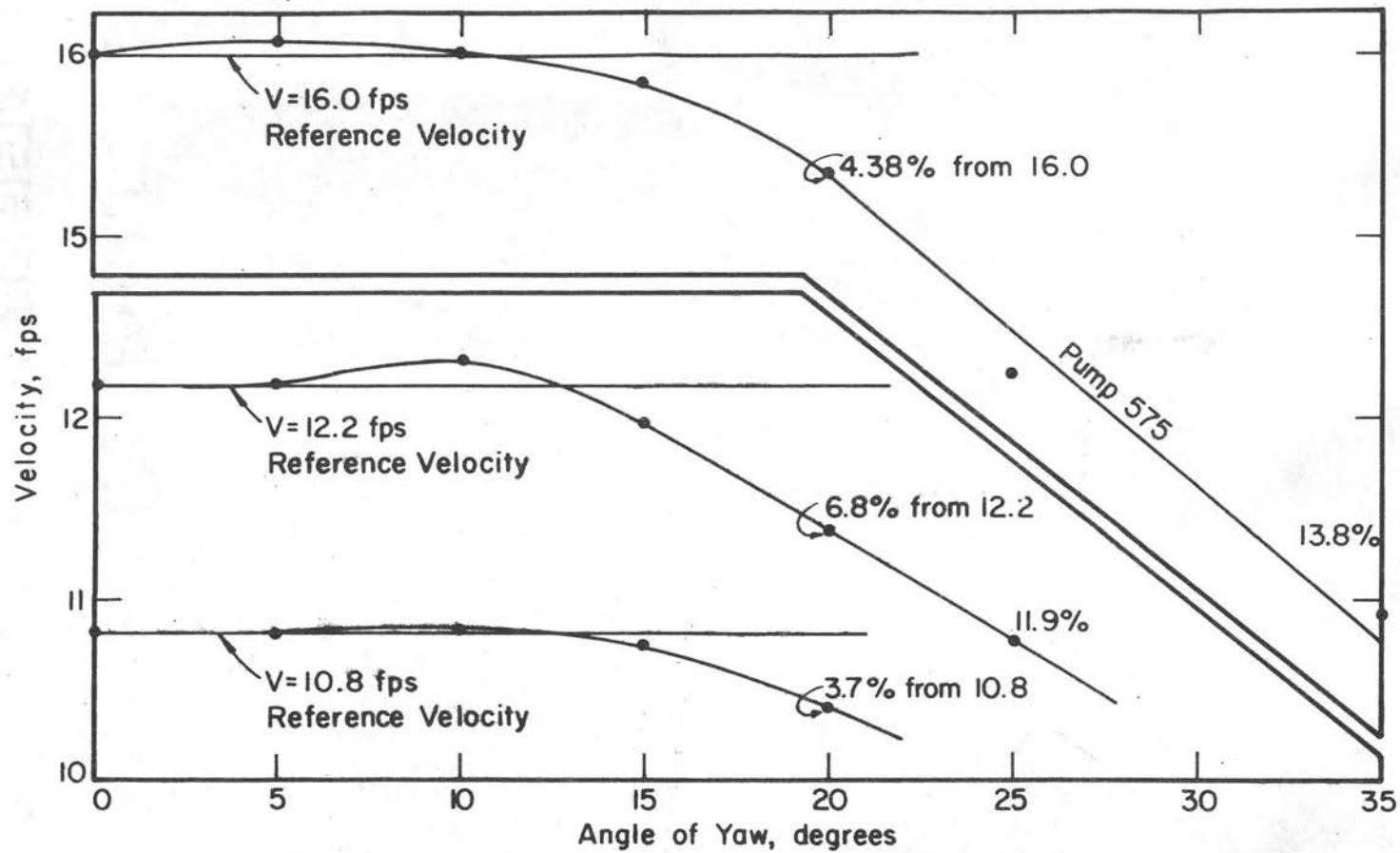
In the region adjacent to the outlet, three-dimensional flow occurred. For this reason, a brief calibration test was conducted to determine the effect of the third component of velocity on the various quantities.

CSU Calibration

The pitch (vertical) probe was positioned at the centerline of the basin at Sta. 5.0 with the centerline of the probe oriented parallel to the centerline of the basin. The flow from the pipe spread symmetrically. Therefore, only a small horizontal angle ($\pm 1^\circ$) occurred along the basin centerline. Three discharges were run; the velocities sensed by the probe were 10.8, 12.2, and 16.0 fps.

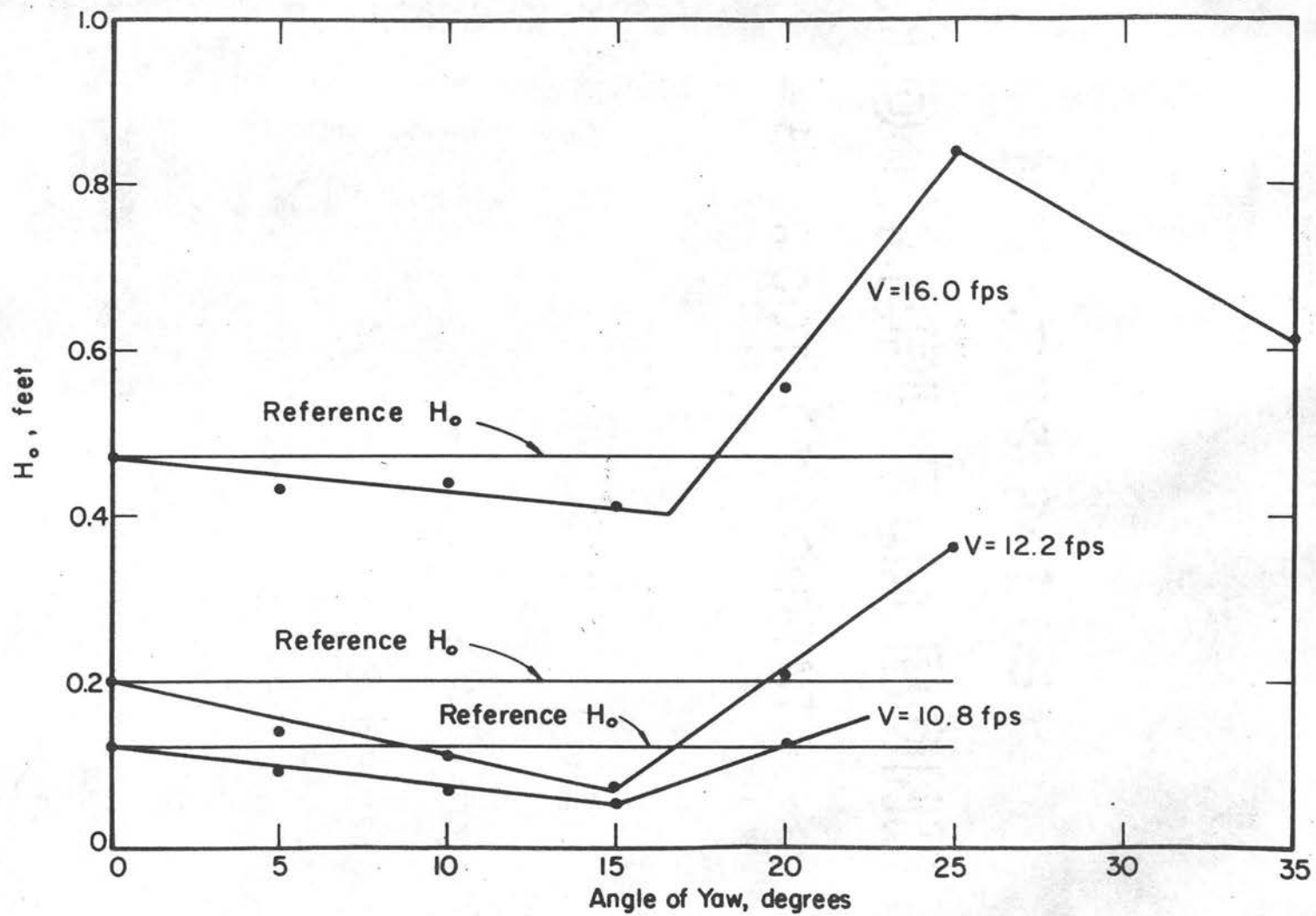
After completing the first three runs, the pitch probe was removed, rotated 5° in the horizontal plane, and replaced in the flow with the nose of the probe in the same spot, i.e., the horizontal angle of attack was 5° . This was repeated systematically with 5° increments. Figure 122 shows the effect on the magnitude of deduced velocity for horizontal attack angles up to 10° ; the variation is trivial. At 20° the deduced velocities were smaller than the true velocities by 3.7%, 6.8%, and 4.4% for velocities of 10.8, 12.2, and 16.0 fps, respectively.

The other calibration was concerned with the effect of the rotation of the probe on deduced pressure head. The data described above was reduced and H_0 , pressure head, was plotted versus the angle of yaw, Fig. 123. The variation of head versus angle of yaw was linear from 0° to 15° , then varied erratically. The data at the outlet section generally had a yaw angle of less than 2.5° ; therefore, the maximum deviation from H_0 was 0.01, 0.02, and 0.015 ft of water for velocities of 10.8, 12.2, and 16.0 fps. Since this deviation is small, no correction was made on the outfall data.



Pitch Probe Calibration
 Angle of Yaw versus Deduced Velocity

Fig. 122



Pitch Probe Calibration
 Angle of Yaw versus Deduced Head

Fig. 123

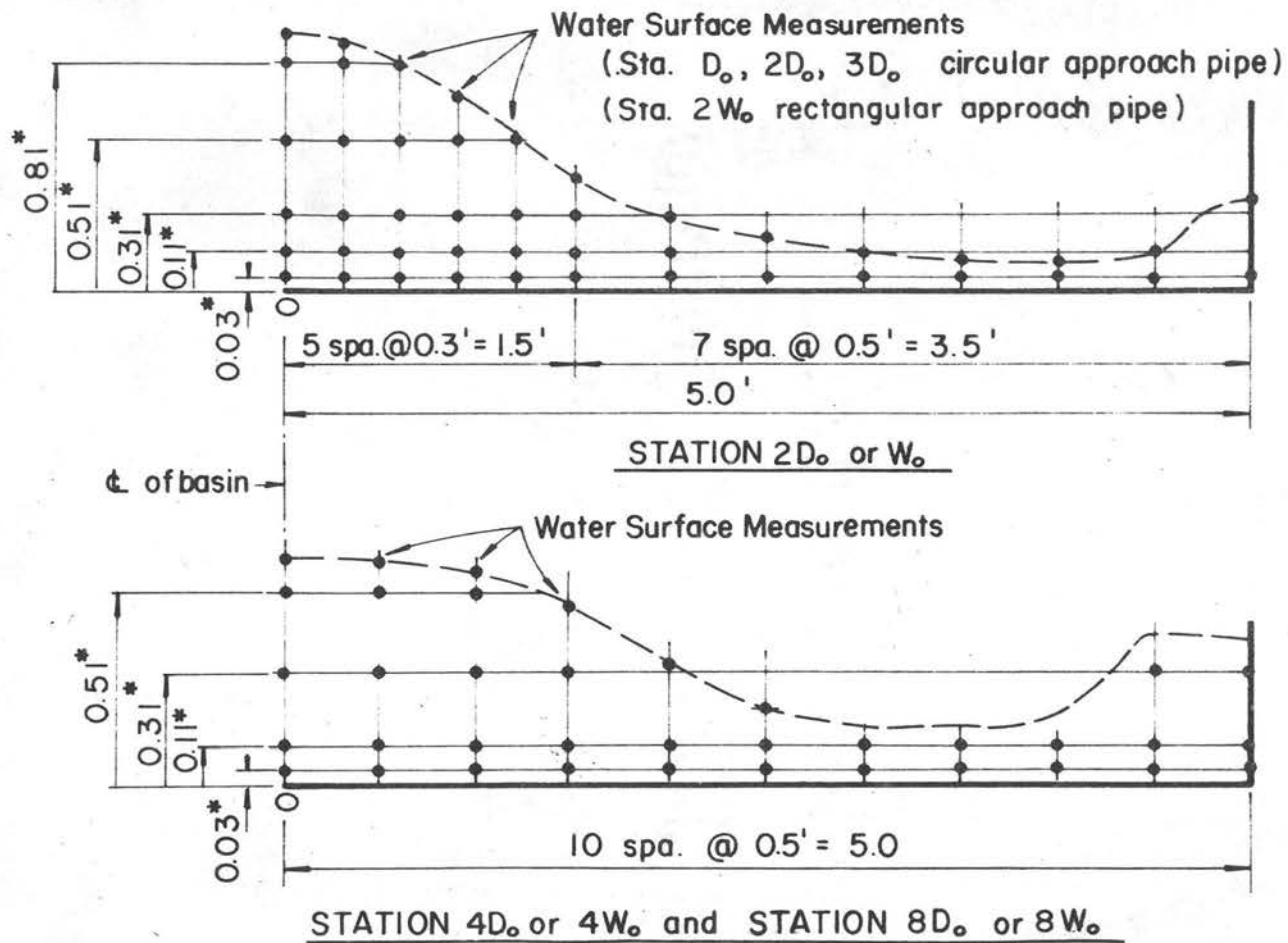
Measuring Procedure

Because of the symmetry of approach pipe, basin, and flow field, it was only necessary to take measurements throughout a half section. After examination of some preliminary data, the various sections were subdivided into appropriate grids and a predetermined coordinate established for the sampling point. Figure 124 displays the measurement grids for the circular and rectangular outlet section, and Fig. 125 displays the grid for sections 2, 4, and 8 pipe widths downstream of the outlet. It was presumed that the relatively steep velocity gradient in the area adjacent to the fixed boundary would have some effect on the measurements. For this reason, the grid points were spaced rather closely near the boundary so as to minimize this effect.

The measuring procedure was as follows. A predetermined discharge was established. The pump was allowed to run 45 minutes prior to any data collection. Because of the long approach pipe (3000 ft \pm) from the pump to the basin, some period of time was required for the flow to stabilize.

The pitch probe was then positioned at the proper station and transverse coordinate, and measurements were completed systematically for the vertical. This was repeated until the section was completed. The pitch probe was then replaced by the yaw probe, and the procedure repeated.

For all data taken at the outlet sections, six readings were recorded for each probe position. After positioning, the liquid in the manometer tubes would stabilize (15 to 30 seconds). The 1, 2, and 3 tube readings (h_1 , h_2 , and h_3) were recorded; the tubes were then reread and recorded. If any of the second group of readings differed



* These dimensions shown are typical but vary with flow conditions. See y coordinate, basic data for exact dimensions.

Measuring Grid at Downstream Sections Fig. 125
 (Section shown is normal to the centerline of the basin)

by more than 0.03 ft from those of the first group, the tubes were reread a third time. The arithmetic average of the two closest sets of readings was used as the data. In general, the readings were quite consistent and rarely was a third set of readings required. This procedure was relaxed somewhat in the downstream sections. Only the yaw probe data were collected. As it was, the amount of data per run was voluminous. For an average run where four sections were sampled, about 700 readings were necessary.

Data defining the water surface elevation to be described in Chapter IV were also recorded at this time.

Test Facility

A rectangular basin with a horizontal floor ($1\frac{1}{4}$ in. sheet aluminum) 10 ft wide and 14 ft long with 12 in. vertical walls was constructed. Two approach pipe sections were examined. For the first series of runs, a 1.45 ft diameter smooth circular pipe twenty ft long with a horizontal invert was installed. This setup was used for run 1 through 7 for energy evaluation purposes at the culvert outlet, and at the station 2 pipe diameters downstream.

A rectangular approach pipe 1.25 ft by 1.25 ft by 20 ft long, with a horizontal invert was used for energy evaluations, run 8 through 13. Data was collected at Stas. 0.0, 2.5, 5.0, and 10.0 for this series of runs.

The pipe inverts were carefully matched to the basin floor so that only a joint separated the two; i.e., there was no vertical discontinuity.

The pipe and basin unit was placed within a large outdoor reinforced concrete flume, previously described.

A rectangular, sharp-crested weir at the lower end of the large flume was used to check the discharges obtained by integration of experimental data. Readings from the point gauges, taken before and after each run, were compared so that any possible change in discharge during the 5 to 8-hour run would be readily apparent.

To avoid tailwater effects from the downstream measuring weir, the floor of the test basin was installed at a height two ft above the concrete floor of the large flume. A variable height dam for the purpose of tailwater control was constructed 35 ft downstream of the pipe outlet. The crest of the dam was maintained at the elevation of the top surface of the basin floor for all runs.

The probes and supporting equipment were mounted on the large instrument carriage spanning from wall to wall of the large flume.

Test Program and Range of Parameters

Seven discharges varying from 9.77 cfs to 23.5 cfs were examined for the 1.45 ft circular approach pipe. The relative depth ratio Y_o/D_o (depth of flow at the outfall section divided by the diameter) ranged from 0.75 cfs to 1.00 cfs. $Q/D_o^{5/2}$ varied from 3.87 cfs to 9.28 cfs. This encompasses the usual range of highway culverts. Data were taken at Stas. 0.0 and 2.9.

For the rectangular approach pipe, six discharges varying from 6.75 cfs to 21.3 cfs were examined. The relative depth ratio Y_o/W_o ranged from 0.61 cfs to 0.94 cfs, and the Froude number $\frac{V_o}{\sqrt{gy_o}}$,

varied from 1.44 cfs to 2.35 cfs, the range of usual culvert operation. Data were collected at Stas. 0:0, 2.5, 5.0, and 10.0.

Table IV lists the significant flow variables, basin geometry, approach pipe geometry, and the deduced energy and momentum coefficients.

The code for the run number example - Run No. 1 - ϕ - Y) is as follows: 1 is the run number, ϕ indicates a circular approach pipe (as contrasted to \square for a rectangular pipe), and Y indicates that the primary data were obtained with the yaw probe (P would indicate pitch probe data).

TABLE IV - FLOW PARAMETERS FOR ENERGY AND MOMENTUM EXPERIMENTS

Run No.	Sta.	Q/2 Integrated (cfs)	Q/2 Weir (cfs)	Area A (ft ²)	Width W _o /2 or D _o /2 (ft)	Mean Depth y (ft)	Average Velocity V = Q/A (fps)	Q/D _o ^{5/2}	V _o /√gW _o	V _o /√gY _o	Power P ft lbs/sec	Spec. Energy E = P/γQ ft lbs/lb	α ₁	α ₂	Press Force + Momen. (lbs)	β ₁	β ₂
Circular Approach Pipe																	
1-φ-Y	0.0	5.04	4.85	0.661	0.725	1.08	7.62	3.99		1.29	580	1.84	0.81	1.07	93.2	0.54	1.01
1-φ-P	0.0	4.89	4.85	0.661	0.725	1.08	7.40	3.87		1.26	548	1.80	0.82	1.07	89.2	0.55	1.01
1-φ-Y	2.9	4.89	4.85	0.780	3.00	0.260	6.27			2.17	518	1.70	1.25	2.24	90.7	1.82	1.33
2-φ-Y	0.0	5.78	5.91	0.731	0.725	1.20	7.90	4.57		1.27	693	1.92	0.74	1.06	107.2	0.43	1.01
2-φ-P	0.0	5.76	5.91	0.731	0.725	1.20	7.88	4.55		1.27	693	1.93	0.75	1.07	106.8	0.44	1.01
2-φ-Y	2.9	5.78	5.91	0.780	3.00	0.260	7.41			2.56	658	1.82	1.36	1.72	108.9	1.79	1.18
3-φ-Y	0.0	6.62	6.85	0.773	0.725	1.28	8.56	5.23		1.33	861	2.08	0.70	1.04	127.8	0.37	1.01
3-φ-P	0.0	6.66	6.85	0.773	0.725	1.28	8.62	5.27		1.34	875	2.11	0.70	1.04	129.6	0.37	1.01
3-φ-Y	2.9	6.66	6.85	0.880	3.00	0.293	7.56			2.46	840	2.02	1.41	1.81	131.8	1.99	1.19
4-φ-Y	0.0	7.87	7.31	0.827	0.725	1.45	9.51	6.22		1.39	1181	2.40	0.65	1.04	164.8	0.32	1.01
4-φ-P	0.0	7.90	7.31	0.827	0.725	1.45	9.55	6.75		1.40	1166	2.37	0.62	1.04	163.4	0.26	1.01
4-φ-Y	2.9	7.90	7.31	0.877	3.00	0.292	9.00			2.94	1150	2.33	1.70	1.46	164.7	2.44	1.05
5-φ-Y	0.0	8.64	8.29	0.827	0.725	1.45	10.43	6.83		1.53	1464	2.72	0.66	1.03	195.6	0.34	1.01
5-φ-P	0.0	8.64	8.29	0.827	0.725	1.45	10.43	6.83		1.53	1429	2.65	0.62	1.03	192.3	0.26	1.01
5-φ-Y	2.9	8.64	8.29	0.917	3.00	0.306	9.42			3.00	1403	2.60	1.96	1.45	196.5	2.71	1.10
6-φ-Y	0.0	10.55	10.18	0.827	0.725	1.45	12.75	8.35		1.87	2375	3.61	0.70	1.02	284.2	0.42	1.01
6-φ-P	0.0	10.58	10.18	0.827	0.725	1.45	12.80	8.36		1.87	2326	3.52	0.64	1.02	280.6	0.29	1.01
6-φ-Y	2.9	10.54	10.18	0.980	3.00	0.327	10.77			3.32	2250	3.42	2.04	1.53	282.5	2.65	1.17
7-φ-Y	0.0	11.71	11.30	0.827	0.725	1.45	14.16	9.27		2.07	3076	4.20	0.72	1.02	345.4	0.45	1.00
7-φ-P	0.0	11.73	11.30	0.827	0.725	1.45	14.18	9.28		2.07	3014	4.11	0.65	1.02	341.1	0.31	1.00
7-φ-Y	2.9	11.72	11.30	0.998	3.00	0.333	11.73			3.59	2871	3.92	2.93	1.38	336.6	4.10	1.10
Rectangular Approach Pipe																	
8-D-Y	0.0	3.40	3.40	0.475	0.625	0.76	7.16		1.13	1.45	321	1.51	0.91	1.03	62.6	0.83	1.00
8-D-P	0.0	3.38	3.40	0.475	0.625	0.76	7.11		1.12	1.44	317	1.50	0.91	1.03	62.2	0.84	1.00
8-D-Y	2.5	3.38	3.40	0.432	3.00	0.144	7.83			3.64	312	1.48	1.71	1.29	57.0	2.38	1.02
8-D-Y	5.0	3.41	3.40	0.459	5.00	0.092	7.43			4.31	301	1.42	2.65	1.38	58.6	3.98	1.09
8-D-Y	10.0	3.36	3.40	0.586	5.00	0.117	5.73			2.95	187	0.89	1.98	1.29	47.2	3.01	1.09
9-D-Y	0.0	4.67	4.64	0.609	0.625	0.98	7.67		1.21	1.37	516	1.77	0.83	1.05	88.4	0.68	1.01
9-D-P	0.0	4.65	4.64	0.609	0.625	0.98	7.64		1.21	1.36	519	1.79	0.85	1.06	88.9	0.73	1.01
9-D-Y	2.5	4.66	4.64	0.567	3.00	0.189	8.22			3.33	506	1.74	1.80	1.34	85.6	2.70	1.03
9-D-Y	5.0	4.66	4.64	0.655	5.00	0.131	7.12			3.47	439	1.51	1.93	1.60	82.0	3.50	1.13
9-D-Y	10.0	4.64	4.64	0.708	5.00	0.141	6.56			3.08	318	1.10	1.91	1.24	72.5	2.93	1.07
10-D-Y	0.0	5.95	6.00	0.652	0.625	1.05	9.11		1.44	1.57	826	2.23	0.86	1.03	127.3	0.74	1.00
10-D-P	0.0	5.94	6.00	0.652	0.625	1.05	9.11		1.44	1.57	822	2.22	0.85	1.03	126.9	0.72	1.01
10-D-Y	2.5	5.94	6.00	0.663	3.00	0.221	8.96			3.35	782	2.11	2.26	1.29	123.4	3.40	1.05
10-D-Y	5.0	5.94	6.00	0.816	5.00	0.163	7.27			3.16	644	1.74	2.07	1.70	114.0	3.91	1.17
10-D-Y	10.0	5.93	6.00	0.764	5.00	0.153	7.77			3.50	540	1.46	2.26	1.19	108.0	3.86	1.06
11-D-Y	0.0	7.30	7.39	0.699	0.625	1.10	10.44		1.65	1.76	1220	2.68	0.86	1.02	171.9	0.73	1.01
11-D-P	0.0	7.38	7.39	0.699	0.625	1.10	10.56		1.67	1.77	1243	2.70	0.83	1.03	174.3	0.68	1.01
11-D-Y	2.5	7.37	7.39	0.759	3.00	0.253	9.72			3.41	1182	2.57	2.30	1.36	167.7	3.29	1.07
11-D-Y	5.0	7.38	7.39	0.732	5.00	0.146	10.05			4.63	1120	2.43	2.51	1.31	163.6	4.11	1.04
11-D-Y	10.0	7.35	7.39	0.812	5.00	0.162	9.05			3.96	876	1.91	2.38	1.20	153.3	4.20	1.06
12-D-Y	0.0	8.32	8.82	0.692	0.625	1.10	12.02		1.90	2.02	1689	3.24	0.87	1.02	218.8	0.76	1.01
12-D-P	0.0	8.48	8.82	0.692	0.625	1.10	12.24		1.93	2.06	1738	3.27	0.82	1.02	223.9	0.66	1.01
12-D-Y	2.5	8.47	8.82	0.820	3.00	0.273	10.33			3.49	1576	2.98	2.70	1.35	209.5	4.02	1.07
12-D-Y	5.0	8.48	8.82	0.743	5.00	0.149	11.42			5.21	1576	2.98	2.92	1.26	209.5	4.68	1.03
12-D-Y	10.0	8.48	8.82	0.842	5.00	0.168	10.05			4.32	1257	2.37	2.62	1.23	195.6	4.52	1.06
13-D-Y	0.0	10.38	10.72	0.736	0.625	1.18	14.10		2.22	2.29	2749	4.25	0.91	1.02	314.3	0.84	1.01
13-D-P	0.0	10.64	10.72	0.736	0.625	1.18	14.46		2.28	2.35	2861	4.31	0.84	1.02	324.4	0.69	1.01
13-D-Y	2.5	10.65	10.72	0.839	2.50	0.335	12.70			3.86	2603	3.92	2.68	1.20	304.0	3.88	1.03
13-D-Y	5.0	10.60	10.72	0.812	5.00	0.162	13.05			5.72	2589	3.92	3.97	1.24	306.0	6.70	1.04
13-D-Y	10.0	10.65	10.72	0.926	5.00	0.185	11.50			4.71	2044	3.09	2.79	1.25	279.0	5.27	1.06

Presentation of Data

 α and β Values

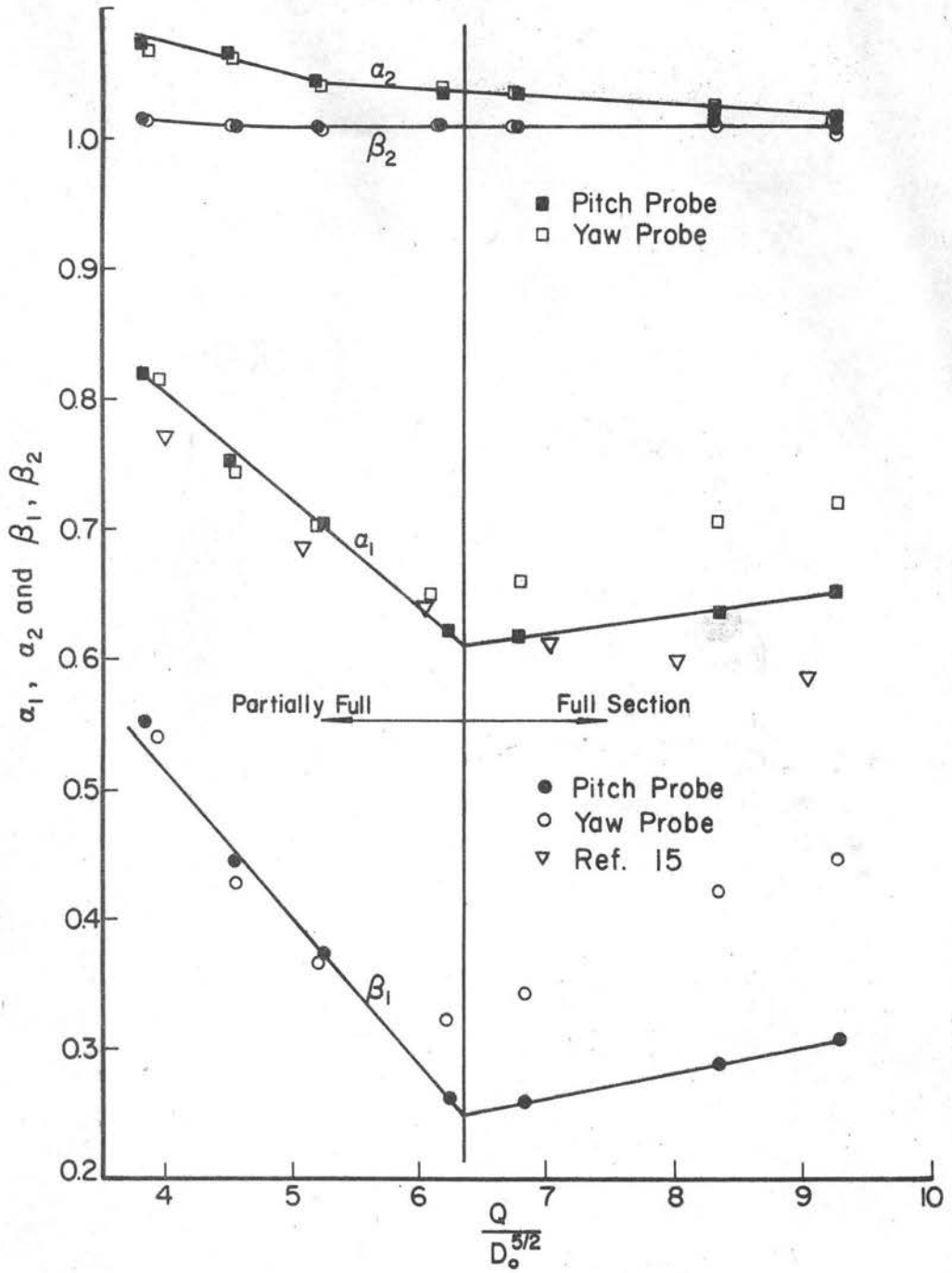
The major interests of this study were the energy correction coefficients (α_1 for the pressure term, α_2 for the velocity term) and the momentum correction coefficients (β_1 for the pressure term and β_2 for the velocity term) at the outfall section.

For the circular approach pipe, these four coefficients are plotted versus the usual circular pipe Froude number $\frac{Q}{D_o^{5/2}}$, Fig. 126. The velocity correction terms α_2 and β_2 are relatively minor.

The pressure correction terms, however, are significant. The coefficients deduced by the CSU data correspond closely to the energy correction coefficients reported in Ref. 15. The CSU data show a definite break where the flow changed from partial section flow to full section flow. The upward trend with the higher discharge shown by the CSU data may be explained as follows. The larger the discharge forced through the full section, the less curvature of the flow; thus the coefficient should increase with increase of flow.

There is good agreement between the CSU energy coefficients and the coefficients presented in Ref. 15. No coefficients, for comparison purposes, were found in the literature for the momentum correction β_1 or for the energy and momentum correction terms for the rectangular pipe.

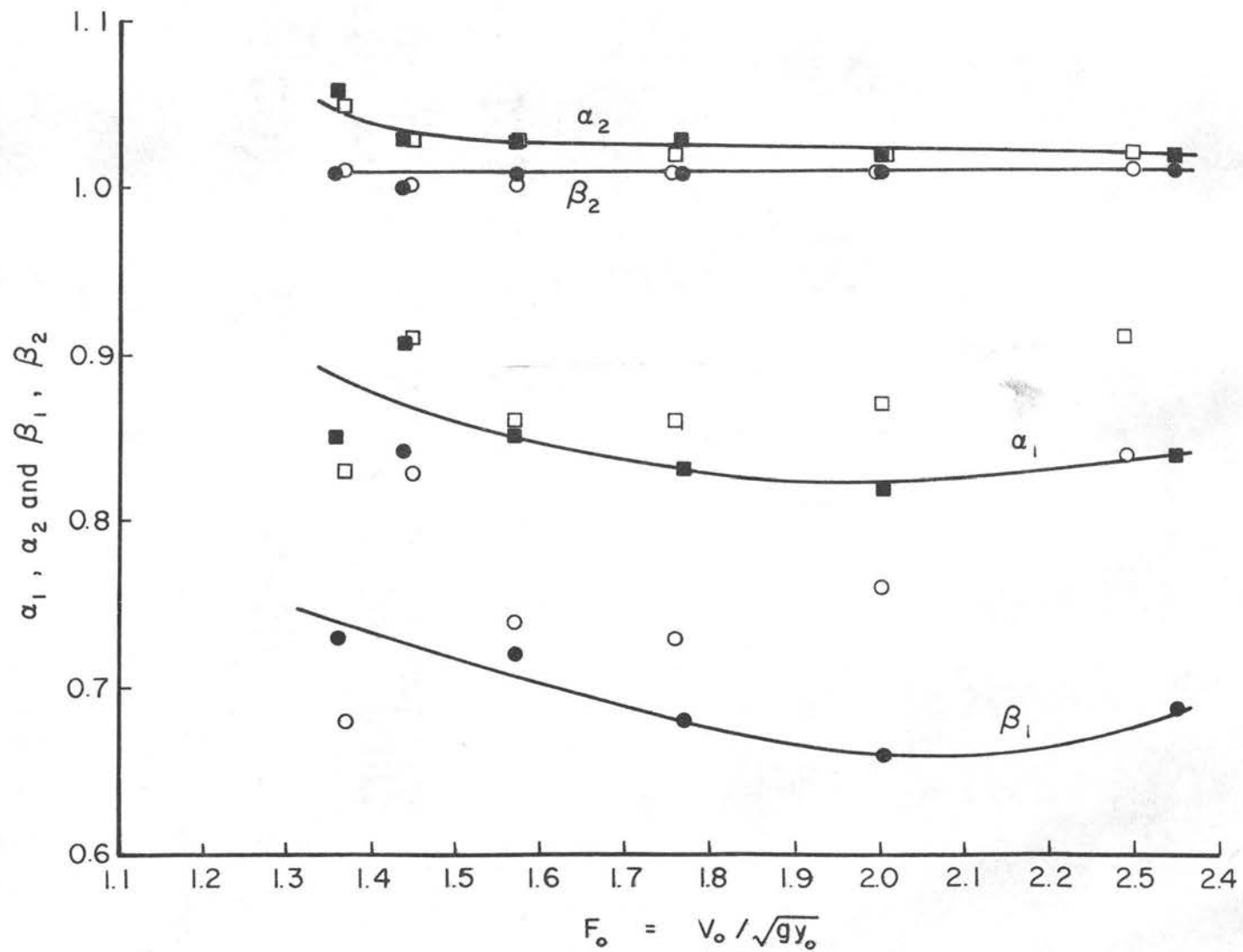
These latter coefficients were, of course, deduced in the same manner as the energy coefficient α_1 which was comparable to that presented in Ref. 15. This is cited as supporting evidence that the technique used in the CSU study yields reasonable values.



Energy and Momentum Coefficients, Out Fall Section
Circular Approach Pipe

Energy and Momentum Coefficients, Outfall Section
Circular Approach Pipe

Fig. 126



Energy and Momentum Coefficients,
Rectangular Approach Pipe

Fig. 127

The correction factors for the rectangular approach pipe are plotted versus the Froude number at the outfall section, $\frac{V}{\sqrt{gy_0}}$, in Fig. 127. Again, the pressure correction coefficient is significantly less than 1.0.

The pressure coefficients for the rectangular pipe are somewhat larger than those for an equivalent flow through a circular outfall section. This is to be expected. The flow is fully supported across the bottom for the rectangular section; thus the flow does not fall off toward the floor quite as rapidly as the partially unsupported, cylindrical tube of water downstream of the circular section. The smaller the amount of the flow undergoing vertical acceleration, the less the deviation from hydrostatic pressure. This results in a larger pressure correction factor.

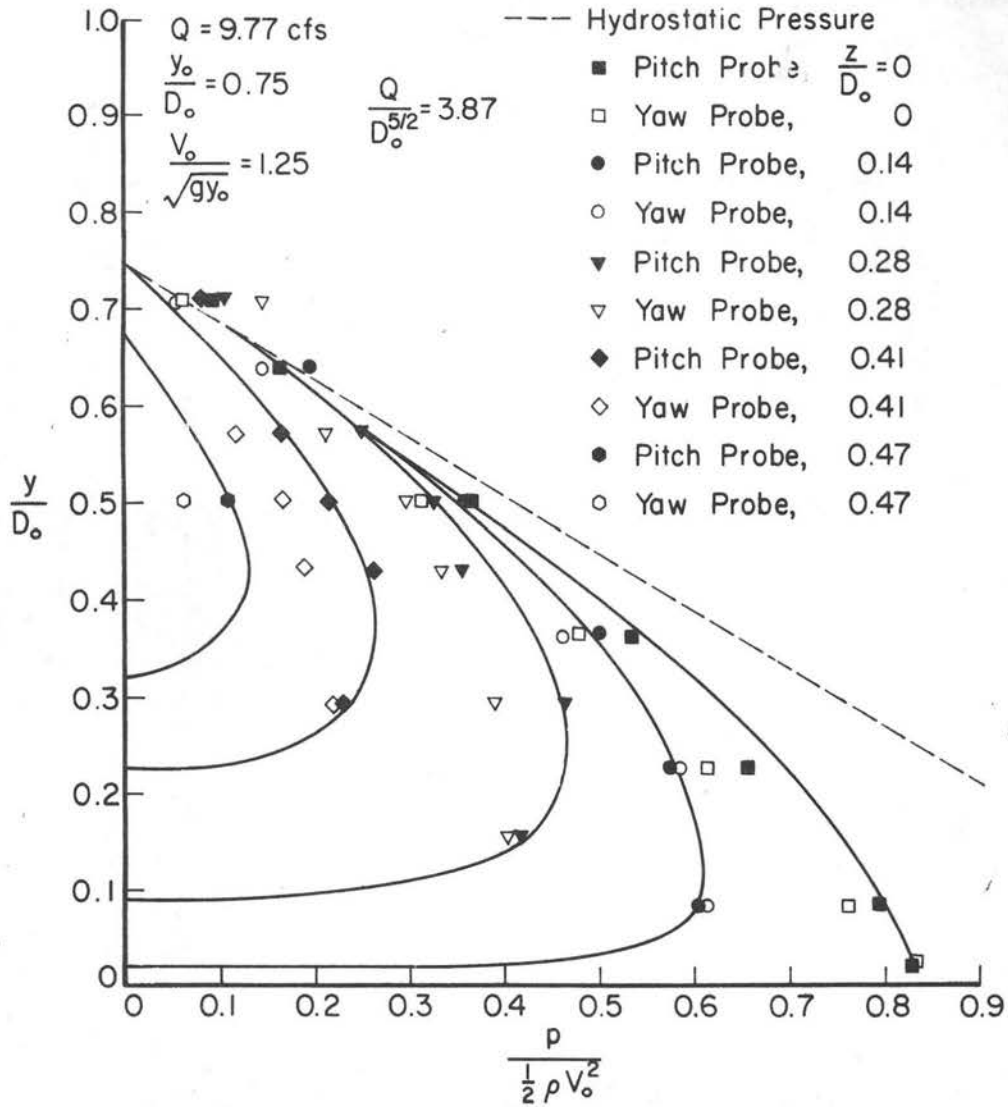
Pressure Distribution

The non-dimensional pressure plots, $\frac{P}{\frac{1}{2}\rho V^2}$, shown in Figs. 128 through 134, graphically display the pressure field at the outfall sections. The deviation from hydrostatic pressure is readily apparent. These plots are not significant for culvert design, but do display the consistency of the data.

There appeared to be a small systematic deviation between the pressures deduced from pitch probe data and those deduced from the yaw probe data.

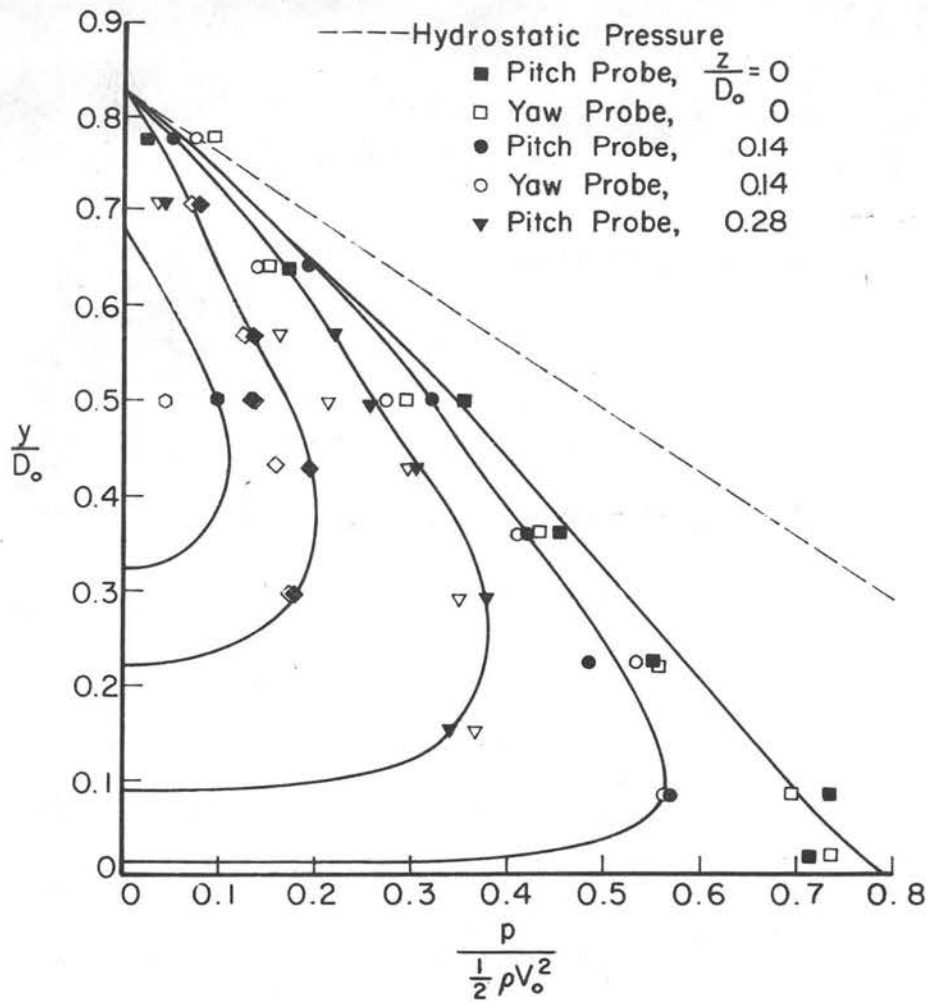
Error Analysis

To try to locate this apparent systematic error, the velocities measured with the pitch probe were plotted, versus the velocities at identical points deduced from the yaw probe data. These data are shown



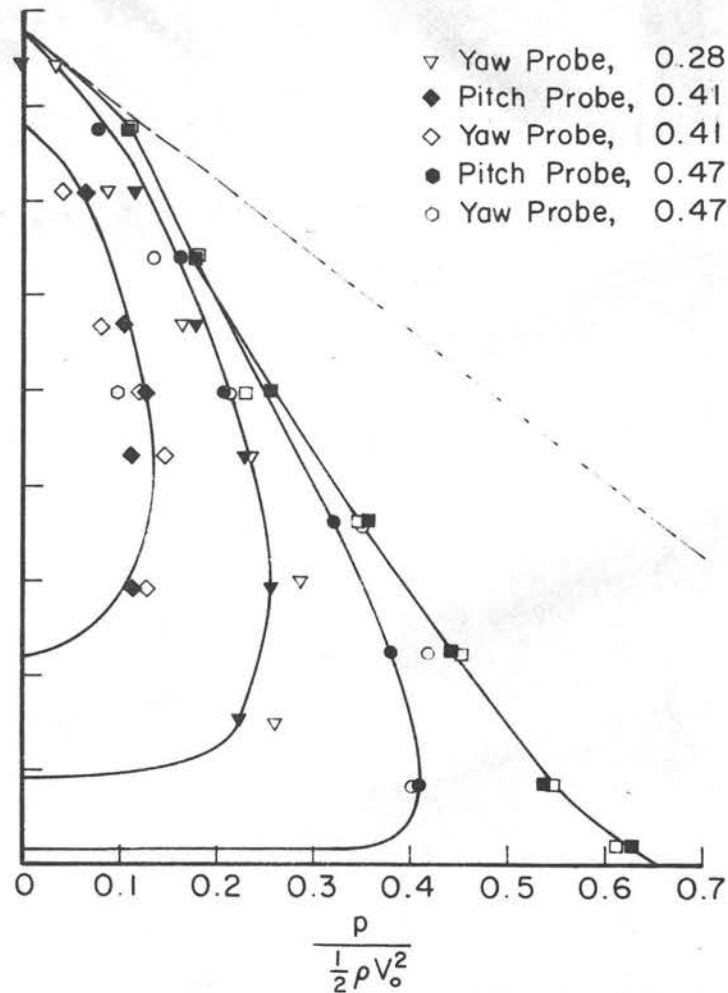
Dimensionless Pressure Plot, Circular Outfall

Fig. 128



$$Q = 11.5 \text{ cfs}, \quad \frac{y_o}{D_o} = 0.83, \quad \frac{V_o}{\sqrt{gy_o}} = 1.27$$

$$\frac{Q}{D_o^{5/2}} = 4.56$$

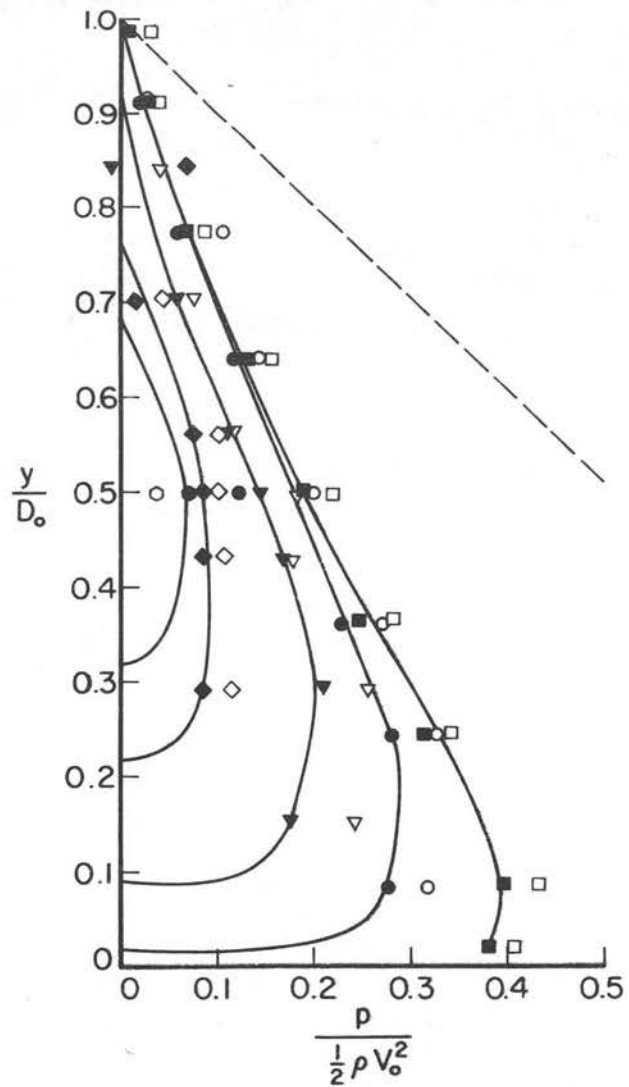


$$Q = 13.3 \text{ cfs}, \quad \frac{y_o}{D_o} = 0.88, \quad \frac{V_o}{\sqrt{gy_o}} = 1.34$$

$$\frac{Q}{D_o^{5/2}} = 5.27$$

Dimensionless Pressure Plots, Circular Outfall

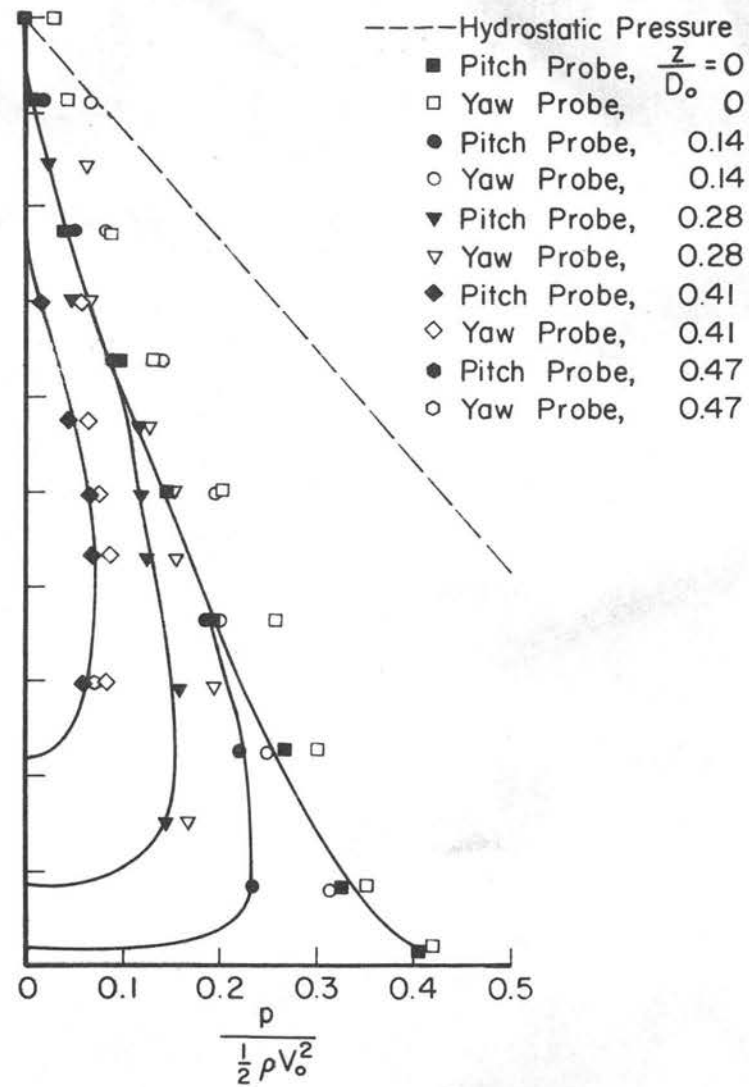
Fig. 129



$$Q = 15.8 \text{ cfs}, \quad \frac{y_o}{D_o} = 1.00$$

$$\frac{V_o}{\sqrt{gy_o}} = 1.40, \quad \frac{Q}{D_o^{5/2}} = 6.25$$

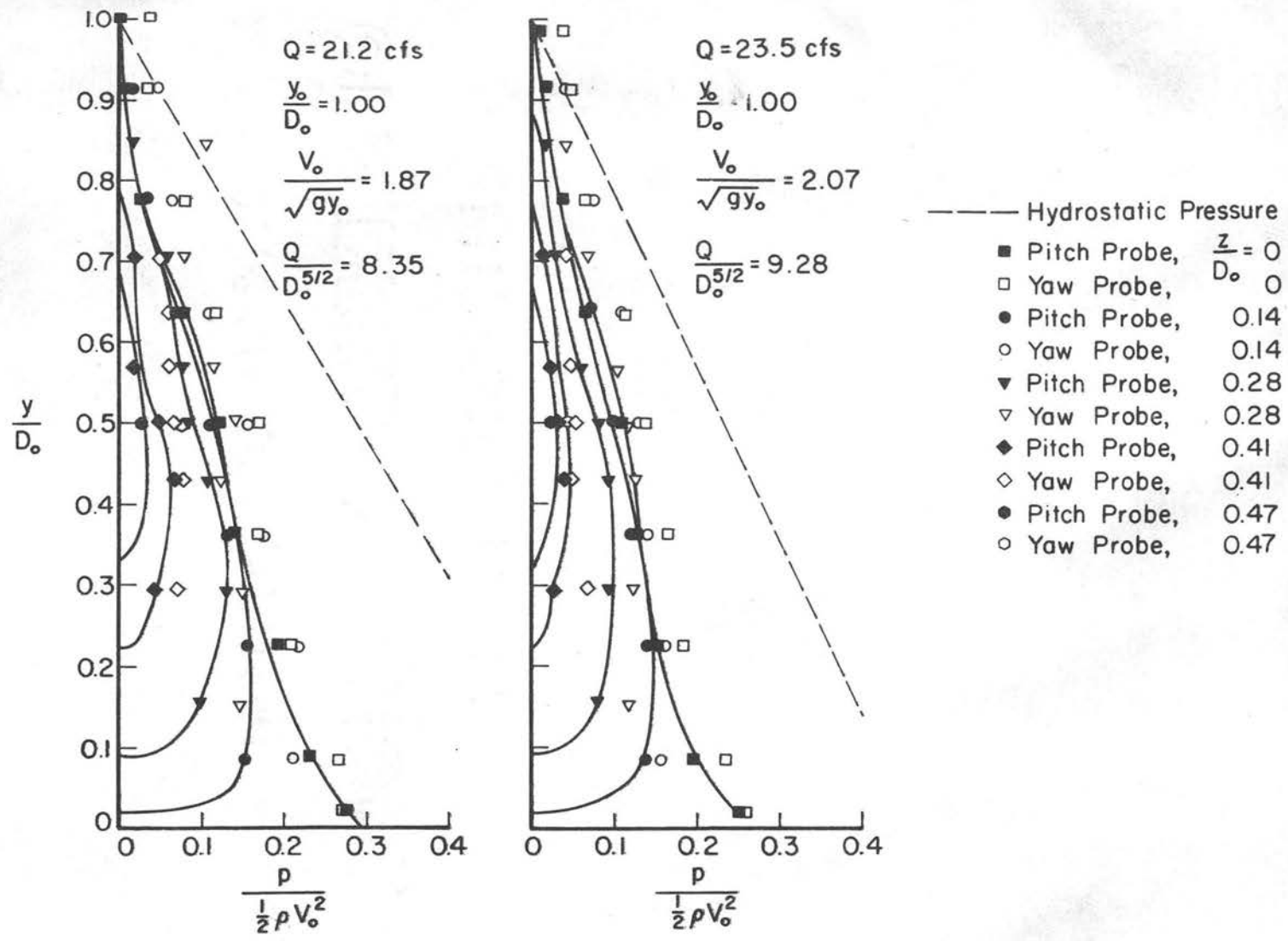
Dimensionless Pressure Plots, Circular Outfall



$$Q = 17.3 \text{ cfs}, \quad \frac{y_o}{D_o} = 1.00$$

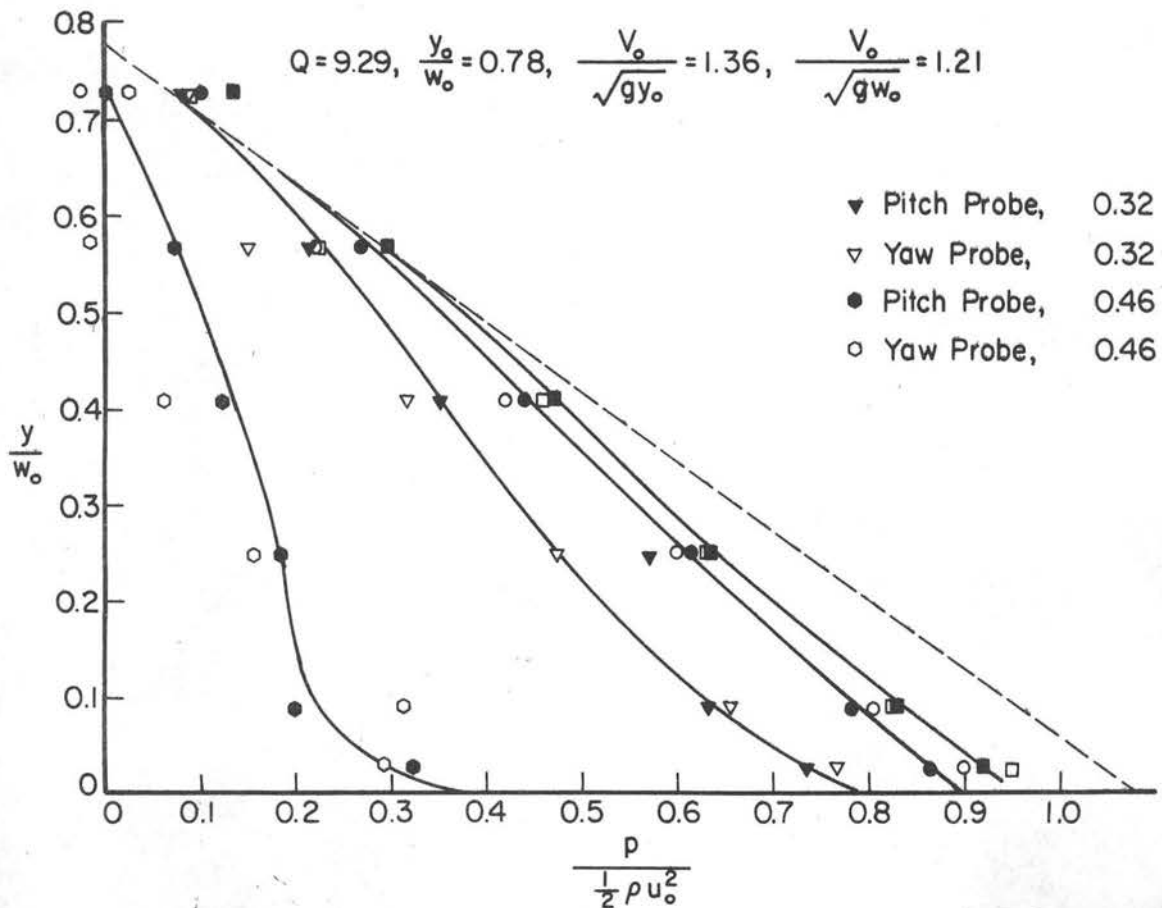
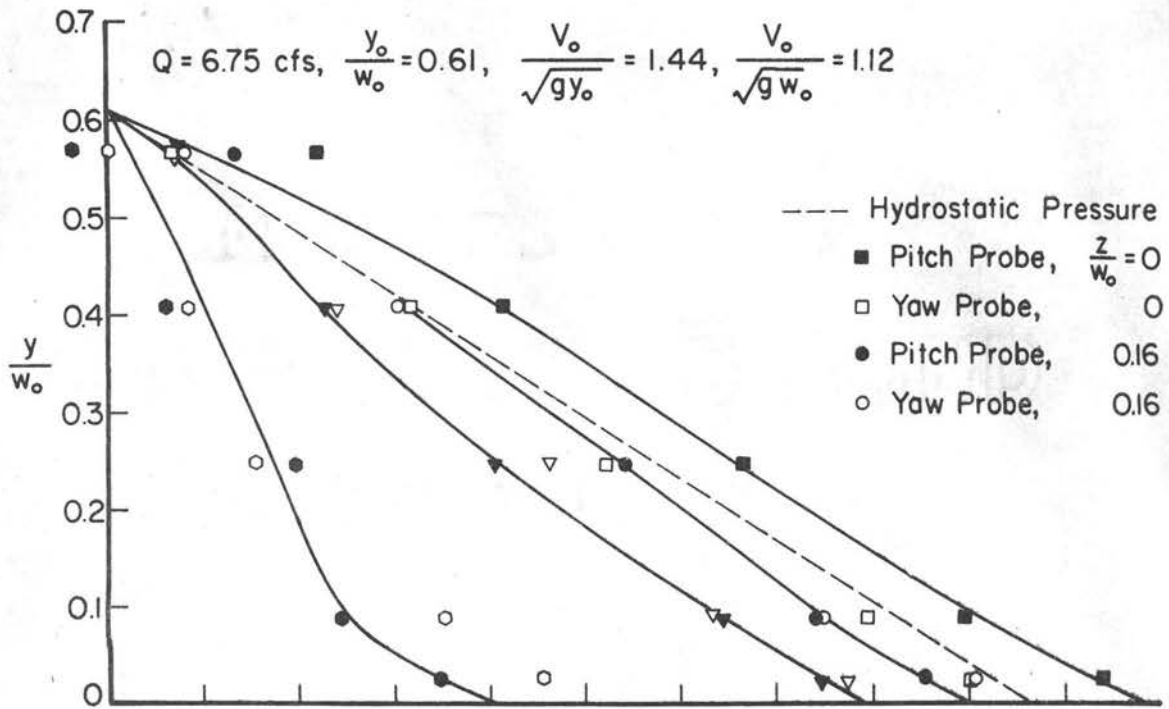
$$\frac{V_o}{\sqrt{gy_o}} = 1.53, \quad \frac{Q}{D_o^{5/2}} = 6.83$$

Fig. 130



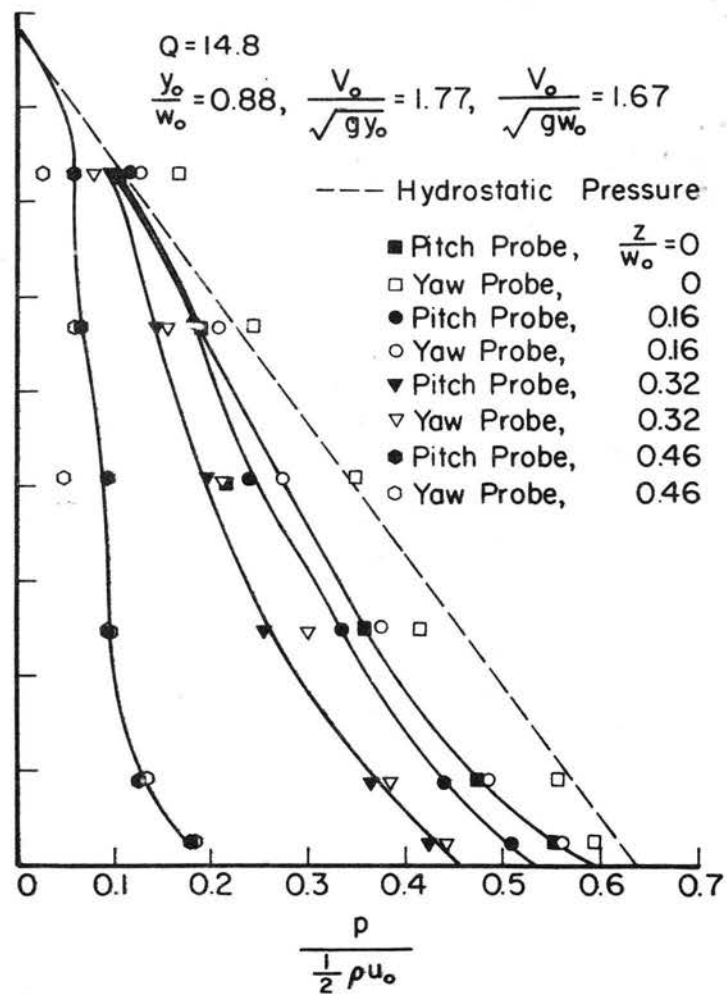
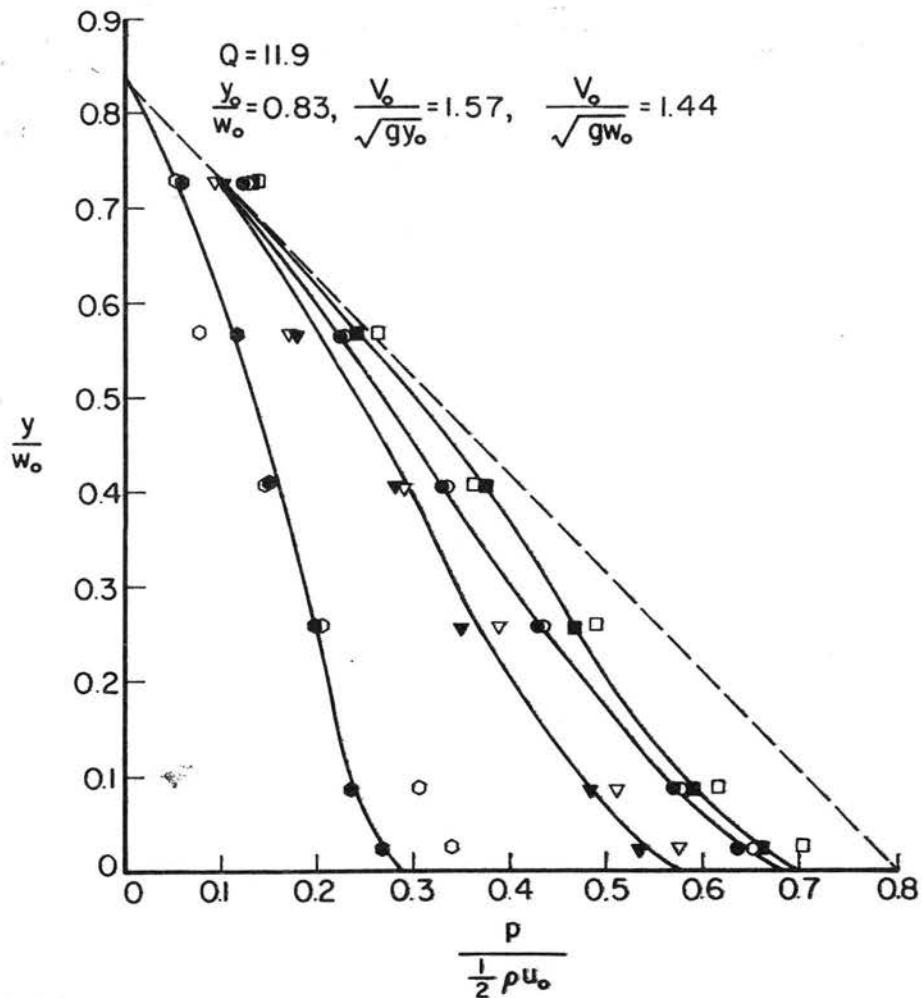
Dimensionless Pressure Plots, Circular Outfall

Fig. 131



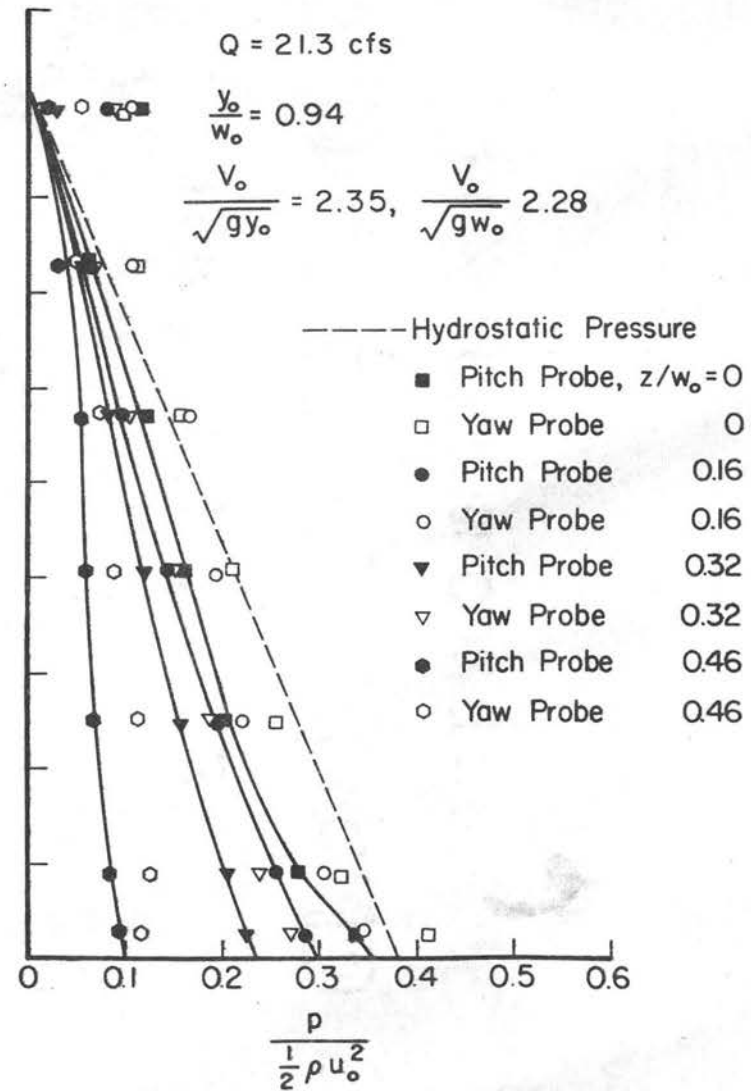
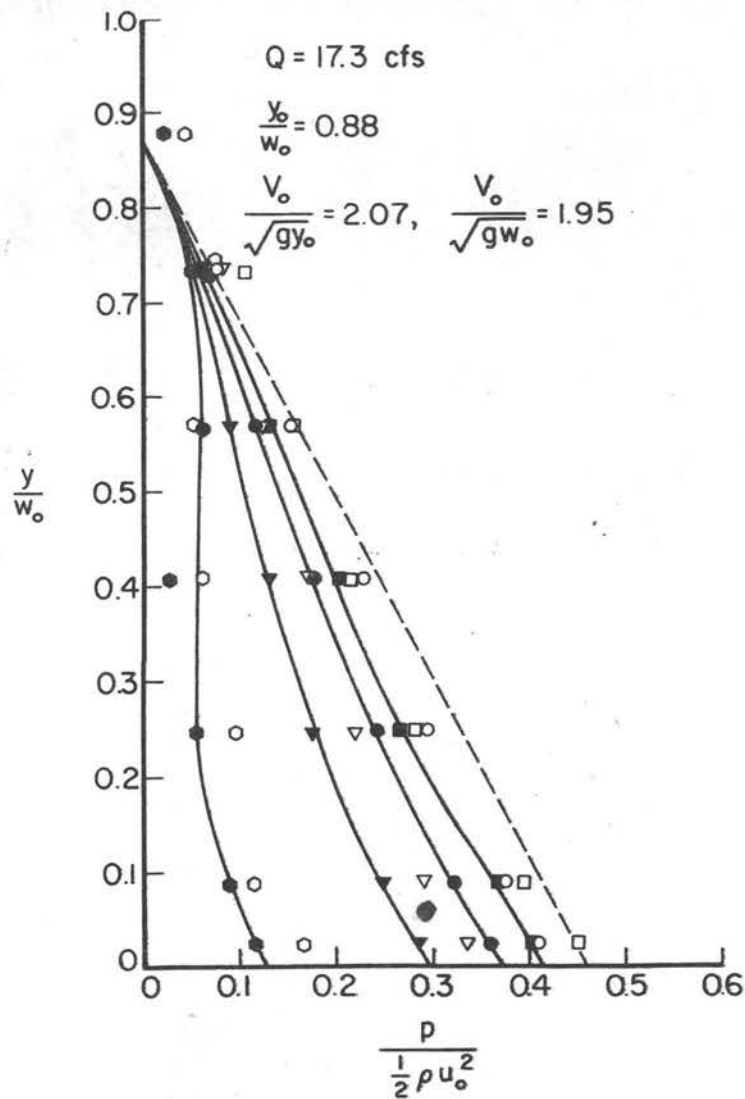
Dimensionless Pressure Plots, Rectangular Outfall

Fig. 132



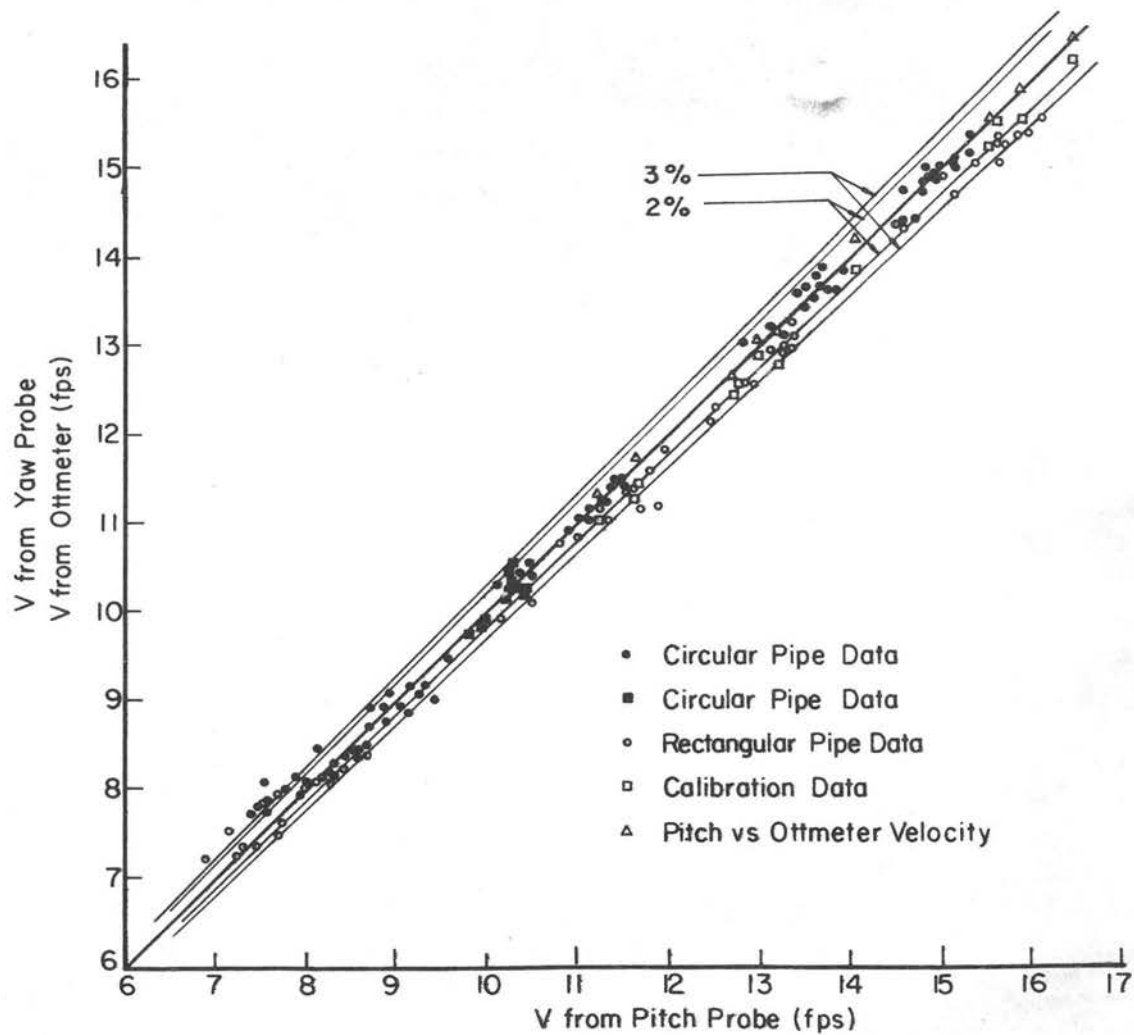
Dimensionless Pressure Plots, Rectangular Outfall

Fig. 133



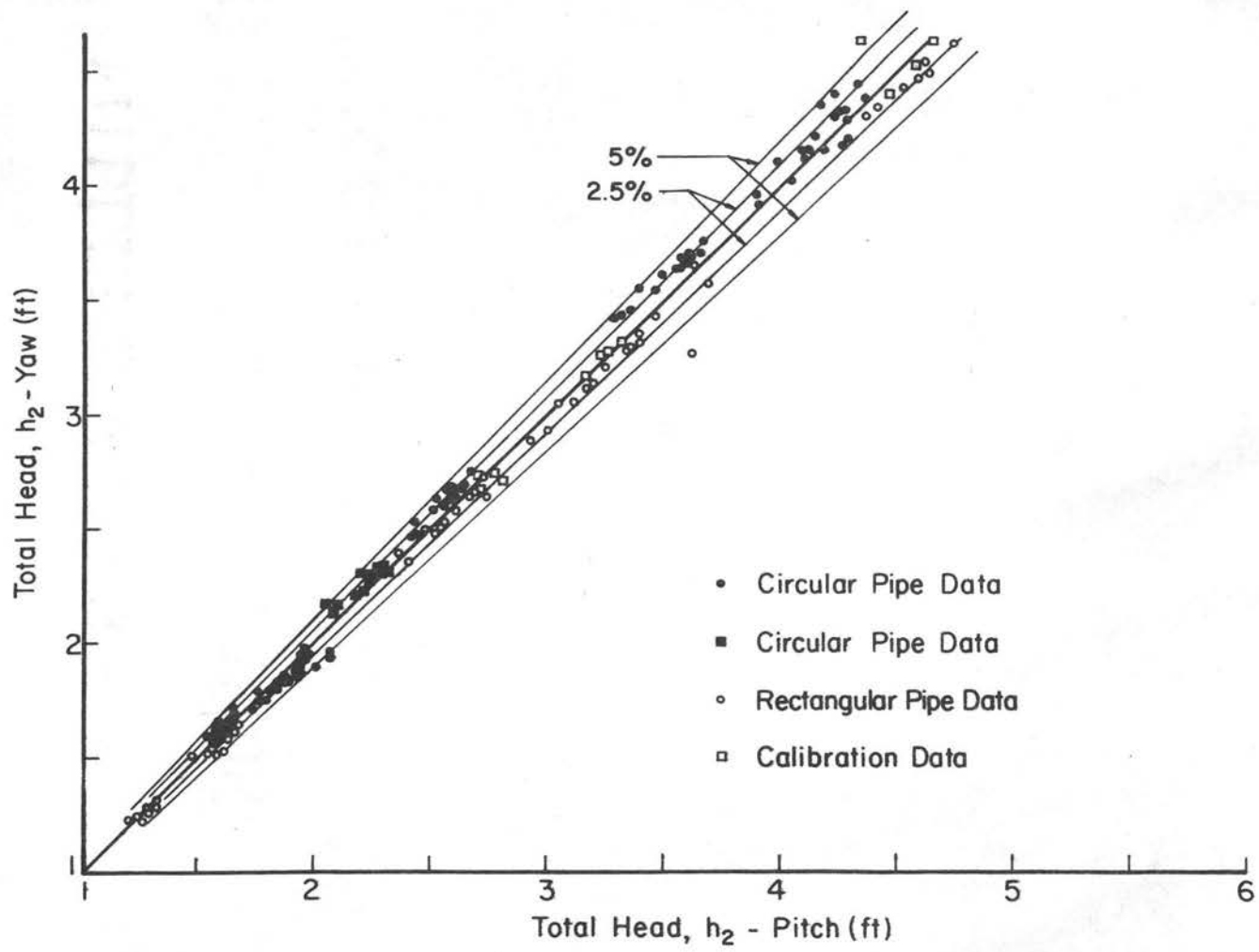
Dimensionless Pressure Plots, Rectangular Outfall

Fig. 134



Velocity Comparison, Pitch Probe versus Yaw Probe
Pitch Probe versus Ott Meter

Fig. 135



Total Head Comparison, Pitch Probe versus Yaw Probe

Fig. 136

in Fig. 135. Additionally, a plot of total head as sensed by each probe at common points was constructed, Fig. 136.

The results were inconclusive. In Fig. 135, with reference to the circular pipe data, it is apparent that for velocities below about 8.5 fps, the yaw probe sensed a larger velocity than the pitch probe. In the region of higher velocities, the velocities from the two probes were comparable.

With reference to the rectangular pipe data, the probes sensed equivalent velocities below 10 fps. For the larger velocities, the pitch probe sensed larger velocities.

In the total head plot, Fig. 136, the pitch probe consistently sensed a larger value of total head than the yaw probe during the circular pipe runs. The reverse situation occurred during the rectangular pipe runs.

It is believed that the reason for the apparent inversions is a slight change in discharge in the intervening time between yaw probe measurements and pitch probe measurements. The usual time lapse between the measurements was about an hour and one half. For the larger discharges, approximately 100,000 cu ft of water was withdrawn from the supply lake during this interval of time. Possibly the pump was drawing from a slightly cooler region of the lake, resulting in a larger coefficient of viscosity of the water. The delivery pipe was 3,000 ft long; thus a slight change in fluid characteristics could account for a small change in discharge. In any event, Figs. 135 and 136 are additional corroborative evidence of the overall consistency of the data.

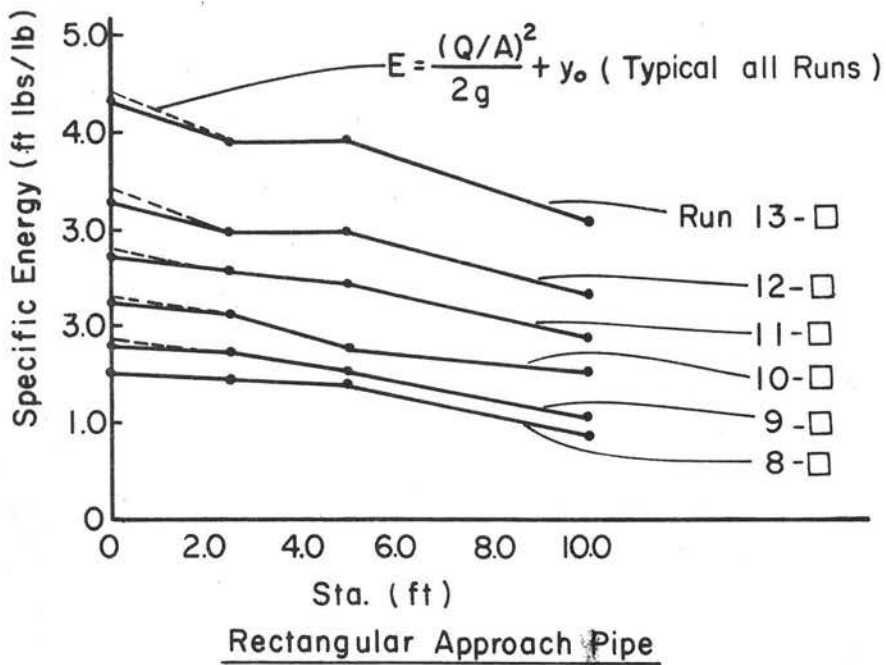
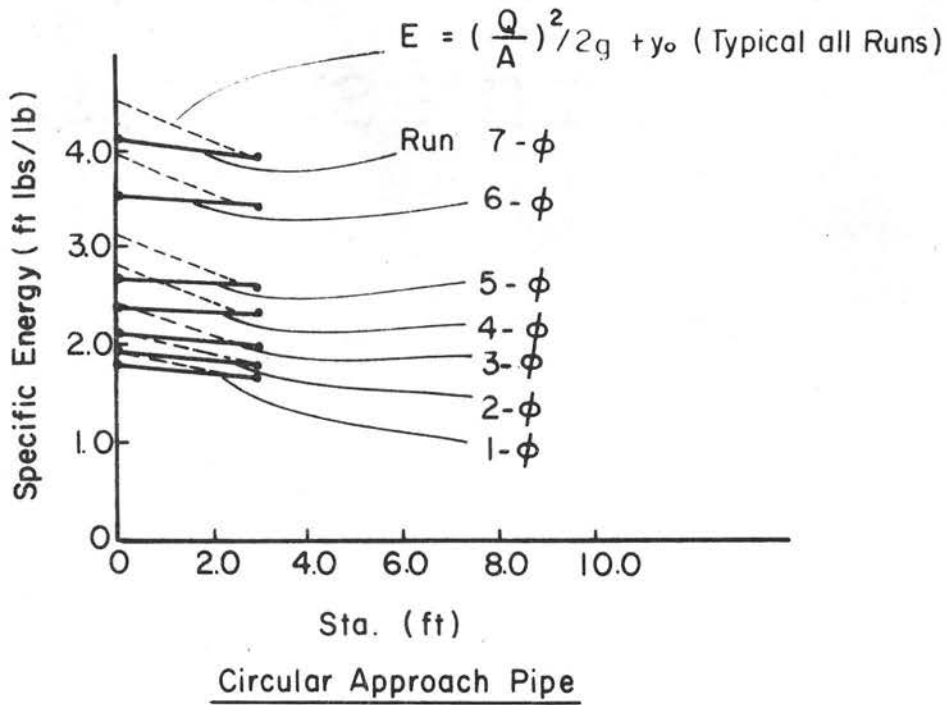
Energy Lines

To compare the energy quantities from station to station it was necessary to adjust the integrated discharges to a common quantity. The discharge obtained by integrating the pitch probe data at Sta. 0.0 was considered the most accurate measurement. The discharges obtained at stations located 2, 4, and 8 pipe diameters downstream were adjusted to the discharge obtained at Sta. 0.0. This was accomplished by shifting the face of the standing wave (the most questionable set of measurements), laterally, a sufficient distance so that the new integrated discharge (using the adjusted areas at the wave front) agreed with the discharge at Sta. 0.0. The adjustments generally amounted to less than 3% of the total discharge. No adjustments were made in the velocities.

Specific energy quantities deduced from the adjusted data are shown in Fig. 137. It is apparent that most of the energy is dissipated in the zone of shallow, high speed flow downstream of Sta. 2.5.

A comparison between energy quantities computed using Eqs. 2-2 and 3-5, is shown at Sta. 0.0. There is a significant difference. This points out the necessity for using corrective factors in the zone of curvilinear flow at the outfall section.

It was not considered practical to publish the voluminous basic data collected during this study. These data and the roughness data described in Chapter V are compiled in a separate data report which is available at cost to interested parties.



Energy Lines Fig. 137
 Run 1 - φP Through 12 - □ - P

Chapter IV

WATER SURFACE CONTOURS AND VELOCITY DISTRIBUTION

Introduction

For basin design, it is necessary that the configuration of the water surface and the approximate magnitude and direction of velocity be predictable in the rapidly varied flow region adjacent to the culvert outlet. The information presented here is valid for any abrupt expansion, where the floor is set at the elevation of the approach pipe invert, continuing at the same slope. The flow in the region adjacent to the outlet will always be supercritical, and, therefore, the outlet is the control section. Oblique or normal hydraulic jumps downstream cannot affect the flow in the supercritical flow region. It is assumed that the slope of the basin is mild or horizontal and thus does not significantly affect the upper flow region.

As a part of the CSU project, a special study entitled, "The Geometry of the Expanding Jet Downstream of Culverts" was made by Roland Stephan (17). Assuming inviscid flow, a numerical, computer-oriented method was devised to solve dimensionless Euler and continuity equations simultaneously. The method was applied to a semi-free (supported on the bottom only) expanding jet. Unfortunately, there were limitations to the program. As can be readily seen by scaling the Euler equations, two flow parameters are important: Euler's number $E = \frac{p}{\frac{1}{2}\rho V^2}$ (where p is the pressure in lbs/sq ft, ρ is the mass density of the fluid, and V_0 is the average velocity at the section), and the Froude number, $Fr = \frac{V_0^2}{gy_0}$, where g is the acceleration of

gravity and y_0 is a length parameter. The Euler parameter poses a problem. The pressure distribution at the outlet section where the water literally falls away is not predictable. Vertical as well as lateral accelerations markedly distort the usually assumed hydrostatic pressure variation. Certainly the pressure distribution for a deep, narrow channel flowing nearly full would vary considerably from that of a wide shallow channel. Where the approach pipe is circular, the pressure variation is even more extreme and not predictable.

By a laborious trial and error procedure, it was possible to solve the numerical equations, Ref. 17, for two specific water surface configurations for the rectangular approach pipe, i.e., a pressure distribution was assumed; the water surface configuration was computed, then compared with previously obtained profiles and the procedure repeated until the profiles matched. To obtain a satisfactory solution for the circular approach pipe, it was necessary to experimentally measure the pressure field for various outlet height-to-width ratios with a systematic increase of Froude number. Once the initial boundary conditions (pressure distribution in particular) were known, the equations could be used with a fair degree of accuracy for predicting the water surface configuration.

Computer-generated output is not used in this chapter. At the time the pressure field was measured, sufficient information was gathered at successive stations downstream to adequately define the water surface and the velocity field. The value of the work in Ref. 17 as far as this chapter is concerned is that by utilizing the measured pressure and the Froude parameter, the water surface was predictable. This is cited as evidence that the equations were properly scaled and

are general; i.e., even though data was collected for only one pipe size, the data should be scalable. As long as the geometric ratios and Froude number are similar, the dimensionless water surface profiles and velocity distribution for circular and rectangular approach pipes presented in this chapter should be general.

Another reference that essentially substantiates the above conclusions is "Design of Channel Expansions," by H. Rouse, B. V. Bhoota, and En-Yun Hsu, (13). In the section "Characteristics of Flow at an Abrupt Expansion," the author delineates the appropriate variables. In the nomenclature of the CSU study, these were Y_0 and V_0 , the depth and mean velocity at the outlet section; W_0 , the width of the rectangular approach channel D_0 for the circular pipe; x and z , the longitudinal and lateral coordinates measured from the outlet section and centerline, respectively; the depth of flow at any point in the basin y ; and gravity g . The variables were combined into the following dimensionless relationship:

$$\frac{Y}{Y_0} = f \left(\frac{x}{y_0}, \frac{z}{y_0}, \frac{W_0}{y_0}, \frac{V_0}{\sqrt{gy_0}} \right) . \quad (\text{Eq. 45, Ref. 13})$$

The relative depth y/y_0 at any point of the flow should depend on the relative coordinate location $\frac{x}{y_0}$ and $\frac{z}{y_0}$, the relative width of the channel outlet $\frac{W_0}{y_0}$, and the Froude number of the approach flow $\frac{V_0}{\sqrt{gy_0}}$.

The authors then proceeded to a graphical solution of the problem based on the "method of characteristics." It is stated that "the method of characteristics, in effect, reduces the functional relationship (Eq. 45 above) to the form

$$\frac{Y}{Y_0} = f_2 \left(\frac{x}{W_0}, \frac{y}{W_0}, \frac{V_0}{\sqrt{gy_0}} \right),$$

by combining the relative coordinate terms x/y_0 and z/y_0 with the initial width-depth ratio W_0/y_0 . This entails the inherent assumption of hydrostatic pressure distribution at all points--that is, the absence of appreciable vertical acceleration." The authors then point out the discrepancy between the hydrostatic pressure assumption and the actual situation for various outlet width to depth ratios. Measured surface contours for three width-depth ratios ($\frac{W_0}{Y_0} = 2, 4, \text{ and } 8$) were plotted and reproduced in this paper as Fig. 148. The authors state that "The deviations with W_0/Y_0 are appreciable but nevertheless secondary to the variation with Froude number."

With reference to Fig. 148, experimental data for Froude numbers of 2, 4, and 8 group reasonably well; however, it is obvious that there is considerable "deviation" of the dimensionless surface contour lines for a Froude number of 1, from the other three larger values. The range of Froude number from 1.0 to 2 is unfortunately the region where a majority of culverts operate.

Three other shortcomings of the information concerning energy basin design, presented in the previously mentioned paper, (13) are:

(a) For a Froude number of one, dimensionless surface contours along the centerline are only presented for a distance of 1.7 pipe diameters.

(b) No information is presented concerning the magnitude or direction of the velocity associated with the water surfaces.

(c) The information shown is probably not applicable for circular approach pipes in the low Froude number range.

To obtain sufficient information for energy basin design, it was necessary to carry out the following experimental program.

Test Program and Procedure

The experimental data described in this section were collected at the same time as the data discussed in Chapter III. The test basin was 10 ft 0 in. wide and 14 ft 0 in. long with vertical walls and a smooth horizontal aluminum floor. Two approach pipes, 1.45 ft internal diameter, smooth, circular pipe, and 1.25 ft by 1.25 ft smooth rectangular pipe, were used.

For the circular pipe, the procedure was to establish the discharge, allowing sufficient time for the system to stabilize, then measure the water surface to the nearest 0.005 ft at cross sections located one, two, and three pipe diameters downstream of the outlet. At the section two pipe diameters downstream, the section where it is proposed to install the first row of roughness elements, Chapter V, sufficient data was collected so that the velocity field is well defined. The yaw probe previously described was used as a point gauge for determining water surface elevations and was also used to obtain the direction and magnitude of velocity. After inspecting the data from the circular pipe runs, the procedure was modified slightly.

For the rectangular approach pipe, velocity data were collected at two cross sections, two pipe widths and four pipe widths downstream. Also, cross-sectional data were dispensed with at sections one and three pipe diameters downstream. The additional velocity data are not essential for design; they do, however, contribute a little more information about the flow field.

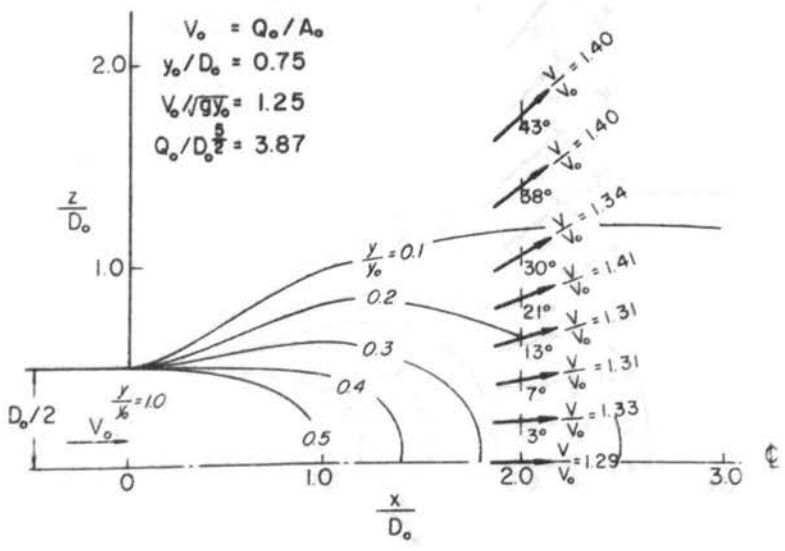
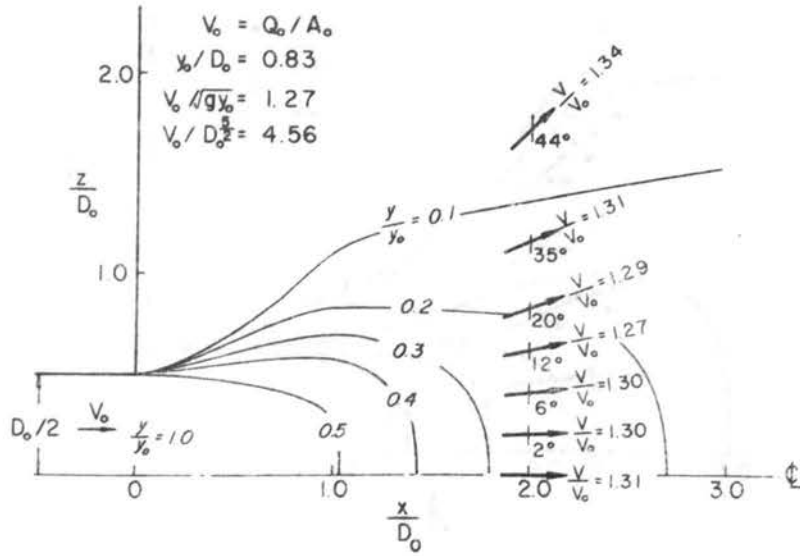
At Stas. $1 D_0$, $2 D_0$, and $3 D_0$, water surface profile data were collected every 0.3 ft transversely in the central portion of the basin and at 0.5 ft increments elsewhere. Velocity data at Stas. $2 D_0$ and $4 D_0$ were collected at the points displayed in Fig. 125, Chapter IV.

For the circular pipe, seven discharges were examined with the value of $\frac{Q}{5/2 P}$, varying from 3.87 cfs to 9.28 cfs. For rectangular approach pipes, six discharges were examined with the Froude numbers $\frac{V}{\sqrt{gy_0}}$ varying from 1.36 cfs to 2.35 cfs. Run numbers and significant flow parameters are listed systematically in Table IV, Chapter III.

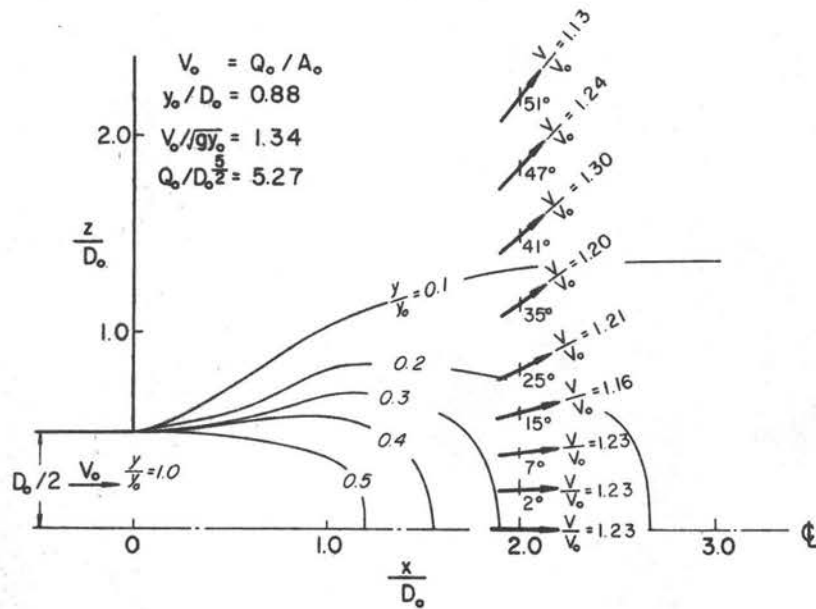
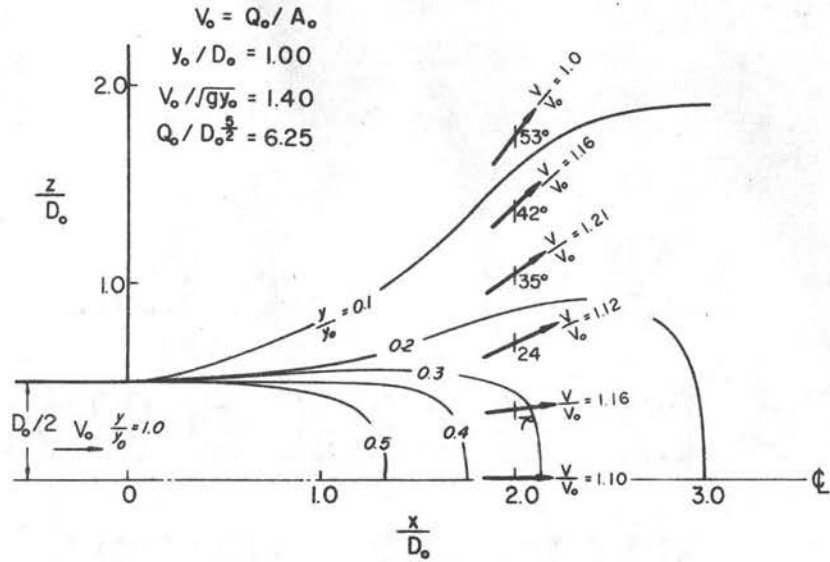
Data Reduction and Presentation

For each flow condition, the measured ordinates of the water degree surface y were scaled (y/y_0) using the depth of water at Sta. 0.0, y_0 , as the reference length. The lateral coordinate z and the longitudinal coordinate x were scaled $\left(\frac{z}{D_0}$ and $\frac{x}{D_0}\right)$ using the width of the approach conduit D_0 , (or W_0) as the reference length. The measured magnitude of velocities V were scaled $\left(\frac{V}{V_0}\right)$, using the mean exit velocity. The angle of the velocity vector is already dimensionless. This is the same dimensionless grouping that was deduced and used in Ref. 17.

The scaled data were then plotted, and contour lines drawn through appropriate points. The completed plots are shown as Figs. 138 through 147. Note that one additional dimensionless parameter, the ratio of the depth of flow at Sta. 0.0 over the width of the approach channel $\left(\frac{y_0}{D_0}$ or $\frac{y_0}{W_0}\right)$, accompanies each of these diagrams. Because of the unpredictability of the pressure at the outlet section and its consequent effect on the flow field, this ratio must be approximately

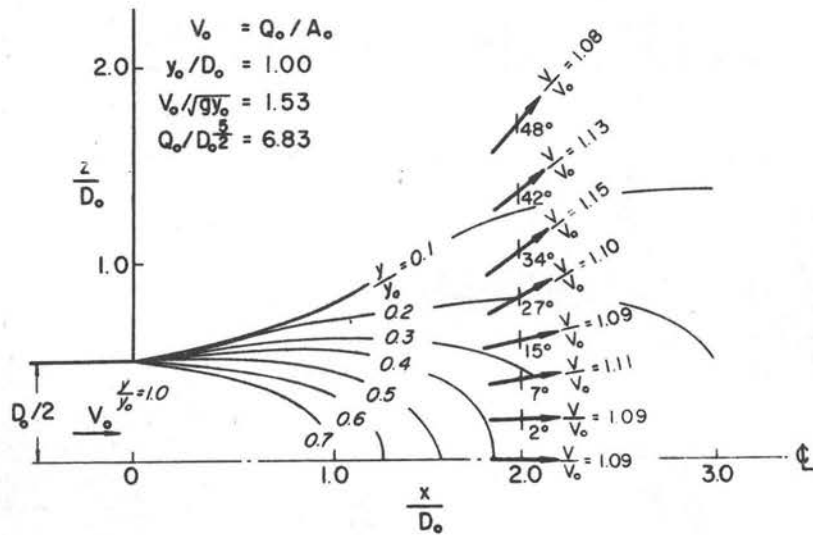
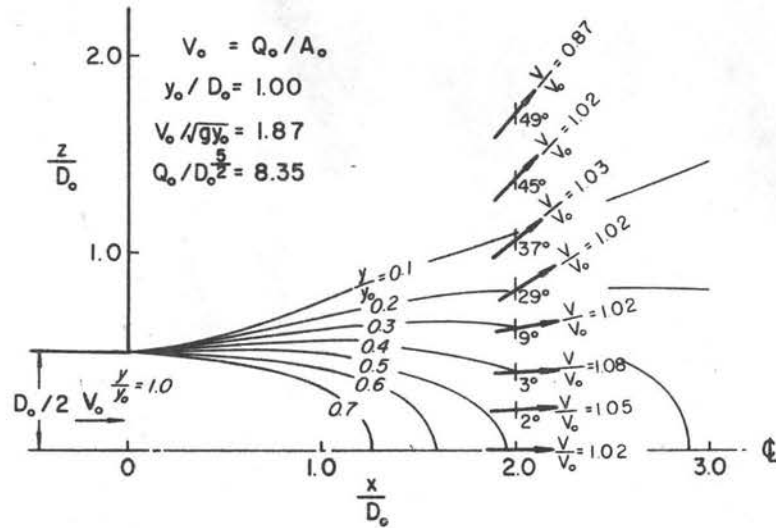


Dimensionless Water Surface Contours and Relative Velocities, Circular Outfall Fig. 138

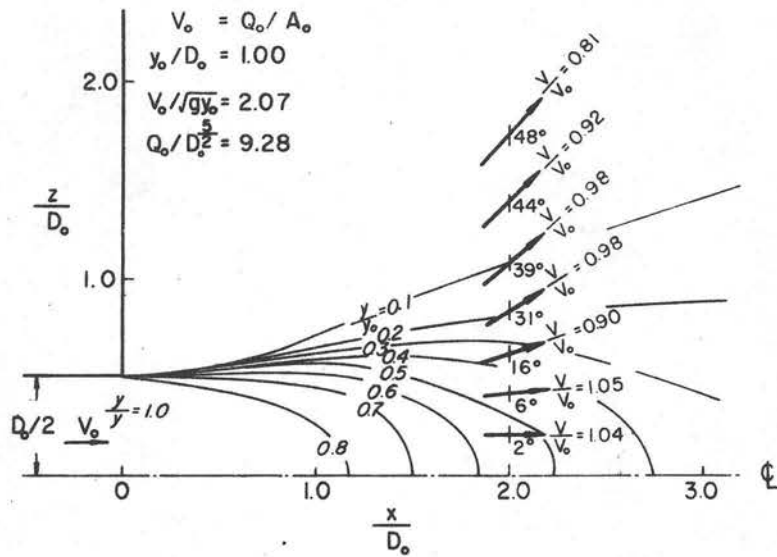


Dimensionless Water Surface Contours and Relative Velocities, Circular Outfall

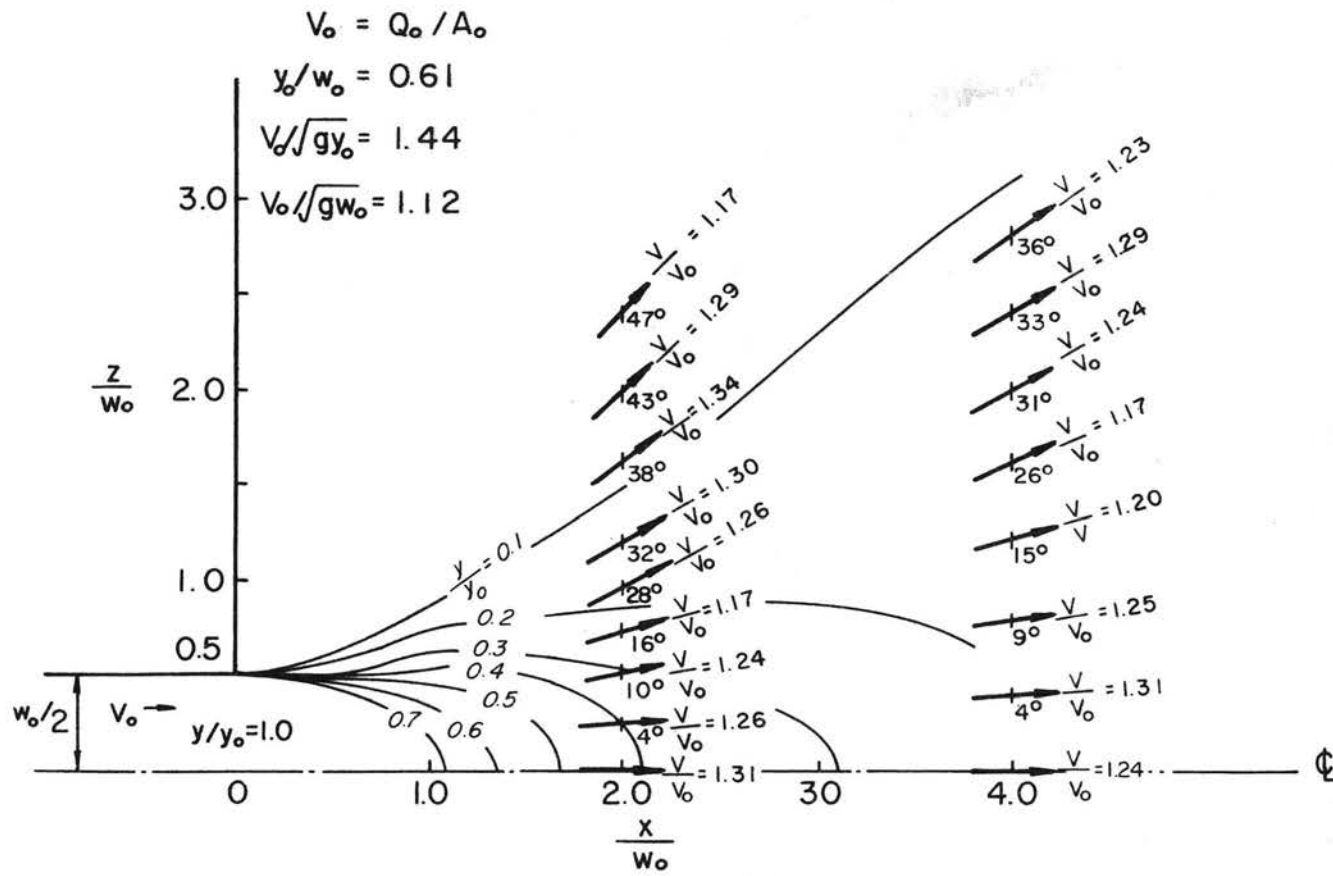
Fig. 139



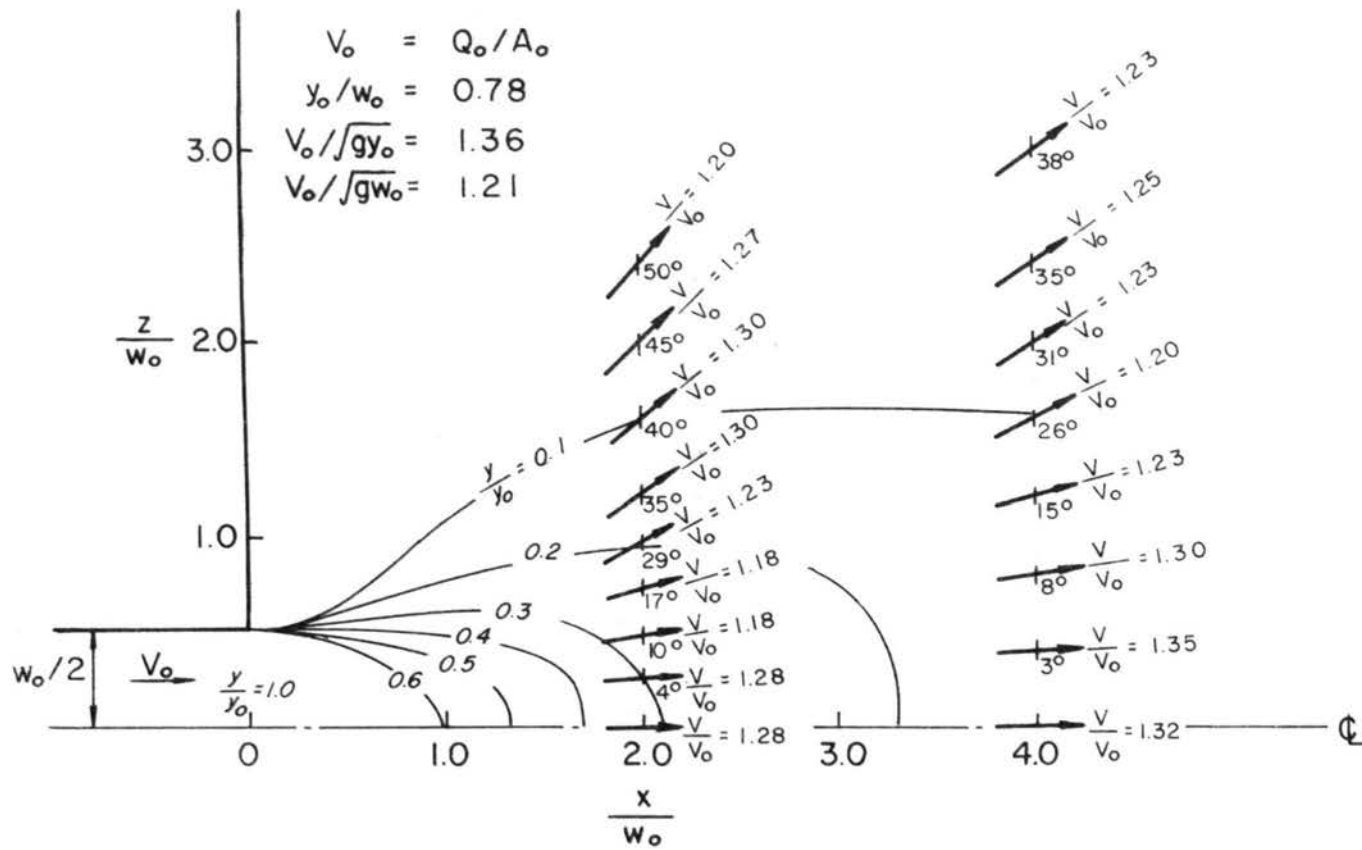
Dimensionless Water Surface Contours and Relative Velocities, Circular Outfall Fig. 140



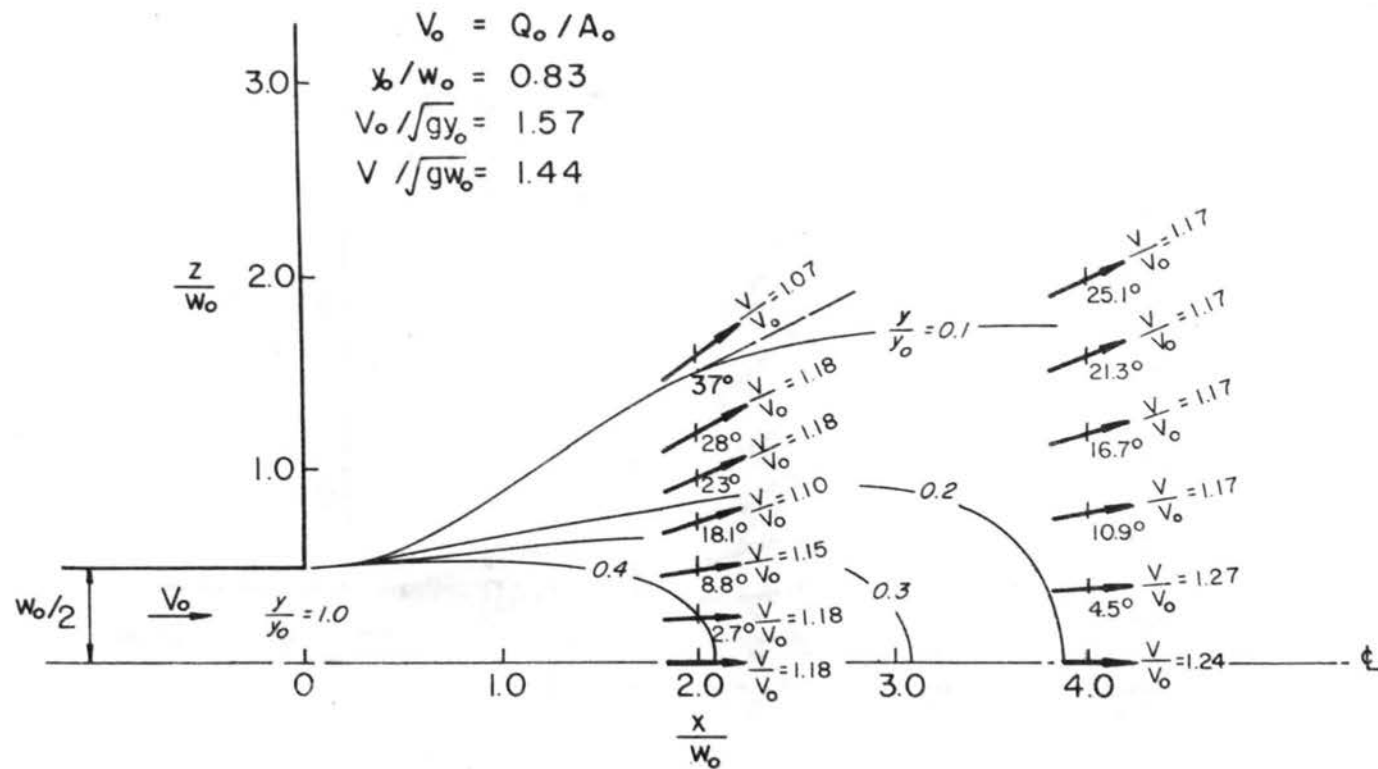
Dimensionless Water Surface Contours and Relative Velocities, Circular Outfall Fig. 141



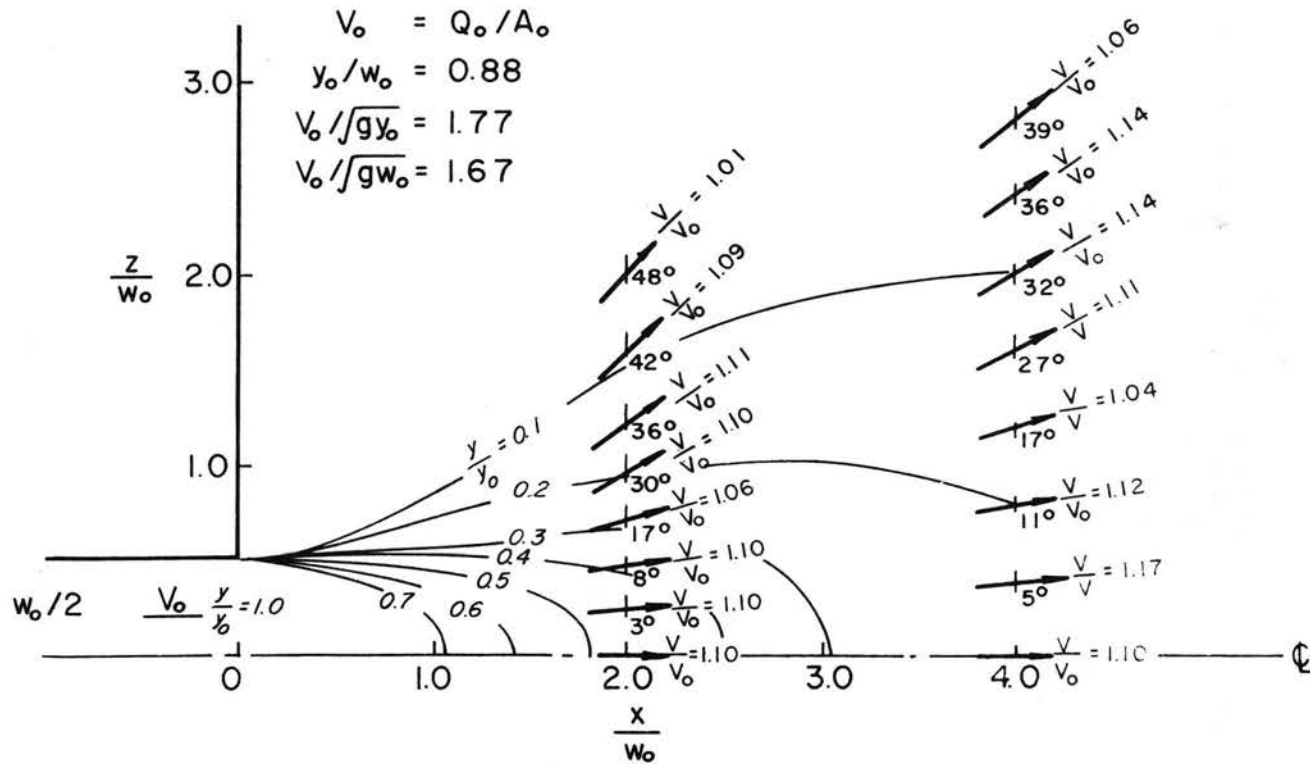
Dimensionless Water Surface Contours and Relative Velocities, Rectangular Outfall Fig. 142



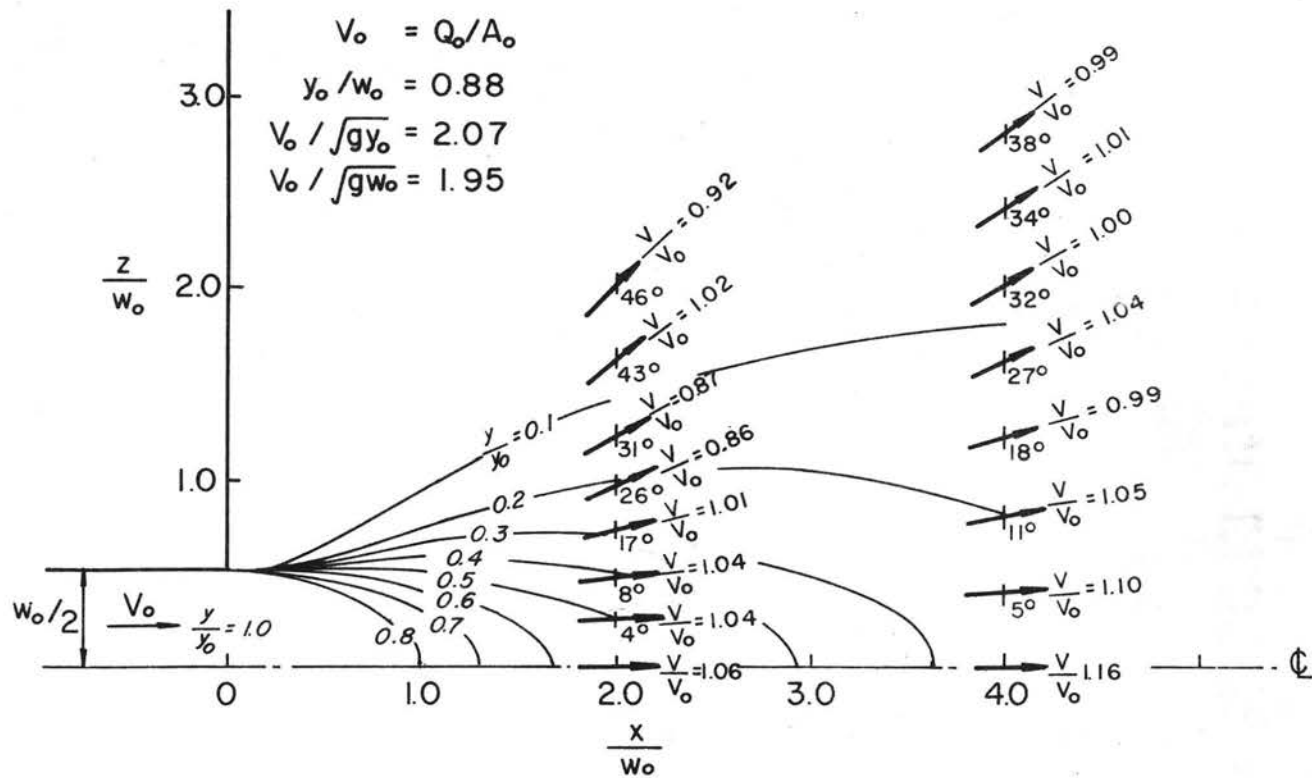
Dimensionless Water Surface Contours and Relative Velocities, Rectangular Outfall Fig. 143



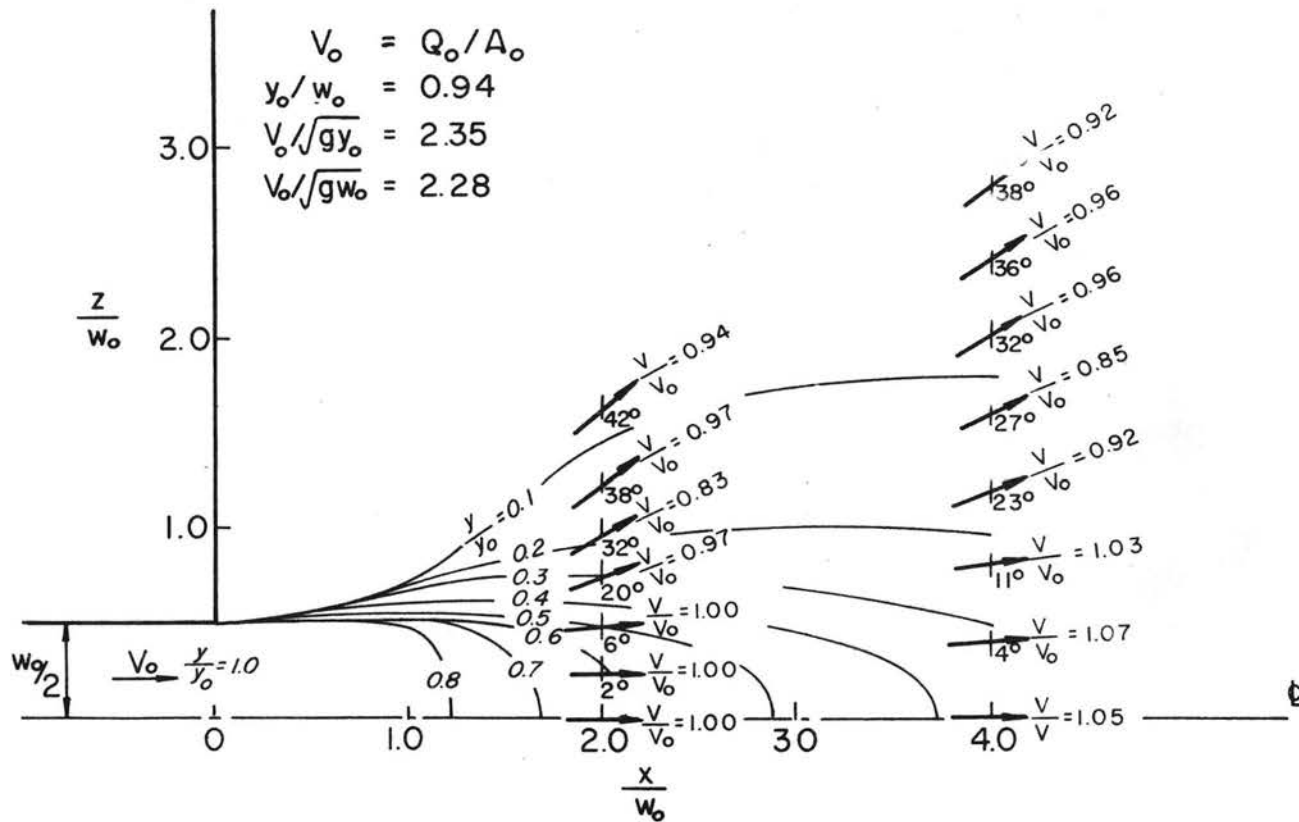
Dimensionless Water Surface Contours and Relative Velocities, Rectangular Outfall Fig. 144



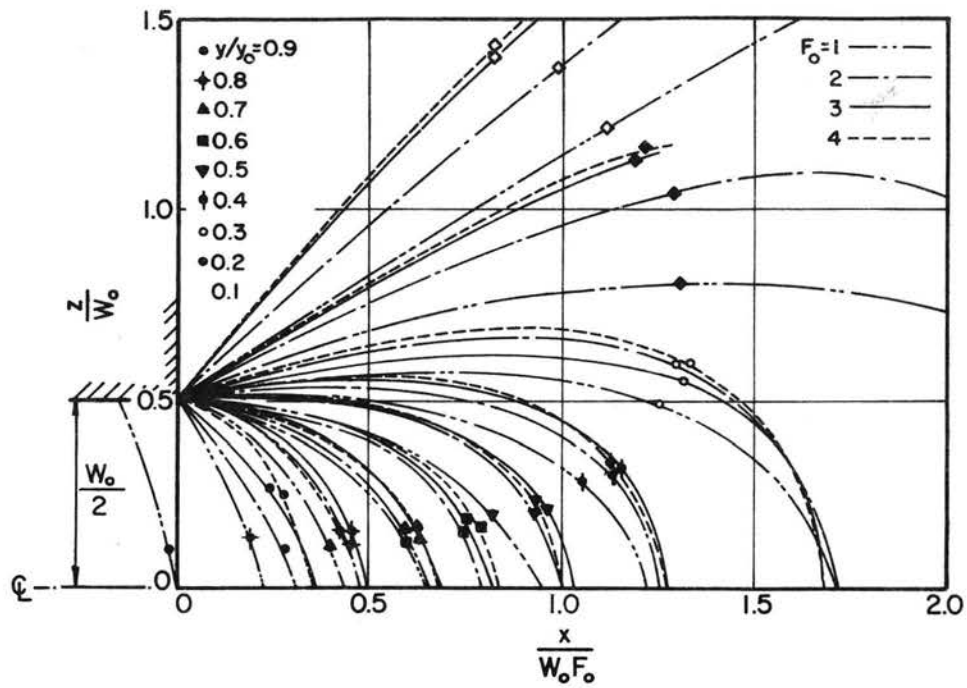
Dimensionless Water Surface Contours and Relative Velocities, Rectangular Outfall Fig. 145



Dimensionless Water Surface Contours and Relative Velocities, Rectangular Outfall Fig. 146



Dimensionless Water Surface Contours and Relative Velocities, Rectangular Outfall Fig. 147



Dimensionless Water Surface Contours
 Reproduced from Ref. 13

Fig. 148

the same for model and prototype. This is particularly important (as can be seen in Fig. 148) for Froude numbers up to 2. For higher Froude numbers, this ratio becomes progressively less significant; i.e., the pressure force, regardless of how it varies, no longer makes up a significant portion of the force-momentum quantity. Velocity dominates the quantity. Figure 148 is recommended for design purposes where the exit Froude number is larger than 2.5.

The plots are essentially self explanatory. Given a pipe size and exit velocity (which can be estimated by conventional culvert hydraulics), the parameters $F_3 = \frac{V_0}{\sqrt{gy_0}}$, $V_0 = \frac{Q_0}{A_0}$ and $\frac{y_0}{D_0}$ are formed. The engineer then selects the dimensionless plot that most closely matches F_0 and $\frac{y_0}{D_0}$ and proceeds with plotting. Because of the rather close grouping of Froude numbers, it is probably not necessary to extrapolate between plots, though it can be done this way. Further discussion of the use of these plots is deferred to the final chapter where application of the figures is described.

Chapter V

DRAG COEFFICIENTS

Problem Statement

The method of analysis proposed for artificially roughened energy basins requires that the coefficient of drag, associated with a particular grouping and size of roughness elements in a basin of specific size, be known. Several circumstances complicate the problem. In the upper portion of the basin over the first few rows of elements, the flow is very irregular and turbulent. The flow, serrated and thrown into the air by the elements, is characterized by a high degree of air entrainment. In many cases, a large separation bubble or vacant gap, open to the atmosphere, forms in the lee of the element. The flow field is not continuous and, therefore, no hope for a theoretical solution exists.

In the literature, there is a large accumulation of information concerning drag coefficients associated with both streamlined and bluff bodies in ambient flow. Most fluid mechanics texts have a table listing approximate values of drag coefficients for rectangular-shaped plates mounted normal to the flow. When a comparison is made between the stream pattern produced by a plate in ambient flow and by a plate protruding into the flow with one edge attached to the boundary, one important difference is noticeable. Where the element is attached to the boundary, the approach velocity at the boundary must be zero, and at least a portion of the element is submerged in the boundary layer. This contrasts with a uniform mean stream velocity of the element in ambient flow in Ref. 20, "Separation Flow Downstream of a Plate Set Normal to a Plane

Boundary," by H. S. Nagabhushanaiah, the boundary layer is shown to have a large effect on the drag coefficient. Depending on the ratio of the boundary layer height divided by the height of the element, the coefficient of drag based on the mean stream velocity varied from 1.2 to 0.3.

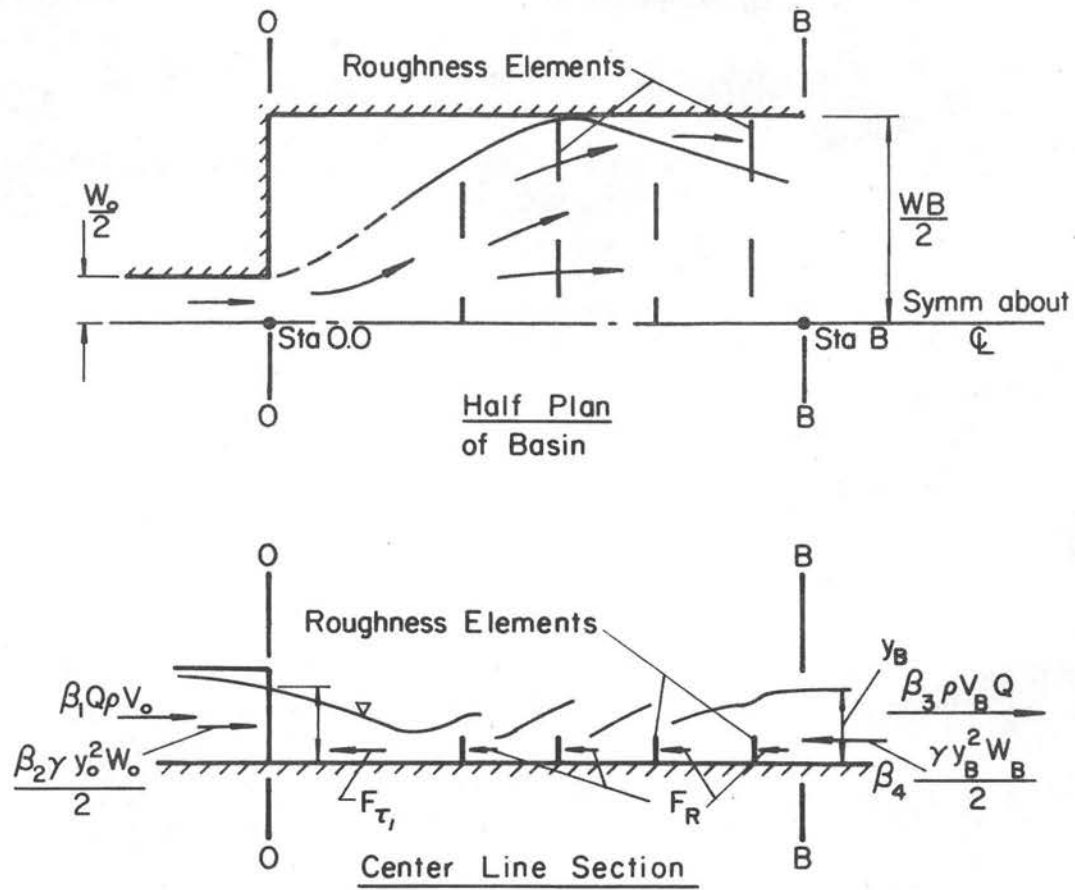
Additionally, the drag coefficient determined for an individual isolated element is not comparable with the overall coefficient derived for a group of elements. The interaction between the fluid and the roughness elements, floor, and basin walls is very complex. Shielding of the downstream elements by those upstream, non-uniform and multi-directional distribution of the fluid as it passes over and around the elements, large scale air entrainment, and burial of some of the downstream elements in the low velocity standing waves originating from the walls combine to drastically reduce the magnitude of the overall coefficient.

This chapter describes the experimental study conducted for the purpose of obtaining usable drag coefficients for various groupings of roughness elements of known dimensions installed in basins of known geometry.

Design Method

The design procedure is based on the impulse-momentum principle. With reference to Fig. 149, the momentum equation written in the direction of flow between Sta. 0.0 and Sta. B is

$$\beta_1 \rho V_0 Q + \beta_2 \gamma \frac{y_0^2}{2} W_0 = F_{\tau_1} + F_R + \beta_3 \rho V_B Q + \beta_4 \gamma \frac{y_B^2}{2} W_B \quad (5-1)$$



Definition Sketch for Drag Coefficient Evaluation

Fig. 149

F_R is the drag force exerted on the flow by the combined group of roughness elements and is defined as

$$F_R = C_D A N \rho \frac{V_a^2}{2} \quad (5-2)$$

where

C_D = dimensionless drag coefficient,

A = frontal area of a roughness element,

N = number of elements, and

V_a = the approach velocity at the first row of roughness elements, defined as the value V , two pipe diameters downstream of the outlet. Knowing Q/A at the outlet, V_a is readily obtained from Figs. 138 through 147, Chapter IV. F_{τ_1} is the shear force exerted by the floor on the flow in the area upstream of the roughness elements and downstream of the outlet. Henceforth, this small quantity is included in the F_R term and is not considered further. Other variables in the equation have been previously defined.

Making use of the continuity equation $Q = V_B W_B Y_B$, where W_B and Y_B are the width and average depth of flow at section B , and V_B is the average velocity passing through the section,

$$Y_B = \frac{Q}{V_B W_B} \quad (5-3)$$

Inserting the value of Y_B and F_R (Eq. 5-2) into Eq. 5-1, the following relationship is obtained:

$$\beta_2 \rho V_o Q + \beta_1 \gamma \frac{y_o^2}{2} W_o = C_D A N \rho \frac{V_a^2}{2} + \beta_3 \rho Q V_B + \beta_4 \frac{\gamma Q^2}{2 V_B^2 W_B} \quad (5-4)$$

This is the design equation. For a given discharge, approach pipe, basin geometry, and a known C_D , an estimate of V_B , exit velocity from the basin, is readily obtained.

Experimental Procedure for Obtaining C_D

Equation 5-4 with slight modification was used to evaluate C_D . The procedure was as follows:

(a) Subject a basin of known dimensions and pattern of roughness elements to a specific discharge.

(b) At a section downstream of the last row of roughness elements, utilize the yaw probe to measure the flow quantities, velocity, and pressure.

(c) Making use of Eq. 3-10 and the measured quantities from step (b), evaluate the quantity

$$\sum_i P_i \Delta A_i + \sum_i \rho V_i^2 \cos^2 \phi_i \cos^2 \phi_i \Delta A_i$$

which was shown in Chapter III to be equivalent to

$$\beta_4 \frac{\gamma Q^2}{2B_B W_B} + \beta_3 \rho Q V_B$$

(d) Evaluate the terms $\beta_2 \rho V_o Q + \beta_1 \frac{y_o^2}{2} W_o$. This information is available from the study of flow properties at Sta. 0.0, described in Chapter III.

(e) Subtract the quantity obtained in step (c) above from the quantity obtained in step (d). The remaining quantity is the drag force exerted by the group of elements on the flow, F_R .

(f) Knowing F_R , solve Eq. 5-2 for C_D .

A complicating circumstance arose. It was impossible to obtain reliable velocity and water surface elevations directly downstream of the elements. For this reason, the measuring station was established at Sta. 11.0, several feet downstream of the last row of elements. To estimate the flow properties directly downstream of the elements, a small correction is necessary for the bed shear between the last row of angles and the measuring station.

The empirical formula used to estimate the smooth floor shear force was

$$F_{\tau_i} = \left(\frac{L_i}{8} \right) \left(\frac{V_{11.0 (i)}^2}{V_{11.0 (o)}^2} \right) F_{\tau_o} \quad (5-5)$$

With reference to centerline profile A, Fig. 150, it was assumed that the smooth floor shear force, F_{τ_o} , was directly proportional to the length of the smooth floor, L_i (width constant), and to the average velocity at Sta. 11.0 squared.

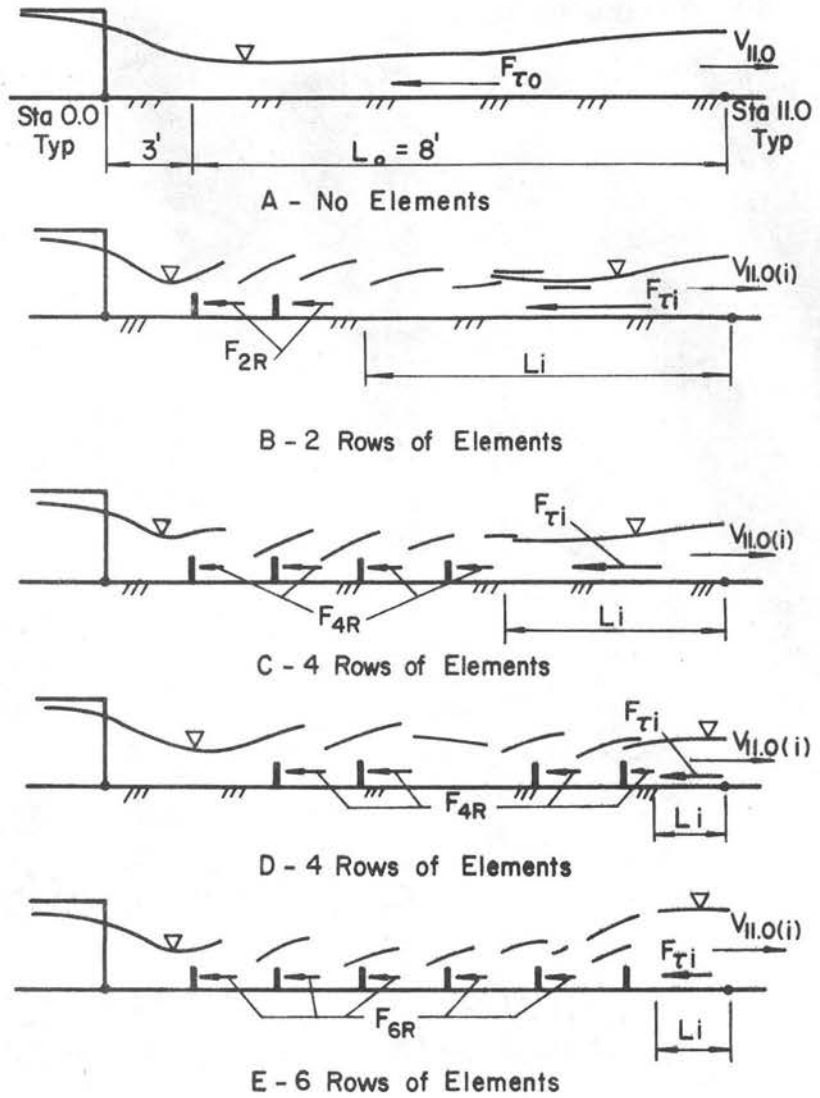
It is known that the friction factor is reduced in flow containing large quantities of entrained air. Also, a significant portion of the flow was airborne, particularly downstream of the first two rows of elements. An approximate compensation for these factors is embodied in the length L_i , chosen for the various element size and patterns.

Values of L_i are given in Table V, shown in Fig. 150, for various heights of elements and number of rows of elements.

$V_{11.0 (i)}$ is the average velocity measured at Sta. 11.0 (Fig. 150) with the particular combination of elements in place; $V_{11.0 (o)}$

TABLE V
Length of Smooth
Floor for Momentum

Basin Type	Height of Element a (inch)	Li (ft)
B	2½	5.4
	1¼	7.0
	1	7.0
C	2½	3.0
	1¼	5.0
	1	6.0
D	2½	3.0
	1¼	5.0
E	2½	0
	1¼	2



Centerline Profiles for Drag Coefficient Evaluation

Fig. 150

is the average velocity measured at Sta. 11.0 with the same discharge but no roughness elements, i.e., smooth floor throughout the basin.

F_{τ_0} is the deficit between the measured momentum at Sta. 0.0 and Sta. 11.0 for the smooth floor basin.

F_{τ_i} was a significant factor only when two rows of elements were used, particularly with the combination of small elements and large discharges. For this reason, the values of C_D computed for two rows of elements are considered to be less reliable than C_D computed for four or six rows. F_{τ_i} was not a significant quantity in the latter two cases.

Problem Analysis

It has been shown by previous studies (Refs. 12, 19, 20) that for both supercritical and subcritical flow, an important correlating parameter is the relative depth y/a , the depth of flow striking the element divided by the height of the element. In the energy dissipating basin where the water is diverted upward by the element, it is obvious that, up to a limiting point at least, the deeper the flow over the element, the larger the quantity of water disturbed by the element and, consequently, the larger the apparent coefficient of drag.

The depth of flow two pipe diameters downstream of the outlet (the approximate location of the first row of elements) was chosen as the scaling length. For design purposes, this length is readily obtained from Figs. 138 through 148, Chapter IV. Since the width of the expanding jet is not controlled by the walls at this point (Sta. $2 D_0$), this height is significant for a basin of any width (when considering only the first two rows of elements). This is not the case for the

remaining rows of elements, i.e., the wider the basin, the shallower the flow for a given discharge. For this reason, an additional correlating factor W_2/W_0 , the basin width divided by the conduit width, is necessary.

The longitudinal spacing of the elements, J , is significant. Because of the complexity of the flow, it did not appear practical to include this factor as a density term. Instead, the ratio J/a is included as a geometric ratio and accompanies each design curve.

The lateral spacing of the element (ZM) is not considered critical. The important point is that the elements in each row occupy half the width of the channel, and that the elements be staggered in successive rows. This insures that there will be no smooth longitudinal corridors through the basin. In order that the elements will serrate the flow and not act as a long sill, it is recommended that the ratio M/a be restricted to a range of 2 to 8.

Test Program

For the primary tests, run 20 R through 71 R, twelve basin and element arrangements were examined. Each basin was subjected to two discharges. The lower discharge was approximately the design discharge (based on the Wyoming Highway Department specifications) for the approach pipe. The higher discharge was approximately 50% larger.

Two heights of elements were used, $a = 1\frac{1}{4}$ in. and $a = 2\frac{1}{2}$ in., for each discharge. A variation of relative depth (y/a) from 1.1 to 2.7 resulted from the combination of two discharges and two element heights.

One pattern of longitudinal and lateral spacing was used for all runs. With two element heights, a twofold variation of J/a , 6.0 and 12.0, was obtained.

For the 1.25 ft square approach pipe, two basin widths, $W_2 = 5$ ft and $W_2 = 10$ ft, were tested. One width of basin, $W_2 = 10$ ft, was used with the 1.45 ft diameter circular approach pipe.

In addition to the primary runs described above, six special runs (72 R through 77 R) were made. The circular approach pipe and 10 ft wide basin were used with two patterns of 4 in. x 1 in. elements. The significant difference between these basins and those used for the primary runs was the size of the elements. The four in. elements were spaced on 18 in. centers laterally; thus large gaps existed between the elements. As expected, high speed cores of water were measured downstream of the field of elements. The coefficient of drag deduced for the small, widely spaced elements was somewhat larger than comparable coefficients of drag for the elements 9 in. long. However, because of the probability of high speed cores of water downstream of the basin, elements spaced laterally at more than twice their length are not recommended.

Table VI systematically lists the 54 runs. Significant flow data, geometric ratios, flow parameters, and deduced coefficients of drag are presented.

The 10 ft by 14 ft basin with a horizontal aluminum floor, described in Chapter IV, was used for all experiments. False walls were installed for the 5 ft basins.

The yaw probe, previously described, was used for all flow measurements. Data gathered at Sta. 11.0 for the purpose of evaluating

TABLE VI - DATA FOR DRAG COEFFICIENT EVALUATION

Run No.	W_0 or D_0 width of pipe (ft)	W_2 width of basin (ft)	W_2/W_0 relative width --	a element height (ft)	M element width (ft)	M/a --	J longi- tudinal spacing (ft)	J/a --	y ave. depth at sta. $2D_0$ (ft)	Y/a relative depth --	Q/Z weir (cfs)	K water surface correction (ft)	Q/Z inte- grated (cfs)	V_{max} at Sta. 0.0 (fps)	V_{max} at Sta. 11.0 (fps)
20R	1.25□	5	4	0.10	0.75	7.2	1.25	12	0.22*	2.1	5.74	.054	5.80	9.9*	5.8
21R									0.28	2.7	8.70	.082	8.81	13.8	7.9
22R									0.22	2.1	6.60	.033	6.61	10.9	6.9
23R									0.28	2.7	8.52	.075	8.56	13.4	8.2
24R									0.22	2.1	6.40	.009	6.40	10.7	6.5
25R									0.28	2.7	8.60	-.010	8.60	13.5	9.3
26R									0.22	2.1	6.30	-.027	6.30	10.5	7.9
27R				0.10	0.75	7.2	1.25	12	0.28	2.7	8.37	-.046	8.38	13.2	10.4
28R				-	-	-	-	-	0.22	-	5.78	0	5.76	9.8	8.9
29R				-	-	-	-	-	0.28	-	8.20	.030	8.20	13.0	12.9
30R				-	-	-	-	-	0.22	1.1	6.06	-.005	6.08	10.2	7.2
31R				0.21	0.75	3.6	1.25	6	0.28	1.4	8.37	-.047	8.38	13.2	9.3
32R									0.22	1.1	5.98	.027	5.98	10.1	6.3
33R									0.28	1.4	8.45	.042	8.46	13.3	7.5
34R									0.22	1.1	6.06	.049	6.09	10.2	5.6
35R									0.28	1.4	8.67	.055	8.74	13.7	6.8
36R									0.22	1.1	6.01	-.040	6.00	10.1	5.8
37R	1.25□	5	4	0.21	0.75	3.6	1.25	6	0.28	1.4	8.65	.140	8.89	13.9	6.8
41R	1.25□	10	7	0.21	0.75	3.6	1.25	6	0.22	1.1	6.16	.005	6.09	10.2	5.2
42R									0.28	1.4	8.92	.017	8.89	13.9	6.6
43R									0.22	1.1	5.79	-.004	5.78	9.9	5.9
44R									0.28	1.4	8.73	.005	8.70	13.6	8.3
45R									0.22	1.1	6.17	.017	6.17	10.3	5.6
46R									0.28	1.4	9.40	.007	9.43	14.6	9.7
47R									0.22	1.1	5.90	-.013	5.90	10.0	7.8
48R				0.21	0.75	3.6	1.25	6	0.28	1.4	8.80	+.051	8.78	13.7	11.0
49R				-	-	-	-	-	0.22	-	6.00	+.023	5.94	10.0	11.0
50R				-	-	-	-	-	0.28	-	8.85	+.045	9.02	14.1	13.0
51R				0.10	0.75	7.2	1.25	12	0.22	2.1	5.91	-.004	5.88	9.9	9.1
52R									0.28	2.7	8.65	+.007	8.62	13.5	12.3
53R									0.22	2.1	5.70	+.023	5.70	9.8	6.9
54R									0.28	2.7	8.55	+.009	8.74	13.7	11.0
55R									0.22	2.1	5.41	+.017	5.38	9.5	5.4
56R									0.28	2.7	8.70	+.026	8.74	13.7	9.3
57R									0.22	2.1	5.75	+.043	5.80	9.9	6.6
58R	1.25□	10	7	0.10	0.75	7.2	1.25	12	0.28	2.7	8.70	+.045	8.77	13.7	9.6
60R	1.45φ	10	7	-	-	-	-	-	0.28	-	5.28	0	5.26	8.7	9.8
61R				0.21	0.75	3.6	1.25	6	0.28	1.4	5.33	0	5.30	8.7	7.5
62R									0.28	1.4	5.25	0	5.19	8.6	5.5
63R									0.28	1.4	5.22	0	5.14	8.6	7.9
64R									0.28	1.4	5.15	0	5.15	8.6	7.6
65R									0.28	1.4	5.41	0	5.32	8.7	8.6
66R									0.33	3.2	8.29	0	8.66	11.5	10.1
67R									0.33	3.2	8.21	0	8.55	11.4	9.4
68R									0.33	3.2	8.36	0	8.66	11.5	10.4
69R									0.33	3.2	8.34	0	8.66	11.5	7.2
70R				0.21	0.75	3.6	1.25	6	0.33	3.2	8.16	0	8.44	11.2	9.8
71R	1.45φ	10	7	-	-	-	-	-	0.33	-	8.51	0	8.80	11.8	11.8
72R	1.45φ	10	7	0.08	0.33	4.0	1.25	15	0.27	3.2	5.15	0	5.15	8.6	9.0
73R									0.29	3.5	6.14	0	6.00	9.2	9.5
74R									0.33	4.0	8.60	0	8.95	11.8	11.5
75R									0.27	3.2	5.18	0	5.15	8.6	8.2
76R									0.29	3.5	6.35	0	6.18	9.3	8.9
77R	1.45φ	10	7	0.08	0.33	4.0	1.25	15	0.33	4.0	8.28	0	9.11	12.1	11.3

*Values given in this column were obtained from data presented in Chapter III.

TABLE VI - DATA FOR DRAG COEFFICIENT EVALUATION - Continued:

Run No.	V ave. at Sta. 0.0 (fps)	V ave. at Sta. 11.0 (fps)	M _{0.0} press. force + mom at Sta. 0.0 (lbs)	M _{11.0} press. force + mom at Sta. 11.0 (lbs)	M _{0.0} - M _{11.0} (lbs)	No. of Elements						C _D Coefficient of Drag		
						Row 1	Row 2	Row 3	Row 4	Row 5	Row 6	2 Rows	4 Rows	6 Rows
						-	-	-	-	-	-	-	-	-
20R	9.0*	4.9	123*	77	46	1.5	2	1.5	2	1.5	2	--	--	.51
21R	12.6	6.9	237	148	89	1.5	2	1.5	2	1.5	2	--	--	.65
22R	9.8	6.1	147	100	47	0	2	1.5	0	1.5	2	--	--	.63
23R	12.3	7.4	227	154	73	0	2	1.5	0	1.5	2	--	--	.78
24R	9.6	6.2	142	99	43	1.5	2	1.5	2	0	0	--	--	.60
25R	12.3	8.1	230	165	65	1.5	2	1.5	2	0	0	--	--	.68
26R	9.5	7.4	138	106	32	1.5	2	0	0	0	0	.68	--	--
27R	12.1	9.2	218	173	45	1.5	2	0	0	0	0	.72	--	--
28R	8.9	8.2	120	105	15	0	0	0	0	0	0	--	--	--
29R	11.8	10.1	210	187	23	0	0	0	0	0	0	--	--	--
30R	9.2	6.7	132	98	34	1.5	2	0	0	0	0	.45	--	--
31R	12.2	8.2	218	162	56	1.5	2	0	0	0	0	.56	--	--
32R	9.1	5.7	128	88	40	1.5	2	1.5	2	0	0	--	--	.32
33R	12.2	6.8	223	146	77	1.5	2	1.5	2	0	0	--	--	.44
34R	9.2	5.0	132	89	43	1.5	2	1.5	2	1.5	2	--	--	.24
35R	12.5	5.8	235	139	96	1.5	2	1.5	2	1.5	2	--	--	.37
36R	9.2	5.3	129	86	43	0	2	1.5	0	1.5	2	--	--	.33
37R	12.7	5.9	240	146	94	0	2	1.5	0	1.5	2	--	--	.51
41R	9.3	4.4	132	73	59	1.5	1	3.5	3	3.5	3	--	--	.22
42R	12.7	5.1	240	127	113	1.5	1	3.5	3	3.5	3	--	--	.29
43R	9.0	4.7	122	74	48	0	2	3.5	0	3.5	3	--	--	.23
44R	12.5	4.8	233	123	110	0	2	3.5	0	3.5	3	--	--	.35
45R	9.3	5.1	134	82	52	1.5	1	3.5	3	0	0	--	--	.31
46R	13.2	6.5	263	167	96	1.5	1	3.5	3	0	0	--	--	.36
47R	9.1	6.3	126	87	39	1.5	1	0	0	0	0	.73	--	--
48R	12.5	8.1	236	170	66	1.5	1	0	0	0	0	.75	--	--
49R	9.1	7.8	127	108	19	0	0	0	0	0	0	--	--	--
50R	12.8	9.8	246	204	42	0	0	0	0	0	0	--	--	--
51R	9.0	6.7	126	94	32	1.5	1	0	0	0	0	.97	--	--
52R	12.4	9.1	230	180	50	1.5	1	0	0	0	0	.66	--	--
53R	8.8	5.7	119	80	39	1.5	1	3.5	3	0	0	--	--	.47
54R	12.5	7.4	236	159	77	1.5	1	3.5	3	0	0	--	--	.56
55R	8.5	4.5	108	65	43	1.5	1	3.5	3	3.5	3	--	--	.35
56R	12.5	6.0	234	140	94	1.5	1	3.5	3	3.5	3	--	--	.45
57R	9.0	5.0	122	76	46	0	2	3.5	0	3.5	3	--	--	.40
58R	12.5	5.9	236	135	101	0	2	3.5	0	3.5	3	--	--	.58
60R	7.6	6.8	97	85	12	0	0	0	0	0	0	--	--	--
61R	7.6	6.1	97	75	22	1.5	1	0	0	0	0	.42	--	--
62R	7.6	4.5	95	62	33	1.5	1	3.5	3	0	0	--	--	.23
63R	7.6	5.4	95	67	28	0	1	3.5	3	0	0	--	--	.20
64R	7.6	5.1	95	66	29	0	0	3.5	3	0	0	.28	--	--
65R	7.6	5.4	98	71	27	1.5	0	3.5	3	0	0	--	--	.21
66R	10.4	6.7	192	144	48	1.5	0	3.5	3	0	0	--	--	.28
67R	10.3	7.0	187	143	44	0	0	3.5	3	0	0	.32	--	--
68R	10.4	7.3	192	149	43	0	1	3.5	3	0	0	--	--	.27
69R	10.4	6.0	192	132	60	1.5	1	3.5	3	0	0	--	--	.32
70R	10.2	7.4	184	144	40	1.5	1	0	0	0	0	.67	--	--
71R	10.6	8.9	197	179	18	0	0	0	0	0	0	--	--	--
72R	7.5	6.2	94	78	16	0	0	3.5	3	0	0	.44	--	--
73R	8.1	6.6	115	97	18	0	0	3.5	3	0	0	.51	--	--
74R	10.8	8.1	204	173	31	0	0	3.5	3	0	0	.73	--	--
75R	7.6	6.1	94	73	21	1.5	2	3.5	3	0	0	--	--	.51
76R	8.2	6.4	116	93	23	1.5	2	3.5	3	0	0	--	--	.59
77R	11.0	8.1	210	173	37	1.5	2	3.5	3	0	0	--	--	.62

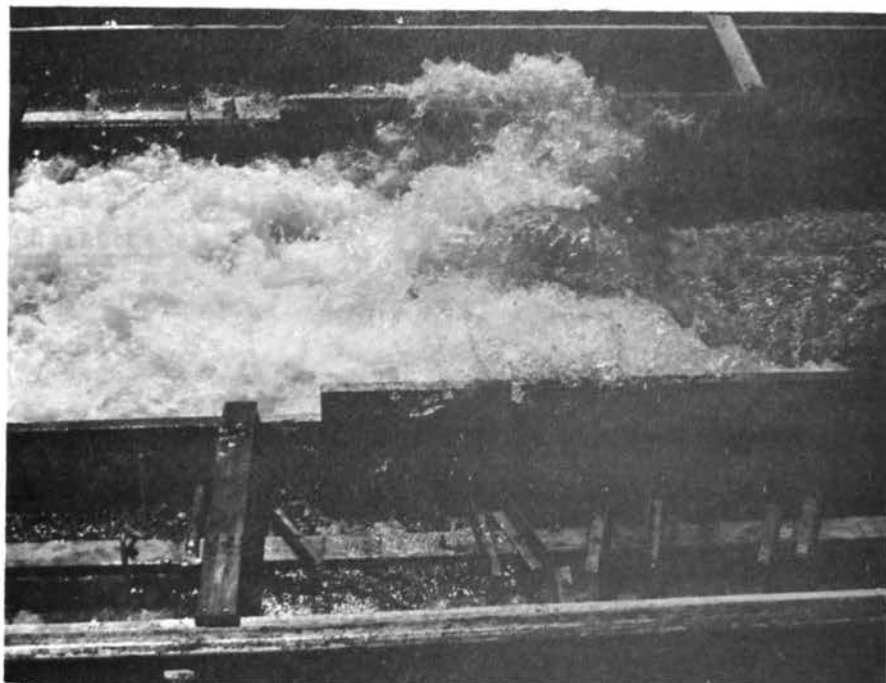
the momentum was measured at the points shown on the sampling grid, Fig. 125. As a check, a measurement of the discharge was obtained at a downstream measuring weir for each run. The major portion of the data was processed with the computer.

A comparison was made between the discharge measured at the weir and the integrated discharge at Sta. 11.0. For runs 41 R through 77 R, there was no significant difference in the two quantities; the maximum deviation was 5%.

Discrepancies of up to plus or minus 15% were noted for runs 20 R through 58 R. With reference to Figs. 151 and 152, it is obvious that any measurement of the water surface profile for some of the runs is at best an estimate.

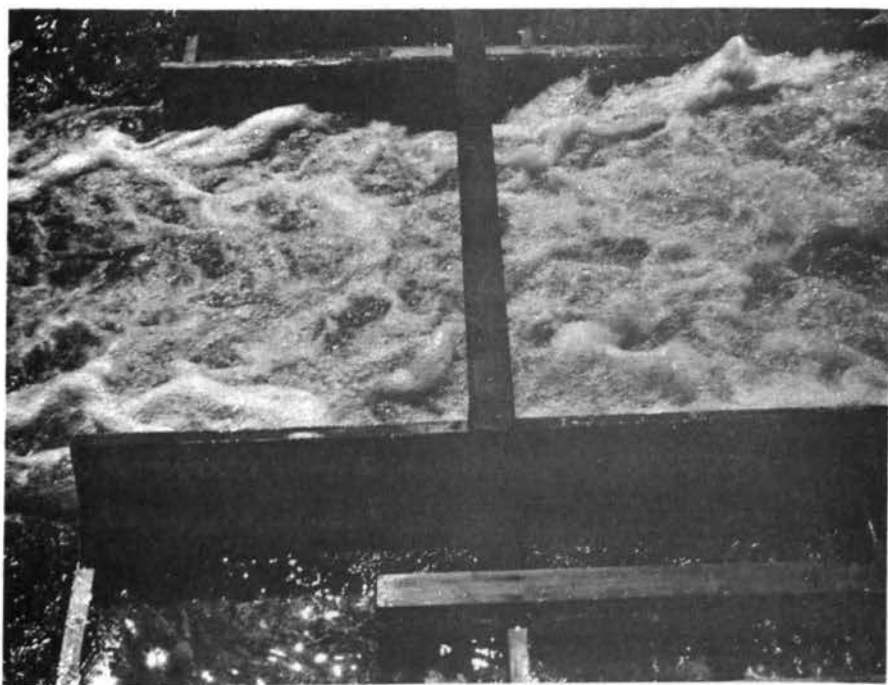
It was assumed that the measured velocities were correct and that the discrepancy between the integrated discharge and weir discharge was due to inaccurate water surface measurements. The water surface elevation was adjusted by adding (or subtracting) an increment of height until the integrated discharge agreed with the weir discharge. The amount of correction applied is shown in Column K of Table VI. Seventy percent of these corrections were less than plus or minus $\frac{1}{2}$ in., well within the measuring tolerance of the roily water surface. Only one run, No. 36 R, looked questionable. A 1-3/4 inch correction was required. Figure 151 shows this particular run. A significant portion of the flow is airborne at the measuring station.

One reason for the larger discrepancy in discharge was the proximity of the roughness elements to the measuring station. When the row 6 elements were in place, the distance between the last row of elements and the measuring station was 1.75 ft.



2½" x 9" Elements Row 2, 3, 5 and 6
 Run 37R Q = 17.3 cfs $\frac{W_2}{W_0} = 4$

Fig. 151



2½" x 9" Elements Row 1, 2, 3, 4, 5 and 6
 Run 35R Q = 17.3 cfs $\frac{W_2}{W_0} = 4$

Fig. 152

Where the first two or four rows of elements were used, the minimum distance between the measuring station and the closest row of elements was 4.25 ft.

Operating Characteristics

The manner in which the basins performed is best illustrated by photographs, Figs. 151 through 160.

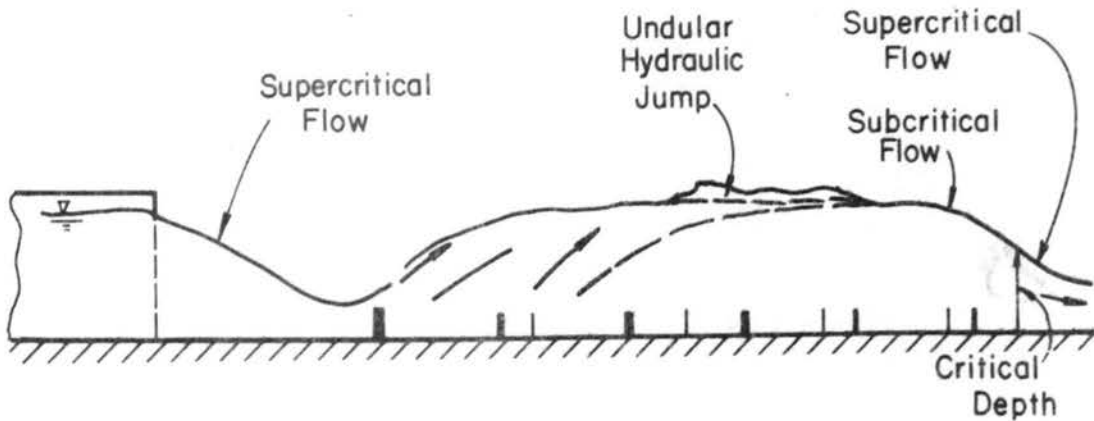
The effect of leaving out the first row of elements is shown in Fig. 151. The first contact between the high speed jet and the elements occurs near the wall. Note the overtopping. The discharge through the basin is about 17.3 cfs, nearly 50% above the design discharge. The measured velocity at Sta. 11.0 (the location of the transverse timber spanning the basin, barely visible in the upper left-hand corner of the picture) averaged 5.9 fps. The velocity of the first row of elements, 8 ft upstream, was approximately 14 fps.

Figure 152 illustrates several features of the basins:

- a) the large quantity of entrained air,
- b) the uniform distribution of the flow downstream of the elements, and
- c) the drawdown downstream of the last row of elements.

This drawdown is equally noticeable in Figs. 154, 155, 157, and 160.

With reference to Fig. 152, the velocities measured at the transverse timber, where the depth of flow is less than 0.5 ft, are larger than the velocities two ft upstream where the flow depth is about 1 ft, the height of the walls. The phenomenon that occurs is illustrated by the sketch below.



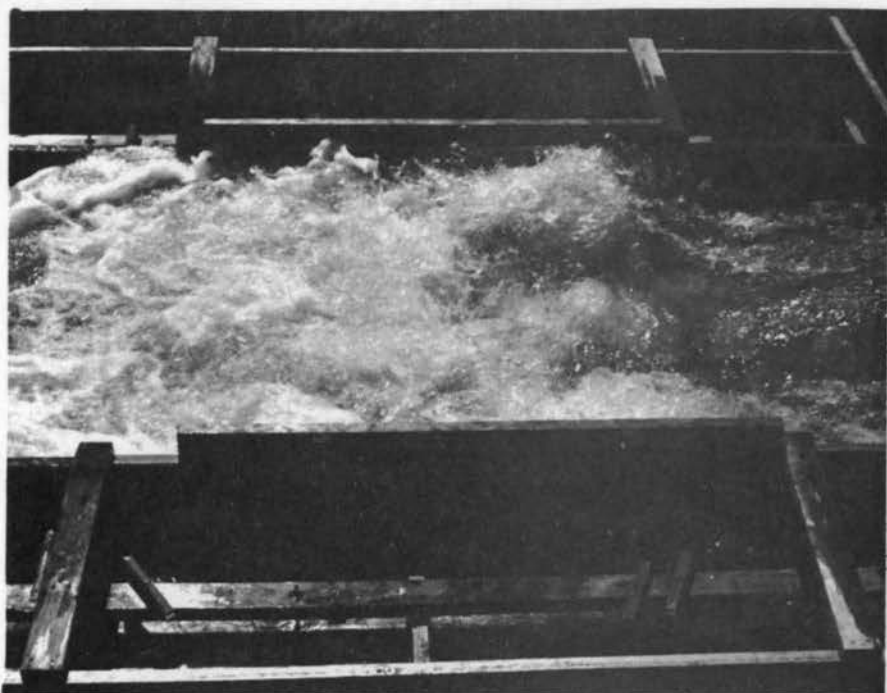
CENTER LINE SECTION

If sufficient downstream tailwater is available, the flow will not return to supercritical. This is an important aspect of the design of the roughened basins and is discussed in Chapter VII.

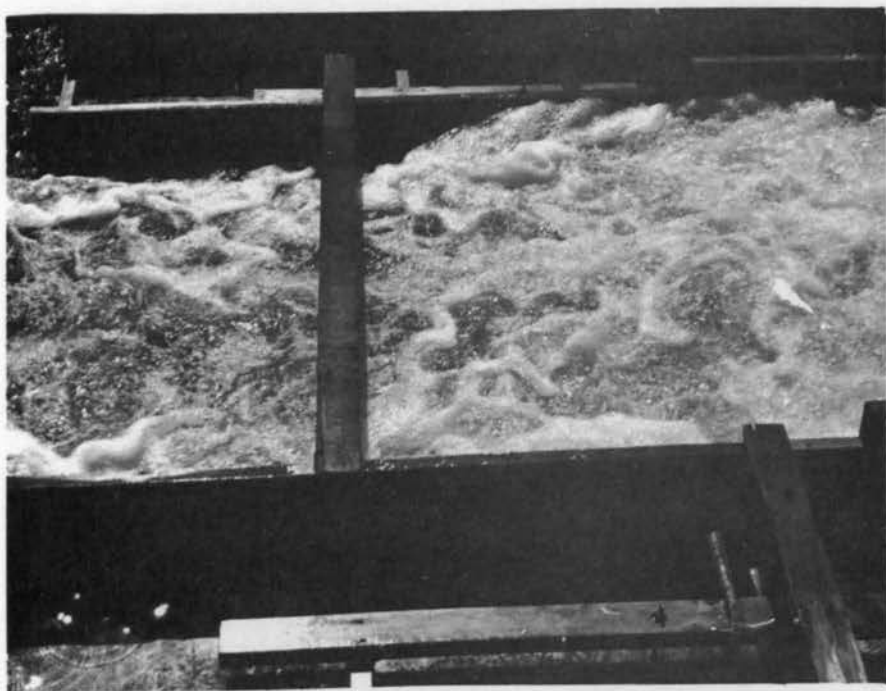
The remainder of the photographs illustrate flow with various relative width ratios, element heights, and number of rows of elements. The captions list significant factors.

Presentation of Data

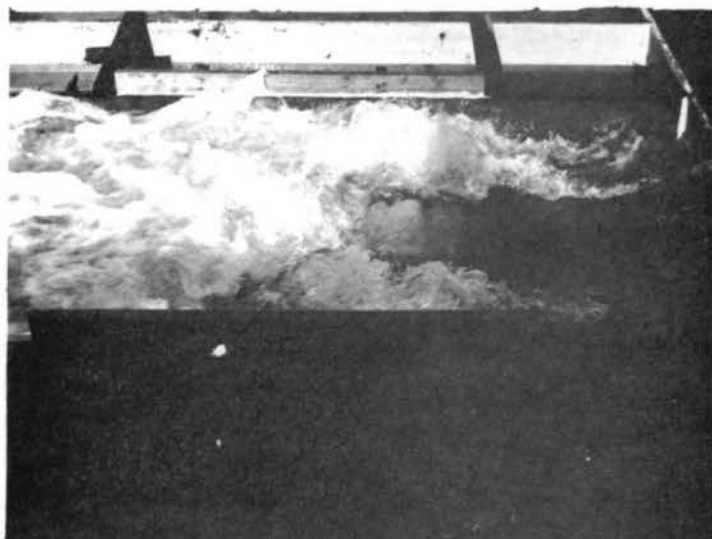
Values of C_D for design use are presented in Figs. 161 through 171. Contained in each sketch are the relative dimensions of the basin, relative height of elements, and relative coordinates (in plan view) of the elements. The coefficients listed are for the particular ratios shown.



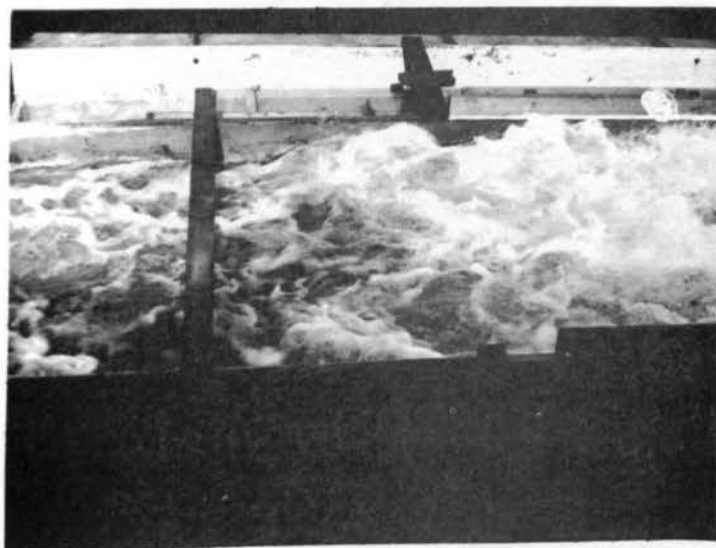
2½" x 9" Elements Row 1, 2, 3, 4, 5 and 6 Fig. 153
 Run 34R Q = 12.1 cfs $\frac{W_2}{W_0} = 4$



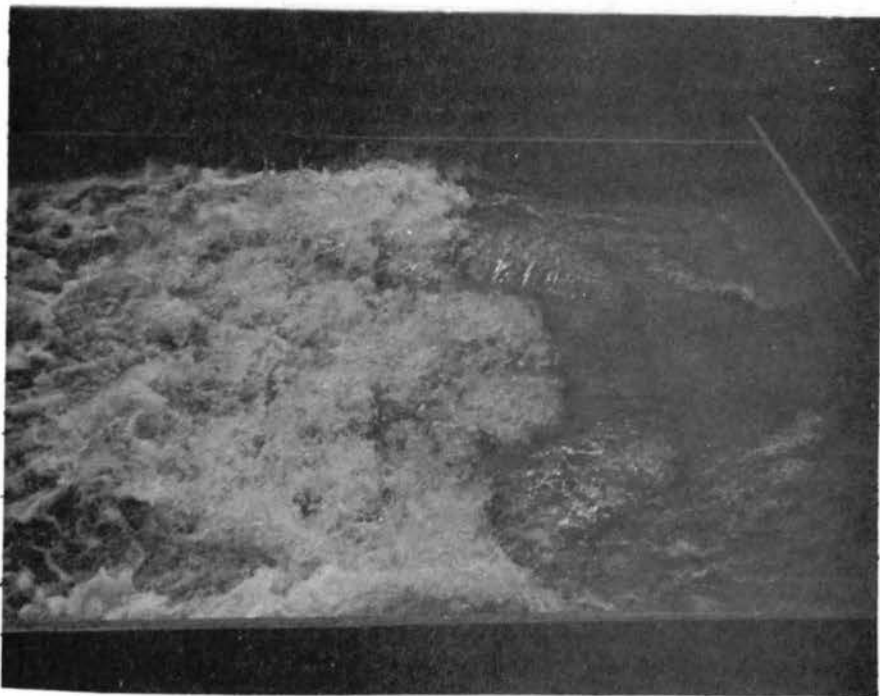
2½" x 9" Elements Row 1, 2, 3, 4, 5 and 6 Fig. 154
 Run 34R Q = 12.1 cfs $\frac{W_2}{W_0} = 4$



2½" x 9" Elements Row 1, 2, 3 and 4 Fig. 155
 Run 32R $Q = 12.0$ cfs $\frac{W_2}{W_0} = 4$

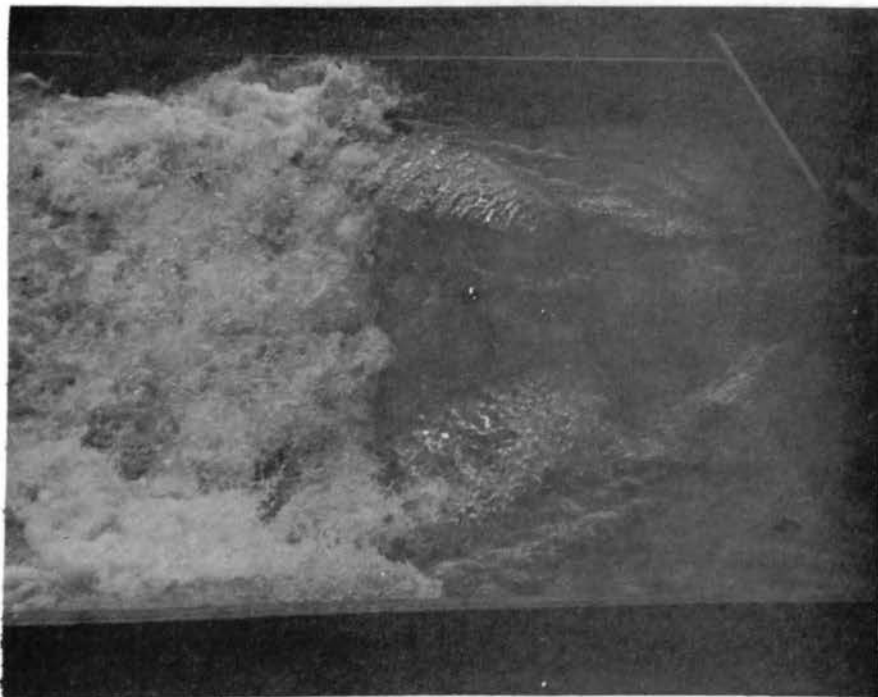


2½" x 9" Elements Row 1, 2, 3 and 4 Fig. 156
 Run 32R $Q = 12.0$ cfs $\frac{W_2}{W_0} = 4$



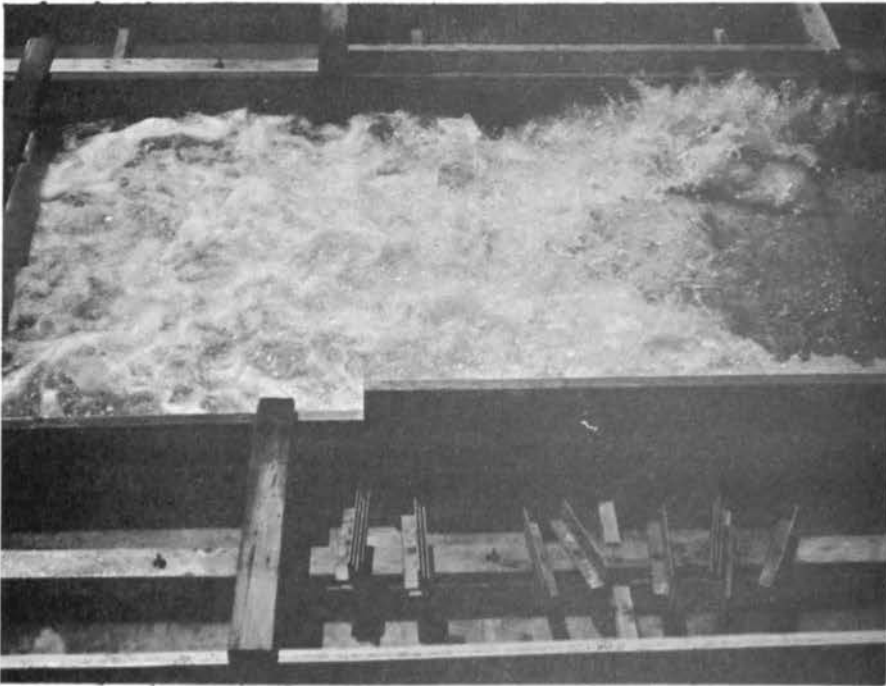
2½" x 9" Elements Row 1, 2, 3 and 4
 Run 41R Q = 12.3 cfs $\frac{W_2}{W_0} = 8$

Fig. 157

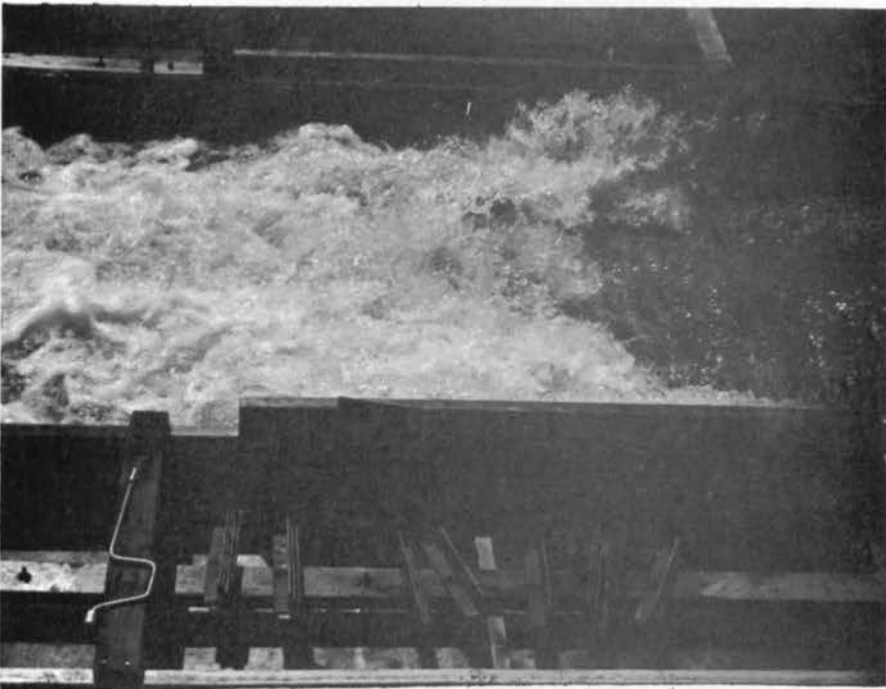


2½" x 9" Elements Row 1, 2, 3, 4, 5 and 6
 Run 42R Q = 17.8 cfs $\frac{W_2}{W_0} = 8$

Fig. 158



1 1/4" x 9" Elements Row 1, 2, 3, 4, 5 and 6 Fig. 159
 Run 21R $Q = 11.5 \text{ cfs}$ $\frac{W_2}{W_0} = 4$



1 1/4" x 9" Elements Row 1, 2, 3 and 4 Fig. 160
 Run 55R $Q = 10.8 \text{ cfs}$ $\frac{W_2}{W_0} = 8$

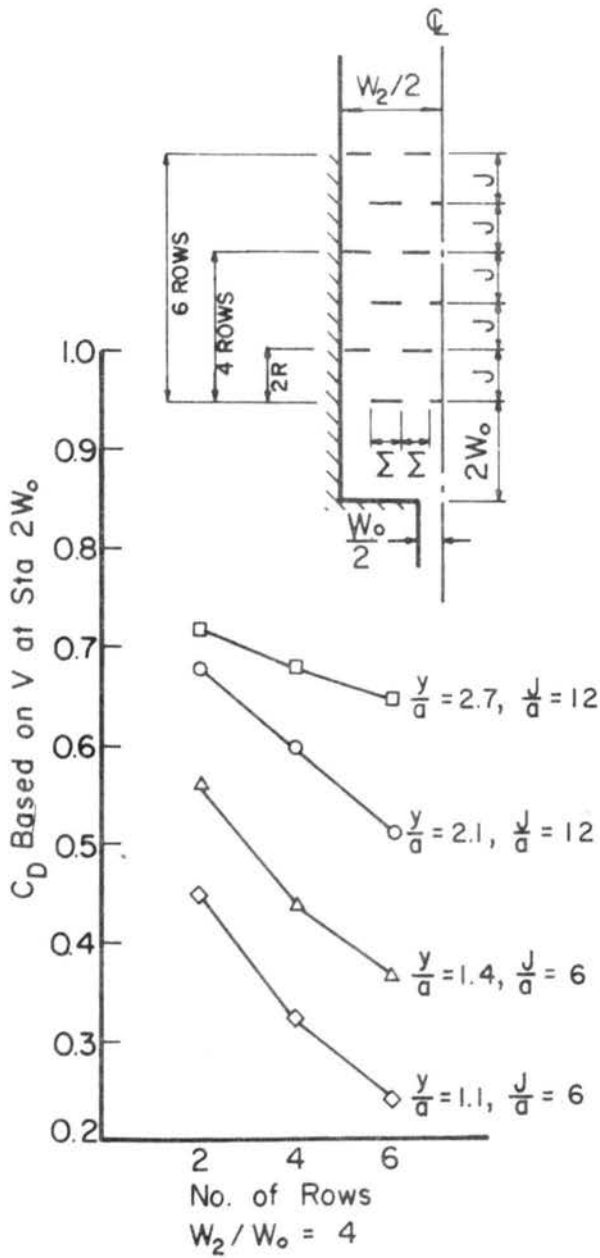


Fig. 161

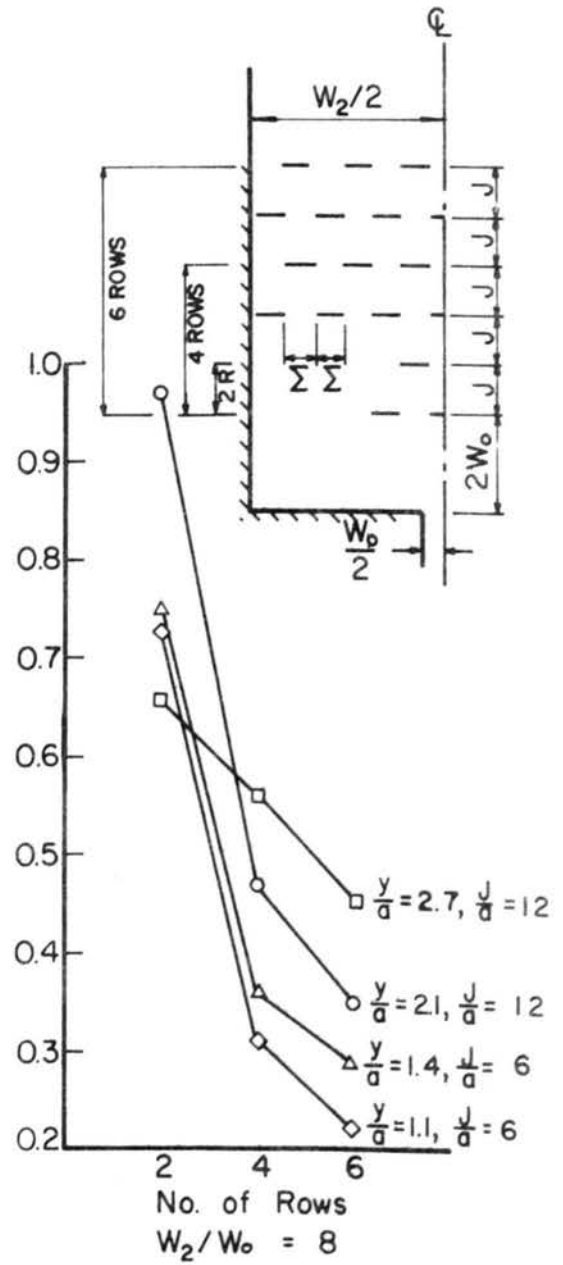


Fig. 162

Coefficients of Drag for Roughness Elements,
Rectangular Approach Pipe

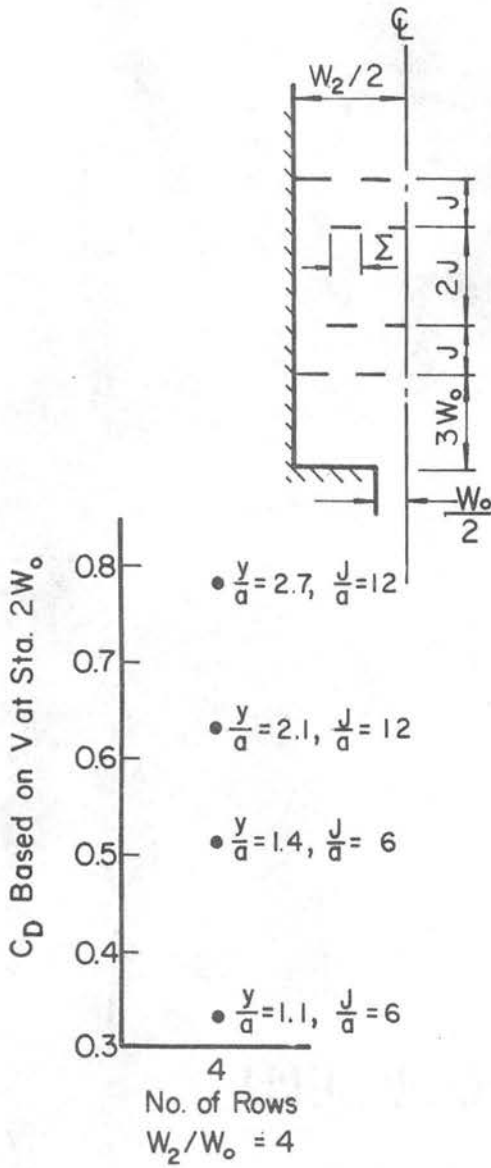


Fig. 163

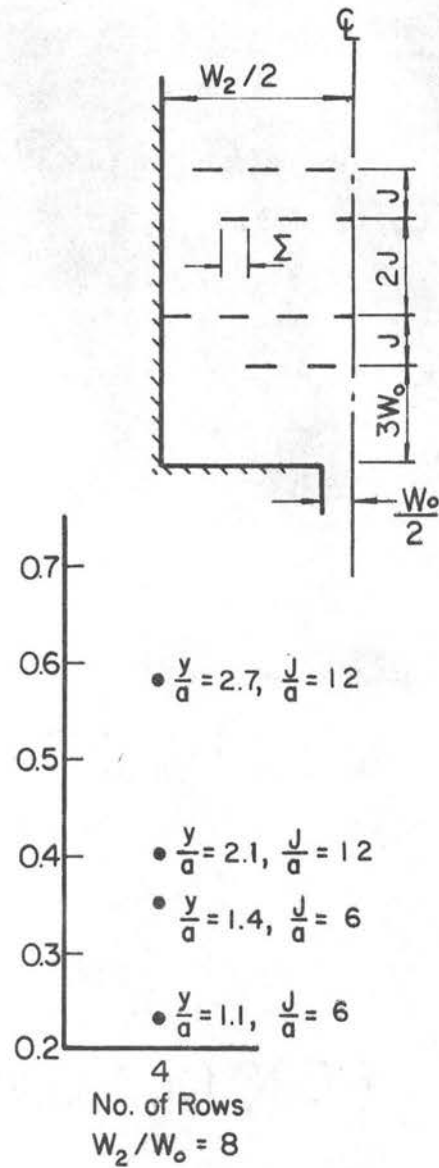


Fig. 164

Coefficients of Drag for Roughness Elements,
Rectangular Approach Pipe

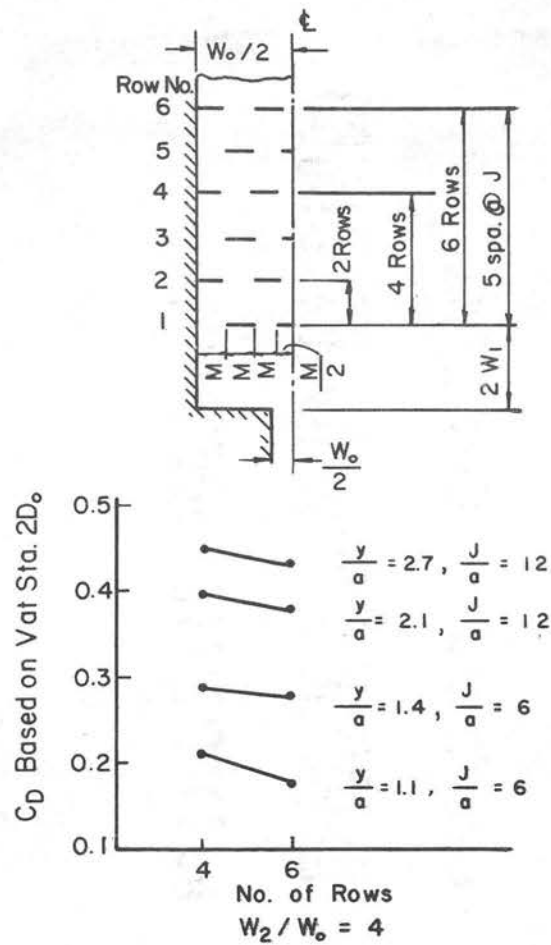


Fig. 165

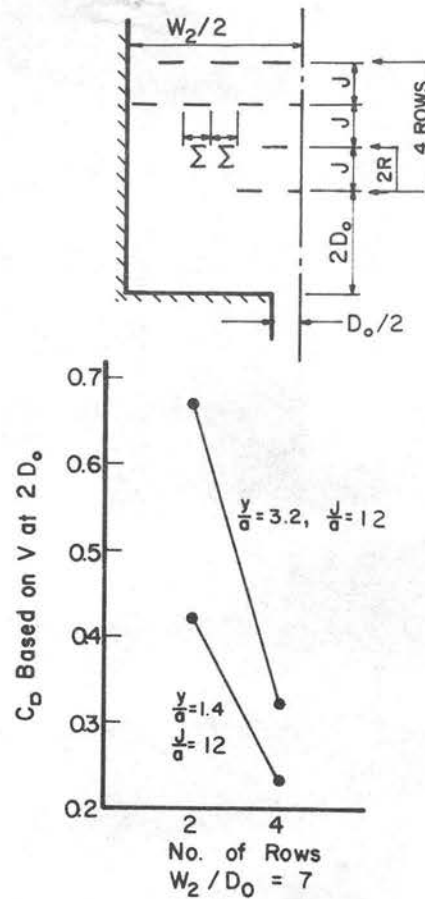


Fig. 166

Coefficients of Drag for Roughness Elements,
Circular Approach Pipe

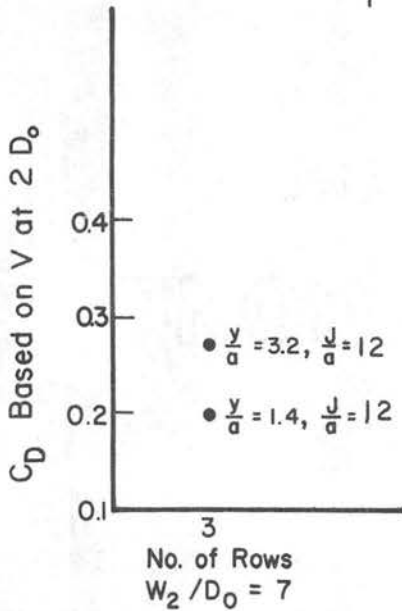
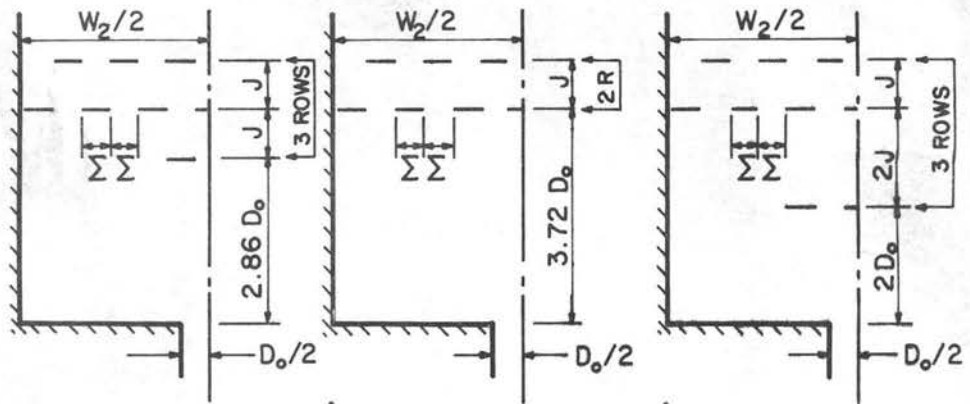


Fig. 167

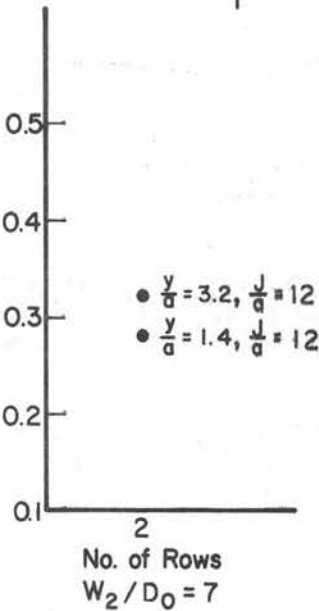


Fig. 168

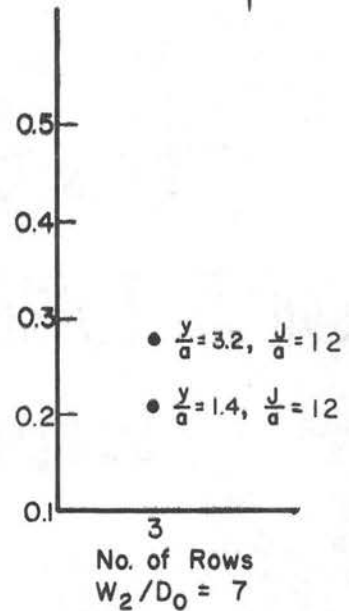
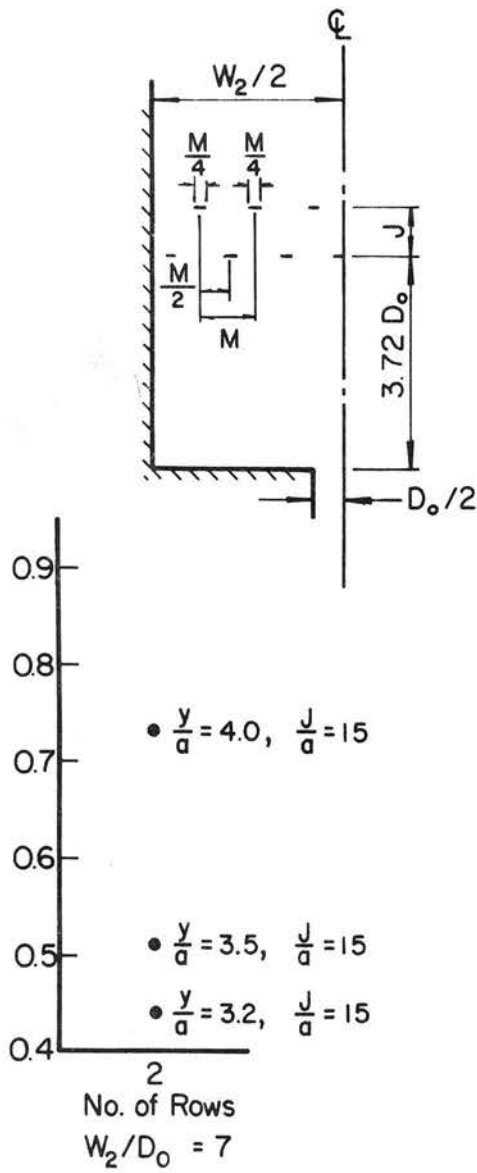


Fig. 169

Coefficients of Drag for Roughness Elements,
 Circular Approach Pipe



Coefficients of Drag for Roughness Elements,
Circular Approach Pipe

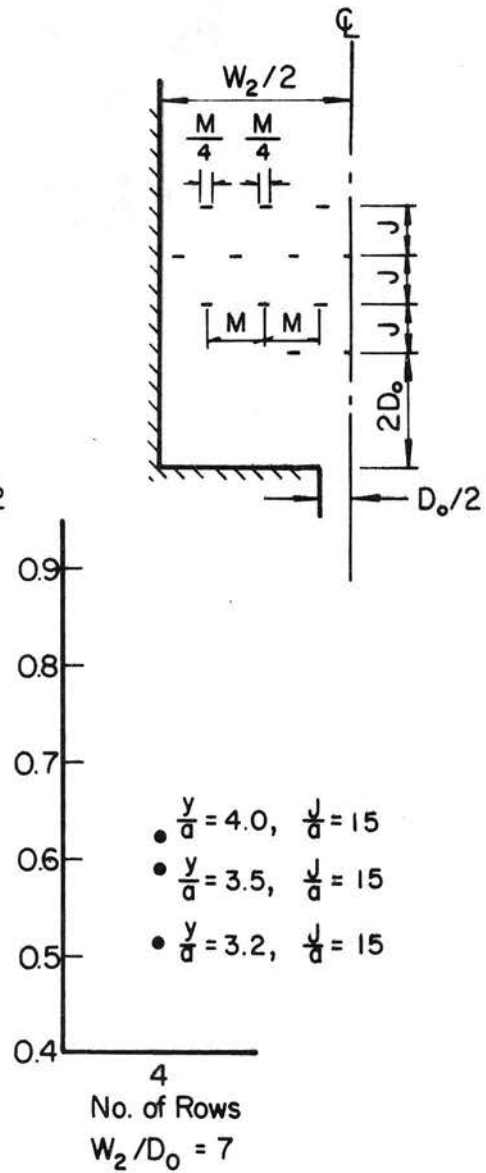


Fig. 171

Fig. 170

With one exception, all plots were constructed from data determined experimentally. Figure 162 was constructed from data obtained by inspection and extrapolation of Figs. 161, 162, and 166.

Basins with two rows of elements are not recommended. Distribution of the flow was not uniform downstream of the elements, particularly for the basins with relative width ratios, W_2/W_D , of seven or eight.

Two rows of elements can be used for triggering a hydraulic jump. If tailwater conditions are known, Eq. 5-4 is directly applicable. All terms in Eq. 5-4 would be known except the drag term, $C_D AN \frac{\rho V_o^2}{2}$. Selecting appropriate values of C_D from the design curves for two rows of elements, A , the required frontal area of the roughness element, is readily determined by trial and error procedure.

The basins with a relative width ratio of four with four or six rows of elements performed in a very satisfactory manner. The rebound flow from the walls is directed back across the elements resulting in a uniform distribution of flow downstream of the elements.

For the wider basins, the flow was diverted to the sides where it tended to concentrate. There was little flow over the central elements, thus they were not effective.

The basins shown in Figs. 170 and 171, where the elements occupy less than one fourth of the basin width, are not recommended. Even with four rows of elements, high speed cores of water were noticeable downstream of the group of elements.

The coefficients of drag deduced from these studies were compared with values deduced from data published by the U.S.B.R.

In Engineering Monograph, No. 25 (2), section 3, Table 4, data from 14 model tests of the Bureau of Reclamation type III basin are presented. In this type of basin, one row of elements is used to trigger the hydraulic jump. Using the data from these studies, it was possible, with a few assumptions, to obtain values of C_D from Eq. 5-4. The magnitude of C_D ranged from 0.68 to 0.92 for 13 of the 14 basins. The data from the other basin yielded a value of $C_D = 1.60$.

The CSU runs that were somewhat similar to these experiments are those with two rows of elements and a W_2/W_0 ratio of 4. Depending on the relative depth of flow, the values of C_D ranged from 0.45 to 0.72. The CSU values should be and are slightly lower because of the shielding of the second row of elements by the front row.

The use of drag coefficients is not restricted to basins downstream of the outfall section. Box culverts could be designed with flared walls at the lower end of the barrel and the elements installed within the barrel, the last rows being on the apron between the wing-walls. This would appear to be more economical than the conventional culvert with a basin downstream. From an aesthetic point of view, the basin would be hidden from the driving public and, additionally, would pose no problem to right-of-way maintenance personnel (mowing, etc.).

The use of the design graphs and suggested design procedures are presented in Chapter VII.

Chapter VI

CHARACTERISTICS OF BASINS WITH HIGH TAILWATER

Problem Statement

High tailwater is defined as the condition where the water surrounding the high speed jet-like core of water downstream of the culvert outlet is as high or higher than the elevation of the crown of the pipe. This situation occurs at culvert outlets where downstream channel constrictions create backwater or where the culvert discharges into a narrow low gradient channel with high banks.

Unknowns that confront the engineer faced with the problem of designing a stable energy dissipating basin where high tailwater conditions prevail are:

- (a) The rate of decay of the high speed velocity core,
- (b) The rate of lateral expansion of the core, and
- (c) The probability of the core being diverted off to one side, thus imperiling the bank.

A literature search yielded three significant papers. "Diffusion of Submerged Jets," by M. L. Albertson, Y. B. Dai, R. A. Jensen, and Hunter Rouse (21), gives a thorough and concise description of the diffusion process and the laws that apparently govern the phenomena. Both two-dimensional jets (long slots) and three dimensional jets (orifices) were examined. For both configurations, the jet discharged into a large volume of quiescent ambient fluid with the same characteristics as the jet. Making full use of dimensional considerations, assuming hydrostatic pressure distribution and dynamic similarity

throughout the flow, and assuming that the longitudinal component of velocity within the diffusion region varied according to the normal probability function at each cross section, the approximate mean characteristics of the diffusion region were derived analytically with the exception of one experimentally derived constant. Distributions of flow volume, momentum flux, energy flux, centerline velocity, longitudinal velocities in the core, radial velocities, mean turbulence characteristics, and the approximate boundary of the expanding jet were presented in both graphical and equation form. Agreement between experimentally obtained data and analytic predictions was good.

In a recent paper, "Diffusion of Slot Jets with Finite Orifice Length-Width Ratios," by V. M. Yevjevich (22), the general diffusion pattern and time average velocity distribution was determined for various orifice length-width ratios. The information from this report in conjunction with that presented in Ref. 21 covers all situations (round orifice, various rectangular orifices with variable length-width ratios, and the infinite slot) for discharge into infinite basins.

"Turbulent Diffusion of the Vertically Upward Jet," by A. Murate and K. Muraoko (23) essentially verifies and extends the results of Ref. 21. The properties of both two and three-dimensional jets directed vertically from the bottom of a basin toward the free surface are discussed. In the region below the stagnation zone at the surface, the data shown in this paper are in agreement with those shown in Ref. 21.

The question arises, how do the diffusion characteristics of a jet bounded on the top by a free surface and on the bottom by a rough (rock lined), essentially rigid boundary compare with the characteristics of a jet diffusing in a basin of infinite size? During the course of

data collection for scoured basins carried out in the summer of 1967, there was an opportunity to obtain a limited amount of data on jet diffusion downstream of culverts. Six runs were carried out with high tailwater.

The remainder of this chapter describes the tests conducted and the data collected, and presents a comparison of this data with results obtained in the three studies described above.

Experimental Apparatus and Procedure

The tests were conducted in the large outdoor flume. Velocities were measured with an Ott minor meter. To obtain a reliable mean value, each point was sampled for a period of 50 seconds. The meter, supported on a point gauge, was mounted horizontally with the axis parallel to the longitudinal centerline of the basin. In all runs, the basin was slowly filled to the specified height. The flow was then increased until the design discharge was obtained.

A smooth circular approach pipe, 1.45 ft in diameter, was used for runs F44 and F45. The basin was approximately 25 ft long with a horizontal floor 6 ft wide and side berms parallel to the centerline sloping 1 on 2, 1 ft high. This condition allowed over-bank flow. The basin was constructed of river rounded rock ranging in size from 6 to 12 in. in diameter with a D_{50} of 8 in. The floor of the basin was placed at approximately the elevation of the pipe invert.

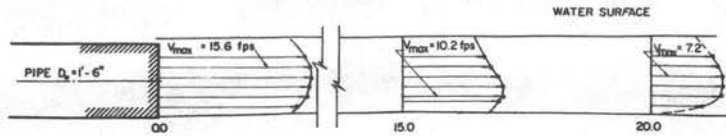
Measurements were taken at two discharges, run No. F44, 22.5 cfs, and run No. F45, 14.6 cfs. The water surface in the basin was maintained about 1.57 ft above the pipe invert, i.e., the crown of the pipe was about 0.12 ft below the average water surface.

Velocity profiles were measured along the centerline of the basin at Stas. 0.0, 5.0, 10.0, and 20.0. Additional velocity measurements were obtained at Stas. 15 and 20 for the purpose of constructing isovel plots. This information is shown in Figs. 172 and 173.

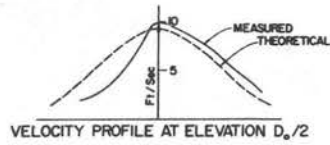
For runs G56 and G57, a 3 ft I.D. smooth pipe was used. The basin was 35 ft long and 20 ft wide with parallel vertical walls 6 ft high. The bed was constructed of rounded rock described in the last paragraph. Two discharges were examined, run G56, 65.4 cfs, and run G57, 84.0 cfs. The water surface was maintained at an elevation 3.05 ft above the pipe invert. A centerline velocity profile was obtained at Sta. 0.0. Sufficient velocity data were taken at Stas. 5.0, 10.0, 15.0, 20.0, and 25.0 to construct the isovel plots shown in Figs. 174 and 175.

For runs K70 (20.9 cfs) and K71 (13.9 cfs), the 1.45 ft diameter smooth steel approach pipe was used. The basin berms were removed and the floor lowered approximately 0.3 ft below the invert. The horizontal floor of the basin was 20 ft wide and 35 ft long, with parallel vertical walls. The rounded material used to construct the basin was much smaller than that used for the previous four runs. The D_{50} was slightly under 5 in. with a D_{max} of 7 in., i.e., the average rock in this series of runs was about one-fourth as heavy as the average rock used previously.

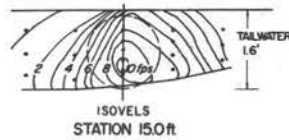
In lieu of holding the tailwater at crown elevation or higher as had been the case for the previous runs, the surface was maintained at an elevation about 0.2 ft below the crown of the pipe. Velocities were measured at Stas. 2.5, 5.0, 7.5, 10.0, 12.5, and 15.0, and for run K71 at Sta. 20.0. During run K70, deposition downstream of the scoured region distorted the flow field and, therefore, measurements



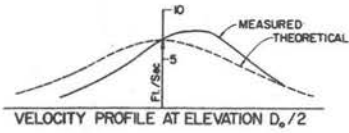
CENTER LINE VELOCITY PROFILES



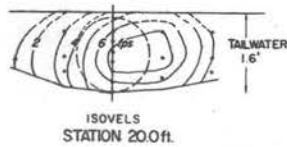
VELOCITY PROFILE AT ELEVATION $D_0/2$



ISOVELS
STATION 15.0 ft.

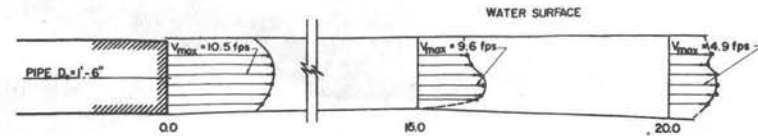


VELOCITY PROFILE AT ELEVATION $D_0/2$

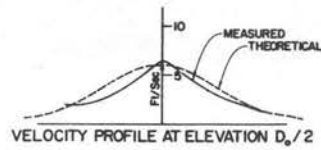


ISOVELS
STATION 20.0 ft.

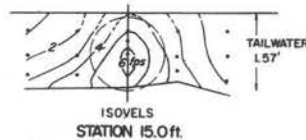
Q = 22.5 cfs
TAIL WATER --- 1.57 ft
PIPE DIAMETER --- 1.45 ft
 D_{90} OF ROCK --- 8 in.
FLAT BED - 6 ft. BOTTOM - 2:1 BERMS
RUN F44 FIG. 172



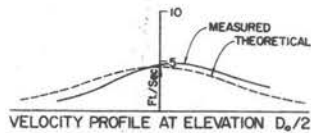
CENTER LINE VELOCITY PROFILES



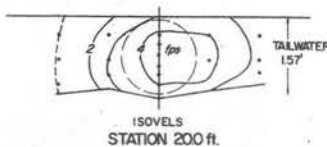
VELOCITY PROFILE AT ELEVATION $D_0/2$



ISOVELS
STATION 15.0 ft.



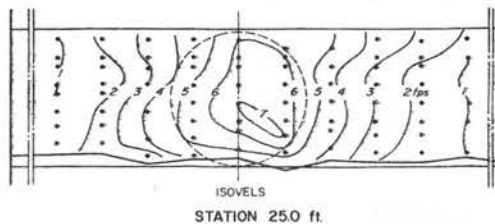
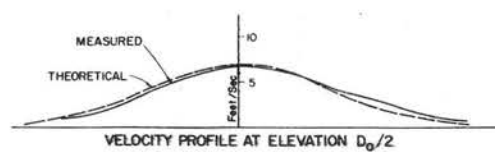
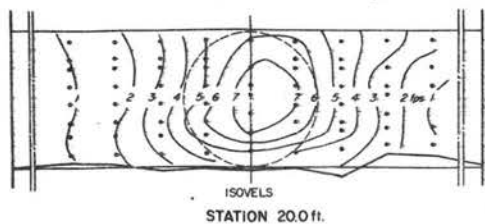
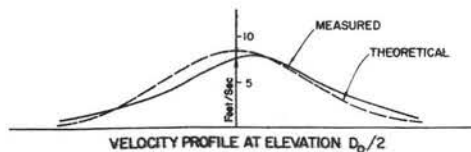
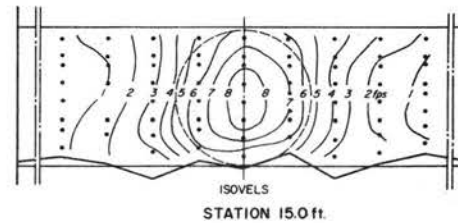
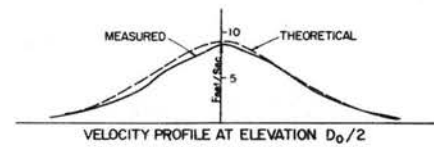
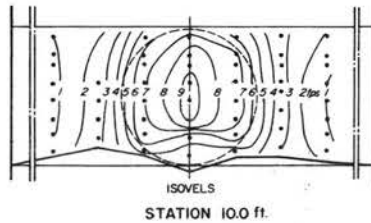
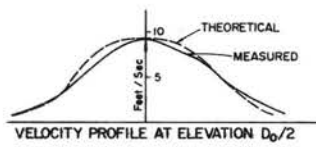
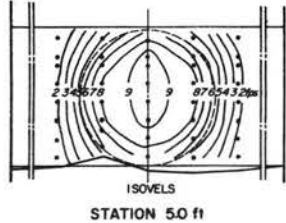
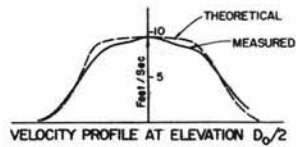
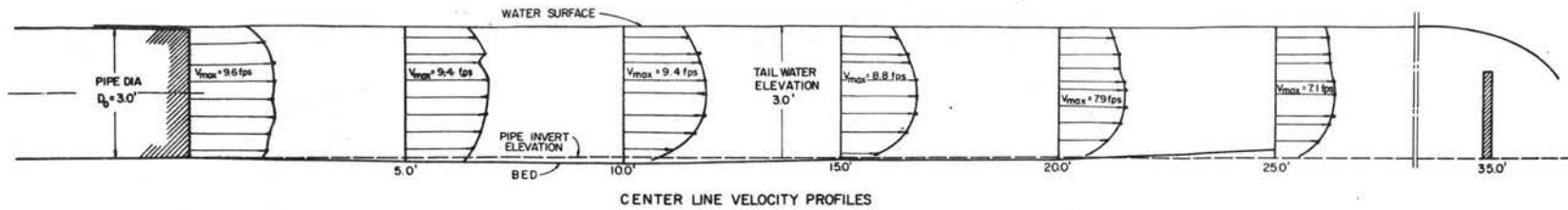
VELOCITY PROFILE AT ELEVATION $D_0/2$



ISOVELS
STATION 20.0 ft.

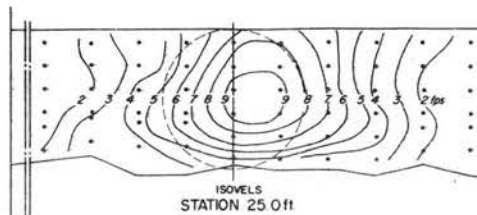
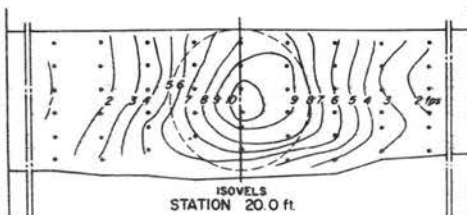
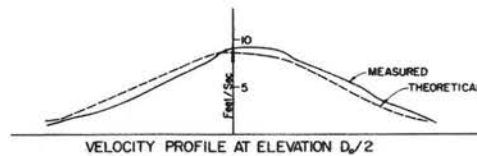
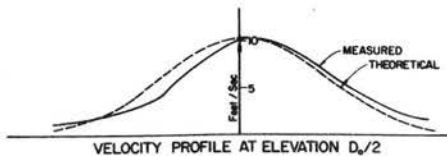
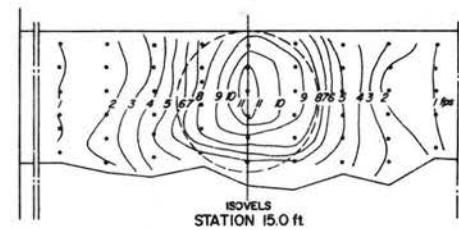
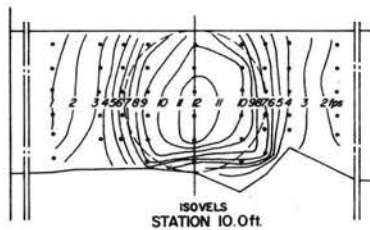
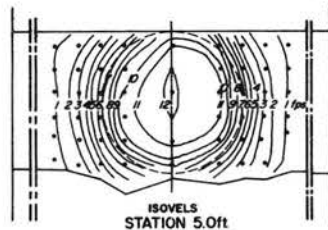
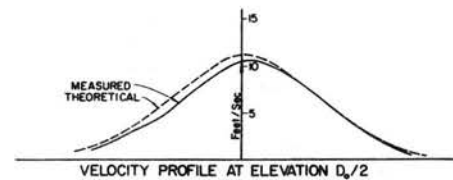
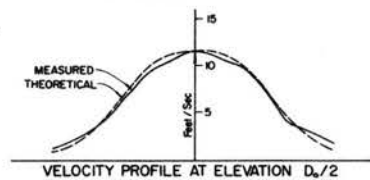
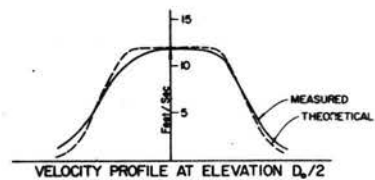
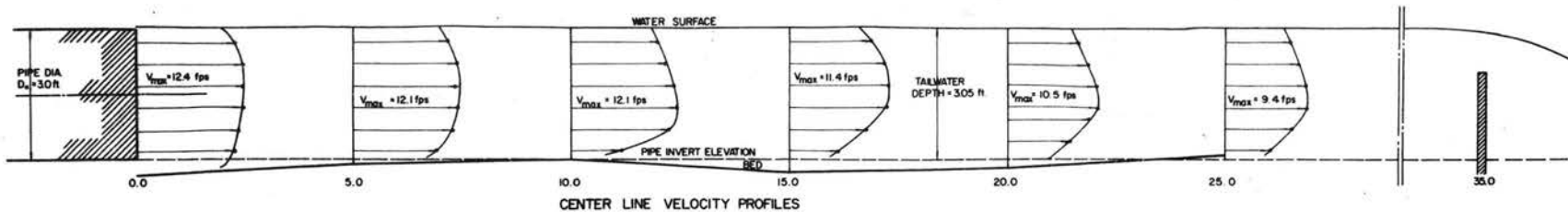
Q = 22.5 cfs
TAIL WATER --- 1.57 ft
PIPE DIAMETER --- 1.45 ft
 D_{90} OF ROCK --- 8 in.
FLAT BED - 6 ft. BOTTOM - 2:1 BERMS
RUN F45 FIG. 173

CENTER LINE VELOCITY PROFILES
ISOVELS
TRANSVERSE VELOCITY PROFILES
(MEASURED & PREDICTED)



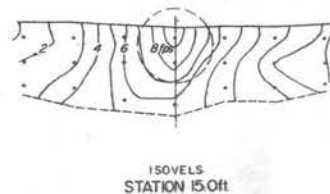
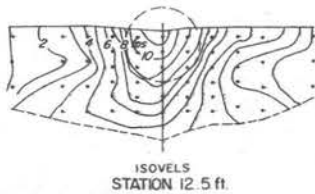
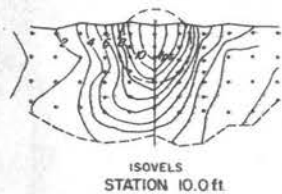
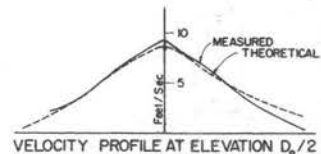
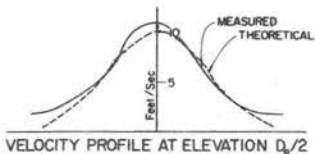
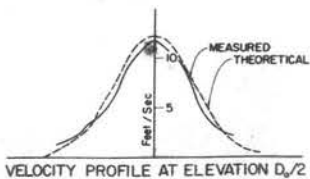
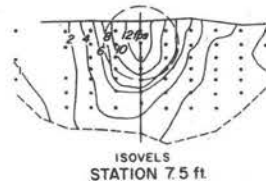
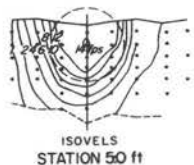
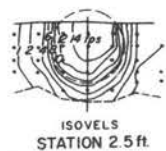
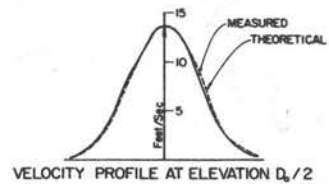
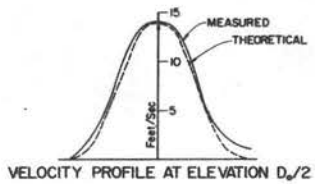
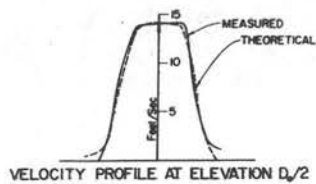
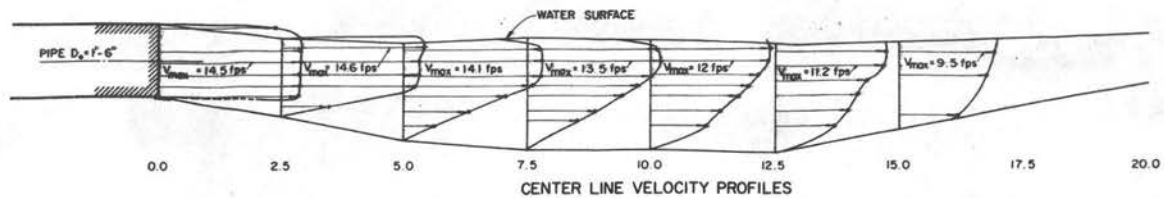
CENTER LINE VELOCITY PROFILES
ISOVELS
TRANSVERSE VELOCITY PROFILES
(MEASURED & PREDICTED)

$Q = 65.4 \text{ cfs}$
TAIL WATER — 3.00 ft.
PIPE DIAMETER — 3.00 ft.
 D_{50} OF ROCK — 8 in.
FLAT BED — 20 ft BOTTOM
RUN G56 FIG. 174



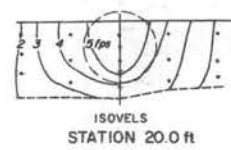
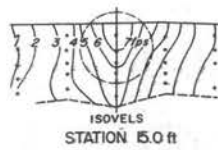
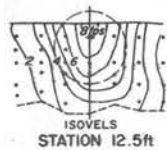
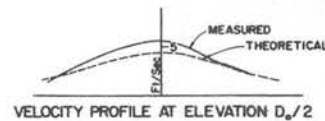
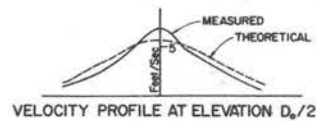
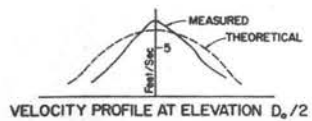
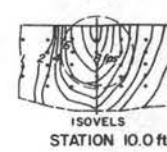
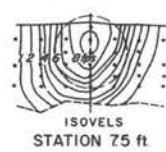
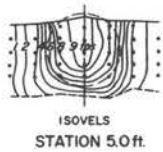
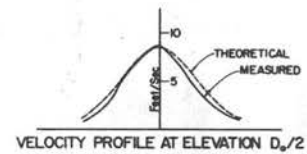
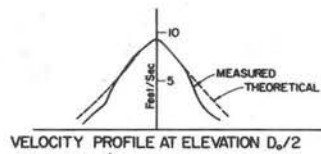
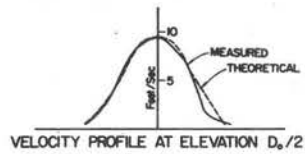
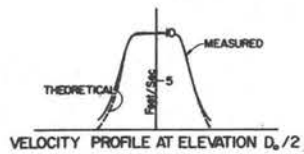
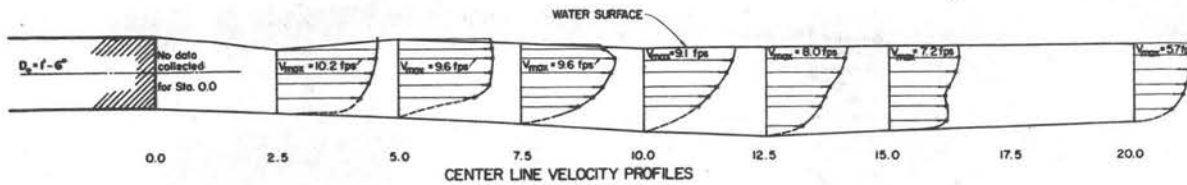
CENTER LINE VELOCITY PROFILES
ISOVELS
TRANSVERSE VELOCITY PROFILES
(MEASURED & PREDICTED)

Q = 84.0 cfs
TAIL WATER --- 3.00 ft.
PIPE DIAMETER --- 3.00 ft.
 D_{50} OF ROCK --- 8 in.
FLAT BED --- 20 ft BOTTOM
RUN G 57 FIG. 175



CENTER LINE VELOCITY PROFILES
ISOVELS
TRANSVERSE VELOCITY PROFILES
(MEASURED & PREDICTED)

$Q = 20.9$ cfs
TAIL WATER --- 1.57 ft
PIPE DIAMETER --- 1.45 ft
 D_{90} OF ROCK --- 8 in.
FLAT BED - 6 ft BOTTOM-2:1 BERMS
RUN K70 FIG. 176



CENTER LINE VELOCITY PROFILES
ISOVELS
TRANSVERSE VELOCITY PROFILES
(MEASURED & PREDICTED)

$Q = 13.9 \text{ cfs}$
 TAIL WATER --- 1.57 ft
 PIPE DIAMETER --- 1.45 ft.
 D_o OF ROCK --- 8 in.
 FLAT BED - 6 ft. BOTTOM-24 BERMS
 RUN K 71 FIG. 177

were not completed at Sta. 20.0. The information collected is shown in Figs. 176 and 177.

Presentation of Data

Figures 172 through 177 display the data collected for the six runs. All plots are to scale, with the appropriate scales appearing on the drawings.

A section along the longitudinal centerline of the basin is shown on the upper portion of each figure. The water surface elevation, centerline profile of the bed, and the vertical distribution of velocity at the centerline are shown for the various sections.

Plots of isovels were constructed from the measured data. The small filled circles indicate points where measurements were taken. The large dotted circle shows the position of the approach pipe relative to the section.

Plotted as a solid line directly above each isovel section is the velocity profile in a horizontal plane at an elevation $D_o/2$ above the pipe invert. The theoretical velocity profile (to be discussed later) based on the mean exit velocity and the approach pipe diameter is shown as a dashed line.

Three facts are apparent from examining the various plots:

1. Lowering the tailwater only one-seventh of the approach pipe diameter allowed the jet to plunge in such a manner as to cause significant scour. It is not known how much of this scour resulted from the plunging effect and how much resulted because of the smaller rock; however, the slope of the water surface indicates the jet was directed toward the floor.

2. Where the jet discharged into the low tailwater basin, the location of the core of maximum velocity is at the surface, whereas the location is at mid-depth or lower for the high tailwater basins.

3. The theoretically predicted velocity profiles are in good agreement with measured values for both tailwater conditions.

Results

To discuss the results in a meaningful manner, it is necessary to present and briefly review some of the information given in Ref. 21. The data collected downstream of the culverts appeared to correlate closely with the data presented for the three-dimensional orifice flow field. For this reason, only the information concerning the orifice flow field is described here.

The flow field was broken down into two zones; the zone of flow establishment adjacent to the outlet and the zone of established flow (see description sketch, Fig. 178). For each of the zones, the writers presented the following relationships:

(a) "Distribution of centerline velocity for flow from orifice,

$$V_{\max}/V_o \text{ versus } X/D_o ,"$$

where V_{\max} = maximum longitudinal velocity at a normal section,

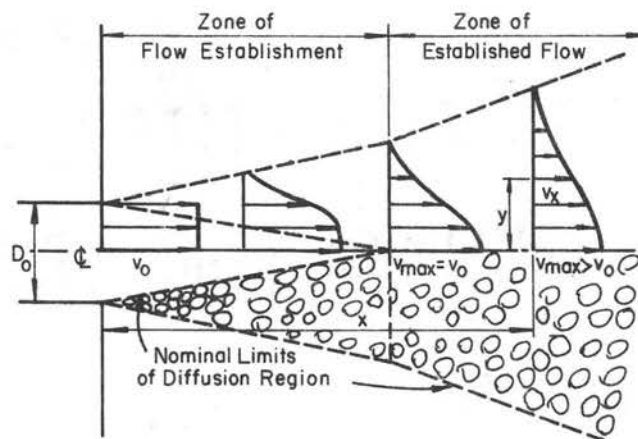
V_o = mean velocity at the outlet section,

x = distance downstream from the outlet, and

D_o = diameter of the outlet pipe.

(b) "Distribution of longitudinal velocity in zone of establishment of flow from orifices,

$$\frac{r - D_o/2}{x} \text{ versus } \frac{V_x}{V_o} ,"$$



Description Sketch Jet Diffusion,
Reproduced from Ref. 22

Fig. 178

where r = radial distance normal to the longitudinal centerline of the basin, and

V_x = longitudinal velocity at point (x,r) .

(c) "Distribution of longitudinal velocity in zone of established flow from orifices,

$$\frac{r}{x} \text{ versus } \frac{V_x}{V_o} \frac{x}{D} \text{ ."}$$

(d) "Distribution of volume, momentum, and energy flux downstream from orifice,

$$\frac{E}{E_o} \text{ versus } \frac{x}{D_o} ; \frac{M}{M_o} \text{ versus } \frac{x}{D_o} / \text{ and } \frac{Q}{Q_o} \text{ versus } \frac{x}{D_o} \text{ ,"}$$

where E = energy flux at Sta. x , = $\int_0^{\infty} V^2 V_x dA$,

E_o = energy flux at outlet section, $V_o^3 A_o$,

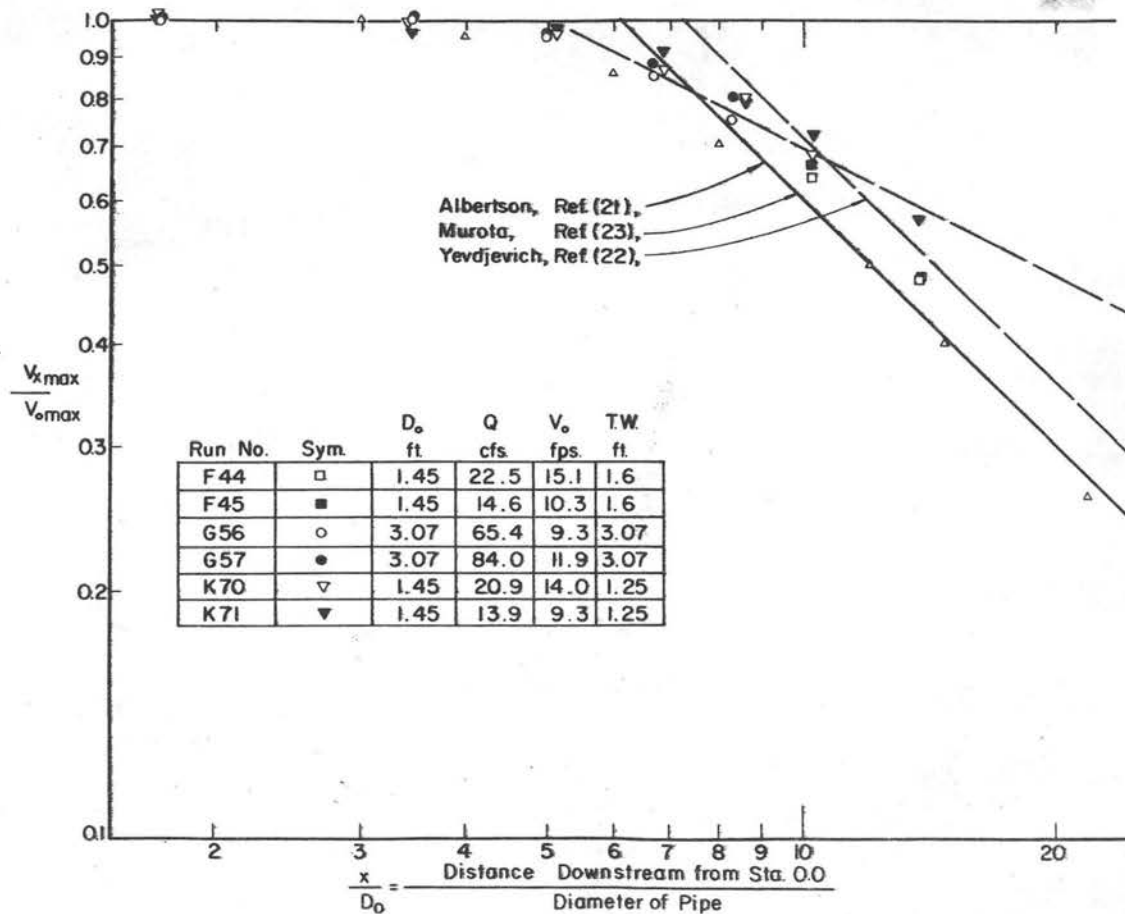
M = momentum flux at Sta. x , = $\int_0^{\infty} (V_x)^2 dA$,

M_o = momentum flux at Sta. 0.0 , $V_o^2 A_o$, and

Q = flow or volume flux through a normal section, $V_o A_o$.

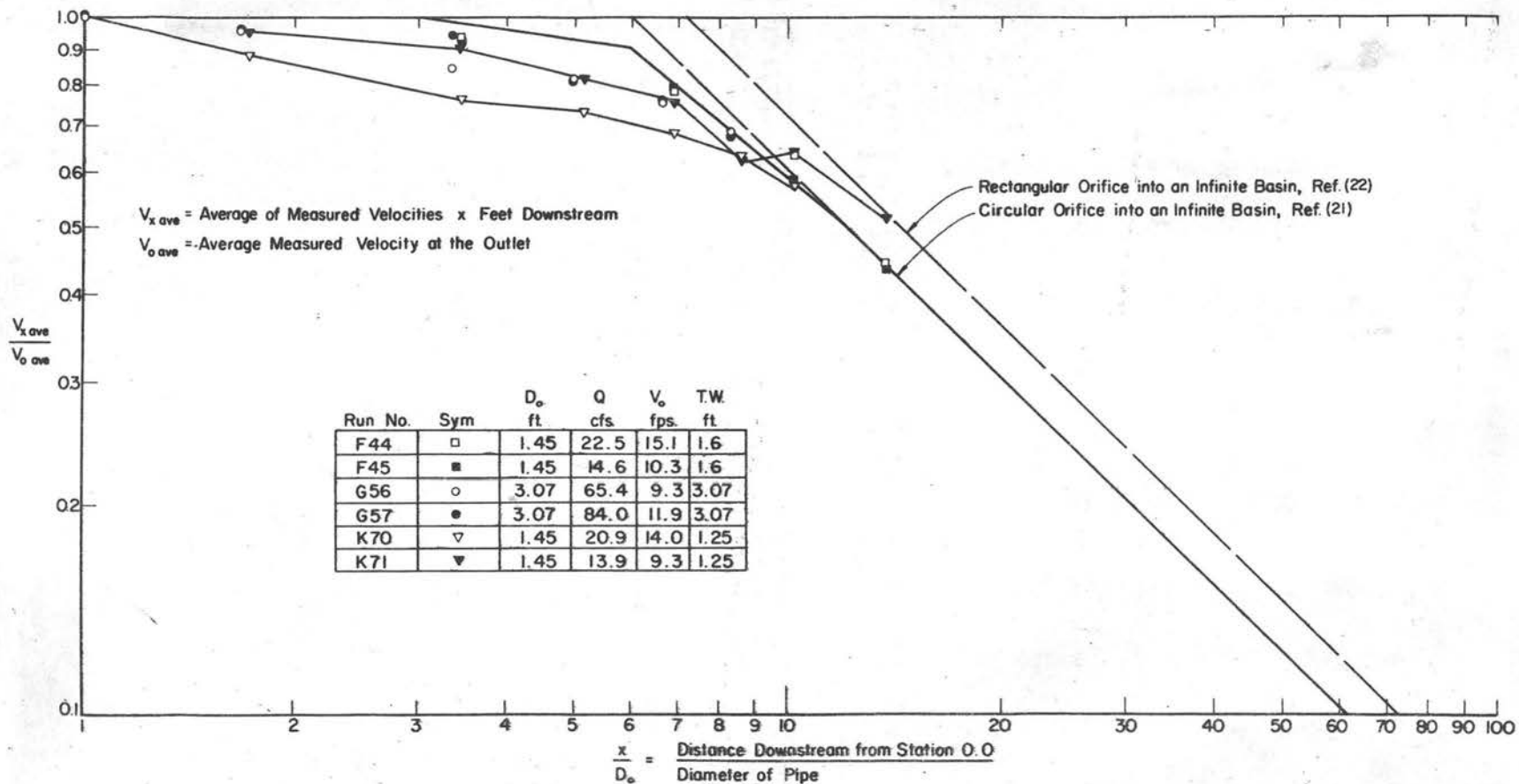
Other significant plots were presented, but only those that relate to the problem at hand are mentioned here.

The data collected downstream of the culvert outlets (6 runs) are superimposed on the plots. To obtain E , M , and Q , for comparison purposes, it was necessary to planimeter the isovel plots, Figs. 172 through 177, and form the appropriate integrals by a summation procedure. It was only possible to integrate to the 1 fps isovel; thus, a trivial portion of the integral (the region 0 to 1 fps) is missing from the quantities.



Distribution of Centerline Velocity
for Flow from Orifice (after Ref. 21)

Fig. 179



Distribution of Centerline Velocity for Flow from Submerged Outlets (after Ref. 21)

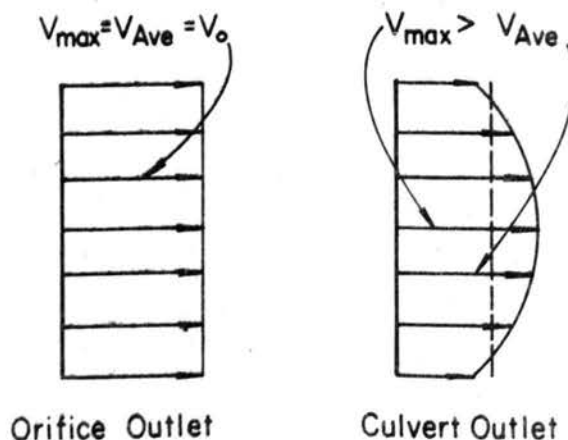
Fig. 180

Unfortunately, economic considerations made it imperative that the prototype basins be of limited length. For this reason data was obtained for only a limited range of x/D_o . The data does carry out to where $V_{x \text{ ave}}/V_{o \text{ ave}}$ is less than 0.5 and is sufficient to establish well defined trends.

$$\frac{V_{x \text{ max}}}{V_{o \text{ max}}} \text{ versus } \frac{x}{D_o} \quad (\text{Figs. 179 and 180})$$

Values of $V_{x \text{ max}}$ were obtained from the measured velocities and are the maximum point velocity in the x-direction at a station. Data from the six runs closely approximate those shown in Ref. 21 for the range $x/D_o < 6.0$ (Fig. 179) and generally fall between the prediction line for the circular pipe and the prediction line for the rectangular approach pipe for the range $x/D_o > 6$. The points which fall to the right of this region are those associated with the low tailwater runs. The core of maximum velocity is close to the surface for the low tailwater runs and, therefore, might not be worrisome from the viewpoint of bed scour.

Because the velocity distribution at the culvert outlet is non-uniform in contrast to the uniform distribution for the orifice, it



seemed more reasonable to compare the arithmetic mean of the velocities measured along a centerline vertical at Sta. x with an arithmetic mean of the velocities measured along a centerline vertical at the outlet. Note that the maximum velocity for the orifice is equal to the mean velocity, which is not the case for usual pipe flow. A plot of $\frac{V_x \text{ ave}}{V_o \text{ ave}}$ versus $\frac{x}{D_o}$, Fig. 180, is superimposed over the prediction curves shown in Fig. 179. In the range $x/D_o < 8.0$, the prediction curve is conservative with the exception of the data for the low tail-water runs. For the range $x/D_o > 8$, the culvert data follows the prediction curve.

Figure 180 is the curve recommended for design purposes. The average velocity is more in agreement with the mean velocity usually specified for conventional design curves.

The $V_o \text{ ave}$ to be used with Fig. 180 for basin design can be obtained by using the formula

$$V_o = KQ/A \quad (6-1)$$

where Q is the design discharge, A is the gross cross-sectional area of the culvert, and K is a constant relating Q/A to the arithmetic mean of the vertical velocity profile. For smooth approach pipes, K was evaluated using data from thirty-four runs. These runs for pipes of 18 and 36 in. diameters. Values of K ranged from 0.96 to 1.16, with an arithmetic mean of 1.07. For design purposes, the value $K = 1.10$ is suggested for smooth pipe.

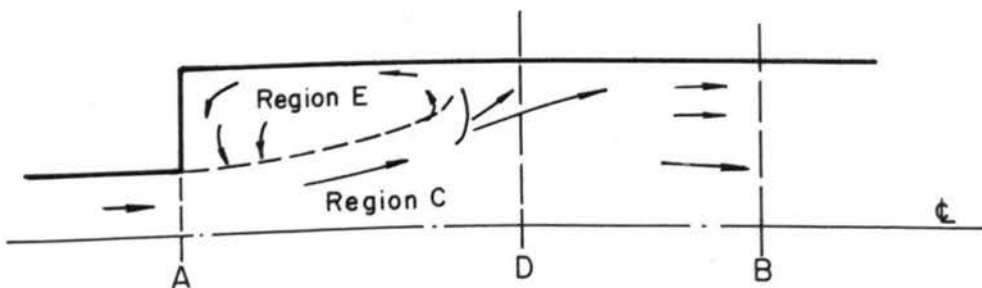
Only two sets of data were available for corrugated pipe. The values of K were 1.14 and 1.21 with the former value associated with

a typical maximum design discharge and the latter value with a Q well over the usual design discharge. It is suggested that $K = 1.15$ be used for corrugated pipe.

Q/Q_0 versus x/D_0 (Fig. 181)

For this relationship, a fundamental difference exists between the infinite basin and a basin of finite width. For the infinite basin, Q increases as the flow proceeds downstream and continuously entrains fluid from the surrounding media. For culvert basin flow, the entrainment can only occur for a limited distance. At the point where the jet expands to the full width of the channel, Q must equal the culvert discharge, barring spatial flow.

The data collected for the runs support this theory. Note that in contrast to the ever increasing Q/Q_0 for the infinite basin, the Q/Q_0 for the culvert basins increases systematically, then levels off and begins to decrease. Again the limited length of basin and the artificial downstream control (spillover weir at Sta. 25 or 35 where only downstream flow is possible) limits the usefulness of the data; however, the trend is well established. A description of the flow field follows.

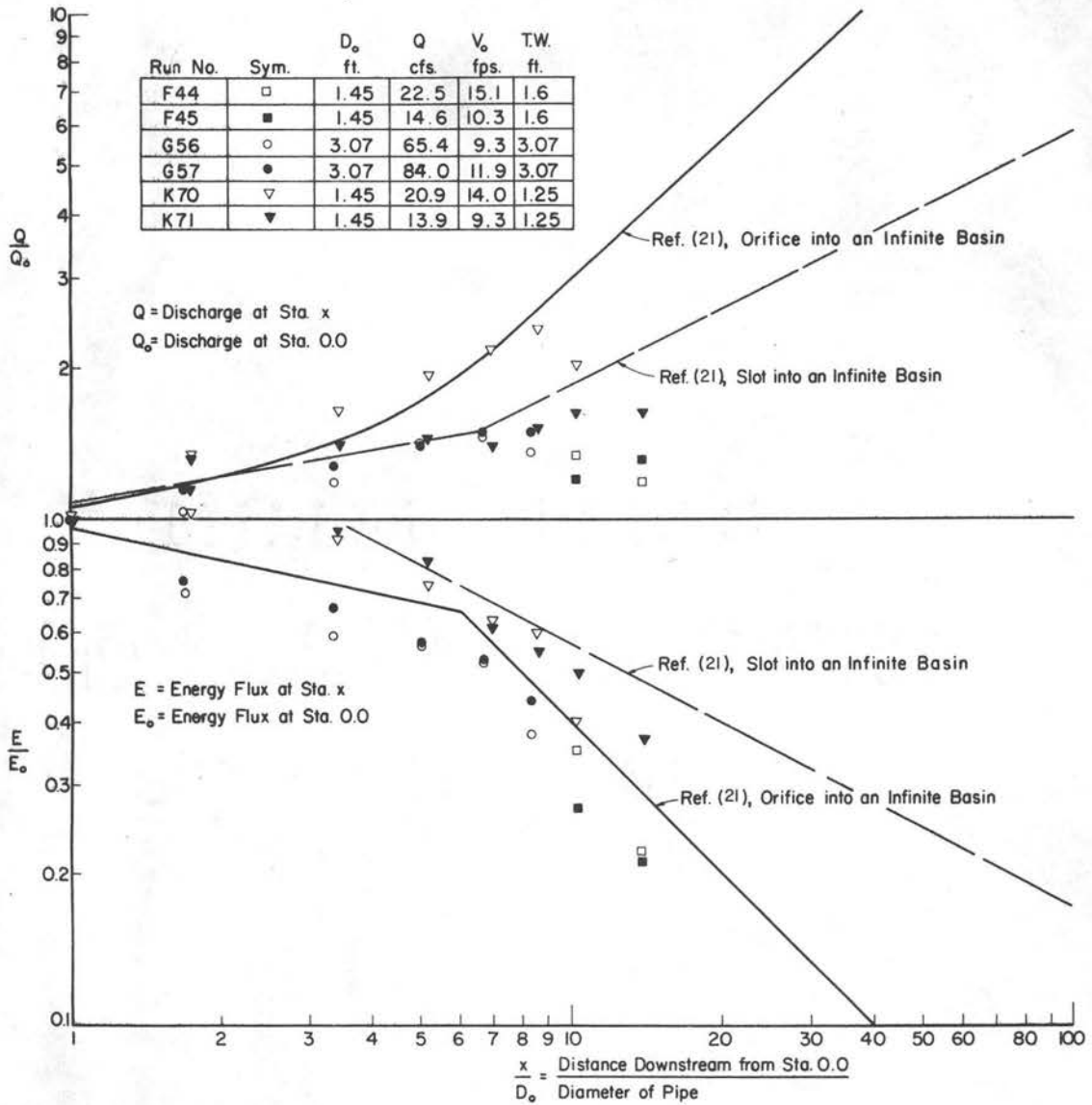


HALF PLAN

At section B, the discharge must be equal to Q_0 at A. In region C, the flow is the sum of Q_0 plus the fluid entrained from region E. To satisfy continuity, there must be upstream flow in region E equal to the amount of fluid entrained by the jet. At D, complex non-uniform, unsteady flow exists. The surface level in region E is lowered, creating sufficient differential elevation between regions D and E to establish upstream flow. The flow is somewhat unsteady. For a brief period of time, the downstream flow would dominate until sufficient differential elevation exists; then the upstream flow would take over. This results in a surging, turbulent flow region.

Having observed many basins in operation, both rigid boundary and scoured basins, it is the opinion of the writer that this continuous entrainment and replacement of water, which must strike a balance, is the driving mechanism of the usually named "eddies" that occur in the separation zone. In shallow rigid boundary basins where depth of flow was on the order of 0.2 ft and the mean diameter of the eddy was 2 to 4 ft (discussed in Chapter II), this circulation was equally obvious. This could not have been the same idle water continuously whirled around but rather was the result of the continuous pumping out and replacement. Note that an upstream velocity of 3 fps can be sustained by a differential in elevation head of 0.14 ft. This difference in elevation can easily exist without detection in a free surface basin of large dimension and high turbulence level.

An experimental program for the study of eddy characteristics, the location of the point of jet impingement, and the critical width where the core of the jet diverts to one side and attaches itself to



Distribution of Volume and Energy Flux
Downstream from Orifice (after Ref. 21)

Fig. 181

the wall is now in the planning stage. Further discussion of these problems awaits the satisfactory completion of this program.

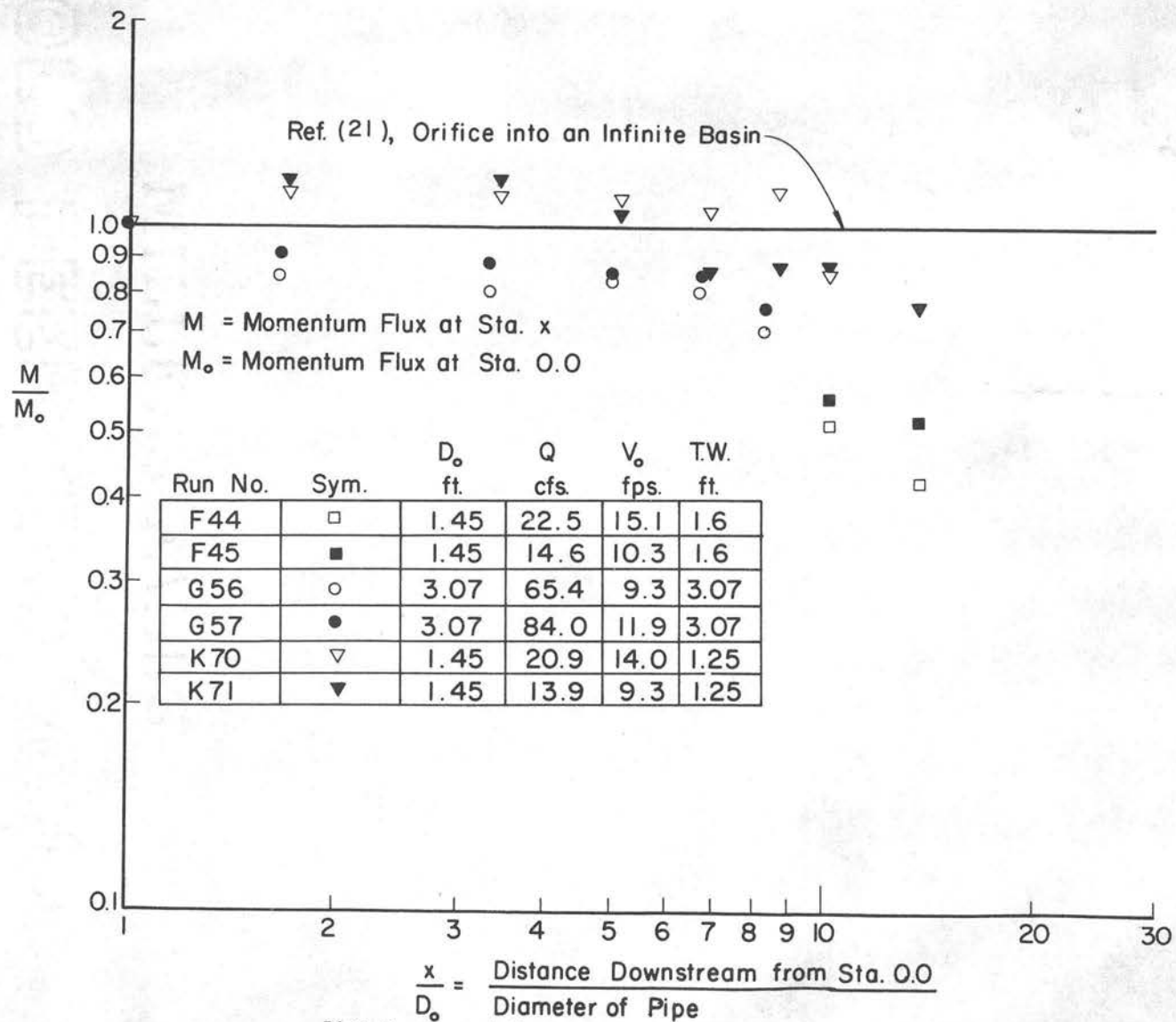
A significant factor affecting bank stability is the pressure fluctuation due to the unsteady surging of the flow where it impinges on the channel bank. This pumping action, in conjunction with the normal wind-generated wave action, is probably the most important factor from the viewpoint of bank erosion.

E/E_0 versus x/D_0 and M/M_0 versus x/D_0 , (Fig. 181 and Fig. 182)

The rate of energy decay, Fig. 181, for the culvert basins appears to follow the same general trend displayed by the infinite basin. In general, the rate of energy loss is somewhat higher for culvert basins. The slight gain of kinetic energy in the region adjacent to the outlet for the low tailwater basins is as it should be. The energy flux described in this chapter refers only to the kinetic energy. Since the water is discharging from a slightly higher elevation, some of the elevation head is converted to velocity head.

Another fundamental difference between the infinite basin and basin of limited dimensions is displayed by the M/M_0 diagram, Fig. 182. For the infinite basin, there is no reduction of momentum as the jet proceeds through the basin because there is no rigid boundary available for developing resistive forces. In the culvert basin, the flow must exert a shear force on the floor (and wall if the basin is narrow) and therefore, a compensating loss of momentum in the downstream direction must occur. This conclusion is substantiated by the data.

For the low tailwater runs, the apparent gain in momentum flux in the upper region of the basin is necessary if a balance between the



Distribution of Momentum Flux Downstream from Orifice (after Ref. 21)

Fig. 182

sum of external forces and momentum flux is maintained at successive stations, i.e., pressure force at the outfall is larger than in the lower tailwater region downstream thus resulting in a compensating larger momentum flux in the lower tailwater region.

Though the information presented in the momentum and energy plots is not readily applicable for design, it does contribute to an understanding of the different modes of flow in the infinite and finite basins.

Rate of Jet Expansion

The rate of jet expansion is also necessary for design. At the time velocity data was collected, it did not appear feasible to determine the line of zero velocity. This is not, of course, a definite line but rather the locus of points in a zone of highly turbulent eddying shear zone where the time average velocity in the downstream direction is zero.

Since the line of 0 velocity is not available, it was decided to compare the jet width at $V_2 = 0.2 V_x$ at the centerline, theoretical, with $V_x = 0.2 V_x$ at the centerline, measured. The comparison is made at a height of $D_o/2$ above the floor. The theoretical velocity can be deduced from Figs. 183 and 184. Results of the comparison are shown in Fig. 185. Though some lateral drift of the jet is apparent, it appears the fit is sufficiently good to warrant the use of the theoretical velocity prediction for design purposes.

Summary

At the outset, it was presumed that because of the differences in boundary conditions the criteria presented in Ref. 21 would have to be significantly modified to be useful for basins of finite dimensions.

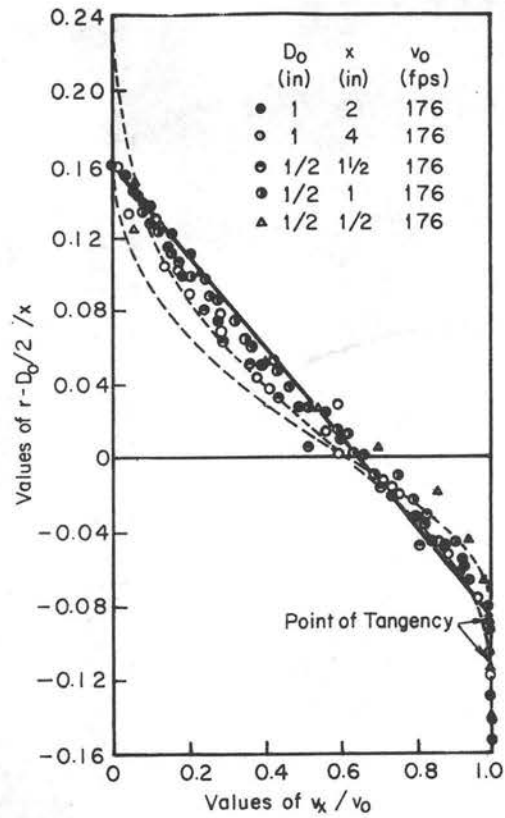


Fig. 183

Distribution of Longitudinal Velocity in
 Zone of Establishment of Flow $\frac{x}{D_0} < 6$
 (after Ref. 21)

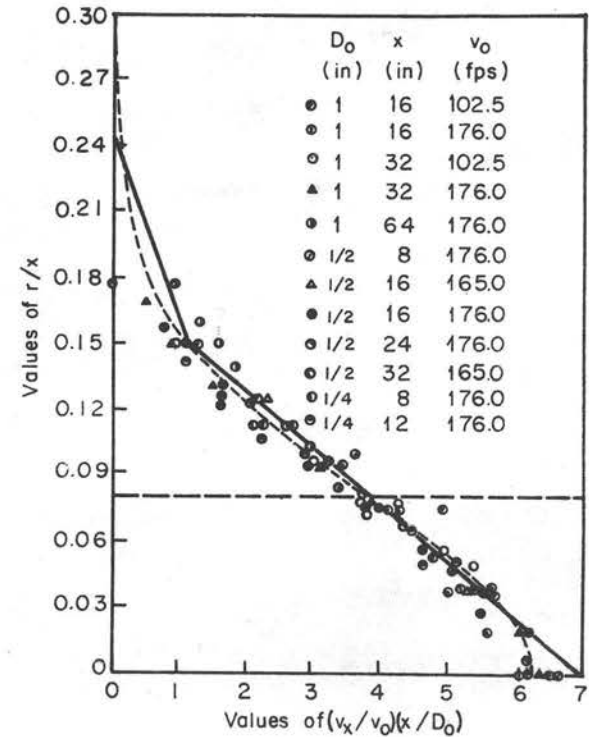
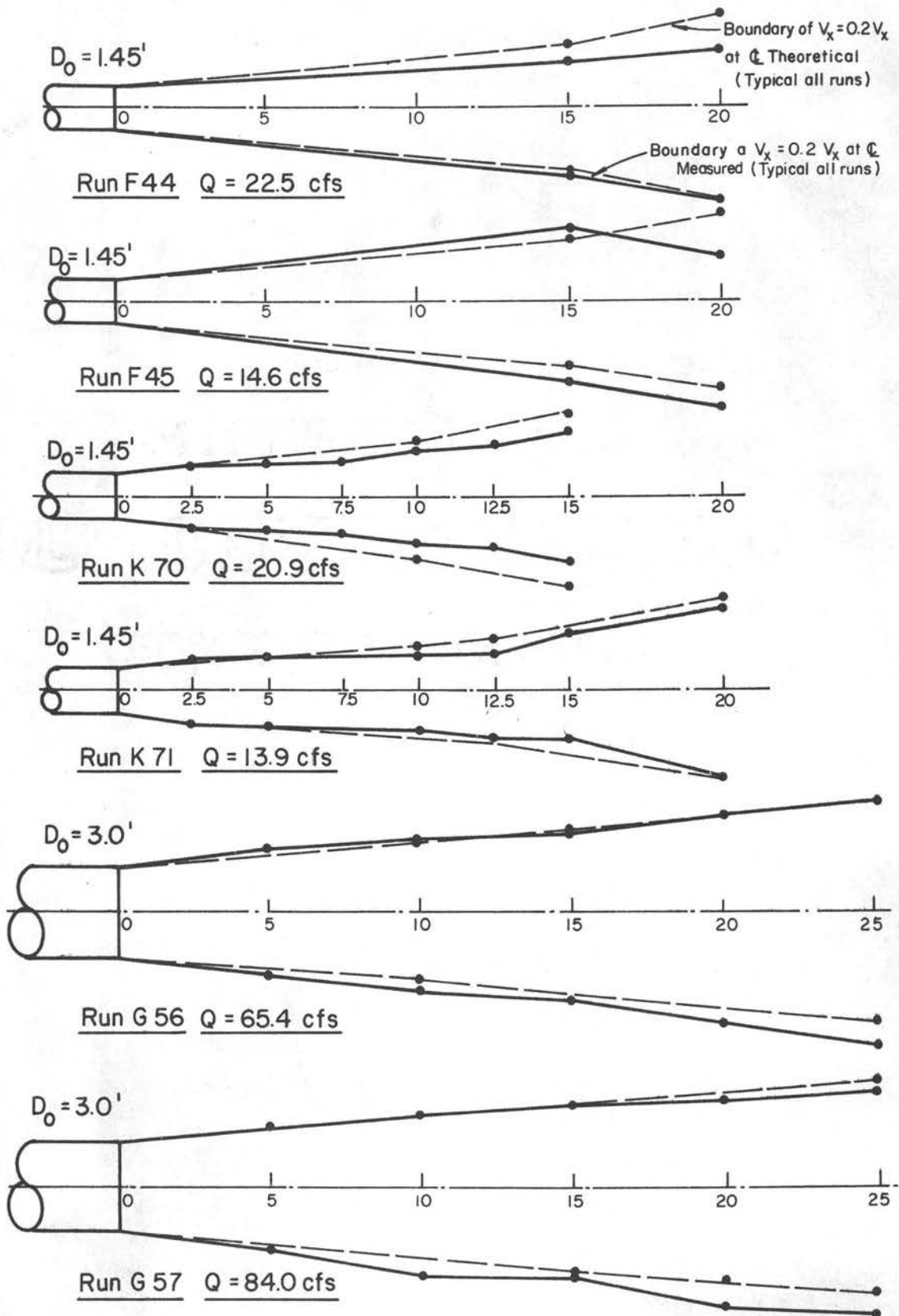


Fig. 184

Distribution of Longitudinal Velocity in
 Zone of Established Flow $\frac{x}{D_0} > 6$



A Comparison of Jet Width, Predicted versus Measured, at Height $D_0/2$

Fig. 185

It appears, after comparing the culvert basin data with data for the infinite jet, that the criteria for velocity distribution and jet dimensions can be used as originally presented.

For simplicity's sake, minor modifications are made in the diagrams. The slight modifications are :

(a) Figure 180

- Create three regions, 1. $x/D < 6$
 2. $6 < x/D < 12.0$
 3. $12.0 < x/D$.

Use the solid line for design purposes. This line passes close to the Albertson, et al., data points and encompasses all data taken for the culvert basins except the low tailwater runs.

Substitute $V_{x \text{ ave}}$ and $V_{o \text{ ave}}$ for pipe flow in lieu of $V_{x \text{ max}}$ and $V_{o \text{ max}}$ for the orifice flow.

(b) Figures 183 and 184

Replace original equation curves with straight line segments. Equations can be written for the straight line segments; however, it is simpler to scale directly from the plots.

It must be kept in mind by the designer that the information presented in this chapter is only useful for high tailwater basins. Consideration must be given to the hydrograph effect. The runoff from significant convective storms would rapidly collect at the inlet with a consequent high velocity discharge into the basin. The rising tailwater would lag considerably, thus allowing the water to pour onto the basin floor as the basin fills. This problem is currently under study and will be reported upon at a later date.

The information presented in this chapter is useful for estimating flow velocities in the channel downstream of the outlet when the culvert is operating under high tailwater conditions.

Chapter VII

DESIGN OF ENERGY BASINS

The design procedure and use of the design aids are most readily explained by the solution of practical problems. The prototype structure used for an example is a 6 ft x 6 ft box culvert. Suggested step by step procedures for the design of each of the three classes of basins (A, B, and C) are presented.

Class A Basin (Fig. 186)

1. Design a Class A basin so that the hydraulic jump will occur within the diverging walls of the basin.

<u>Given</u>	6 ft x 6 ft box culvert	$W_o = 6$ ft
	Depth of flow at outfall of culvert	$y_o = 4$ ft
	Design discharge	$Q = 420$ cfs
	Downstream tailwater depth	$y_B = 4$ ft
	Horizontal apron	

Compute

$$V_o = \frac{Q/2}{A/2} = \frac{210}{(3)(4)} = 17.5 \text{ fps}$$

Use Eq. 2-1, $u = 3 F_o$, to determine flare,

$$F_o = \frac{V_o}{\sqrt{gy_o}} = \frac{17.5}{\sqrt{(32.2)(4)}} = \underline{\underline{1.54}}$$

$$u = 3 F_o = 4.62 \text{ use } \underline{\underline{4.5}}$$

$$\text{Tan}\theta = \frac{1}{u} = \frac{1}{4.5} = \underline{\underline{0.222}}$$

With reference to Fig. 186, for a given Q and tailwater depth y_B , the momentum flux and pressure force at point x (slightly downstream of the hydraulic jump) is (assuming hydrostatic pressure variation and uniform distribution of velocity)

$$M_x = \rho(Q/2) V_x + \frac{W_2}{2} \frac{\gamma y_B^2}{2} \quad (7-1)$$

At point x ,

$$Q/2 = V_x \frac{W_2}{2} y_B$$

or

$$V_x = \frac{Q/2}{W_2/2 y_B} \quad (7-2)$$

$$W_2/2 = L_1 \text{ Tan}\theta \quad (7-3)$$

Substituting Eq. 7-2 and Eq. 7-3 into Eq. 7-1,

$$M_x = \rho \left(\frac{Q}{2} \right) \left(\frac{Q/2}{L_1 \text{ Tan}\theta y_B} \right) + \frac{L_1 (\text{Tan}\theta) (\gamma) (y_B)^2}{2} \quad (7-4)$$

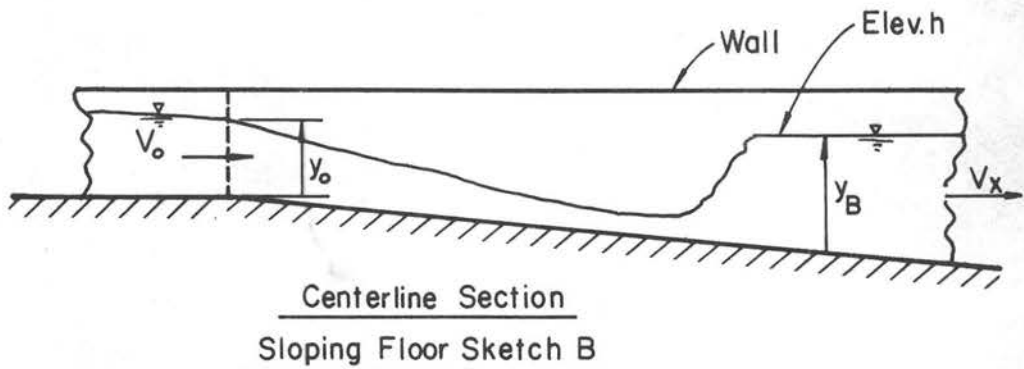
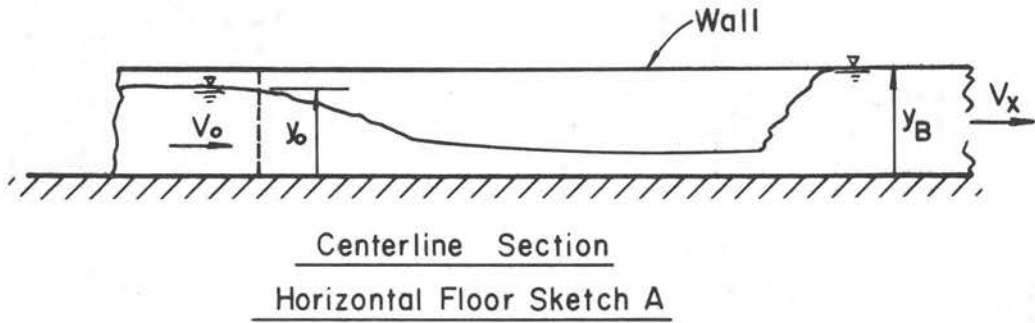
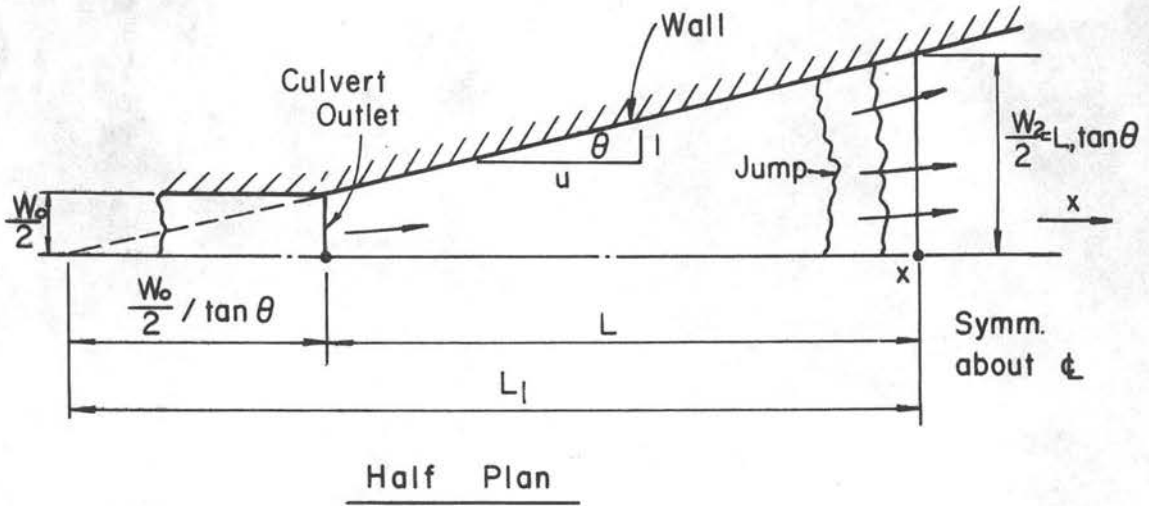
Given Q , y_B , and θ , there is a value of M_x associated with each value of L_1 .

Compute values of M_x for several values of L_1 , i.e., let $L_1 = 25'$, $30'$, $35'$, etc., determine M_x for each L_1 .

Substituting given values of Q , $\text{Tan}\theta$, y_B , ρ and γ , into Eq. 7-4,

$$M_x = \frac{(1.94)(210)^2}{L_1(0.222)(4)} + \frac{L_1(0.222)(62.4)(4)^2}{2},$$

$$M_x = \frac{96,500}{L_1} + L_1(110.7)$$



Class A Basin Fig. 186

TABLE VII

L_1 ft	L ft	$\frac{96,500}{L_1}$ lbs	$L_1 (110.7)$ lbs	M_x lbs
35	21.5	2760	3880	6640
40	26.5	2410	4430	6840
45	31.5	2140	4990	7130
50	36.5	1930	5540	7470
55	41.5	1750	6100	7850
60	46.5	1610	6650	8260
65	51.5	1480	7200	8680
70	56.5	1330	7750	9130

The next step is to compute the momentum at the outfall section,

$$M_o = \frac{\beta_1 \gamma y_o^2}{2} \left(\frac{W_o}{2} \right) + \beta_2 \rho V_o Q/2 \quad .$$

Compute

$$F_o = \frac{V_o}{\sqrt{g y_o}} = \frac{17.5}{\sqrt{(32.2)(4)}} = \underline{\underline{1.54}}$$

For rectangular approach pipe, $F_o = 1.54$

$$\text{Fig. 127} \quad \beta_1 = 0.71$$

$$\beta_2 = 1.01$$

$$M_o = (0.71)(62.4) \frac{(4)^2}{2} \frac{(6)}{2} + (1.01)(1.94)(17.5) \frac{(420)}{2}$$

$$= 1060 + 7200 = 8260 \text{ lbs} \quad .$$

Comparing this value to the values of M_x versus L_1 Table VII, it is apparent that $M_o \approx M_x$ at $60 \text{ ft} < L_1 < 65 \text{ ft}$. This is an estimate

of the location of the hydraulic jump. Note that L_1 is not the length of the basin, L . With reference to the half plan, Fig. 186,

$$L = L_1 - \frac{W_0}{2} \tan\theta .$$

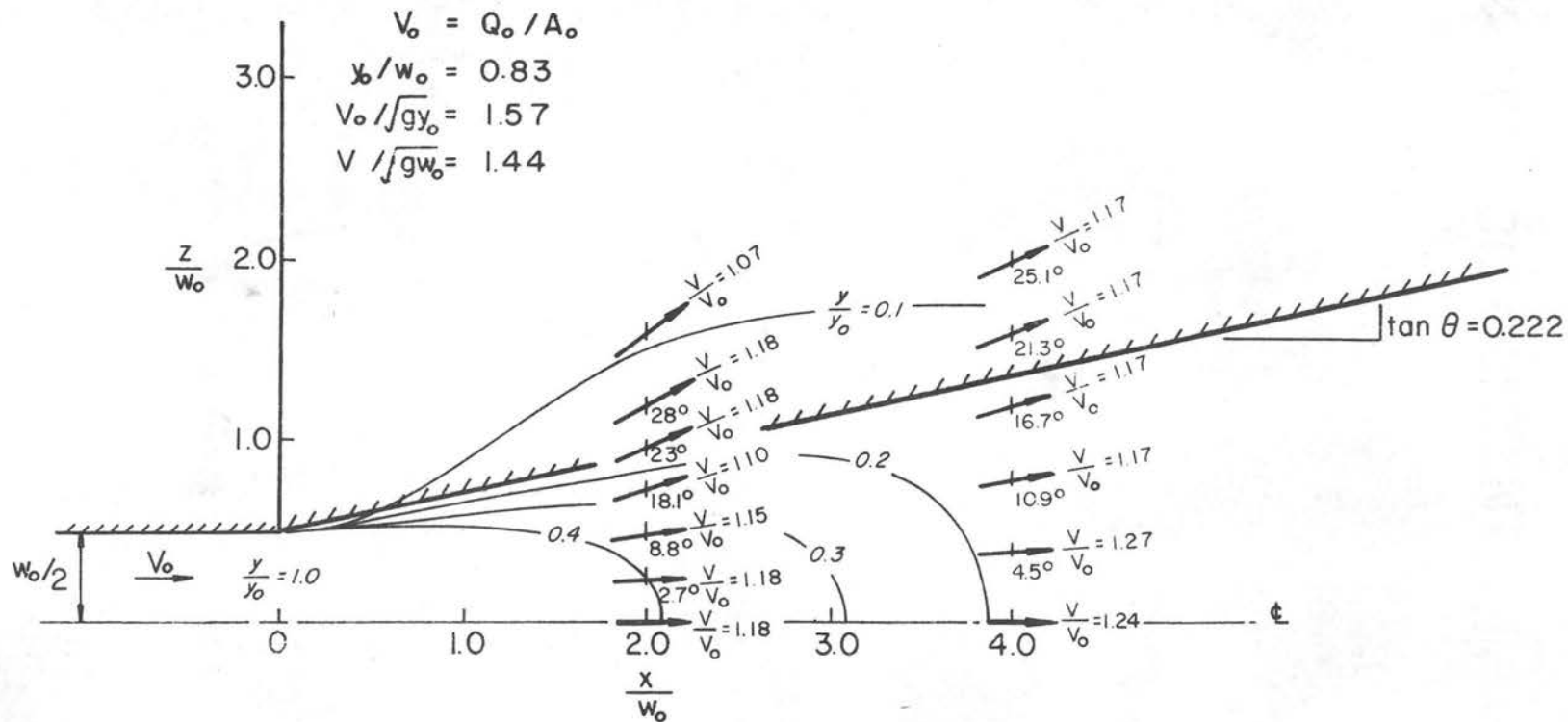
In the analysis, the shear force exerted by the floor on the flow, and the pressure force exerted by the diverging walls on the flow have not been considered. The two forces tend to cancel each other. The floor shear is the larger of the two. By ignoring the wall and floor forces, a conservative estimate of L is obtained.

If a more precise estimate of L is required, it is suggested that the back water curve of the supercritical flow through the diverging basin be computed. The flow is supercritical, therefore the control section (and starting point for backwater computations) is upstream.

The rapidly varied flow region near the outfall section presents a problem. It is suggested that backwater computations be started at Sta. $\frac{x}{W_0} = 2$.

Using values of $F_0 = 1.54$, previously computed, and $\frac{y_0}{W_0} = \frac{4'}{6'} = 0.67$, the dimensionless plot of water surface profiles and velocity vectors (for flow with similar parameters, $F_0 = 1.57$, $\frac{y_0}{W_0} = 0.83$), Fig. 144, is selected. This data is superposed over a half plan of the proposed basin, Fig. 187.

At St. $\frac{x}{W_0} = 2.0$ it is apparent that the wall would have little effect on the flow field (the wall falls outside the $\frac{y}{y_0}$ contour of 0.2) therefore a good estimate of the velocity can be obtained by averaging the $\frac{V}{V_0}$ values shown between the centerline of the basin and the wall,



Dimensionless Water Surface Contours and
Relative Velocities
Class A Basin

Fig. 187

$$\frac{V}{V_0} = \frac{1.18 + 1.18 + 1.15 + 1.10}{4} = 1.15 \quad .$$

The mean velocity passing through the sections is $V = V_0(1.15) = (17.5)(1.15) = 20.1$ fps. The width of the basin at Sta. $\frac{x}{W_0} = 2$ is $3.0 + (2)(6)(\tan\theta) = (3.0) + (12)(0.222) = 5.67$ ft. The mean depth is

$$\frac{Q/2}{(\text{width})(V)} = \frac{210}{(5.67)(20.1)} = 1.84' \quad .$$

With a known depth of flow and mean velocity at the starting section and given flare angle for the walls, backwater computations using the standard step method (see page 279, Ref. 9) is a routine (though laborious) procedure.

To locate the jump, values of V_L (velocity at $x = L$) and y_L (depth at $x = L$) from the backwater computations are used to compute the quantity $M_L = \rho Q/2 V_L + \frac{\gamma y_L^2 w_L/2}{2}$ for various values of L . When M_L for a specific L equals the quantity shown in column 5 of Table VII for an equal length L , the jump will occur.

Whichever method is used to locate the approximate position of the jump, the basin must be extended several feet beyond the theoretical position. It is shown in Ref. 24 that the length of the circular hydraulic jump (a situation similar to the flared basin) is about 3.5 to 4.5 the depth of flow (y_b) at the heel of the jump. It is suggested that a minimum of $6 y_b$ be added to L (Fig. 186) for design purposes.

Additionally, exit velocities from the basin should be checked for the minimum tailwater condition. The standard step method carried out for the design length of basin would yield this information. A means of shortening the basin is to increase the tailwater depth. One way of accomplishing this is to slope the basin steeply into the ground.

In the analysis (see sketch B, Fig. 186) it is assumed that tailwater height, elevation h , is a known quantity. To obtain the quantities similar to those shown in Table VII, the variation of y_B has to be considered, i.e.,

$$M_x = \frac{(1.94)(210)^2}{L_1(0.222)(y_B)} + \frac{L_1(0.222)(62.4)(y_B)^2}{2}$$

Knowing elevation h , the elevation of the invert at the culvert outfall, and the slope of the floor, y_B is readily determinable for any value of L_1 . Also, if the backwater curve is computed, the longitudinal slope of the floor must be considered.

In the design of this basin, the walls must be of sufficient height that tailwater cannot flow over the walls and submerge the high velocity flow upstream of the jump. If this basin is submerged by tailwater, a flow field similar to that described in Chapter VI can occur.

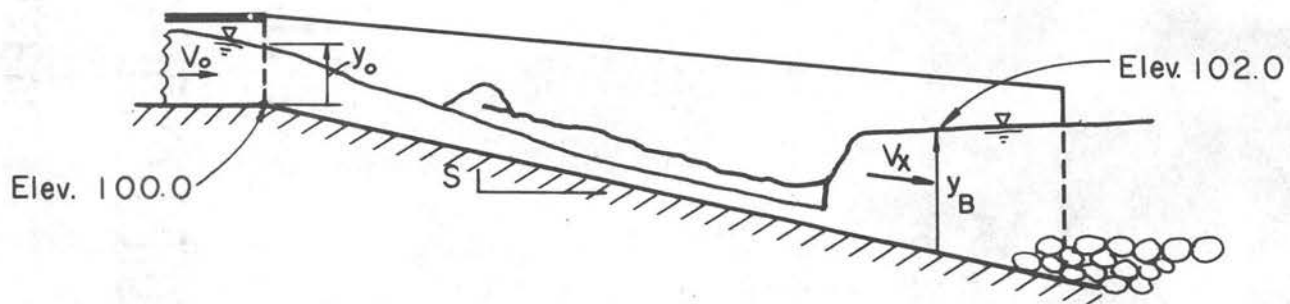
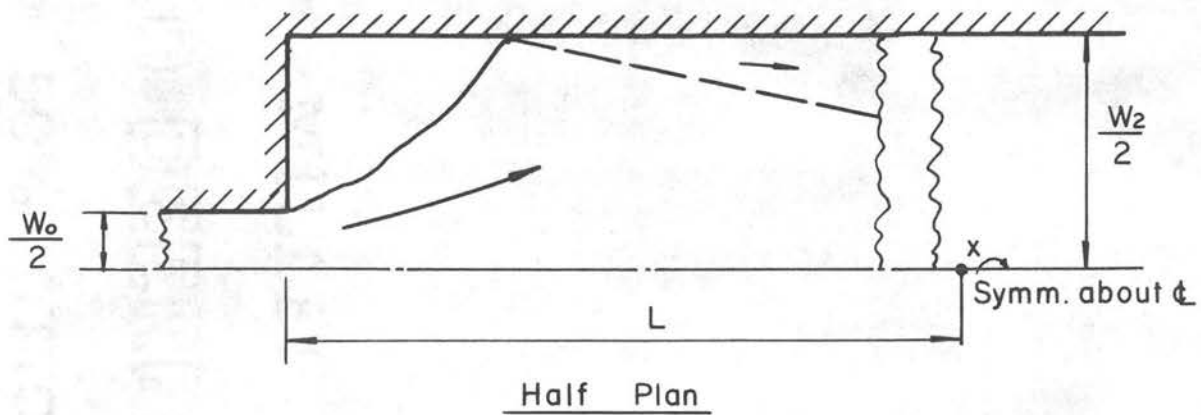
Class B Basin (Fig. 188)

This basin is the least tractable of the three classes and should only be used with strict tailwater control. The simplest way to ensure adequate tailwater is to slope the basin into the channel.

Design a Class B basin for the following situation:

Alternate A

Given 6 ft x 6 ft box culvert	$W_0 = 6 \text{ ft}$
Depth of flow at culvert outfall	$y_0 = 4 \text{ ft}$
Design discharge	$Q = 420 \text{ cfs}$
Downstream tailwater elevation	102.0
Invert elevation at culvert outlet	100.0



Centerline Section
 Sloping Floor Sketch C

Class B Basin Fig. 188

Longitudinal slope of basin 10%

Designer's choice $\frac{W_2}{W_0} = 4.0$ $W_2 = 24$ ft

Work with $\frac{1}{2}$ section.

Compute the momentum at outfall section.

See previous computations, $M_0 = 8260$ lbs.

Combining Eq. 7-1 and the continuity equation $V_x = \frac{Q/2}{W_2/2 y_B}$

the momentum in the x-direction at Sta. L (sketch C, Fig. 188) is

$$M_x = \rho \left(\frac{Q}{2} \right) \frac{Q/2}{W_2/2 y_b} + \left(\frac{W_2}{2} \right) \frac{\gamma y_B^2}{2}$$

Equate M_x to M_0 above, substitute known values of Q , ρ , γ , and W_2 and solve for the subcritical flow depth y_B :

$$(1.94)(210) \left(\frac{210}{12} \right) \frac{1}{y_B} + \left(\frac{24}{2} \right) \left(\frac{62.4}{2} \right) y_B = 8260 \quad (7-5)$$

Solve above equation by trial and error for positive values of y_B .

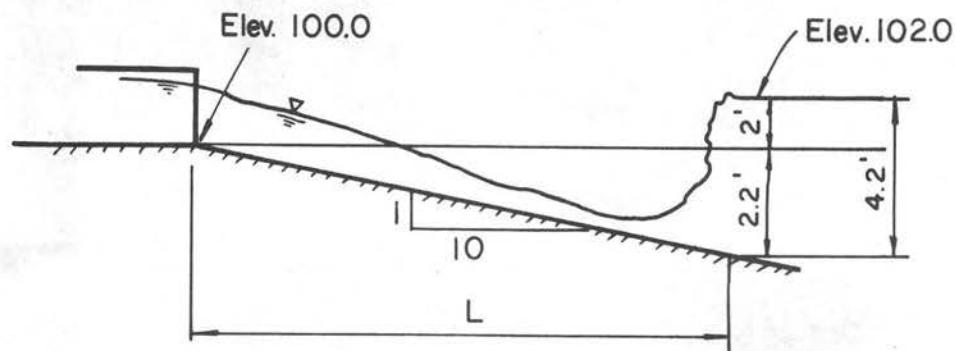
y_B supercritical = 0.9 ft

y_B subcritical = 4.2 ft.

Elevation of invert given as 100.0

Tailwater elevation given as 102.0

Slope given as 10% .



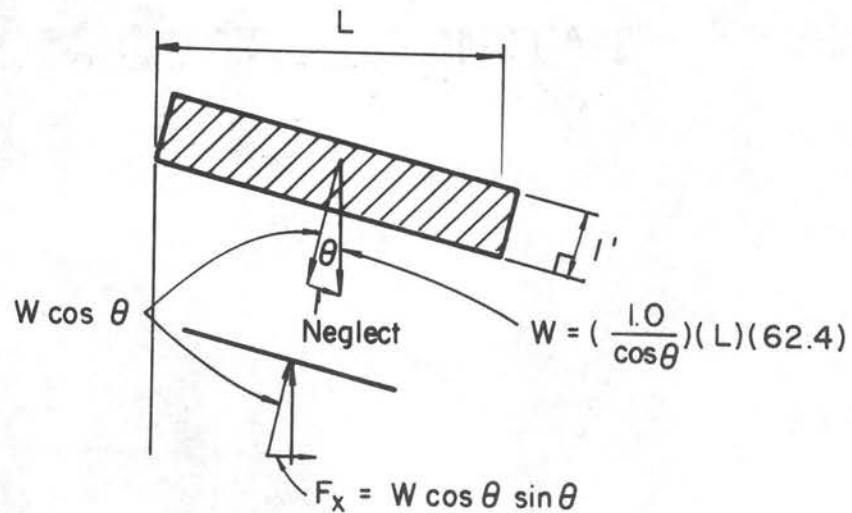
SKETCH D

$$L(0.10) = 4.2 - 2.0 = 2.2$$

$$\underline{\underline{L = 22 \text{ ft.}}}$$

Note: The weight of the water has not been considered. There is a force component in the x-direction produced by the sloping floor on the body of water. There is also a shear force exerted by the floor on the water which partially cancels the weight force (the shear would, of course, exactly cancel the weight component if parallel flow exists).

For a conservative estimate of L , neglect the shear force. Compute the weight component in the x-direction of the body of water 22 ft. long, 12 ft. wide, and 1 ft. deep.



SKETCH E

$$F_x = (1.0)(22)(12)(62.4) \frac{1}{10} = \underline{\underline{1650 \text{ lbs}}}$$

Add 1650 lbs plus a questimate of 600 lbs to the right side of Eq. 7-5 and recompute y_b .

$$\frac{7130}{y_B} + 375 y_B^2 = 8260 + 1650 + 600 = 10,510 .$$

By trial and error solution,

$$y_B \text{ subcritical} \approx \underline{\underline{5.0 \text{ ft}}} .$$

Recompute L (sketch D), $L = \frac{5.0 - 2.0}{0.10}$, $L = \underline{\underline{30 \text{ ft}}} .$

Check $F_x \cdot F_x = \left(\frac{30}{22}\right) (1650) = 2250 \text{ lbs}$ which is the amount previously added to Eq. 7-5. Since the bed shear force directed upstream was not considered, this is a conservative estimate of L .

If a horizontal floor is required, the following procedure is suggested.

Alternate B

Given

6 ft x 6 ft box culvert	$W_o = 6 \text{ ft}$
Design discharge	$Q = 420 \text{ cfs}$
Depth of flow at culvert outlet	$y_o = 4 \text{ ft}$
Downstream tailwater	3 ft

Estimate the exit velocity from a Class A basin.

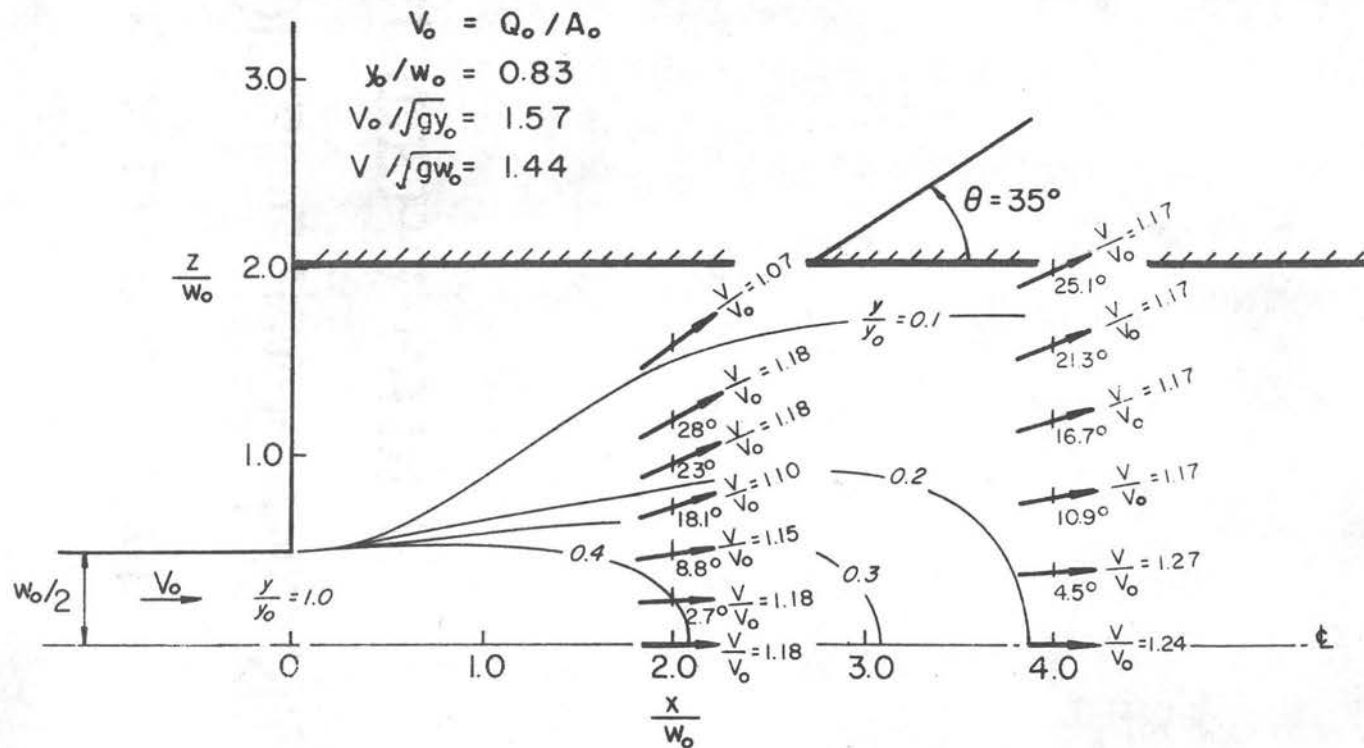
Designer's choice $\frac{W_2}{W_o} = 4$, $W_2 = (4)(6) = 24 \text{ ft}$.

F_o previously computed = 1.54,

$$\frac{y_o}{W_o} = \frac{4}{6} = 0.67 .$$

Select dimensionless water surface profile and velocity vectors, Fig.

144. Superimpose a rectangular basin with $\frac{Z}{W_o} = 2$ over the dimensionless plot, Fig. 189.



Dimensionless Water Surface Contours and Relative Velocities
Class B Basin

Fig. 189

Assumption 1

Extend the $\frac{y}{y_0} = 0.1$ contour to the wall. The intersection is assumed to be the point of impingement. Scale angle θ , $\theta \approx 35^\circ$. Use Ippen's criterion for estimating the angle of the standing wave.

$$\theta = 35^\circ$$

$$F_1 = \frac{V_1}{\sqrt{gy_1}}, \text{ from relative velocity plot, } \frac{V_1}{V_0} = 1.07 \text{ near}$$

$$\text{the wall, } V_1 = (1.07)(17.5) = \underline{\underline{18.7 \text{ fps}}}$$

Assumption 2

$$y_1 = 0.1 y_0$$

$$y_1 = (0.1)(4) = \underline{\underline{0.4 \text{ ft}}}$$

$$F_1 = \frac{V_1}{\sqrt{gy_1}} = \frac{19.7}{\sqrt{(32.2)(0.4)}} = \underline{\underline{5.2}}$$

Using Fig. 190,

$$\text{Know } \theta = 35^\circ$$

$$F_1 = 5.2$$

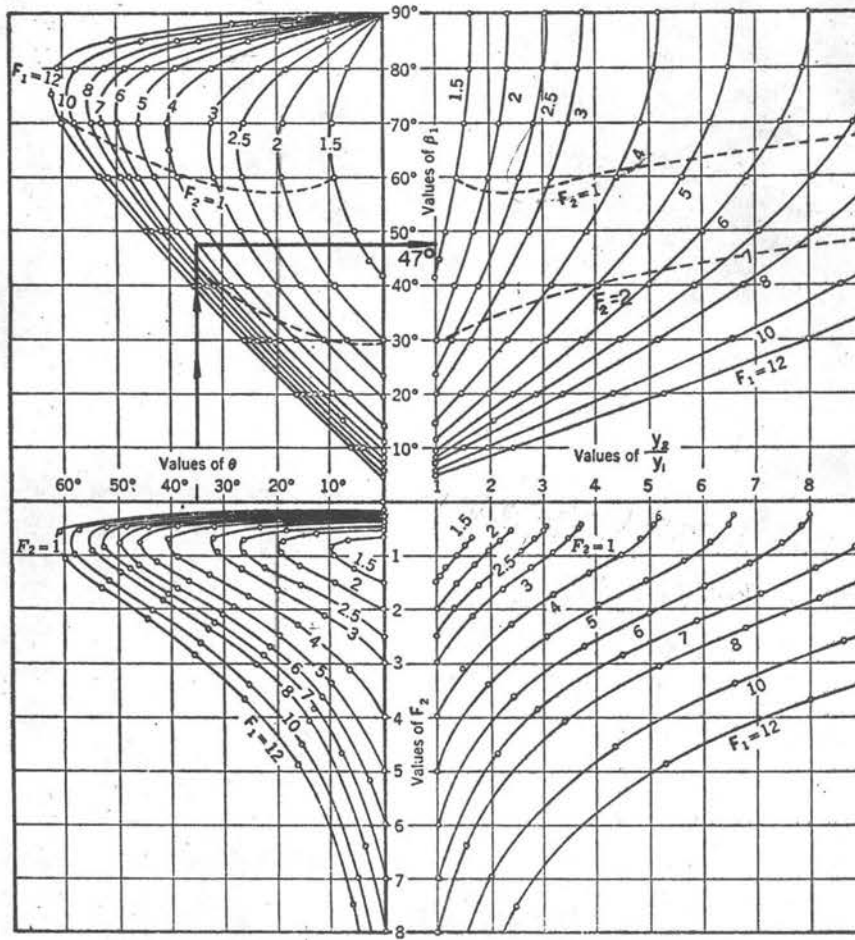
$$\text{Find } \beta_1 = 47^\circ$$

Ippen's criterion for $\frac{y_2}{y_1}$ is unsatisfactory for the prediction of y_2 ; therefore, use $\frac{y_2}{y_1} = 3.5$. This approximate formula is discussed in detail in Chapter II.

$$y_2 = (3.5)(y_1) = (3.5)(0.4) = \underline{\underline{1.40 \text{ ft}}}$$

At Sta. x downstream of the intersection of the standing wave,

$$V \approx \frac{Q/2}{(W_2/2)y_2} = \frac{210}{(12)(1.4)} = \underline{\underline{12.5 \text{ fps}}}$$



General Relations Among F_1 , θ , B , y_2/y_1 , and F_2 for Oblique Hydraulic Jumps (after A. T. Ippen, Ref. 11) Fig. 190

The momentum in the x-direction at Sta. x is

$$M_x = \rho Q/2 V_x + \gamma \frac{y_b^2}{2} \frac{W_2}{2} = (1.94)(210)(12.5) + \frac{(62.4)(1.4)^2(12)}{(2)}$$

$$= 5100 + 735 = \underline{\underline{5835 \text{ lbs}}}$$

Tailwater depth is given as 3 ft. Assuming the entire section is occupied by downstream flow,

$$V \approx \frac{Q/2}{(W_2/2)(y_B)} = \frac{210}{(12)(3)} = 5.83 \text{ fps}$$

Momentum of the flow 3 ft deep and 12 ft wide is

$$\rho Q/2V + \frac{\gamma y_B^2}{2} \frac{W_2/2}{2} = (1.94)(210)(5.83) + \frac{(62.4)(3)^2(12)}{2}$$

$$= 2370 + 3370 = \underline{\underline{5740 \text{ lbs}}}$$

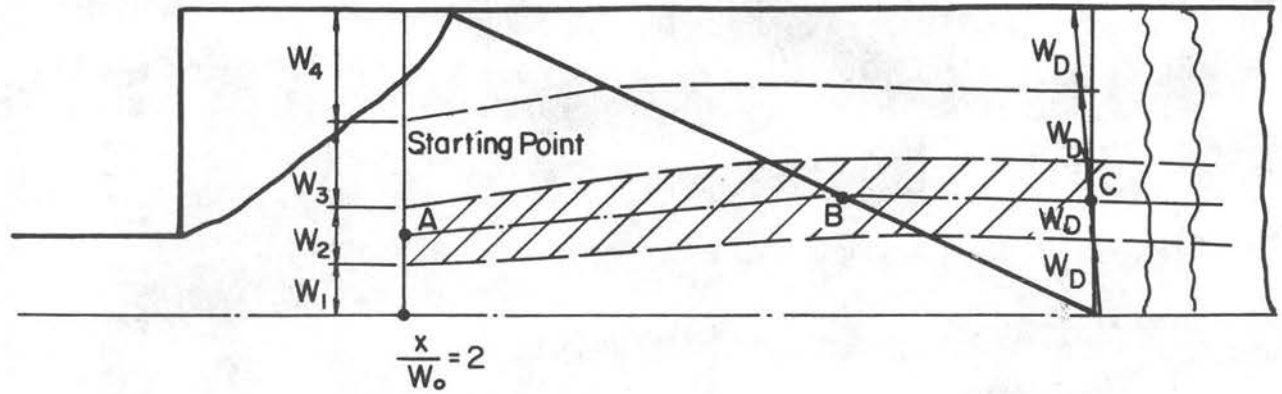
This is slightly less than the momentum flux shown above (5835 lbs); therefore the jump would not occur within the basin. The outlet velocity would be approximately the velocity shown at Sta. x above, $V = 12.5 \text{ fps}$. Without the basin, the velocity at the outfall of the culvert would have been $V = (1.18)(17.5) = \underline{\underline{21.6 \text{ fps}}}$.

If further refinement of the design procedure is warranted, the following method is suggested:

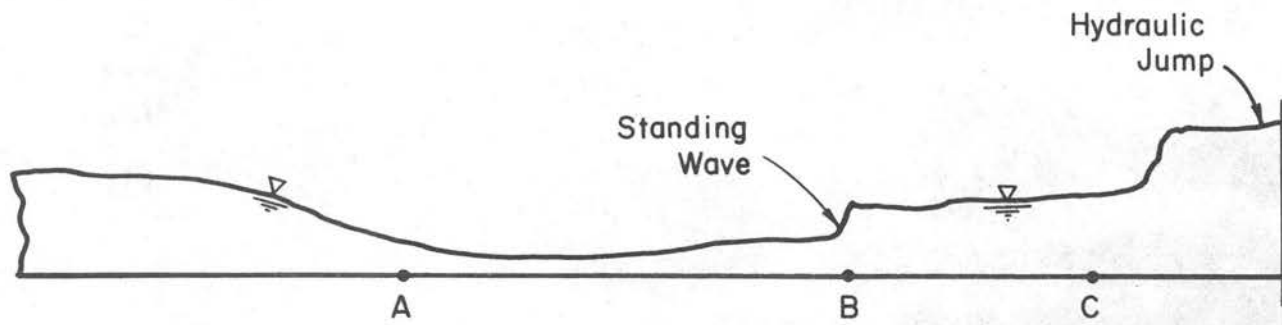
Alternate C

a) Superimpose the basin over dimensionless water profiles, determine point of impingement and the bearing of the standing wave in the same manner as described under Alternate B.

b) Subdivide the basin into 4 (or more) stream tubes each carrying an equal discharge. (See Fig. 191).



Half Plan



Section Along Stream Tube

Definition Sketch for Backwater Computations
Class B Basin

Fig. 191

$$Q/2 = 210 \text{ cfs}$$

$$\frac{Q/2}{4} = 52 \text{ cfs} .$$

Begin computations at Sta. $\frac{x}{W_0} = 2.0$. In the central portion of the basin $\frac{V}{V_0} = 1.18$ and $\frac{y}{y_0} \approx 0.42$. Therefore $V = (1.18)(V_0) = (1.18)(17.5) = 20.6 \text{ fps}$; $y = (0.42)(4) = 1.68$.

$$W_1 , \text{ width of first stream tube} = \frac{52 \text{ cfs}}{(y)(V)} = \frac{52}{(1.68)(20.6)} = \underline{\underline{1.50 \text{ ft}}} .$$

Compute W_2 and W_3 in the same manner, and assume W_4 is the remaining width of the basin. With reference to Fig. 191, compute the backwater curve for stream tube 1, 2, 3, and 4.

Example Stream tube 2:

1. Starting point A,

Given depth, mean velocity and width of stream tube (just computed).

2. Assumption, subdivide channel downstream of standing wave into 4 equal widths, W_D and project the stream tube boundaries back to the standing wave.

3. Using the standard step procedure, compute backwater curve for each of the 4 stream tubes from point A to point B. Determine the depth of flow at point B from backwater computations.

4. Use the relationship $\frac{y_2}{y_1} = 3.5$ to obtain depth of flow downstream of wave.

5. Estimate the velocity of the flow downstream of the standing wave, $V = \frac{Q/8}{W_D y_2}$.

6. Continue backwater computations in the downstream direction using y_2 , W_D , and V from Step 5.

7. Periodically check the depth of flow from tube to tube to insure the depths are approximately equal. If they are not, average the depths. Use this new depth in the computations.

8. From point C on downstream, the backwater curve is assumed common for all tubes. The location of the jump from this point on downstream (or the estimate of exit velocity from the basin) is routine. As an example, see page 403, Ref. 9.

The basin must be designed in such a way that the jet will not be totally submerged (basins with high tailwater, Chapter VI). The flow must plunge and spread so that a high Froude number jump can occur. To insure this, the invert of the pipe at the outlet section must be set sufficiently high. In addition, the walls of the basin must be higher than the tailwater so that water cannot spill into the basin and submerge the jet.

Class C Basin (Fig. 192)

Given

Design Discharge $Q = 420$ cfs

6 ft x 6 ft box $W_0 = 6$ ft

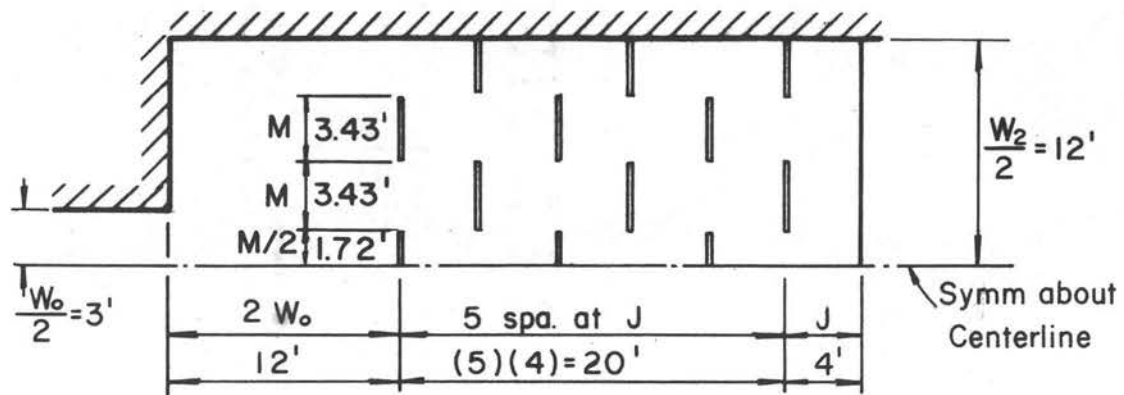
Depth of flow at outfall of box $y_0 = 4$ ft

Designer's choice: $\frac{W_2}{W_0} = 4$, $\frac{y_0}{a} = 1.1$, 6 rows of elements.

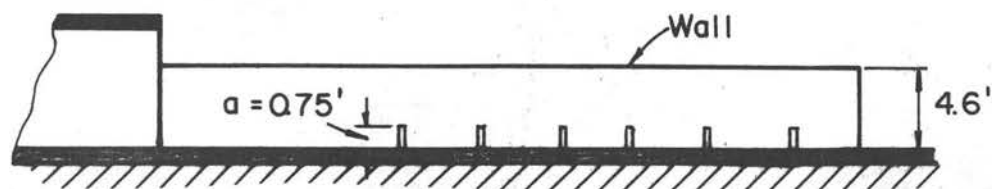
Note work with $\frac{1}{2}$ of basin,

$$\frac{W_2}{W_0} = 4 \quad , \quad W_2 = W_0 4 = (6)(4) = 24 \text{ ft}$$

$$\frac{Q}{2} = 210 \text{ cfs} \quad , \quad y_0 = 4 \text{ ft} \quad , \quad \frac{W_0}{2} = 3 \text{ ft}$$



Half Plan



Centerline Section

Class C Basin

Fig. 192

$$V_o = \frac{Q/2}{\text{Area}} = \frac{210}{W_o/2(y_o)} = \frac{210}{(3)(4)} = \underline{\underline{17.5 \text{ fps}}}$$

$$F_o = \frac{V_o}{\sqrt{gy_o}} = \frac{17.5}{\sqrt{(32.2)(4)}} = \underline{\underline{1.54}}$$

From Fig. 127: $\beta_1 = \underline{\underline{0.71}}$

$$\beta_2 = \underline{\underline{1.01}}$$

Estimate from Fig. 144: $\frac{y}{y_o} = 0.21$, $y = y_o(0.21) = (4)(0.21) = \underline{\underline{0.84 \text{ ft}}}$ at $\frac{x}{W_o} = 2$,

$$\begin{aligned} \frac{V_a}{V_o} &= 1.18 & V_a &= (1.18) V_o \\ & & &= (1.18)(17.5) = 20.6 \text{ fps.} \end{aligned}$$

Height of Element-A

Designer's choice, $\frac{y}{a} = 1.1$

$y = 0.84$, $\frac{y}{a} = 1.11$, therefore $a = 0.76 \text{ ft}$, use $a = \underline{\underline{0.75 \text{ ft}}}$.

Length of Element-m

See Fig. 161, $3\frac{1}{2}$ space/ $\frac{W_2}{2}$,

Area of element-A = (m)(a) = (3.43)(0.75) = 2.57 sq ft

Longitudinal Spacing of Elements-J

From Fig. 161 for $\frac{y}{a} = 1.1$, $\frac{J}{a} = 6.0$, $J = (6.0)(0.75) = \underline{\underline{4 \text{ ft}}}$.

Number of Elements-N

Count those shown in Fig. 161, $N = \underline{\underline{10.5}}$.

Determine C_D

Fig. 161, for 6 rows of elements, $\frac{y}{a} = 1.1$, $C_D = \underline{\underline{0.23}}$.

Estimate velocity at outfall of basin, V_B . Use design Eq. 5-4,

$$\beta_1 \gamma \frac{y_o^2}{2} \frac{W_o}{2} + \beta_2 \rho V_o \frac{Q}{2} = C_D N A \rho \frac{V_a^2}{2} + \beta_3 \rho \frac{Q}{2} V_B + \beta_4 \frac{\gamma (Q/2)^2}{2 V_B^2 W_B/2}$$

$$\gamma = 62.4 \text{ lbs/ft}^3 \quad C_D = 0.23 \quad \beta_3 = 1 \quad V_o = 17.5 \text{ fps}$$

$$\gamma = 1.94 \frac{\text{lbs sec}^2}{\text{ft}^4} \quad \beta_1 = 0.71 \quad \beta_4 = 1 \quad y_o = 4 \text{ f}$$

$$\beta_2 = 1.01 \quad W_o = 6 \text{ ft}$$

$$W_B = W_2 = 24 \text{ ft}$$

$$Q = 420 \text{ cfs}$$

Assume β_3 and $\beta_4 = 1$ in the uniform zone at the outfall of the basin. All other values in the equation have been determined above, except V_B , the unknown. Substitute known values into above equation.

$$(0.71)(62.4) \frac{(4)^2}{2} \left(\frac{6}{2} \right) + (1.01)(1.94)(17.5)(210) = (0.23)(10.5)(2.57)$$

$$(1.94) \frac{(20.1)^2}{2} + (1.94)(210) V_B + \frac{(62.4)}{2} \frac{(210)^2}{V_B^2 \frac{(24)}{2}}$$

Solving for V_B

$$407 V_B + \frac{114,600}{V_B^2} = 5830$$

There are three possible values of V_B , one value is negative and meaningless, the other two are significant. The lower value is associated with subcritical flow, the higher value is the conjugate velocity. Solving the equation above,

$$V_B \text{ subcritical} = 5.7 \text{ fps and}$$

$$V_B \text{ supercritical} = 12.5 \text{ fps}$$

The depths of flow at the outfall corresponding to these velocities are

$$d_B = \frac{Q/2}{(W_2/2) V_B}$$

$$d_B \text{ subcritical} = \frac{210}{(12)(5.7)} = 3.1 \text{ ft}$$

$$d_B \text{ supercritical} = \frac{210}{(12)(12.5)} = 1.4 \text{ ft} .$$

As mentioned in Chapter V for basins with $y/a < 1.4$, the jumps always occurred within the angle field. If insufficient tailwater existed, the flow passed back through the critical depth with supercritical flow in the channel downstream of the basin.

If tailwater is less than 1.4 ft, flow will be supercritical and the outfall velocity will be about 12.5 fps. If tailwater is 3.1 ft or higher (it is difficult to imagine a natural channel carrying 420 cfs at a depth less than this), the exit velocity will be about 5.7 fps or less.

If the exit velocity and depths are satisfactory, the basin dimensions are as follows:

$$\text{Length} = 2 W_0 + 5 J + 1 J \quad (\text{Add } J \text{ downstream of last row of elements.})$$

$$= (2)(6) + (5)(4) + 4 = 36 \text{ ft}$$

$$\text{Width} = (4)(W_0) = (4)(6) = 24 \text{ ft}$$

$$\begin{aligned} \text{Height of basin walls} &= d_B \text{ subcritical} + \text{freeboard} \\ &= 3.1 + 1.5 = 4.6 \text{ ft.} \end{aligned}$$

Size of element 0.75 x 3.43

No. required 2 x 10.5 = 21

Longitudinal spacing of elements = 4 ft

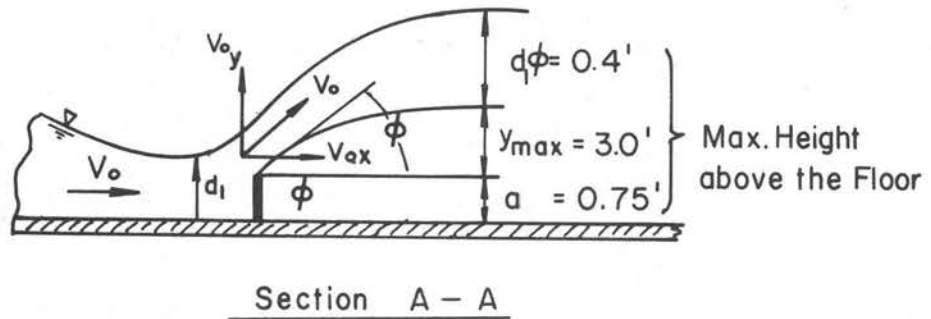
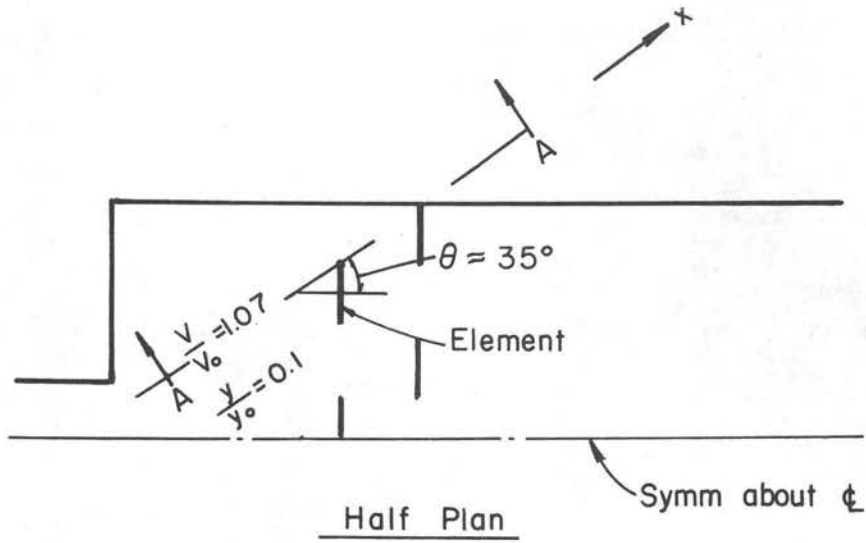
Lateral spacing of elements = $2 M = \underline{\underline{6.8 ft}}$

If V_B deduced from Eq. 5-4 is close to critical velocity (this was not the case in the example solved above) and the tailwater depth downstream of the basin is, coincidentally, near critical depth, an unstable water surface (standing waves, etc.) is probable. If tailwater depth is near critical, the basin should be redesigned in such a way as to ensure adequate depth. Widening the basin or lowering the downstream portion of the basin are two effective means of attaining a suitable depth. The latter solution is generally more economical.

Even though V_B deduced from Eq. 5-4 is near critical velocity, this does not imply that the exit velocity from the basin is near critical velocity. What it does imply is that the momentum of the flow has been reduced to the minimum level possible for the particular combination of discharge and basin width. If the tailwater depth is near critical depth, the exit velocity will be near critical velocity. If the tailwater depth is larger than critical depth the exit velocity will be subcritical. If the tailwater depth is less than critical velocity the exit velocity will be supercritical. The latter mode of operation is illustrated and discussed in Chapter V.

One other problem exists. This is the rooster tail of water downstream of the first two rows of elements. Referring to Fig. 193, a method of estimating the trajectory of the rooster tail is shown. The method is based on the energy equation.

Example: at the first row of elements, using criteria shown on Fig. 144,



Trajectory Equations

$$V_{0x} = V_0 \cos \phi \quad V_{0y} = V_0 \sin \phi$$

$$y_{\max} = V_{0y}(t) - \frac{1}{2}gt^2 \quad x = V_{0x}(t)$$

Definition Sketch, Trajectory Equations

Fig. 193

$$V = (1.07)(17.5) = 18.7 \text{ fps}$$

$$\frac{y}{y_0} \approx 0.1, \quad y = (0.1)(4) = 0.40 \text{ ft, i.e., } d_1 = \underline{\underline{0.40 \text{ ft}}}$$

$$y = V_{oy}(t) - \frac{1}{2} g(t)^2 .$$

$$\text{Assume } \phi = 45^\circ .$$

$$\text{Determine } t @ y = 0 .$$

$$V_{ox} = V_0 \cos 45^\circ = (18.7)(0.707) = 13.2 \text{ fps}$$

$$V_{oy} = V_0 \sin 45^\circ = 13.2 \text{ fps}$$

$$\text{Determine } t @ y = 0 .$$

$$0 = 13.2 (t) - \frac{32.2}{2} t^2 ,$$

$$t = 0 \text{ or } t = 0.91 \text{ sec} , \quad \frac{t}{2} = 0.455 \text{ sec}$$

$$y_{\max} \approx V_{ox} \left(\frac{t}{2}\right) - \frac{1}{2} g \left(\frac{t}{2}\right)^2$$

$$= (13.2)(0.455) - \frac{1}{2} (32.2)(0.455)^2$$

$$= 6.0 - 3.3 = 2.7 \text{ ft} .$$

The maximum height of the top of the water above the floor is:

$$a + y_{\max} + \text{depth of flow } d_1 = 0.75 + 2.7 + 0.4 = \underline{\underline{3.85 \text{ ft}}}$$

Locate distance to y_{\max} .

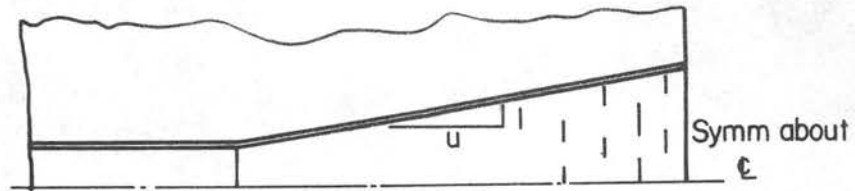
$$x = V_{ox} \left(\frac{t}{2}\right) = (13.2)(0.455) = \underline{\underline{6 \text{ ft}}} .$$

By superimposing these values on the plan of the basin (Fig. 193) it can be determined if the walls are high enough to contain the rooster tails.

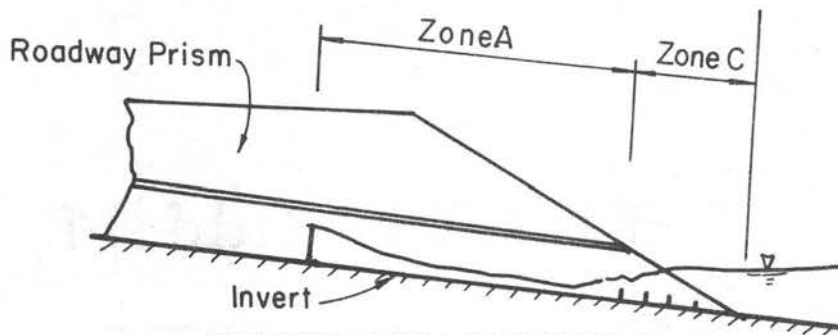
Combined Basin

An alternate basin which would be equally effective and probably more economical than the Class C basin is shown below.

Zone A of the basin would be designed by the procedure described for Class A basins. The depth and velocity of flow at the upstream row of elements can be estimated from the Class A basin computations. Given the depth of flow and velocity at the first row of elements, the zone C portion of the basin is then designed as a Class C basin.



HALF PLAN

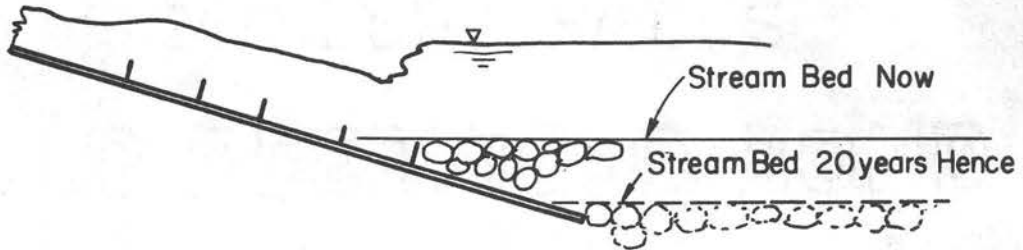


CENTER LINE SECTION

A particularly good feature of this arrangement is positive tailwater control. The invert elevation at the end of the basin can be set low enough to insure adequate tailwater

If the channel downstream is degrading, the floor can be extended as far as is necessary to accommodate future degradation.

Silting in of the elements should not be a problem. Judging from the vigorous action of the water shown in Figs. 153 through 160, deposition in the upper portion of the basin would be rapidly eroded and washed downstream.



PARTIAL CENTER LINE SECTION

High Tailwater Basins

Given: 6 ft x 6 ft box culvert, $Q = 420$ cfs, culvert flowing full (high tailwater), determine the maximum velocity in the channel 60 ft downstream of the outlet.

$$\text{Compute } \frac{x}{W_o} \approx \frac{x}{D_o} = \frac{60}{6} = 10 \quad . \quad (\text{Note: Substitute } W_o \approx D_o \text{ for rectangular approach pipe.})$$

From Fig. 180

$$\frac{V_{x \text{ ave}}}{V_{o \text{ ave}}} = 0.6$$

$$V_{o \text{ ave}} = (1.10) \frac{Q}{\text{area}} = (1.10) \frac{420}{36} = \underline{\underline{12.8 \text{ fps}}}$$

$$V_{x \text{ ave}} = (V_{o \text{ ave}}) (0.6) = (12.8) (0.6) = \underline{\underline{7.7 \text{ fps}}} \quad .$$

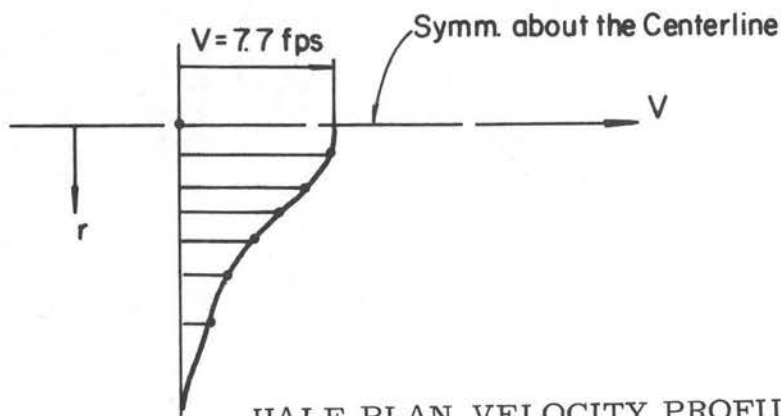
Plot the velocity distribution at $\frac{x}{W_0} = 10$ at an elevation $\frac{W_0}{2}$. Compute: $x = (10)(W_0) = \underline{60}$

$$\frac{V_0 W_0}{x} = \frac{(12.8)(6)}{60} = 1.28$$

Select values of $\frac{V_x}{V_0} \frac{x}{D} = 6, 5, 4, \text{etc.}$ Using these values of $\frac{V_x}{V_0} \frac{x}{D}$, obtain values of $\frac{r}{x}$ from Fig. 184. Compute r and V_x .

$\frac{V_x}{V_0} \frac{x}{D_0}$	$\frac{r}{x}$	$r = x \left(\frac{r}{x} \right)$	$V_x = \left(\frac{V_x x}{V_0 D_0} \right) \left(\frac{V_0 D_0}{x} \right)$
6	0.03	1.8	7.7
5	0.06	3.6	6.4
4	0.075	4.5	5.1
3	0.100	6.0	3.8
2	0.13	7.8	2.5
1	0.17	10.3	1.8
0	0.24	14.4	0

Plot velocity profile.



HALF PLAN VELOCITY PROFILE
AT ELEVATION $W_0/2$, STATION 60.0

The jet may not remain along the centerline of the channel. In the runs with the large pipe in the outdoor flume ($\frac{W_2}{W_0} \approx 6$) the jet oscillated from side to side but never attached to the wall. Insufficient basin length may have precluded attachment. During the high tailwater run described in Chapter II, run 43, where $\frac{W_2}{W_0} = 4$, the jet did attach to the wall. Jet attachment is a possibility in the prototype basin if the downstream channel is relatively narrow with high banks.

There are two possible solutions to the attachment dilemma. One solution is to maintain the invert elevation sufficiently high so that the jet will plunge. This requires a rigid basin or a heavily riprapped floor. The other solution is to increase the cross sectional area of culvert so that the exit velocity is tolerable. The culvert exit is assumed submerged; therefore, if the flare is sufficiently gradual, the entire section will be occupied by the flow.

Chapter VIII

CONCLUSIONS

Rational methods of design for rigid boundary energy dissipating basins have been developed. Existing criteria which have been shown to be applicable for the design of energy basins include: the Blaisdell criterion for wall flare, Ippen's relationship for predicting the angle of the standing wave, and Albertson et al., relationships for determining the properties of the flow field downstream of a culvert outlet operating with high tailwater.

Design aids developed during the CSU study include suitable dimensionless momentum coefficients β_1 and β_2 which correct for non-hydrostatic pressure distribution and non-uniform distribution of velocity at the outfall section of circular or rectangular pipes; dimensionless water surface contours and velocity vectors for free jets supported on the bottom only, downstream of circular and rectangular abrupt expansions; drag coefficients for roughness elements of known size and pattern; and a means of estimating the height of oblique standing waves.

The major contribution of this paper is the integration of the various criterion into a systematic step-by-step design procedure. Though attention has been directed toward the design of energy basins downstream of culvert outfalls, the design procedures are directly applicable to the design of many other energy dissipating structures.

The suggested methods of analysis must be thought of as mathematical models useful for basin analysis. They do not precisely describe the basins.

With reference to the hydraulic jump described in Chapter II for the Class B basins (smooth floor), the face of the jump continuously migrated up and down the channel, sometimes moving two pipe diameters from its average location. This basin was operating under ideal conditions, i.e., fixed tailwater and constant discharge. Certainly the prediction of the position of a hydraulic jump in a prototype structure, with unsteady discharge and variable tailwater conditions (compounded by severe winds which frequently accompany convective storms), is a rather questionable procedure. The suggested design procedures for the smooth basins are little better than order of magnitude estimates.

The artificially roughened basins have many advantages. By manipulation of element size and relative widths of basin, it is possible to obtain any specified exit velocity.

The velocities deduced by the momentum equations for the roughened basins are average velocities. With reference to values of V_{\max} at Sta. 11.0 and V_{ave} at Sta. 11.0 shown in Table VI, the maximum measured point velocity exceeded the mean velocity by as much as 20 percent in some cases. It is suggested that this problem be handled by using appropriate factors of safety.

The design aids do not contain factors of safety. The selection of appropriate factors of safety is left to the discretion of the engineer.

The basins operate well under a large range of discharges. The absence of curved surface, usually associated with energy basins, is another plus feature.

If the roughened basins are subjected to flow with bed material of cobble size (such as is found in torrential mountain streams), the elements must be constructed of sturdy material.

In some instances, particularly where tailwater is low, the most economic installation may be a roughened basin where the flow is spread laterally and the velocity is reduced by 30 to 50 percent, followed by a riprapped floor.

The criteria presented in this paper are sufficient to design basins constructed integrally with the culvert barrel for box culverts and to design energy dissipating basins attached to the outfall of circular or rectangular pipes.

A logical extension of the work described in this paper is a test program for the purpose of obtaining design criteria for end sections of circular (or arch) pipes which could be commercially manufactured. The end section should be an integral part of the culvert, terminating in the same manner as conventional end sections, flush with the roadway prism. Roughness elements could be used to break up the jet and to reduce the velocities to a suitable level.

BIBLIOGRAPHY

BIBLIOGRAPHY

1. Blaisdell, Fred W., "Development and Hydraulic Design, Saint Anthony Falls Stilling Basin," ASCE Trans., Vol. 113, pp. 483-520, 1948.
2. U.S. Bureau of Reclamation, Engineering Monograph No. 25, "Hydraulic Design of Stilling Basins and Bucket Energy Dissipators," Technical Information Branch, Denver Federal Center, Denver, Colorado, 1958.
3. O'Loughlin, B. E., "Culvert Investigations by Hydraulic Models," Harbours and Rivers Branch, Hydraulic Laboratory, Manly Vale. N. S. W., Australia, 1960.
4. U.S. Army Corps of Engineers, "Shore Protection Planning and Design," Beach Erosion Board, Tech. Rep. No. 4, U.S. Government Printing Office, Washington, D. C., 1961.
5. Murphy, T. E., Grace, J. L., "Riprap Requirements for Overflow Embankments," Highway Research Board Record, No. 30, Washington, D. C., 1963.
6. California Division of Highways, "Bank and Shore Protection in California Highway Practice," Sacramento, California, 1960.
7. Blaisdell, Fred W., "Flow through Diverging Open Channel Transitions at Supercritical Velocities," Soil Conservation Service, U.S. Deptment of Agriculture, Washington, D. C., S.C.S. - TP-76, pp. 15, April 1949.
8. Sandborn, V. A., "Metrology of Fluid Mechanics," CET66-67S033, Colorado State University, Fort Collins, Colorado, p. 107 and p. 276, June 1967.
9. Chow, Ven T., "Open Channel Hydraulics," McGraw Hill Book Co., New York, 1959.
10. Watts, F. J., Simons, D. B., Richardson, E. V., "Variation of α and β Values in a Lined Open Channel," Journal of the Hydraulics Division, ASCE, Vol. 93, No. HY6, Proc. Paper 5593, November 1967.
11. Ippen, Arthur T., "Mechanics of Supercritical Flow," ASCE Trans., Vol. 116, pp. 268-295, 1951.
12. Sayre, William W., and Albertson, M. L., "Roughness Spacing in Rigid Open Channels," ASCE Trans., Vol. 128, Part 1, pp. 343-372, 1963.

13. Rouse, Hunter, Bhoota, B. V., and Hsu, En-Yun, "Design of Channel Expansions," ASCE Trans., Vol. 116, pp. 347-363, 1951.
14. Raharatnam, N., and Subramanya, K., "Hydraulic Jump Below Abrupt Symmetrical Expansions," Journal of the Hydraulics Division, ASCE Vol. 94, No. HY2, Proc. Paper 5860, March 1968.
15. Granch, John L., "Second Progress Report on Hydraulics of Culverts Pressure and Resistance Characteristics of a Model Pipe Culvert," National Bureau of Standards, U.S. Department of Commerce, Washington, D. C., 4911, October 1956.
16. Rajaratnam, N., and Muralidhar, D., "Yaw and Pitch Probes," Technical Report, Department of Civil Engineering, University of Alberta, Edmonton, Canada, 1967.
17. Stephan, Roland, "The Geometry of the Expanding Jet Downstream of Culverts," M.S. Thesis, Colorado State University, Fort Collins, Colorado, March 1968.
18. Nagabhushanaiah, H. S., "Separation Flow Downstream of a Plate Set Normal to a Plane Boundary," Ph.D. Thesis, Colorado State University, Fort Collins, Colorado, November 1961.
19. Herbich, J. B., and Shulits, S., "Large Scale Roughness in Open Channel Flow," Journal of the Hydraulic Division HY6, pp. 203-229, November 1964.
20. Koloseus, H. J., and Davidian, J., "Free-Surface Instability Correlations and Roughness-Concentration Effects on Flow Over Rough Surfaces," Geological Survey Water-Supply Paper 1592-C, D, U.S. Government Printing Office, Washington, D. C., 1966.
21. Albertson, M. L., Dai, Y. B., Jensen, R. A., and Rouse, H., "Diffusion of Submerged Jets," ASCE Trans. Vol. 115, pp. 639-697, 1950.
22. Yevjevich, V. M., "Diffusion of Slot Jets with Finite Orifice Length-Width Ratios," Hydraulics Paper No. 2, Colorado State University, Fort Collins, Colorado, 1966.
23. Murota, A., and Muraoka, K., "Turbulent Diffusion of the Vertically Upward Jet," Proceedings of the Twelfth Congress of the IAHR, Vol. 4, Part 1, Colorado State University, Fort Collins, Colorado, 1967.
24. Ahmad, Duad, "Circular Hydraulic Jump," M.S. Thesis, Colorado State University, Fort Collins, Colorado, June 1967.